Stony Brook University

GRAPHENE NANORIBBONS ELICIT CELL SPECIFIC UPTAKE AND DRUG DELIVERY VIA ACTIVATION OF EPIDERMAL GROWTH FACTOR RECEPTORS

A Dissertation Presented

by

Sayan Mullick Chowdhury

to

The Graduate School

in Partial Fulfillment of the

Requirements

for the Degree of

Doctor of Philosophy

in

Molecular and Cellular Biology

Stony Brook University

August 2014

Stony Brook University

The Graduate School

Sayan Mullick Chowdhury

We, the dissertation committee for the above candidate for the

Doctor of Philosophy degree, hereby recommend

acceptance of this dissertation.

Balaji Sitharaman - Dissertation Advisor
Associate Professor of Biomedical Engineering, Stony Brook University

Kenneth R Shroyer -Chairperson of Defense
Professor and Chair of Pathology, Stony Brook University

Richard A.F. Clark
Professor of Biomedical Engineering, Stony Brook University

Patrick Hearing
Professor of Molecular Genetics and Microbiology, Stony Brook University

Anne E McElroy
Professor of Marine and Atmospheric Sciences, Stony Brook University

This dissertation is accepted by the Graduate School

Charles Taber
Dean of the Graduate School

Abstract of the Dissertation

GRAPHENE NANORIBBONS ELICIT CELL SPECIFIC UPTAKE AND DRUG DELIVERY VIA ACTIVATION OF EPIDERMAL GROWTH FACTOR RECEPTORS

by

Sayan Mullick Chowdhury

Doctor of Philosophy

in

Molecular and Cellular Biology

Stony Brook University

2014

Ligands such as peptides, antibodies or other epitopes bind and activate specific cell receptors, and can be employed for targeted cellular delivery of pharmaceuticals such as drugs, genes and imaging agents. In this dissertation, I investigate the *in vitro* and hematological compatibility of oxidized graphene nanoribbons, non-covalently functionalized with PEG-DSPE (1, 2-distearoyl-*sn*-glycero-3-phosphoethanolamine-N[amino(polyethyleneglycol)]) (O-GNR-PEG-DSPE) and evaluate its potential as a drug delivery agent. Although, O-GNR-PEG-DSPE was found to interact with RBC membrane and induce structural changes in them, they did not affect other hematological parameters. *In vitro* studies showed that these particles activate epidermal growth factor receptors (EGFRs) and elicit cell specific uptake and concentration dependent toxicity in cells over-expressing these receptors. Receptor activation was found to occur through a mechanism involving membrane depolarization and influx of extracellular Ca^{2+}. This activation generates a dynamin-dependent macropinocytosis-like response, and results in

significant O-GNR-PEG-DSPE uptake into cells with high EGFR expression. Cells with an integrated human papillomavirus (HPV) genome also show increased uptake due to the modulation of the activated EFGR by the viral protein E5. I demonstrate that this cell specific uptake of O-GNR-PEG-DSPE can be exploited to achieve significantly enhanced drug efficacies even in drug resistant cells and xenograft tumors. These results have implications towards the development of active targeting and delivery agents without ligand functionalization for use in the diagnosis and treatment of pathologies that over-express EGFR or mediated by HPV.

DEDICATION

I would like to dedicate this dissertation to my parents, Subrata and Suparna Mullick Chowdhury and brother Sreyan Mullick Chowdhury. I will forever be grateful for their encouragement, love and support throughout the years.

TABLE OF CONTENTS

List of Tables

List of Figures

Chapter 1

Chapter 2

Chapter 3

Chapter 4

Acknowledgments

I would like to extend my sincere gratitude to the following people for the continuous help and support I received from them. Firstly, I would like to thank my parents who have always stood by my decisions and supported me through everything. I would like to express my deepest gratitude to Dr Balaji Sitharaman, my advisor, for giving me the opportunity to work in his lab and being so supportive throughout my graduate career. I am also grateful to my committee members Dr Kenneth Shroyer, Dr Richard Clark, Dr Anne McElroy and Dr Patrick Hearing for their advice and guidance throughout my PhD.

I would also like to thank Gaurav Lalwani, Yahfi Talukdar, Shruti Kanakia, Jason Rashkow, Shawn Xie, Stephen Lee, Behzad Farshid, Cassandra Surhland, Justin Fang, Jimmy Toussaint and other past and present lab members in Dr Sitharaman's Lab who have helped me whenever I needed.

I will forever be indebted to many of my friends and colleagues who have supported me in these four years. A special thanks to Urmi Majumdar for her unending support and encouragement and Subham Dasgupta for being such a great friend, colleague and roommate.

This dissertation would not have been possible without the help and support of Dr Guo Wei Tian and Susan Van Horn of Central Microscopy in Stony Brook and staff of the animal facility in Stony Brook Hospital.

This work was supported by funding from National Institutes of Health (grant No. 1DP2OD007394-01), and the Wallace. H. Coulter Foundation.

Publications

1.Mullick Chowdhury S, Lalwani G, Zhang K, Yang JY, Neville K, Sitharaman B. Cell specific cytotoxicity and uptake of graphene nanoribbons. **Biomaterials.** 2013;34:283-93

2.Mullick Chowdhury S, Kanakia S, Toussaint JD, Frame MD, Dewar AM, Shroyer KR, Moore W& Sitharaman B. In vitro Hematological and In vivo vasoactivity assessment of dextran functionalized graphene.**Scientific Reports** .2013; 3: 2584

3. Mullick Chowdhury S, Manepalli P, Sitharaman B. "Graphene Nanoribbons Elicit Cell Specific Uptake and Delivery Via Activation of EGFR Enhanced by HPVE5" **Acta Biomaterialia**, 2014 (In Press)

4.Kanakia S, Toussaint JD, **Mullick Chowdhury S,** Lalwani G, Tembulkar T, Button T, Shroyer KR, Moore W & Sitharaman B. Physicochemical characterization of a novel graphene-based magnetic resonance imaging contrast agent.2013 **International Journal of Nanomedicine**. 8, 2821–2833

5. Frame MD, Dewar AM, **Mullick Chowdhury S,** Sitharaman B. Vasoactive Effects of Stable Aqueous Suspensions of Single Walled Carbon Nanotubes in Hamsters and Mice.2014..**Nanotoxicology**. 8.8:867-875

6. Kanakia S, Toussaint J , **Mullick Chowdhury S**, Tembulkar T, Lee S, Jiang Y, Lin R, Shroyer KR, Moore W, Sitharaman B **"**Dose Range Finding, Acute Toxicity and Safety Pharmacology of Intravenously Administered Functionalized Graphene Nanoparticle Formulations" **Biomaterials**.2014;35:7022-7031

Organization of Dissertation

The ultimate goal of this doctoral research is to evaluate the potential of graphene nanoribbons as a chemotherapeutic drug delivery agent. To this end, this dissertation will discuss the *in vitro* and hematological toxicity of these nanostructures, explore their uptake mechanism in cell lines, and evaluate their chemotherapeutic drug delivery efficiency *in vitro* and *in vivo*. Based on the data reported in subsequent chapters, the introduction chapter is aimed at providing a brief overview of EGFR, its role in inducing cancer, treatment options available clinically and the importance of chemotherapy. This chapter also explains the importance of drug delivery agents and the advantages that graphene provides as a drug delivery agent. The second and third chapter of this dissertation introduces graphene nanoribbons and evaluates their *in vitro* and hematological toxicity respectively. The fourth chapter explores the mechanism of cellular uptake of these nanostructures and reports their *in vitro* targeted drug delivery efficiency in multiple cell lines by utilizing the uptake mechanism. The fifth chapter reports the *in vivo* drug delivery efficiency of graphene nanoribbons and also presents the molecular basis of the uptake mechanism of the particles. The sixth and last chapter provides the conclusion of the work completed and potential future directions of this reported work.

Chapter 1

INTRODUCTION

1.1 EGFR and its role in cancer

Epidermal growth factor receptors (EGFR) (also known as HER1 and ErbB1) are glycoprotein trans-membrane receptors (polypeptide containing 1186 amino acids) comprised of an extracellular ligand binding domain, an intracellular kinase domain, and a trans-membrane hydrophobic anchor sequence (Figure 1)(Voldborg et al., 1997). These receptors are part of the ErbB family which also includes three other types of receptors (ErbB2, ErbB 3 and ErbB4)(Erjala et al., 2006). All members of the ErbB family of receptors contain a tyrosine kinase domain that gets activated on ligand binding(Hinohara et al., 2012). There are eight known ligands that can activate EGFR. These are epidermal growth factor (EGF), transforming growth factor alpha (TGF-Alpha), Epigen, Neuregulin-2β, heparin binding EGF like growth factor, betacellulin, amphiregulin and epiregulin(Henriksen et al., 2013). On ligand binding, the EGF receptors transform from an inactive monomeric to an active dimeric state by dimerization with another monomeric receptor of its own kind (homodimerization i.e. EGFR with EGFR), or another member of the Erb B family (heterodimerization)(Yarden and Schlessinger, 1987). EGFR dimerization activates the tyrosine kinase domain of the receptors resulting in auto-phosphorylation of several tyrosine residues in the C terminal domain of the receptors (Tyrosines 992, 1045, 1068, 1148 and 1173)(Downward et al., 1984). Post auto-phosphorylation, activation of several downstream signaling cascades are initiated through proteins that can bind the phosphor tyrosine through their SH_2 domains(Oda et al., 2005). The downstream cascades initiated include MAPK (Mitogen activated protein kinase), JNK (Janus kinase) and Akt (Protein

kinase B) pathways(Oda et al., 2005). These pathways take part in cell growth, proliferation, migration, adhesion and DNA synthesis(Figure 1)(Oda et al., 2005). After activation, the receptors are internalized into vesicular endosomal structures(Rush et al., 2012). However, even after internalization, the phosphorylated EGFR is still catalytically active and can interact with downstream signaling proteins(Wang et al., 2002). These endosomal structures containing internalized EGFR have to be acidified to merge into the lysosome for degradation of EGFR and attenuation of signaling(Wang et al., 2002). EGFR signaling attenuation is initiated by ubiquitination of EGFR tail protruding into the cytoplasm from the endosomes(Sigismund et al., 2013). This ubiquitination results in recognition of the EGFR sorting complex that directs the EGFR containing endosomes to the lysosomes(Sigismund et al., 2013). Compromise of this ubiquitination and degradation pathway often results in EGFR recycling back to the membrane and continuation of signaling(Alwan et al., 2003).

Epidermal growth factor receptor activation and resultant signaling cascades are responsible for promoting growth and proliferation in cells(Carpenter and Cohen, 1979, Mitsudomi and Yatabe, 2010). Hence, aberrations in their expression, activation and signaling pathways can result in abnormal cellular growth (i.e. formation of tumors or cancerous growth)(Nicholson et al., 2001, Mitsudomi and Yatabe, 2010). Cancer formation usually takes place due to increased proliferation of cells, cell invasion, metastasis, resistance to apoptosis and increased angiogenesis, all of which are directly or indirectly influenced by enhanced EGFR signaling(Figure 1)(Baselga, 2002). As such, cancers caused due to mutations in EGFR are highly infiltrative and aggressive in nature(Nicholson et al., 2001). Enhancement of EGFR signaling occurs due to either amplification or mutation of the EGFR gene(Voldborg et al., 1997). Three types of deletion mutations of the EGFR extracellular domain have been reported

to cause cancerous growth(Voldborg et al., 1997). EGFRvI represents a mutated EGFR with completely deleted extracellular domain that does not respond to EGF but remains constitutively active(Voldborg et al., 1997). EGFR vII represents a mutated EGFR with 83 aa deletion in domain IV of the extracellular domain, found primarily in glioblastoma (Voldborg et al., 1997). EGFRvIII represents a mutated EGFR that does not contain domain I and II (amino acids 6-273) of the extracellular domain. This deletion results in over-amplification of this mutated EGFR, contributing in enhanced EGFR signaling(Voldborg et al., 1997). Also, EGFRvIII fails to get internalized after activation, thus prolonging the signaling cascade. Similar mutations leading to EGFR over-expression in cells have been identified as the cause for several kinds of cancer(Voldborg et al., 1997). EGFR over-expression is reported in most cases of breast cancer(Rimawi et al., 2010), non small cell lung cancer and glioblastoma multiformae (Rusch et al., 1997, Barker II et al., 2001). Human papilloma virus mediated cancers (cervical cancer, head and neck cancer, vulvar cancer etc) have also been shown to over-express these receptors(Kim et al., 2007). The most important and frequently studied oncogenic EGFR mutations are those in its intracellular tyrosine kinase domain (Tang et al., 2005, Wang et al., 2006). Mutations in the tyrosine kinase domain of EGFR may activate these receptors without their ligand, keeping the receptor constitutively active(Wang et al., 2006, Voldborg et al., 1997). Some mutations like those in the C-terminal amino acids 957-1022 (required for endocytosis) has been reported to enhance EGFR signaling by preventing their endocytosis, ubiquitination and degradation (Voldborg et al., 1997).

1.2 Human Papilloma Virus mediated EGFR over expressing tumors

Human papilloma viruses (HPV) are small, non enveloped DNA viruses that belong to the *papovaviridae* family of viruses(Parkin., 2006). Clinical, scientific and epidemiological data suggests that HPV infection accounts for ~5.2% of cancers worldwide, (Schiffman et al., 2007)including cervical, vulvar, penile, and oropharyngeal cancer (Schiffman et al., Muñoz et al., 2004, Watson et al., 2008). Till date, more than twelve oncogenic, high risk HPV strains have been identified. Among these stains, HPV16 and HPV 18 cause majority of the HPV related cancers (~70%)(Muñoz et al., 2004, Watson et al., 2008, Schiffman et al.). Although, currently, cervical cancer is the most common form of HPV mediated cancer, research indicates that by 2020 oropharyngeal cancer will take over as the leading form of HPV mediated cancer in the United States(Chaturvedi et al., 2011).

The human papilloma virus genome contains a double stranded DNA that can code for 8 proteins which are named early (E) or late (L) according to the time in the viral life cycle they are expressed. E1, E2, E4 and E5 proteins are important for replication of the viral genome in the host. E1 plays a role in preventing the viral genome from integrating into the host, and along with E2 initiates the viral gene expression. E6 and E7 are the two primary oncoproteins which inactivate tumor suppressing p53 and pRb proteins respectively. (Yim and Park, 2005). The hydrophobic E5 protein down regulates the major histocompatibility complex 1(MHC1) to prevent infected cells from being eliminated through the immune system and also plays a role in ligand activated cell proliferation through the epidermal growth factor receptors(Chen et al., 2004). E1 and E2 regulate the production of the E6 and E7 oncoproteins to prevent possible cancerous growth. L1 and L2 are capsid proteins that are produced only when viral genome needs to be packaged before leaving the host (Cricca et al., 2009).

HPV can infect, develop and reproduce in keratinocytes or keratin producing epithelial cells only(Delvenne et al., 2001). The capsid proteins of the virus, L1 and L2, play an important role in the uptake of the viruses through interaction with heparan sulphate proteoglycans on the surface of host cells (Rommel et al., 2005). Recent evidence also suggests that integrin-alpha 6 acts as a co-receptor in the uptake mechanism (Bousarghin et al., 2003). It has been reported that *in vivo,* virions initially bind to the basement membrane before they move into the keratinocyte or epithelial cell population. However, *in vitro* the virions show a direct receptor mediated uptake (Horvath et al., 2010, Da Silva et al., 2007).

Once inside the cell the HPV amplifies its genome to maintain ~ 50 copies per infected cell (Meyers et al., 2002). At this point the virus may choose to remain latent inside the host cells, or it may start proliferating and subsequently show symptoms of infection. HPV genome amplification is usually a tightly regulated process that changes with the stage of epithelial differentiation. Keratinocytes and outer epithelial layer cells contain ~1000 copies of the HPV episome, and also produce the L1 and L2 proteins which package the HPV genome for release (Zhao et al., 1998, Finnen et al., 2003). HPV latency can last from months to 20 years or more. In cervical cancer, latency period between HPV infection and low grade cervical dysplasia is~5 years and between low grade lesions to the development of invasive cancer is ~15 years (Meijer et al., 2000). Low grade lesions are characterized by presence of the HPV genome as an episome whose protein expression is independent of the host genome. E6 and E7 oncoproteins are not expressed at the low grade lesion stage (Lee et al., 2011). The conversion of a low grade lesion into a high grade lesion is characterized by integration of the HPV genome into the host genome such that transcription of HPV genome is regulated by both HPV and host regulatory elements. This invasive stage is characterized by increased expression of E6 and E7 oncoproteins due to

loss of E1 and E2 expression which normally regulate the level of these oncoproteins (Cricca et al., 2009, Collins et al., 2009). This increased expression of the oncoproteins also lead to genomic instability that results in genome integration and finally progression to malignancy.

The HPV E5 is a hydrophobic, trans-membrane, 83 amino acid poly-peptide that is unable to immortalize kerationocytes, but increases the proliferative life of these cells *in vitro* (Barbaresi et al., 2010). In some studies it has been shown that in presence of the ligand, HPV E5 inhibits the down regulation of EGFR (Figure 2) (Ashby et al., 2001). This inhibition of EGFR down regulation takes place in the endosomal compartment once the EGFR in endocytosed. E5 acts on the ATPases to prevent endosomal acidification and hence prevention of EGFR degradation (Figure 2)(Ashby et al., 2001). This result in a 2-5 times increase in EGFR expression and phosphorylation on the surface of the cells as the EGFR is recycled back to the surface. HPV E5 expression in an infected cell depends on the stage of HPV infection and also the portions and number of HPV genomes that has fused with the host genome (Figure 2)(Tsai and Chen, 2003). In the initial stages of infection when the HPV genomes are present mainly as episomes, E5 protein is highly expressed in the cells (Muto et al., 2011). On integration the expression of E5 depends on the number of integrated HPV E5 genomes. Two HPV 16 cell lines SiHa and CaSki have ~1-2 and ~500-600 HPV genomes integrated in the host genome and produce corresponding amounts of E5 protein whereas HeLa cells have 40-50 HPV-18 integrated genomes (Samama et al., 2002). A recent study using 40 HPV-16 positive tissue samples has shown that E5 protein was primarily expressed in the lower third of the epithelium in low-grade squamous intraepithelial lesions (SILs) and throughout the whole epithelium in high-grade SILs (Chang et al., 2001).

1.3 Treatment for EGFR over-expressing cancers

The main treatment options for cancer are use of signaling pathway inhibitors, antibodies against over-expressed receptors, surgery, chemotherapy and radiation therapy or their combination(Recht et al., 1996, Woodburn, 1999). The choice of treatment is dependent on the type of tumor, its physiological location and stage of its diagnosis (Sant et al., 2009, Heidenreich et al., 2011, Flehinger et al., 1992). If it is possible to take the tumor out of the body then surgery is usually the preferred choice. This is usually the case if the tumor growth is detected early and the cancer has not spread to other organs(Flehinger et al., 1992, Ohgami et al., 1999). In case of late diagnosis (i.e. detection at the invasive stage), chemotherapy and radiation therapy are the preferred choices(Paik et al., 2000, Shah and Lydiatt, 1995). Also, in case of surgery, it might not be possible to remove the complete tumor from the body and hence chemotherapy and radiation therapy need to be used for removal of the remnant tumor cells(Roth et al., 1994). A treatment option that has been considered for EGFR over-expressing tumors includes use of antibodies against the receptors(Ciardiello and Tortora, 2008). Anti EGFR antibodies bind to the ligand binding pocket of the receptors, thus blocking ligand mediated EGF activation(Ciardiello and Tortora, 2008). Two anti-EGFR antibodies Cetuximab (a mouse human IgG1 antibody) and Panitumumab (humanized IgG2 antibody) have been widely used for this purpose.(Ciardiello and Tortora, 2008) However, several forms of primary and acquired resistance have been reported for antibody based treatment of EGFR over-expressing tumors(Chong and Jänne, 2013). BRAF (B-Raf) mutation and PTEN (Phosphatase and tensin homolog) deletion are two common mechanisms of primary resistance to antibody treatment in colon cancer (Laurent-Puig et al., 2009, Sartore-Bianchi et al., 2009). Similarly mechanisms of acquired resistance in colon cancer include S492R mutation (Figure 3) and alternative pathway activation [e.g. KRAS (K-Ras) and

MET (Mesenchymal–epithelial transition) pathway activation] (Montagut et al., 2012, Diaz Jr et al., 2012, Misale et al., 2012, Liska et al., 2011). For cancers caused due to mutations in the tyrosine kinase domain of EGFR, tyrosine kinase inhibitors like gefitinib, erlotinib and sunitinib have been used(Ghoreschi et al., 2009). Similar to antibody treatment, both primary and acquired resistance to tyrosine kinase inhibitors has been observed in different cancers(Chong and Jänne, 2013). For example, in lung cancer, T790M mutation (Figure 3) or BIM (a member of Bcl-2 family of proteins) deletion is responsible for primary resistance.(Ng et al., 2012, Inukai et al., 2006, Wu et al., 2011) The T790M mutation can also be an acquired resistance to tyrosine kinase inhibitor treatment(Kobayashi et al., 2005). Activation of the alternate pathways like DAPK (Death associated protein kinase), BRAF (B-Raf), and JAK2 (Janus Kinase 2) are also acquired resistance to tyrosine kinase inhibitors (Ohashi et al., 2012, Harada et al., 2012, Koch et al., 2012). Studies have shown that all patients of pancreatic, colorectal, lung and head and neck cancer receiving antibody or tyrosine kinase inhibitor treatment ultimately develop resistance(Chong and Jänne, 2013). Hence chemo or radiation therapies are usually the more effective methods for treatment of tumors with oncogenic EGFR mutation or over-expression.

1.4 Detection and treatment of HPV induced cancers

The common methods for detection of a HPV infection include Pap smear tests, colposcopy and direct inspection for HPV DNA in patient cell samples (Denny et al., 2000). Vaccines have been invented for prevention of HPV infections in both males and females. However, these vaccines need to be taken early in life (21 years for male and 26 years for female) (Hutchinson and Klein, 2008). Once the HPV infection has progressed to cancerous lesion stage the current methods of

treatment include surgery, radiation therapy and chemotherapy. Surgery procedures include cryosurgery, loop electrosurgical excision procedure, electrocautery and laser therapy. However, survival rate for patients is very low, and functional outcomes are often compromised in these surgical procedures. Thus, the patient often requires either radiation therapy or chemotherapy (Wang et al., 2012). Sub-lethal doses of radiation therapy are also used in combination with surgery, alone or with chemotherapy for tumors which cannot be operated (Worden et al., 2008). Chemotherapy is the most common approach for treatment of HPV mediated cancers and depending on the stage of the cancer it may be the first mode of treatment before surgery or radiation therapy (Smith et al., 2011). Hycamtin and cisplatin were approved for therapy of cervical cancer by FDA in 2006. Presently, cisplatin is the most frequently used drug for chemotherapy of HPV mediated cancers. However, recent studies have showed that EGFR over-expressing HPV mediated cancers are less responsive to present chemotherapy treatments compared to other tumors (Kumar et al., 2008). Thus better chemotherapeutic methods need to be developed for treatment of HPV mediated cancers that frequently over-express EGFR.

1.5 Drug delivery agents for chemotherapy

The major drawback to systemic chemotherapy has been the effect that anti-cancer drugs have on non-cancerous cells. There are multiple classes of chemotherapy drugs: alkylating agents, antimetabolites, anthracyclines etc (Yeh et al., 2004) and each has its own set of negative effects on healthy tissue. Alkylating agents have been shown to cause long term bone marrow damage(van Os et al., 1998) and even leukemia, while anthracyclines can permanently damage the heart (Suter and Meier, 2002). The problem of negative effects on healthy tissue is further

compounded by the poor cellular uptake shown by many cancer cells for a variety of chemotherapeutic drugs such as doxorubicin, a commonly used anthracycline(Kik et al., 2009). One of the major limitations of these drugs is their low therapeutic index (ratio of the lethal dose to the effective dose of a drug) (Haley and Frenkel, 2008, Gombotz and Pettit, 1995). The two leading reasons for the low therapeutic index value are: (a) low drug concentrations at the target site (solid tumors) upon systemic administration; and (b) systemic toxicity on normal tissues leading to potentially severe side effects on patients (Haley and Frenkel, 2008). The major reason for low drug concentrations at target site is low drug bioavailability due to binding of hydrophobic drug to proteins. Thus, drug delivery systems have been developed that improve the bioavailability of the drug and alter the drug's biodistribution to improve its accumulation at the tumor site. These drug delivery agents, which are mainly micro and nanoparticles, are characterized by efficient drug loading and delivery to target site. The various categories of nanoparticles that have been explored in this regard include metal based nanoparticles (gold, silver) (Chan, 2007, Anandhakumar et al., 2012), lipid based nanoparticles (liposome, micelles) (Drummond et al., 1999, Liu et al., 2000) dendrimers(Gillies and Frechet, 2005), polymer based nanoparticles (Haxton and Burt, 2009), biological nanoparticles (viruses)(Ren et al., 2010),and carbon based nanoparticles (carbon nanotubes, fullerenes, graphene) (Elhissi et al., 2011, Zakharian et al., 2005, Zhang et al., 2010). The delivery of drug to the tumor site using these nanoparticles can happen by either an active or a passive uptake mechanism (Danhier et al., 2010). The passive diffusion or convection of nanoparticle through leaky tumor vasculature into the tumor is referred as passive delivery. Nanoparticles, due to their sizes, gain access to the tumor interstitium and can be retained in the tumor for extended times, and this phenomenon is known as the enhanced permeability-and-retention (EPR) (Gombotz and Pettit, 1995). EPR has

been proposed as the dominant phenomena responsible for the higher drug delivery efficacy of the nanoparticles by passive tumor uptake mechanism. The active nanoparticle uptake mechanism is based on targeted drug delivery. Nanoparticle based drug delivery systems that target tumors have been under investigation for a number of years also because of the advantages they provide in terms of controlled drug release and increased effectiveness of drug delivery to target sites. To ensure the drug loaded nanoparticles are targeted to the tumor site specifically, they are functionalized with antibodies, peptides and carbohydrate moieties. The receptors for these attached moieties are often over-expressed in tumors and thus these nanoparticles are taken up in the tumors. Nanoparticles with biocompatible coatings have also been utilized for the delivery of drugs by evading the immune system. Poly Lactic Acid (PLA), Poly Lactic Acid co Glycolic Acid (PLGA) and Poly ethylene glycol (PEG) based micro and nanoparticles have been approved by the FDA for drug delivery applications (Makadia and Siegel, 2011). Recently, DOXIL, a doxorubicin (chemotherapeutic drug) liposome formulation has been approved by the FDA for drug delivery applications also (Barenholz, 2012). Genexol-PM, a micelle based agent for delivery of the drug paclitaxel has also been FDA approved for treatment of breast cancer (Oerlemans et al., 2010).

Currently, the chemotherapeutic treatment of EGFR over-expressing (which includes HPV induced) cancers is either through oral ingestion or intravenous injection of the drug. However, there are no FDA approved drug delivery agents which can target chemotherapeutic drugs specifically to EGFR over-expressing tumors. Thus, there is a critical need for the development of such an agent.

1.6 Graphene as a delivery agent

Graphene is a two-dimensional planar carbon nanostructure which is made up of a densely packed network of sp^2-hybridized carbon atoms arranged in a honeycomb crystal lattice formation (Geim and Novoselov, 2007, Novoselov et al., 2004, Liu et al., 2010, Paratala et al., 2012). This material has attracted a great deal of attention due to its unique nanoscopic properties, and for its potential in various material and biomedical science applications (Schedin et al., 2007, Lin et al., 2011, Sordan et al., 2009). Its scientific significance and potential transformative impact were underscored by the 2010 Nobel Committee with the award of the Nobel Prize in Physics for work on 'the thinnest material known'. A recent report also predicts that graphene may overtake carbon nanotubes in commercial applications (Paratala et al., 2012).

The physical and chemical properties of graphene make it particularly useful for a variety of imaging, therapeutic and drug-delivery applications, and thus, it can be considered a multifunctional nanoparticle (Sun et al., 2008). As mentioned earlier, efficient delivery of chemotherapeutic drugs into cancer cells needs the use of drug delivery agents because of three main reasons. Firstly, most chemotherapeutic drugs are hydrophobic in nature, have very low solubility in physiological solvents and needs to be carried by an agent. Secondly, drug delivery agents can load high volumes of drug onto themselves for delivery. Thirdly, drug delivery agents can deliver loaded drugs to specific target sites thus increasing the specificity of the drug action. Graphene has proved to be better than other drug delivery agents in all three areas mentioned. Graphene oxide, the oxidized form of graphene can be dispersed well in physiological solutions because of the carboxylic, hydroxyl and epoxide groups on its surface and is the form of graphene mainly used for drug delivery purposes (Schedin et al., 2007). The external carbon sheath of graphene can be covalently or non-covalently functionalized with biological moieties

that target specific cell or tissues types and/or pharmaceutical agents (Sun et al., 2008, Huang et al., 2011).

The other advantage that graphene provides over other drug delivery agents is its high aromatic drug loading capacity (Sun et al., 2008). The hydrophobic drug loading of graphene is possible because of the stacking of aromatic rings of the drug (pi-pi stacking) on the flat bed of carbon atoms that graphene provides (Figure 4)(Sun et al., 2008). This kind of non covalent attachment of graphene has its own advantages including easy but slow release of the drug when in an acidic environment (in cancer cells)(Sun et al., 2008). Slow release of the drug ensures that there is a continuous release of the drug for a better and efficient chemotherapeutic treatment. Moreover, graphene can be functionalized covalently or non-covalently (e.g. hydrophobic interactions) very easily by ligands which can increase the aqueous stability of graphene or target the graphene to cancer tissues. Solubilizing and targeting ligands may include monoclonal antibodies, lipids, folic acid, proteins and carbohydrate moieties which help in the uptake of graphene into cancer cells by endocytosis (Figure 4) (Sun et al., 2008, Huang et al., 2011). The exact circumstance under which the drug release occurs is also very important because drug release in tissues other than target tissues will cause unwanted cell death.

As mentioned earlier, drug loading on graphene is very high. Although functionalization of graphene to facilitate targeting decreases its drug loading capacity it is still much higher than other drug delivery agents (e.g. most liposomal drug delivery agents can load ~10% w/w of the drug (Fattal et al., 1991). *Sun et al* were the first group to show that nanographene sheets are biocompatible and can be used to load high amounts of hydrophobic aromatic drug (e.g. doxorubicin and SN38)(Sun et al., 2008). Functionalization of the graphene sheets with antibodies was also achieved by this group so that the graphene sheets could be specifically

targeted to cancer cells (Raji B cell lymphoma) (Sun et al., 2008). To provide better stabilization in physiological solvents the same group reported functionalization of graphene oxide with amine terminated PEG. The PEG coating, being biocompatible by itself provided further biocompatibility to the graphene structures and they were used to transport drugs into colorectal cancer cells (HCT-116) (Huang et al., 2011). Another way to make graphene oxide physiologically more stable is functionalization with chitosan (Bao et al., 2011). 5-fluorouracil could be successfully loaded and delivered on chitosan functionalized graphene (Fan et al., 2013). Mixed drug treatment of cancer is very a very common practice to treat cancer. To see if mixed drug loading of graphene is possible *Zhang et al* used folic acid conjugated nano graphene oxide to load with mixed anti-cancer drugs and delivered them to cancer cells(Zhang et al., 2010). *Yang et al* have achieved a dual targeting system of graphene based drug delivery in which they have attached super paramagnetic Fe_3O_4 to graphene and then further functionalized it with folic acid (Yang et al., 2011). Dual targeting was achieved by both the folic acid (folic acid receptors are over expressed in cancer cells) and by a guided magnetic field which would guide the super paramagnetic particle attached graphene oxide into the cancer cells. Previous work from the same group (*Yang et al* 2009) where they had used only Fe_3O_4 to functionalize graphene oxide had yielded a drug(doxorubicin) loading of ~ 1.08 mg/mg of graphene oxide(Yang et al., 2009). However, on attachment of the folic acid/ Fe_3O_4, the drug loading decreased to ~ 0.387 mg/mg of graphene oxide indicating that additional functionalization was taking up space on the graphene oxide and thus reducing drug loading(Yang et al., 2011). Thus, drug loading and functionalization for targeting seem to have inverse relationship. One has to be compromised to achieve the other. As mentioned earlier, the release of the drug at the right place and in the right conditions is important to determine how efficient the drug delivery is. *Yang et*

al found out that drugs loaded on graphene oxide releases drugs efficiently only at an acidic pH (pH 4) and the release over time decreased gradually as one went from acidic to basic pH (Yang et al., 2011). Similar results with other drugs and different functionalization has been demonstrated in other studies (*Rana et al.*)(Rana et al., 2011). Alternately, the space between graphene sheets can be filled with biologically important atoms and molecules (Figure 5) (Paratala et al., 2012). Here, the graphene acts as a biological cargo vehicle which transports and delivers imaging and/ or therapeutic agents (Figure 5). Furthermore, graphene itself can be used as a therapeutic agent by exploiting its unique physical properties. For example, the strong optical absorption properties of graphene in the visible or near infrared region could facilitate tumor ablation with targeted hyperthermia of graphene containing cells (Huang et al., 2011).Other advantages of using graphene for therapeutic purposes, and as delivery vehicles include its nanoscale size, which enhances its retention and permeability into diseased tissues (e.g. tumors.). Additionally, its large surface area allows attachment of multiple functional groups for the targeted delivery of multiple therapeutic entities (Huang et al., 2011). Work is just beginning on the idea of harnessing graphene as a chemotherapeutic agent for the targeted treatment of cancer. The multifunctional characteristics of this material may allow it to overcome some of the problems that chemotherapeutics have suffered to date.

Many recent studies have shown that once injected *in vivo,* graphene shows passive targeting and accumulation in tumors. This is probably because of its thin dimensions and small size. Yang et al showed that pegylated graphene oxide accumulates preferably in mice xenograft tumors when injected though the tail vein (Yang et al., 2010). Miao et al repeated this study and in addition showed that drug loaded graphene nanoparticles can be used for effective passive targeting and chemotherapy of tumors (Miao et al., 2013). Similar studies by Yue et al have shown same

results in mice because of the previously mentioned EPR (enhanced permeation and retention) effect (Yue et al., 2013). These studies indicate that drug loaded graphene nanostructures would be very efficient as agents for passive accumulation in tumors where they can be taken up into tumor cells and thus increase bioavailability of the loaded drug inside the tumor.

1.7 Graphene Nanoribbons

Previous biomedical research using graphene based nanostructures including the studies discussed in section 1.6 have focused on graphene derived from oxidation and exfoliation of graphite. Recently, graphene nanoribbon, a new form of graphene, has been synthesized by oxidative unzipping of multiwalled carbon nanotubes [117]. These graphene nanostructures, apart from being structurally different from graphite derived graphene also contain more carboxyl and hydroxyl groups on their surface [118]. Hence, graphene nanoribbons should be potentially easier to functionalize for targeting, and improvement of their stability in biological media. However, currently, there are no reported studies that explore the potential biomedical applications of this particular form of graphene. The global aim of this and subsequent chapters of this dissertation is to test the biocompatibility of these nanostructures and assess their ability to deliver chemotherapeutic drugs in *vitro* and *in vivo*.

1.9 References

Alwan, H. A., Van zoelen, E. J. & Van leeuwen, J. E. 2003. Ligand-induced lysosomal epidermal growth factor receptor (EGFR) degradation is preceded by proteasome-dependent EGFR de-ubiquitination. *Journal of Biological Chemistry,* 278**,** 35781-35790.

Anandhakumar, S., Mahalakshmi, V. & Raichur, A. M. 2012. Silver nanoparticles modified nanocapsules for ultrasonically activated drug delivery. *Materials Science and Engineering: C,* 32**,** 2349-2355.

Ashby, A. D., Meagher, L., Campo, M. S. & Finbow, M. E. 2001. E5 transforming proteins of papillomaviruses do not disturb the activity of the vacuolar H+-ATPase. *Journal of General Virology,* 82**,** 2353-2362.

Bao, H., Pan, Y., Ping, Y., Sahoo, N. G., Wu, T., Li, L., Li, J. & Gan, L. H. 2011. Chitosan-Functionalized Graphene Oxide as a Nanocarrier for Drug and Gene Delivery. *Small,* 7**,** 1569-1578.

Barbaresi, S., Cortese, M. S., Quinn, J., Ashrafi, G. H., Graham, S. V. & Campo, M. S. 2010. Effects of human papillomavirus type 16 E5 deletion mutants on epithelial morphology: functional characterization of each transmembrane domain. *Journal of General Virology,* 91**,** 521-530.

Barenholz, Y. C. 2012. Doxil®—the first FDA-approved nano-drug: lessons learned. *Journal of Controlled Release,* 160**,** 117-134.

Barker II, F. G., Simmons, M. L., Chang, S. M., Prados, M. D., Larson, D. A., Sneed, P. K., Wara, W. M., Berger, M. S., Chen, P. & Israel, M. A. 2001. EGFR overexpression and radiation response in glioblastoma multiforme. *International Journal of Radiation Oncology* Biology* Physics,* 51**,** 410-418.

Baselga, J. 2002. Why the epidermal growth factor receptor? The rationale for cancer therapy. *The Oncologist,* 7**,** 2-8.

Bousarghin, L., Touzé, A., Sizaret, P.-Y. & Coursaget, P. 2003. Human papillomavirus types 16, 31, and 58 use different endocytosis pathways to enter cells. *Journal of virology,* 77**,** 3846-3850.

Carpenter, G. & Cohen, S. 1979. Epidermal growth factor. *Annual review of biochemistry,* 48**,** 193-216.

Chan, W. C. 2007. *Bio-applications of Nanoparticles,* Springer.

Chang, J.-L., Tsao, Y.-P., Liu, D.-W., Huang, S.-J., Lee, W. & Chen, S.-L. 2001. The expression of HPV-16 E5 protein in squamous neoplastic changes in the uterine cervix. *Journal of biomedical science,* 8**,** 206-213.

Chaturvedi, A. K., Engels, E. A., Pfeiffer, R. M., Hernandez, B. Y., Xiao, W., Kim, E., Jiang, B., Goodman, M. T., Sibug-Saber, M., Cozen, W., Liu, L., Lynch, C. F., Wentzensen, N., Jordan, R. C., Altekruse, S., Anderson, W. F., Rosenberg, P. S. & Gillison, M. L. 2011. Human papillomavirus and rising oropharyngeal cancer incidence in the United States. *Journal of Clinical Oncology,* 29**,** 4294-4301.

Chen, Y.-F., Lin, C.-W., Tsao, Y.-P. & Chen, S.-L. 2004. Cytotoxic-T-lymphocyte human papillomavirus type 16 E5 peptide with CpG-oligodeoxynucleotide can eliminate tumor growth in C57BL/6 mice. *Journal of virology,* 78**,** 1333-1343.

Chong, C. R. & Jänne, P. A. 2013. The quest to overcome resistance to EGFR-targeted therapies in cancer. *Nature medicine,* 19**,** 1389-1400.
Ciardiello, F. & Tortora, G. 2008. EGFR antagonists in cancer treatment. *New England Journal of Medicine,* 358**,** 1160-1174.
Collins, S. I., Constandinou-Williams, C., Wen, K., Young, L. S., Roberts, S., Murray, P. G. & Woodman, C. B. 2009. Disruption of the E2 gene is a common and early event in the natural history of cervical human papillomavirus infection: a longitudinal cohort study. *Cancer Research,* 69**,** 3828-3832.
Cricca, M., Venturoli, S., Leo, E., Costa, S., Musiani, M. & Zerbini, M. 2009. Disruption of HPV 16 E1 and E2 genes in precancerous cervical lesions. *Journal of virological methods,* 158**,** 180-183.
Da Silva, D. M., Fausch, S. C., Verbeek, J. S. & Kast, W. M. 2007. Uptake of human papillomavirus virus-like particles by dendritic cells is mediated by Fcγ receptors and contributes to acquisition of T cell immunity. *The Journal of Immunology,* 178**,** 7587-7597.
Danhier, F., Feron, O. & Préat, V. 2010. To exploit the tumor microenvironment: Passive and active tumor targeting of nanocarriers for anti-cancer drug delivery. *Journal of Controlled Release,* 148**,** 135-146.
Delvenne, P., Hubert, P., Jacobs, N., Giannini, S., Havard, L., Renard, I., Saboulard, D. & Boniver, J. 2001. The organotypic culture of HPV-transformed keratinocytes: an effective in vitro model for the development of new immunotherapeutic approaches for mucosal (pre) neoplastic lesions. *Vaccine,* 19**,** 2557-2564.
Denny, L., Kuhn, L., Risi, L., Richart, R. M., Pollack, A., Lorincz, A., Kostecki, F. & Wright Jr, T. C. 2000. Two-stage cervical cancer screening: an alternative for resource-poor settings. *American journal of obstetrics and gynecology,* 183**,** 383-388.
Diaz Jr, L. A., Williams, R. T., Wu, J., Kinde, I., Hecht, J. R., Berlin, J., Allen, B., Bozic, I., Reiter, J. G. & Nowak, M. A. 2012. The molecular evolution of acquired resistance to targeted EGFR blockade in colorectal cancers. *Nature,* 486**,** 537-540.
Downward, J., Parker, P. & Waterfield, M. 1984. Autophosphorylation sites on the epidermal growth factor receptor. *Nature,* 311**,** 483-485.
Drummond, D. C., Meyer, O., Hong, K., Kirpotin, D. B. & Papahadjopoulos, D. 1999. Optimizing liposomes for delivery of chemotherapeutic agents to solid tumors. *Pharmacological reviews,* 51**,** 691-744.
Elhissi, A., Ahmed, W., Hassan, I. U., Dhanak, V. R. & D'Emanuele, A. 2011. Carbon nanotubes in cancer therapy and drug delivery. *Journal of drug delivery,* 2012.
Erjala, K., Sundvall, M., Junttila, T. T., Zhang, N., Savisalo, M., Mali, P., Kulmala, J., Pulkkinen, J., Grenman, R. & Elenius, K. 2006. Signaling via ErbB2 and ErbB3 associates with resistance and epidermal growth factor receptor (EGFR) amplification with sensitivity to EGFR inhibitor gefitinib in head and neck squamous cell carcinoma cells. *Clinical Cancer Research,* 12**,** 4103-4111.
Fan, X., Jiao, G., Zhao, W., Jin, P. & Li, X. 2013. Magnetic Fe 3 O 4–graphene composites as targeted drug nanocarriers for pH-activated release. *Nanoscale,* 5**,** 1143-1152.
Fattal, E., Rojas, J., Roblot-Treupel, L., Andremont, A. & Couvreur, P. 1991. Ampicillin-loaded liposomes and nanoparticles: comparison of drug loading, drug release and in vitro antimicrobial activity. *Journal of microencapsulation,* 8**,** 29-36.

Finnen, R. L., Erickson, K. D., Chen, X. S. & Garcea, R. L. 2003. Interactions between papillomavirus L1 and L2 capsid proteins. *Journal of virology,* 77**,** 4818-4826.
Flehinger, B., Kimmel, M. & Melamed, M. 1992. The effect of surgical treatment on survival from early lung cancer. Implications for screening. *CHEST Journal,* 101**,** 1013-1018.
Geim, A. K. & Novoselov, K. S. 2007. The rise of graphene. *Nature materials,* 6**,** 183-191.
Ghoreschi, K., Laurence, A. & O'Shea, J. J. 2009. Selectivity and therapeutic inhibition of kinases: to be or not to be? *Nature immunology,* 10**,** 356-360.
Gillies, E. R. & Frechet, J. M. 2005. Dendrimers and dendritic polymers in drug delivery. *Drug discovery today,* 10**,** 35-43.
Gombotz, W. R. & Pettit, D. K. 1995. Biodegradable polymers for protein and peptide drug delivery. *Bioconjugate chemistry,* 6**,** 332-351.
Haley, B. & Frenkel, E. Nanoparticles for drug delivery in cancer treatment. Urologic Oncology: Seminars and original investigations, 2008. Elsevier, 57-64.
Harada, D., Takigawa, N., Ochi, N., Ninomiya, T., Yasugi, M., Kubo, T., Takeda, H., Ichihara, E., Ohashi, K. & Takata, S. 2012. JAK2-related pathway induces acquired erlotinib resistance in lung cancer cells harboring an epidermal growth factor receptor-activating mutation. *Cancer science,* 103**,** 1795-1802.
Haxton, K. J. & Burt, H. M. 2009. Polymeric drug delivery of platinum-based anticancer agents. *Journal of pharmaceutical sciences,* 98**,** 2299-2316.
Heidenreich, A., Bellmunt, J., Bolla, M., Joniau, S., Mason, M., Matveev, V., Mottet, N., Schmid, H.-P., Van der Kwast, T. & Wiegel, T. 2011. EAU guidelines on prostate cancer. Part 1: screening, diagnosis, and treatment of clinically localised disease. *European urology,* 59**,** 61-71.
Henriksen, L., Grandal, M. V., Knudsen, S. L. J., Van Deurs, B. & Grøvdal, L. M. 2013. Internalization mechanisms of the epidermal growth factor receptor after activation with different ligands. *PloS one,* 8**,** e58148.
Hinohara, K., Kobayashi, S., Kanauchi, H., Shimizu, S., Nishioka, K., Tsuji, E.-I., Tada, K.-I., Umezawa, K., Mori, M. & Ogawa, T. 2012. ErbB receptor tyrosine kinase/NF-κB signaling controls mammosphere formation in human breast cancer. *Proceedings of the National Academy of Sciences,* 109**,** 6584-6589.
Horvath, C. A., Boulet, G. A., Renoux, V. M., Delvenne, P. O. & Bogers, J. 2010. Mechanisms of cell entry by human papillomaviruses: an overview. *Virol J,* 7.
Huang, P., Xu, C., Lin, J., Wang, C., Wang, X., Zhang, C., Zhou, X., Guo, S. & Cui, D. 2011. Folic acid-conjugated graphene oxide loaded with photosensitizers for targeting photodynamic therapy. *Theranostics,* 1**,** 240.
Hutchinson, D. J. & Klein, K. C. 2008. Human papillomavirus disease and vaccines. *American Journal of Health-System Pharmacy,* 65**,** 2105-2112.
Inukai, M., Toyooka, S., Ito, S., Asano, H., Ichihara, S., Soh, J., Suehisa, H., Ouchida, M., Aoe, K. & Aoe, M. 2006. Presence of epidermal growth factor receptor gene T790M mutation as a minor clone in non–small cell lung cancer. *Cancer Research,* 66**,** 7854-7858.
Kik, K., Wasowska-Lukawska, M., Oszczapowicz, I. & Szmigiero, L. 2009. Cytotoxicity and cellular uptake of doxorubicin and its formamidine derivatives in HL60 sensitive and HL60/MX2 resistant cells. *Anticancer research,* 29**,** 1429-1433.
Kim, S. H., Koo, B. S., Kang, S., Park, K., Kim, H., Lee, K. R., Lee, M. J., Kim, J. M., Choi, E. C. & Cho, N. H. 2007. HPV integration begins in the tonsillar crypt and leads to the

alteration of p16, EGFR and c-myc during tumor formation. *International Journal of Cancer*, 120**,** 1418-1425.
Kobayashi, S., Boggon, T. J., Dayaram, T., Jänne, P. A., Kocher, O., Meyerson, M., Johnson, B. E., Eck, M. J., Tenen, D. G. & Halmos, B. 2005. EGFR mutation and resistance of non–small-cell lung cancer to gefitinib. *New England Journal of Medicine*, 352**,** 786-792.
Koch, W. M., Sidransky, D. & Chang, X. 2012. Methylation of death-associated protein kinase is associated with cetuximab and erlotinib resistance. *Cell Cycle*, 11**,** 1656-1663.
Kumar, B., Cordell, K. G., Lee, J. S., Worden, F. P., Prince, M. E., Tran, H. H., Wolf, G. T., Urba, S. G., Chepeha, D. B. & Teknos, T. N. 2008. EGFR, p16, HPV Titer, Bcl-xL and p53, sex, and smoking as indicators of response to therapy and survival in oropharyngeal cancer. *Journal of Clinical Oncology*, 26**,** 3128-3137.
Laurent-Puig, P., Cayre, A., Manceau, G., Buc, E., Bachet, J.-B., Lecomte, T., Rougier, P., Lievre, A., Landi, B. & Boige, V. 2009. Analysis of PTEN, BRAF, and EGFR status in determining benefit from cetuximab therapy in wild-type KRAS metastatic colon cancer. *Journal of Clinical Oncology*, 27**,** 5924-5930.
Lee, K., Lee, A.-Y., Kwon, Y. K. & Kwon, H. 2011. Suppression of HPV E6 and E7 expression by BAF53 depletion in cervical cancer cells. *Biochemical and biophysical research communications*, 412**,** 328-333.
Lin, Y.-M., Valdes-Garcia, A., Han, S.-J., Farmer, D. B., Meric, I., Sun, Y., Wu, Y., Dimitrakopoulos, C., Grill, A. & Avouris, P. 2011. Wafer-scale graphene integrated circuit. *science*, 332**,** 1294-1297.
Liska, D., Chen, C.-T., Bachleitner-Hofmann, T., Christensen, J. G. & Weiser, M. R. 2011. HGF rescues colorectal cancer cells from EGFR inhibition via MET activation. *Clinical Cancer Research*, 17**,** 472-482.
Liu, M., Kono, K. & Fréchet, J. M. 2000. Water-soluble dendritic unimolecular micelles:: Their potential as drug delivery agents. *Journal of Controlled Release*, 65**,** 121-131.
Liu, W., Jackson, B. L., Zhu, J., Miao, C.-Q., Chung, C.-H., Park, Y.-J., Sun, K., Woo, J. & Xie, Y.-H. 2010. Large scale pattern graphene electrode for high performance in transparent organic single crystal field-effect transistors. *ACS nano*, 4**,** 3927-3932.
Makadia, H. K. & Siegel, S. J. 2011. Poly lactic-co-glycolic acid (PLGA) as biodegradable controlled drug delivery carrier. *Polymers*, 3**,** 1377-1397.
Meijer, C. J., Snijders, P. J. & Brule, A. 2000. Screening for cervical cancer: should we test for infection with high-risk HPV? *Canadian Medical Association Journal*, 163**,** 535-538.
Meyers, C., Bromberg-White, J. L., Zhang, J., Kaupas, M. E., Bryan, J. T., Lowe, R. S. & Jansen, K. U. 2002. Infectious virions produced from a human papillomavirus type 18/16 genomic DNA chimera. *Journal of virology*, 76**,** 4723-4733.
Miao, W., Shim, G., Lee, S., Lee, S., Choe, Y. S. & Oh, Y.-K. 2013. Safety and tumor tissue accumulation of pegylated graphene oxide nanosheets for co-delivery of anticancer drug and photosensitizer. *Biomaterials*, 34**,** 3402-3410.
Misale, S., Yaeger, R., Hobor, S., Scala, E., Janakiraman, M., Liska, D., Valtorta, E., Schiavo, R., Buscarino, M. & Siravegna, G. 2012. Emergence of KRAS mutations and acquired resistance to anti-EGFR therapy in colorectal cancer. *Nature*.
Mitsudomi, T. & Yatabe, Y. 2010. Epidermal growth factor receptor in relation to tumor development: EGFR gene and cancer. *FEBS journal*, 277**,** 301-308.
Montagut, C., Dalmases, A., Bellosillo, B., Crespo, M., Pairet, S., Iglesias, M., Salido, M., Gallen, M., Marsters, S. & Tsai, S. P. 2012. Identification of a mutation in the

extracellular domain of the Epidermal Growth Factor Receptor conferring cetuximab resistance in colorectal cancer. *Nature medicine,* 18**,** 221-223.

Muñoz, N., Bosch, F. X., Castellsagué, X., Díaz, M., De Sanjose, S., Hammouda, D., Shah, K. V. & Meijer, C. J. L. M. 2004. Against which human papillomavirus types shall we vaccinate and screen? the international perspective. *International Journal of Cancer,* 111**,** 278-285.

Muto, V., Stellacci, E., Lamberti, A. G., Perrotti, E., Carrabba, A., Matera, G., Sgarbanti, M., Battistini, A., Liberto, M. C. & Focà, A. 2011. Human papillomavirus type 16 E5 protein induces expression of beta interferon through interferon regulatory factor 1 in human keratinocytes. *Journal of virology,* 85**,** 5070-5080.

Ng, K. P., Hillmer, A. M., Chuah, C. T., Juan, W. C., Ko, T. K., Teo, A. S., Ariyaratne, P. N., Takahashi, N., Sawada, K. & Fei, Y. 2012. A common BIM deletion polymorphism mediates intrinsic resistance and inferior responses to tyrosine kinase inhibitors in cancer. *Nature medicine,* 18**,** 521-528.

Nicholson, R., Gee, J. & Harper, M. 2001. EGFR and cancer prognosis. *European Journal of Cancer,* 37**,** 9-15.

Novoselov, K. S., Geim, A. K., Morozov, S., Jiang, D., Zhang, Y., Dubonos, S., Grigorieva, I. & Firsov, A. 2004. Electric field effect in atomically thin carbon films. *science,* 306**,** 666-669.

Oda, K., Matsuoka, Y., Funahashi, A. & Kitano, H. 2005. A comprehensive pathway map of epidermal growth factor receptor signaling. *Molecular systems biology,* 1.

Oerlemans, C., Bult, W., Bos, M., Storm, G., Nijsen, J. F. W. & Hennink, W. E. 2010. Polymeric micelles in anticancer therapy: targeting, imaging and triggered release. *Pharmaceutical research,* 27**,** 2569-2589.

Ohashi, K., Sequist, L. V., Arcila, M. E., Moran, T., Chmielecki, J., Lin, Y.-L., Pan, Y., Wang, L., De Stanchina, E. & Shien, K. 2012. Lung cancers with acquired resistance to EGFR inhibitors occasionally harbor BRAF gene mutations but lack mutations in KRAS, NRAS, or MEK1. *Proceedings of the National Academy of Sciences,* 109**,** E2127-E2133.

Ohgami, M., Otani, Y., Kumai, K., Kubota, T., Kim, Y.-I. & Kitajima, M. 1999. Curative laparoscopic surgery for early gastric cancer: five years experience. *World journal of surgery,* 23**,** 187-193.

Paik, S., Bryant, J., Tan-Chiu, E., Yothers, G., Park, C., Wickerham, D. L. & Wolmark, N. 2000. HER2 and choice of adjuvant chemotherapy for invasive breast cancer: National Surgical Adjuvant Breast and Bowel Project Protocol B-15. *Journal of the National Cancer Institute,* 92**,** 1991-1998.

Paratala, B. S., Jacobson, B. D., Kanakia, S., Francis, L. D. & Sitharaman, B. 2012. Physicochemical characterization, and relaxometry studies of micro-graphite oxide, graphene nanoplatelets, and nanoribbons. *PloS one,* 7**,** e38185.

Parkin, D. M. 2006. The global health burden of infection-associated cancers in the year 2002. *International Journal of Cancer,* 118**,** 3030-3044.

Rana, V. K., Choi, M. C., Kong, J. Y., Kim, G. Y., Kim, M. J., Kim, S. H., Mishra, S., Singh, R. P. & Ha, C. S. 2011. Synthesis and Drug-Delivery Behavior of Chitosan-Functionalized Graphene Oxide Hybrid Nanosheets. *Macromolecular Materials and Engineering,* 296**,** 131-140.

Recht, A., Come, S. E., Henderson, I. C., Gelman, R. S., Silver, B., Hayes, D. F., Shulman, L. N. & Harris, J. R. 1996. The sequencing of chemotherapy and radiation therapy after

conservative surgery for early-stage breast cancer. *New England Journal of Medicine,* 334**,** 1356-1361.
Ren, Y., Wong, S. M. & Lim, L. Y. 2010. Application of plant viruses as nano drug delivery systems. *Pharmaceutical research,* 27**,** 2509-2513.
Rimawi, M. F., Shetty, P. B., Weiss, H. L., Schiff, R., Osborne, C. K., Chamness, G. C. & Elledge, R. M. 2010. Epidermal growth factor receptor expression in breast cancer association with biologic phenotype and clinical outcomes. *Cancer,* 116**,** 1234-1242.
Rommel, O., Dillner, J., Fligge, C., Bergsdorf, C., Wang, X., Selinka, H. C. & Sapp, M. 2005. Heparan sulfate proteoglycans interact exclusively with conformationally intact HPV L1 assemblies: Basis for a virus-like particle ELISA. *Journal of medical virology,* 75**,** 114-121.
Roth, J. A., Fossella, F., Komaki, R., Ryan, M. B., Putnam, J., Lee, J. S., Dhingra, H., De Caro, L., Chasen, M. & McGavran, M. 1994. A randomized trial comparing perioperative chemotherapy and surgery with surgery alone in resectable stage IIIA non-small-cell lung cancer. *Journal of the National Cancer Institute,* 86**,** 673-680.
Rusch, V., Klimstra, D., Venkatraman, E., Pisters, P., Langenfeld, J. & Dmitrovsky, E. 1997. Overexpression of the epidermal growth factor receptor and its ligand transforming growth factor alpha is frequent in resectable non-small cell lung cancer but does not predict tumor progression. *Clinical Cancer Research,* 3**,** 515-522.
Rush, J. S., Quinalty, L. M., Engelman, L., Sherry, D. M. & Ceresa, B. P. 2012. Endosomal accumulation of the activated epidermal growth factor receptor (EGFR) induces apoptosis. *Journal of Biological Chemistry,* 287**,** 712-722.
Samama, B., Plas-Roser, S., Schaeffer, C., Chateau, D., Fabre, M. & Boehm, N. 2002. HPV DNA detection by in situ hybridization with catalyzed signal amplification on thin-layer cervical smears. *Journal of Histochemistry & Cytochemistry,* 50**,** 1417-1420.
Sant, M., Allemani, C., Santaquilani, M., Knijn, A., Marchesi, F. & Capocaccia, R. 2009. EUROCARE-4. Survival of cancer patients diagnosed in 1995–1999. Results and commentary. *European Journal of Cancer,* 45**,** 931-991.
Sartore-Bianchi, A., Di Nicolantonio, F., Nichelatti, M., Molinari, F., De Dosso, S., Saletti, P., Martini, M., Cipani, T., Marrapese, G. & Mazzucchelli, L. 2009. Multi-determinants analysis of molecular alterations for predicting clinical benefit to EGFR-targeted monoclonal antibodies in colorectal cancer. *PloS one,* 4**,** e7287.
Schedin, F., Geim, A., Morozov, S., Hill, E., Blake, P., Katsnelson, M. & Novoselov, K. 2007. Detection of individual gas molecules adsorbed on graphene. *Nature materials,* 6**,** 652-655.
Schiffman, M., Castle, P. E., Jeronimo, J., Rodriguez, A. C. & Wacholder, S. Human papillomavirus and cervical cancer. *The Lancet,* 370**,** 890-907.
Schiffman, M., Castle, P. E., Jeronimo, J., Rodriguez, A. C. & Wacholder, S. 2007. Human papillomavirus and cervical cancer. *The Lancet,* 370**,** 890-907.
Shah, J. P. & Lydiatt, W. 1995. Treatment of cancer of the head and neck. *CA: a cancer journal for clinicians,* 45**,** 352-368.
Sigismund, S., Algisi, V., Nappo, G., Conte, A., Pascolutti, R., Cuomo, A., Bonaldi, T., Argenzio, E., Verhoef, L. G. & Maspero, E. 2013. Threshold-controlled ubiquitination of the EGFR directs receptor fate. *The EMBO journal,* 32**,** 2140-2157.
Smith, I., Rosenblatt, E., Sanguineti, G., Bishop, J. A., Richmon, J. D. & Pai, S. 2011. Extracapsular Extension in Lymph Node Metastasis from HPV-Associated Squamous

Cell Carcinoma of the Oropharynx. *Otolaryngology--Head and Neck Surgery,* 145**,** P65-P66.
Sordan, R., Traversi, F. & Russo, V. 2009. Logic gates with a single graphene transistor. *Applied Physics Letters,* 94**,** 073305.
Sun, X., Liu, Z., Welsher, K., Robinson, J. T., Goodwin, A., Zaric, S. & Dai, H. 2008. Nano-graphene oxide for cellular imaging and drug delivery. *Nano research,* 1**,** 203-212.
Suter, T. & Meier, B. 2002. Detection of anthracycline-induced cardiotoxicity: is there light at the end of the tunnel? *Annals of Oncology,* 13**,** 647-649.
Tang, X., Shigematsu, H., Bekele, B. N., Roth, J. A., Minna, J. D., Hong, W. K., Gazdar, A. F. & Wistuba, I. I. 2005. EGFR tyrosine kinase domain mutations are detected in histologically normal respiratory epithelium in lung cancer patients. *Cancer Research,* 65**,** 7568-7572.
Tsai, T.-C. & Chen, S.-L. 2003. The biochemical and biological functions of human papillomavirus type 16 E5 protein. *Archives of virology,* 148**,** 1445-1453.
Van Os, R., Robinson, S., Sheridan, T., Mislow, J. M., Dawes, D. & Mauch, P. M. 1998. Granulocyte colony-stimulating factor enhances bone marrow stem cell damage caused by repeated administration of cytotoxic agents. *Blood,* 92**,** 1950-1956.
Voldborg, B. R., Damstrup, L., Spang-Thomsen, M. & Poulsen, H. S. 1997. Epidermal growth factor receptor (EGFR) and EGFR mutations, function and possible role in clinical trials. *Annals of Oncology,* 8**,** 1197-1206.
Wang, C.-C., Lai, C.-H., Huang, Y.-T., Chao, A., Chou, H.-H. & Hong, J.-H. 2012. HPV genotypes predict survival benefits from concurrent chemotherapy and radiation therapy in advanced squamous cell carcinoma of the cervix. *International Journal of Radiation Oncology* Biology* Physics,* 84**,** e499-e506.
Wang, S. E., Narasanna, A., Perez-Torres, M., Xiang, B., Wu, F. Y., Yang, S., Carpenter, G., Gazdar, A. F., Muthuswamy, S. K. & Arteaga, C. L. 2006. HER2 kinase domain mutation results in constitutive phosphorylation and activation of HER2 and EGFR and resistance to EGFR tyrosine kinase inhibitors. *Cancer cell,* 10**,** 25-38.
Wang, Y., Pennock, S., Chen, X. & Wang, Z. 2002. Endosomal signaling of epidermal growth factor receptor stimulates signal transduction pathways leading to cell survival. *Molecular and cellular biology,* 22**,** 7279-7290.
Watson, M., Saraiya, M., Ahmed, F., Cardinez, C. J., Reichman, M. E., Weir, H. K. & Richards, T. B. 2008. Using population-based cancer registry data to assess the burden of human papillomavirus-associated cancers in the United States: Overview of methods. *Cancer,* 113**,** 2841-2854.
Woodburn, J. 1999. The epidermal growth factor receptor and its inhibition in cancer therapy. *Pharmacology & therapeutics,* 82**,** 241-250.
Worden, F. P., Kumar, B., Lee, J. S., Wolf, G. T., Cordell, K. G., Taylor, J. M., Urba, S. G., Eisbruch, A., Teknos, T. N. & Chepeha, D. B. 2008. Chemoselection as a strategy for organ preservation in advanced oropharynx cancer: response and survival positively associated with HPV16 copy number. *Journal of Clinical Oncology,* 26**,** 3138-3146.
Wu, J.-Y., Yu, C.-J., Chang, Y.-C., Yang, C.-H., Shih, J.-Y. & Yang, P.-C. 2011. Effectiveness of Tyrosine Kinase Inhibitors on "Uncommon" Epidermal Growth Factor Receptor Mutations of Unknown Clinical Significance in Non–Small Cell Lung Cancer. *Clinical Cancer Research,* 17**,** 3812-3821.

Yang, K., Zhang, S., Zhang, G., Sun, X., Lee, S.-T. & Liu, Z. 2010. Graphene in mice: ultrahigh in vivo tumor uptake and efficient photothermal therapy. *Nano letters,* 10**,** 3318-3323.

Yang, X., Wang, Y., Huang, X., Ma, Y., Huang, Y., Yang, R., Duan, H. & Chen, Y. 2011. Multi-functionalized graphene oxide based anticancer drug-carrier with dual-targeting function and pH-sensitivity. *Journal of materials chemistry,* 21**,** 3448-3454.

Yang, X., Zhang, X., Ma, Y., Huang, Y., Wang, Y. & Chen, Y. 2009. Superparamagnetic graphene oxide–Fe 3 O 4 nanoparticles hybrid for controlled targeted drug carriers. *Journal of materials chemistry,* 19**,** 2710-2714.

Yarden, Y. & Schlessinger, J. 1987. Epidermal growth factor induces rapid, reversible aggregation of the purified epidermal growth factor receptor. *Biochemistry,* 26**,** 1443-1451.

Yeh, E. T., Tong, A. T., Lenihan, D. J., Yusuf, S. W., Swafford, J., Champion, C., Durand, J.-B., Gibbs, H., Zafarmand, A. A. & Ewer, M. S. 2004. Cardiovascular complications of cancer therapy diagnosis, pathogenesis, and management. *Circulation,* 109**,** 3122-3131.

Yim, E.-K. & Park, J.-S. 2005. The Role of HPV E6 and E7 Oncoproteins in HPV-associated Cervical Carcinogenesis. *Cancer Res Treat,* 37**,** 319-324.

Yue, Z., Lv, P., Yue, H., Gao, Y., Ma, D., Wei, W. & Ma, G. 2013. Inducible graphene oxide probe for high-specific tumor diagnosis. *Chem. Commun.,* 49**,** 3902-3904.

Zakharian, T. Y., Seryshev, A., Sitharaman, B., Gilbert, B. E., Knight, V. & Wilson, L. J. 2005. A fullerene-paclitaxel chemotherapeutic: synthesis, characterization, and study of biological activity in tissue culture. *Journal of the American Chemical Society,* 127**,** 12508-12509.

Zhang, L., Xia, J., Zhao, Q., Liu, L. & Zhang, Z. 2010. Functional graphene oxide as a nanocarrier for controlled loading and targeted delivery of mixed anticancer drugs. *Small,* 6**,** 537-544.

Zhao, K.-N., Sun, X.-Y., Frazer, I. H. & Zhou, J. 1998. DNA packaging by L1 and L2 capsid proteins of bovine papillomavirus type 1. *Virology,* 243**,** 482-491.

1.10 Figures

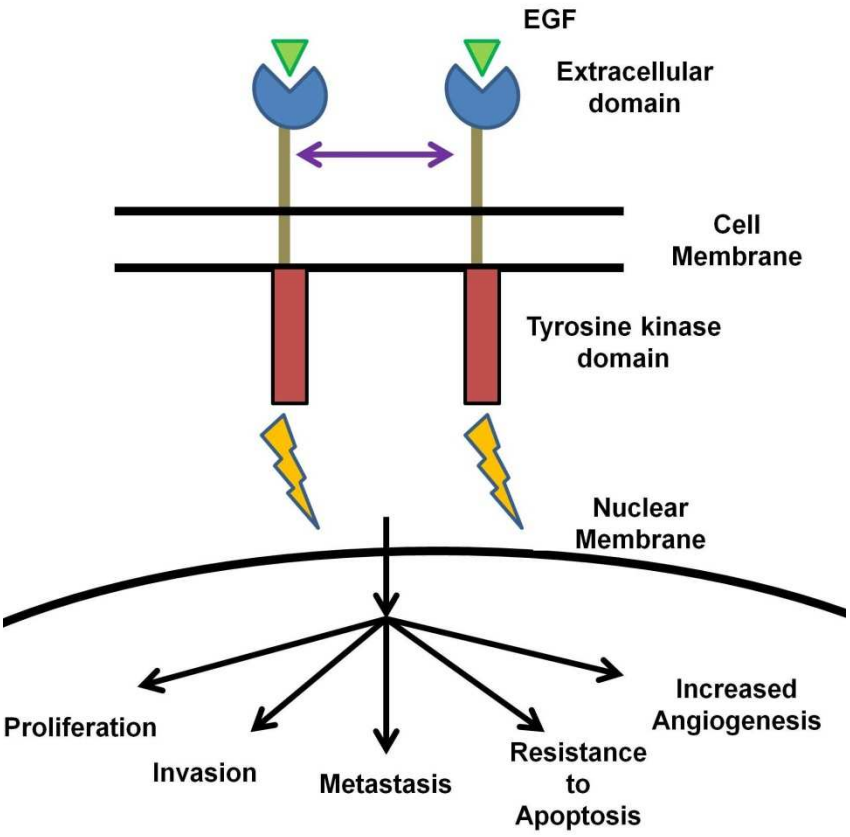

Figure 1 Schematic representation of EGF receptor activation and its associated growth related effects

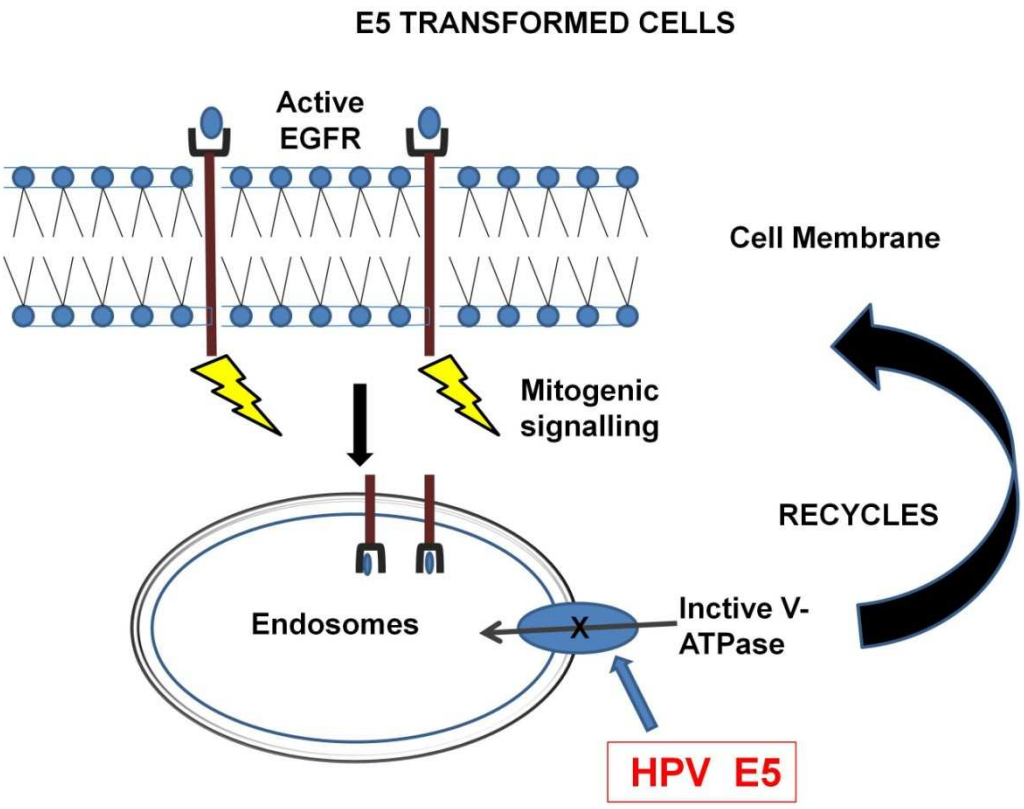

Figure 2 Schematic representation of EGFR recycling in HPV infected cells

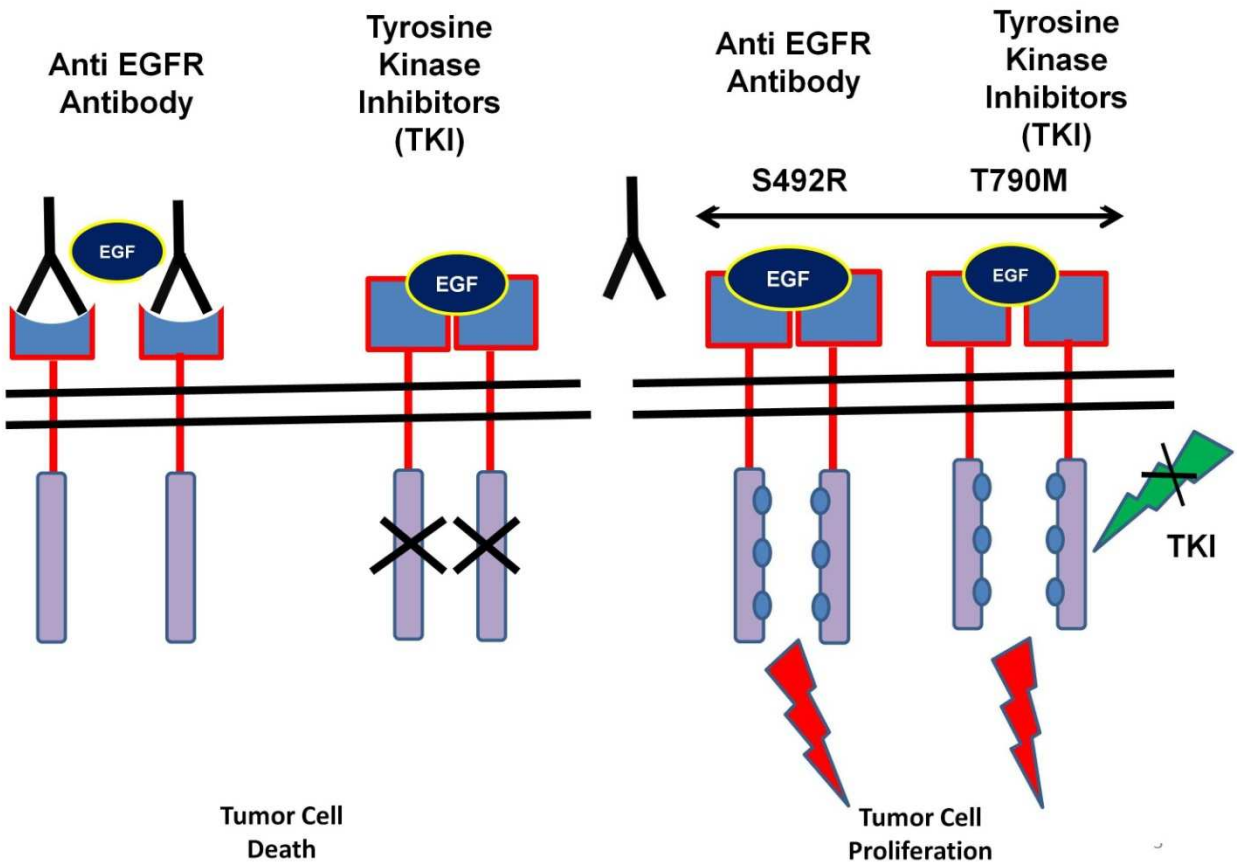

Figure 3 Schematic representation of resistance due to T790M mutation in anti EGFR treated and tyrosine kinase inhibitor treated cells.

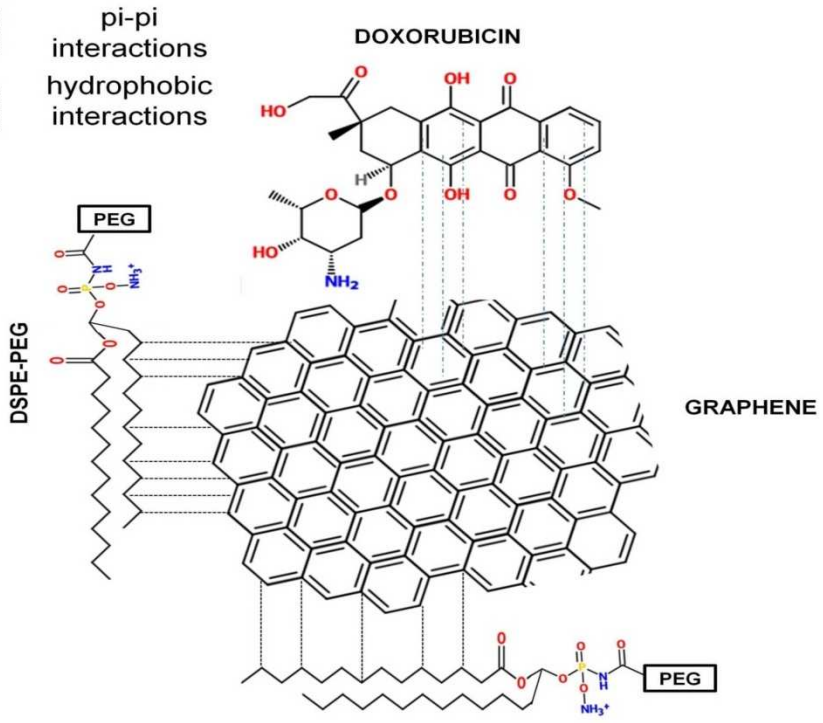

Figure 4 Loading of aromatic and hydrophobic moieties onto graphene using pi stacking and hydrophobic interactions.

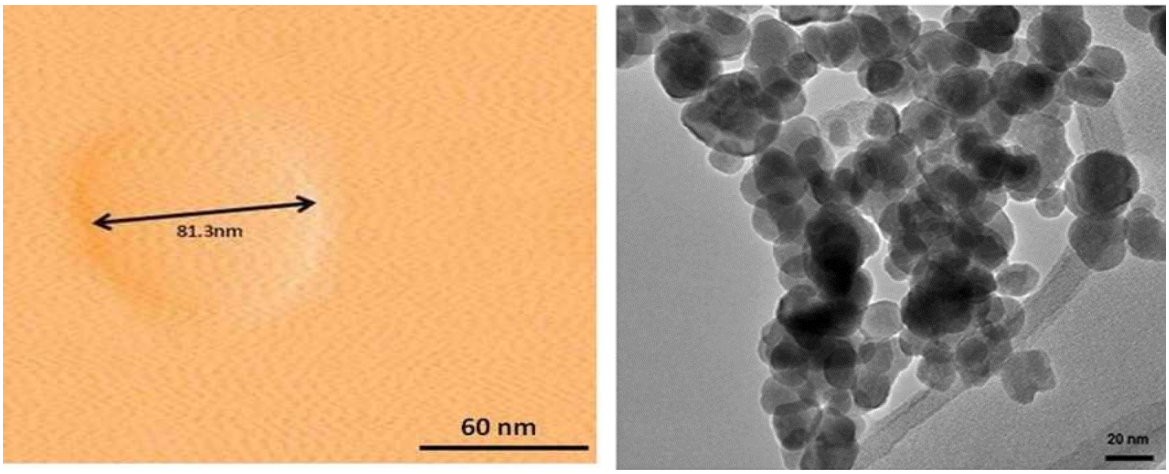

Figure 5 Atomic Force Microscopy (left image) and Transmission electron microscopy (right image) images of graphene nanoparticles synthesized from oxidation and exfoliation of graphite and intercalated with Mn^{2+} ions. (Images from Paratala et al 2012 and Mullick Chowdhury et al 2013)

Chapter 2

GRAPHENE NANORIBBONS AND THEIR *IN –VITRO* TOXICITY

Preface

Portions of this chapter have been reproduced from

Mullick Chowdhury S, Lalwani G, Zhang K, Yang JY, Neville K, Sitharaman B. Cell specific cytotoxicity and uptake of graphene nanoribbons. Biomaterials. 2013;34:283-93 with permission from Elsevier publishing group.

The authors listed in the above manucript have contributions towards the data reported in this chapter.

2.1 Introduction

Graphene, a two-dimensional (2-D) carbon nanostructure, has attracted a great deal of attention due to its unique nanoscopic properties, and has shown potential for various material, and biomedical science applications (Novoselov et al., 2004, Liu et al., 2010, Schedin et al., 2007, Lin et al., 2011, Sordan et al., 2009, Sun et al., 2008, Huang P, 2011, Yang et al., 2009, Paratala et al., 2012). Recent reports predict that graphene might overtake carbon nanotubes in commercial applications(Geim and Novoselov, 2007). Evaluation of the cyto- and bio-compatibility is necessary to develop graphene nanomaterial for *in vitro* or *in vivo* biomedical applications. Additionally, in the future, use of these materials for a wide range of commercial materials science applications will increase the possibility of their release into the environment.

Compared to carbon nanostructures such as fullerenes (Nakamura and Isobe, 2003), metallofullerenes (Sitharaman and Wilson, 2007) and carbon nanotubes (Lacerda et al., 2006, Liu et al., 2009b), few reports are available on the toxicity of graphene *in vitro* (Singh et al., 2011, Sasidharan et al., 2011, Chang et al., 2011), and *in vivo* (Yang et al., 2010, Wang et al., 2011). Solution-based techniques based on the modified Hummer's method (chemical oxidation of graphite followed by ultrasonic cleavage) have been used in the synthesis of graphene nanoparticles for these toxicity studies, as they allow preparation of graphene in macroscopic amounts necessary for these studies and eventual applications (Hummers and Offeman, 1958). Recently, Kosynkin, Tour, and co-workers have pioneered an oxidative method that allows the synthesis of graphene nanoparticles in macroscopic amounts by the longitudinal unzipping of multi walled carbon nanotubes (Kosynkin et al., 2009). These nanoparticles referred as graphene nanoribbons may also be suitable for a variety of biomedical applications provided they are cyto-

, and bio-compatible. In this chapter, I assess, and evaluate the cytotoxicity of oxidized-graphene nanoribbons (O-GNRs) water-solubilized with the amphiphilic polymer PEG-DSPE (hereafter referred to as O-GNR-PEG-DSPE) at various concentrations (0-400µg/ml) and time points (24-72 hours) in four different cell lines (HeLa, MCF7, SKBR, NIH3T3).

2.2 Materials and Methods

2.2.1 Synthesis of oxidized graphene nanoribbons formulations:

O-GNRs were synthesized from multi walled carbon nanotubes (Sigma Aldrich, New York) using a slight modification (centrifugation was used for purification rather than filtration) of the previously reported procedure (Kosynkin et al., 2009). Briefly, multi walled carbon nanotubes (MWCNTs) (150 mg) were suspended in 30ml of concentrated sulphuric acid (H_2SO_4) for 2-4 hours. Potassium permanganate ($KMnO_4$, 750mg, 4.75 mmol) was added, and the mixture was stirred for 1 hour. The reaction was heated at 55-70^oC in an oil bath for an additional 1 hour until completion, cooled to room temperature, and washed with dilute aqueous hydrochloric acid. Ethanol and ether were added for flocculation, and the product was isolated by centrifugation at 3000 rpm for 30 minutes. The sample was then dried overnight in a vacuum oven.

Dried O-GNR samples were weighed, and dispersed in 2ml of PEG-DSPE(1,2-distearoyl-*sn*-glycero-3-phosphoethanolamine-N-[amino(polyethylene glycol)]) solution (best dispersion was achieved using 1.2 mg/ml of PEG-DSPE), or DI water to obtain the different concentrations. The dispersions were first bath sonicated (Ultrasonicator FS30H, Fischer Scientific,Pittsburgh, PA) for 15 minutes followed by probe sonication for 180 seconds (2 seconds on and 1 second off cycle, 20% amplitude, Cole Parmer Ultrasonicator LPX 750) to ensure homogenous O-GNR

suspensions. Freshly-prepared O-GNR-PEG-DSPE formulations were used for all the cell studies.

2.2.2 Raman Spectroscopy

Raman spectra of O-GNRs was obtained using an Enwave Pro Raman-L Spectrophotometer equipped with a CCD detector, and a 532 nm laser, at 20% of maximum laser strength (500mW). Samples were prepared by dissolving 10µg of O-GNRs in 1 ml of PEG-DSPE solution (containing 1.2 mg of PEG-DPSE). The Raman spectra of PEG-DSPE solution was used as the baseline.

2.2.3 Sample preparation for Transmission Electron Microscopy

Samples for high resolution transmission electron microscopy (HRTEM) were prepared by dispersing the O-GNR in 1:1 mixture of water/ethanol by probe sonication for 1 min (Cole Parmer Ultrasonicator LPX 750) followed by ultracentrifugation at 5000 rpm for 5 mins. The supernatant was dropped onto 300 mesh size, holey lacey carbon grids on a copper support (Ted Pella, Inc., Redding, CA). HRTEM was performed using JOEL 2100F high-resolution analytical TEM (Center for Functional Nanomaterials, Brookhaven National Laboratory) at an accelerating voltage of 200kV.

2.2.4 Cell Culture

Four different cell lines Henrietta Lacks cells (HeLa) derived from cervical cancer, National Institute of Health 3T3(NIH-3T3) mouse fibroblast cells, Sloan Kettering breast cancer cells (SKBR3) and Michigan cancer foundation-7 breast cancer cells (MCF7) were used in the

experiments. All cell lines were obtained from ATCC (Manassas, VA, USA). HeLa cells and NIH-3T3 mouse fibroblasts were grown in DMEM medium, SKBR3 cells were grown in McCoy's medium and MCF7 cells were grown in RPMI 1600 medium. All the media were supplemented with 10% fetal bovine serum and 1 % penicillin-streptomycin. Cells were incubated at 37^{o}C in a humidified atmosphere of 5% CO_2, and 95% air.

2.2.5 Alamar Blue Assay

Cell viability in terms of mitochondrial integrity, and overall cellular metabolism was measured by alamar blue assay (Invitrogen, Grand Island, NY). Cells from the three different cell lines (SKBR3, MCF7 and HeLa) were plated at 5 x 10^3 cells per well in 96 well plates, and incubated for 18 hours. Before commencing with the assay, old media was replaced with 200µl of fresh media in each well. 50µl of O-GNR PEG-DSPE stock solutions at various concentrations were added to every well for a final treatment concentration of 10µg/ml, 50µg/ml, 100µg/ml, 200µg/ml, 300µg/ml and 400µg/ml. The cells were incubated at 37^{o}C for 24, and 48 hours. After each time point, the media was removed, and wells were rinsed twice with Dulbecco's phosphate buffer saline (DPBS) before adding 100µl of fresh media, and 10µl of Alamar Blue reagent. The plates were again incubated for 2 hours at 37^{o}C. Fluorescence readings of the wells were recorded by Cytofluor fluorescence multiwell plate reader (Series H4000 PerSeptive Biosystems, Framingham, MA) with excitation at 530 nm, and emission at 580 nm. Fluorescence reading for cells in the culture medium containing only PEG-DSPE was used for baseline correction. The cell viability in terms of % of control cells is expressed as the percentage of $(F_{test} - F_{blank})/(F_{control} - F_{blank})$,where F_{test} is the fluorescence of the cells exposed to nanoribbon sample, $F_{control}$ is the

fluorescence of the unexposed control sample and F_{blank} is the fluorescence of the wells without any cells.

2.2.6 Neutral Red Assay

Cell viability in terms of lysosomal integrity was measured by neutral red assay (Sigma-Aldrich, New York). SKBR3, MCF7 and HeLa cells were plated at 5 x 10^3 cells per well in 96 well cell culture plates, and incubated for 18 hours. Next, the cell culture media from each well was removed, and replaced with 200 µl of fresh media. Similar to the Alamar Blue assay, 50µl of O-GNR-PEG-DSPE stock solutions at various concentrations were added to every well for a final treatment concentration of 10µg/ml, 50µg/ml, 100µg/ml, 200µg/ml, 300µg/ml, and 400µg/ml. The cells were incubated at 37^{o}C for 24 and 48 hours. After each time point, the media was removed, and the wells were rinsed multiple times with DPBS. After the DPBS washes, 100µl of fresh media was added to each well along with 10 µl of neutral red reagent (0.33% in DPBS), followed by incubation for 2 hours at 37^{o}C. The neutral red reagent was removed, and cells were treated with 100µl of Neutral red assay fixative for 1 min followed by 100µl of Neutral Red assay solubilization reagent. Absorbance of culture media containing O-GNR-PEG-DSPE at 490nm was used for baseline correction in all the groups. Absorbance readings of the plates were taken in a BIOTEK ELx 800 absorbance micro plate reader at 490 nm. Cell viability in terms of % of control cells is expressed as $(OD_{test} - OD_{blank})/(OD_{control} - OD_{blank})$, where OD_{test} is the optical density of the cells exposed to nanoribbon sample, $OD_{control}$ is the optical density of the control sample, and OD_{blank} is the optical density of the wells without any cells.

2.2.7 Trypan Blue Assay

Cell mortality of SKBR3, MCF7 and HeLa cells was investigated by trypan blue assay. All the 3 cell lines were plated in 6-well culture plates at a concentration of 10^6 cells per well, and incubated for 18 hours prior to media change, and O-GNR-PEG-DSPE treatment. The wells were incubated with O-GNR-PEG-DSPE solutions at concentrations of 10µg/ml, 50µg/ml, 100µg/ml, 200µg/ml, 300µg/ml, and 400µg/ml for 12 hours. Next, the cells were trypsinized using with 300 µl trypsin–EDTA solution. The supernatant was mixed with trypsin detached cells, and centrifuged at 1500 rpm for 3 minutes. 1ml of trypan blue reagent was added to the pellet, and the cells were counted using a hemocytometer. Cell mortality (%) was expressed as the percentage of dead cells out of the total number of cells. Cells cultured in the absence of O-GNR-PEG-DSPE served as control. Mortality of cells in the presence of DSPE-PEG was also tested.

2.2.8 Lactate Dehydrogenase Assay

Membrane integrity of cells exposed to O-GNR-PEG-DSPE was evaluated by lactate dehydrogenase assay (LDH) Kit (Sigma-Aldrich, New York). SKBR3, MCF7 and HeLa cells were plated at a density of 5 x 10^3 cells per well in 96 well cell culture plates, and incubated for 18 hours. Post media changes, and treatments of the cells at O-GNR-PEG-DSPE concentrations (10-400µg/ml similar to the previous assays, the cells were incubated at 37^{o}C for 24, 48, and 72 hours). After each time point, media was collected from individual wells, and centrifuged at 1200 rpm for 5 minutes. 50µl of the media supernatant was added to a fresh 96 well plate along with LDH assay reagent, and incubated for 45 minutes. The absorbance values were recorded at 490 nm. Positive control was prepared by adding 10 µl of lysis solution to the control cells, 45

min before centrifugation. The LDH leakage (% of positive control) is expressed as the percentage of $(OD_{test} - OD_{blank})/(OD_{positive} - OD_{blank})$, where OD_{test} is the optical density of the control cells, or cells exposed to O-GNR-PEG-DSPE, $OD_{positive}$ is the optical density of the positive control cells, and OD_{blank} is the optical density of the wells without cells. Absorbance of culture media containing PEG-DSPE was used for baseline correction in all the groups.

2.2.9 Clonogenic assay

Cell division and colony forming capacity of the cells exposed to the O-GNR-PEG-DSPE formulations were evaluated using clonogenic assay. HeLa and MCF7 cells were plated at a density of 50 cells per well in 6 well plates. After 18 hours of incubation, old media was removed, and 1.6 ml of fresh media along with 400µl of various O-GNR-PEG-DSPE stock solutions was added to yield final treatment concentrations of 1µg/ml, 10µg/ml and 30µg/ml. The cells were incubated at 37^{o}C for 7 days, and media was changed every 2 days. Post incubation, the culture media was removed, cells were subjected to multiple DPBS washes, and fixed using ice cold methanol. Cell colonies were viewed, and imaged by a bright-field microscope (Axiovision 4.0, Zeiss, Germany). Cells cultured without O-GNR-PEG-DSPE or with PEG-DSPE served as the controls.

Image processing toolbox in MATLAB was used to quantify the sizes of each of the colonies obtained after O-GNR-PEG-DSPE treatment. Briefly, bright field images were subjected to a series of image processing steps such as thresholding, edge detection, contrast enhancement, median filtering, erosion, and dilation followed by quantification of the region properties. Colony area, computed using image processing (square pixels) was converted to μm^2 based on

the pixel area, scale and magnification of the bright-field images. Multiple colonies were analyzed for every O-GNR-PEG-DSPE treatment group

2.2.10 Live Cell Assay

The toxicity of O-GNR-PEG-DSPE on HeLa and NIH 3T3 cells was assessed by a LIVE cell assay using Calcein-AM fluorescence as the indicator for live cells. NIH 3T3 and HeLa cells were plated at a density of 5 x 10^3 cells per well in 96 well cell culture plates for 15 hours, were subjected to media changes, and treated with the O-GNR-PEG-DSPE at concentrations between 10-250µg/ml.. The cells were incubated at 37^{o}C for 24 hours in the presence of the O-GNR-PEG-DSPEs. Next, the cell culture media was removed, and the wells were subjected to multiple DPBS washes. 100µl of Calcein AM (2µM) was added to each well, and incubated at 37^{o}C for 1 hour. Fluorescence readings of the plates were recorded using Cytofluor fluorescence multiwell plate reader (PerSeptive Biosystems, Framingham, MA) at excitation, and emission wavelengths of 485 and 530 nm, respectively. Cells lysed by treatment with lysis solution served as the negative control (F_{min}). Cell without O-GNR-PEG-DSPE treatment served as positive control ($F_{max)}$. The percentage of viable cells was calculated as (F_{sample} -F_{min})/ (F_{max} - F_{min}) x 100.

2.2.11 TEM of cells incubated with the O-GNR-PEG-DSPE formulations

Six well plates with surfaces covered with ACLAR® film (Electron Microscopy Sciences, Hatford, PA) were plated with cells at a density of 5x 10^5 cells per plate, and exposed to O-GNR-PEG-DSPE for 3 hours. At the end of three hours, cells were fixed with 2.5% electron microscopy grade glutaraldehyde (Electron Microscopy Sciences, Hatford, PA) in 0.1 M PBS.

After fixation, the films containing fixed cells were placed in 2% osmium tetroxide in 0.1 M PBS, dehydrated through graded ethanol washes, and embedded in durcupan resin (Sigma-Aldrich, St. Louis, USA). Areas with high cell densities were blocked, cut into 80 nm ultra-thin sections using an Ultracut E microtome (Reichert-Jung, Cambridge, UK), and placed on formvar-coated copper grids. The sections were then viewed with a Tecnai Bio Twin G transmission electron microscope (FEI, Hillsboro, OR), at 80 kV. Digital images were acquired using an XR-60 CCD digital camera system. (AMT, Woburn, MA). 12 cells per treatment condition were analyzed.

2.2.12 Cell Attachment

The effect of O-GNR-PEG-DSPE on the attachment of cells was tested by incubating HeLa, MCF7, and SKBR3 cells with 10µg/ml of nanoparticles for 48 hours, and comparing the remaining number of cells to that of the untreated control (Figure 11).

MCF7, HeLa, or SKBR3 cells were plated at 25 x 10^4 cells per plate in 10 cm plates, and incubated for 24 hours. 1 ml of O-GNR PEG-DSPE stock solution was added to each plate for a final treatment concentration of 10µg/ml. The plates were incubated for 48 hours, after which the cell media was removed, the plate were washed multiple times with DPBS. The cells were then trypsinized, and their number counted using a hemocytometer.

2.2.13 ROS generation

The production of reactive oxygen species (ROS) in normal cells is greatly increased when they are under stress. ROS generation in HeLa cells, and MCF7 cells treated with 20µg/ml, and 40 µg/ml O-GNR-PEG-DSPE were quantified using 2', 7'-dichlorofluorescin diacetate (Sigma

Aldrich) (Figure 12). 2', 7'-dichlorofluorescin diacetate is cell permeable, and oxidized in the presence of ROS to produce green fluorescence. The fluorescence intensity is directly proportional to the amount of ROS produced.

MCF7 or HeLa cells were plated at 25 x 10^3 cells per well in 96 well plates, and incubated for 18 hours. Before commencing with the assay, old media was replaced with 200 µl of a 20 µM working solution of 2', 7'-dichlorofluorescin diacetate in each well, and incubated for 45 minutes. Next, this solution was replaced by 200 µl of DPBS (containing 10% FBS) followed by addition of 50 µl of O-GNR PEG-DSPE stock solutions to each well for final treatment concentrations of 20µg/ml, or 40µg/ml. The O-GNR PEG-DSPE concentrations were incubated for 2 hours, and then aspirated out. The wells were washed with DPBS, and 200µl of DPBS (with 10% FBS) was added to each well. Fluorescence readings of the wells were recorded by a Cytofluor fluorescence multiwell plate reader (Series H4000 PerSeptive Biosystems, Framingham, MA) with excitation at 485 nm and emission at 530 nm. Fluorescence reading for cells in the culture medium containing only PEG-DSPE was used as the untreated control.

2.2.14 Depletion of media

The effect of O-GNR-PEG-DSPE on the depletion of media was tested by incubating HeLa, MCF7 or SKBR3 cells to media pre-exposed to the nanoparticles (Figure 13). Media for the three different cell lines (DMEM, RPMI or McCoy's medium) were prepared by exposing the media to 100µg/ml O-GNR-PEG-DSPE for 4 hours followed by removal of the nanoparticles using high speed centrifugation. The supernatant was used as the cell culture media.

MCF7, HeLa or SKBR3 cells were plated at 25 x 10^4 cells per plate in 10 cm plates, and incubated for 24 hours. Next the old media was replaced by the media pre-exposed to O-GNR-

PEG-DSPE, and incubated for 48 hours. Following this incubation, the cells were trypsinized, and cell number was counted using a hemocytometer. Cells grown in normal media were considered as the untreated control.

2.2.15 Statistical Analysis

All data are presented as mean + standard deviation. (n = 4 for trypan blue assay, and n = 6 for all other assays). Square root transformation was used to transform percentage data to approximate a normal distribution, and these transformed data were used for further statistical analyses. Students‘t’ test was used to analyze the differences among groups. One-way anova followed by Tukey Kramer post hoc analysis was used for multiple comparisons between groups. All statistical analyses were performed using a 95% confidence interval ($p < 0.05$).

2.3 Results:

2.3.1 TEM and Raman Spectroscopy O-GNRs

Figure 1A displays a low resolution TEM micrograph showing multiple O-GNRs. As seen in the figure, the graphene nanoribbons have fully unzipped layers of graphene sheets. The TEM image clearly shows that the nanoribbons are multilayered (arrows) due to the unzipping of the MWCNTs. The graphene oxide nanoribbons structure appears mostly uniform and smooth, with few defects. Analyses of multiple TEM images show that O-GNRs have an average width of 125- 220 nm, and lengths between of 500 – 2500 nm. Figure 1B, C and D are representative high resolution TEM (HRTEM) images of the synthesized O-GNRs that show straight smooth edges with no edge-roughness. The inter-layer spacing of graphene sheets measured from HRTEM

micrograph is ~ 0.34 nm, which is in agreement with the values reported for pristine graphene (Miyazaki H, 2008).

Figure 2A shows a representative Raman spectrum of the O-GNRs. The spectrum shows the characteristic G band at 1580 cm^{-1} attributed to the doubly degenerate E_{2g} state and the D band at 1332 cm^{-1}, attributed to the zone boundary phonons (Ferrari et al., 2006). Figure 2B shows a digital photograph of O-GNRs dispersed in water or PEG-DSPE solution (6 mg PEG- DSPE in 5 ml of water) at a concentration of 1 mg/ml, and kept undisturbed for 3 hours. The O- GNRs dispersed in the PEG-DSPE solution appear darker, and homogenous than those dispersed in water.

2.3.2 Alamar Blue Assay

In this fluorescence-based assay, the non-fluorescent dye Alamar blue (resazurin) acts as an electron acceptor for enzymes like nicotinamide adenine dinucleotide phosphate (NADP), and is converted to a pink fluorescent dye. The amount of non-fluorescence to fluorescence conversion is dependent on the metabolic state of cells. Increased metabolic activity produces more conversion, and hence more fluorescence. Figure 3A and B show the plot of percent cell viability as a function of O-GNR-PEG-DSPE concentration (10-400μg/ml) at the 24, and 48 h time point, respectively. At both the time points, all the three cell types showed a decrease in cell viability with increase in incubation concentrations and the largest decrease in cell viability was observed at the maximum incubation concentration of 400μg/ml. At this concentration, the SKBR3 cells shows ~ 10% and 22% decrease in cell viability at the 24 and 48 h time point, respectively. MCF7 cells show a 15% and 20% decrease in cell viability at the 24 and 48 h time point,

respectively. At the same incubation concentration, HeLa cells show a 60%, and 63% decrease in cell viability at the 24 and 48 h time point, respectively. 50% cell death was observed for the HeLa cells at 200μg/ml incubation concentration at both the time points.

2.3.3 Neutral Red assay

In this colorimetric assay, healthy cells take up, and store the neutral red dye in lysosomes, which is released in the presence of solubilization buffer(Repetto et al., 2008). Healthy cells with intact lysosomes hold more neutral red dye than dead cells, or cells undergoing apoptosis. Figure 4A and 4B shows the viability of 3 cell lines (SKBR3, MCF7 and HeLa), incubated with the O-GNR-PEG-DSPE solutions for 24 and 48 hours at concentrations between 10-400μg/ml. At both the time points, all the three cell types showed a decrease in cell viability with increase in incubation concentrations. At the highest concentration of 400μg/ml, SKBR3 cells show maximum cell death with 17% and 20% decrease in cell viability, and MCF7 cells show a 20% and 22% decrease in cell viability at the 24 and 48 hour time point, respectively. HeLa cells show a 60%, and 58% decrease in cell viability at the 24 and 48 hour time point, respectively. 50% cell death was observed for the HeLa cells at 200μg/ml incubation concentration at both the time points.

2.3.4 Trypan Blue Assay

This assay is based on the principle of dye exclusion to differentiate between living, and dead cells. Living cells with intact cell membranes prevents the trypan blue dye from entering them, whereas dead cells with compromised leaky cell membranes allow the dye to pass through. This allows dead cells stained by the dye to be visualized under a bright field microscope. Figure 5

shows the cell mortality (cell death) observed in the 3 cell lines (SKBR3, MCF7 and HeLa), when incubated with 10-400µg/ml O-GNR-PEG-DSPE solution for 12 hours. Also included are the results of the controls; untreated cells, and cells treated with only the PEG-DSPE solution. The controls do not show any noticeable cell death in the three cell types. MCF7 cells show no cell death at 10µg/ml, ~5% cell mortality at 50µg/ml, and no statistically significant increase upto 400µg/ml treatment concentrations. SKBR3 cells show ~5% cell mortality at 10µg/ml incubation concentration, and a dose -dependent increase with ~ 13% cell death at 400µg/ml treatment concentration. HeLa cells show ~5% cell mortality at 10µg/ml incubation concentration and a dose-dependent increase with ~ 36% cell death at the highest treatment concentration of 400µg/ml.

***2.3.5 LDH Assay**:*

This assay measures the cytosolic enzyme lactate dehydrogenase (LDH) released in the media by dying cells possessing compromised cell membranes. The released LDH oxidizes lactate to pyruvate which converts iodonitrotetrazolium (INT) present in the assay reagent to formazan; a water soluble molecule with an absorbance peak at 490nm (Lewinski et al., 2008), readily detectable by optical absorption spectroscopy. Figure 6A-C shows %LDH release from the three cell lines incubated with various concentrations of O-GNR-PEG-DSPE (10-400µg/ml), for 24, 48 and 72 h. The results of the controls; untreated cells and cells treated with only the PEG-DSPE solution are also shown. The controls (untreated cells) shows different LDH release with SKBR3 and HeLa cells showing slightly higher LDH release at the three time points (24,48 and 72 hours) compared to MCF7 cells which does not show any statistically significant increase in %LDH release with increase in O-GNR-PEG-DSPE incubation concentrations, at all the three

time points (Figure 6A-C). At the highest applied concentration (400µg/ml), MCF7 cells show the maximum LDH release of ~45% LDH compared to positive control (lysis solution) at the 24 hour time point, which remains almost same (~40%) at the 72 hour time point. SKBR3 cells also show no statistically significant increase in %LDH release with increase in O-GNR-PEG-DSPE incubation concentrations, at all the three time points (Figure 6A-C). SKBR3 cells incubated with 400µg/ml O-GNR-PEG-DSPE solution show a LDH release of ~45% at the 24 and 48 hour time point which increases to ~55% at the 72 hour time point. HeLa cells show an increase in %LDH release with increase in O-GNR-PEG-DSPE incubation concentrations, at all the three time points (Figure 6A-C). They show ~95% LDH release at the 24 hour time point when compared to positive control, which increases to ~105% at the 72 hour time point.

2.3.6 Clonogenic Assay:

The clonogenic assay is a widely-accepted method to quantify the proliferation rate, and capacity of colony formation of cancer cells in presence of one or more xenobiotic compounds (Franken et al., 2006). The colony forming capacity of an individual cancer cell can be assessed by either counting the number of colonies or by estimating the size of the colonies produced by the individual cells at various concentrations of the xenobiotic compound. Figure 7 shows representative bright-field optical images of HeLa and MCF7 cell colonies after 7 days. These images are of control groups (untreated cells or only PEG-DSPE solution) and experimental groups (cells incubated with O-GNR-PEG-DSPE solutions at various concentrations). Figure 7A and Figure 7B are bright-field images of HeLa cell colonies formed by the control cells (untreated cells). Figure 7C and Figure 7D are bright-field images of HeLa cell colonies formed when cells were incubated with only the PEG-DSPE solution. Figure 7E-H show colonies of

HeLa cells formed by cells incubated with 1µg/ml (Figure 7E-F), and 10µg/ml (Figure 7G-H) of O-GNR-PEG-DSPE solution. HeLa cell colonies, albeit of smaller sizes compared to controls could only be observed for cell incubated at these concentrations. At the O-GNR-PEG-DSPE incubation concentration of 30µg/ml, individual HeLa cells could be observed till day 3 of incubation. However, no observable cell colonies were observed at day 7(results not shown). MCF7 cell colonies formed in the absence (control) and presence of O-GNR-PEG-DSPE solution (incubated at 30µg/ml concentration) are shown in Figures 7 I-J and K-L, respectively. Qualitatively, from the images, the MCF7 cell colony sizes for all groups were similar. Image processing performed to calculate the colony area (Figure 7M) showed no significant difference between the untreated control (HeLa and MCF7 cells), HeLa cells treated with only PEG-DSPE , and MCF7 cells incubated with 30µg/ml O-GNR-PEG-DSPE (average colony area ~ 3-8 x 10^5 μm^2). However, HeLa cells showed smaller colony areas of ~ 1.5x10^5 μm^2 and 1x10^5 μm^2 at incubation concentrations of 1 and 10µg/ml respectively.

2.3.7 Live Cell Assay

The LIVE cell assay involves the addition of calcein-AM. Esterases found inside the cytoplasm of living cells cleave the acetomethoxy group (AM) from calcein-AM, and entrap the calcein inside living cells, which emits green fluorescence, and can be quantified to assess cell viability (Bratosin et al., 2005). Figure 8 shows the cell viability of NIH-3T3, and HeLa cells, when incubated with increasing concentrations of O-GNR-PEG-DSPE formulations for 24 hours. Both the cell types showed a decrease in cell viability with increase in incubation concentrations. However, the decrease in cell viability with increase in incubation concentration was much

steeper for the HeLa cells compared NIH 3T3 cells. At the highest incubation concentration (250µg/ml), ~85% of the NIH-3T3 cells, and ~60% of the HeLa cells remain viable.

2.3.8 Cellular Uptake

Representative TEM images of HeLa and MCF7 cells incubated with 20µg/ml O-GNR-PEG-DSPE solution are shown in Figure 9, and Figure 10, respectively. Figure 9 A shows O-GNR-PEG-DSPE aggregates (yellow arrow) at the periphery of a HeLa cell. The same image also shows O-GNR-PEG-DSPEs located in a pit with the membrane enveloping around it suggesting that this aggregate is getting endocytosed (blue arrows). A part of the membrane from the same cell can also be seen moving towards a larger aggregate (red arrows) suggesting a macropinocytotic mode of uptake being also present. Figure 9 B shows a HeLa cell with its cytoplasm (red arrows) moving towards the O-GNR-PEG-DSPEs (yellow arrow), and engulfing them in a mechanism similar to macropinocytosis. Figure 9 C shows large O-GNR-PEG-DSPE aggregates inside a HeLa cell. The aggregates are enclosed within a vesicular structure (red arrows) lying outside the nucleus. The structures are similar in appearance to early endosomes (endosomal matrix is less dense matrix than cytoplasm) which generally transport endocytosed material to lysosomes after maturation. Figure 9D shows another vesicle carrying the O-GNR-PEG-DSPEs. Analysis of multiple TEM images indicates that most of the O-GNR-PEG-DSPEs uptaken into the HeLa cells were present in vesicles within the cell, and rarely found outside the cells. Additionally, no O-GNR-PEG-DSPE aggregates were found inside the nucleus of the HeLa cells, or associated with any cellular organelles. Figure 9E and F shows TEM images of HeLa cells incubated with 20µg/ml O-GNR-PEG-DSPE for 24 hours. The images show swollen intracellular vesicles (Figure 9E), and disrupted plasma membrane (Figure 9F) shown with red

arrows) commonly observed in necrotic cells. Figure 10 A –B shows MCF 7 cells with most of the O-GNR-PEG-DSPE aggregates (yellow arrows) in the periphery of the cells, and no or very few aggregates within the cells. Figure 10 C shows O-GNR –PEG-DSPE aggregates (circled in red) lying between two MCF-7 cells (nucleus shown with black arrows). Figure 10 D shows the morphology of MCF7 cells exposed to the O-GNR-PEG-DSPEs. The cells appear healthy, and do not show any apparent changes in the gross morphology.

2.4 Discussion

The objective of this study was to assess, and evaluate the cytotoxicity of O-GNR-PEG-DSPE formulations. Towards this end, O-GNR-PEG-DSPE solutions at various concentrations (0-400 µg/ml) were treated at various time points (24-72 hours) on four different cell lines (HeLa, MCF7, SKBR and NIH3T3). The four cells were chosen since, they are widely accepted model cell lines used for screening *in vitro* cytotoxicity, and cytocompatibility (Clothier et al., 1997). The TEM images (Figure 1) clearly show multilayered (arrows) O-GNRs due to the unzipping of the MWCNTs. The starting material, MWCNTs, have an outer diameter of 40- 70 nm. Upon unzipping, the MWCNTs should open up completely to have breadths of ~ 125 – 220 nm (π x diameter). The analysis of the TEM images (15 nanoribbons were analyzed) indicates that the width of the graphene nanoribbons is ~125-220 nm, which is in the range expected for fully flat ribbons. The Raman spectrum (Figure 2A) shows a more prominent D-band peak compared to the raman spectrum of multiwalled carbon nanotubes reported previously by our group, due to increased disorder in the sp^2 domains, and reduction of the crystal size due to oxidation (Kosynkin et al., 2009, Lalwani et al., 2013). The O-GNR-PEG-DSPE solutions were homogeneous, and stable up to the 3 hour time point (Figure 2B). The O-GNRs dispersed in

water settled down with time. Nevertheless, at the end of 3 hours, substantial amounts (~50%) of O-GNRs still remained in the solution. This observation is in line with other reports (Sun et al., 2008). The presence of carboxyl and hydroxyl groups along the edges of the nanoribbons leads to their increased dispersibility in water (Kosynkin et al., 2009). However, the O-GNRs flocculate in presence of ionic salts typically present cell culture media. Thus, addition of a biocompatible coating such as PEG-DSPE stabilizes the O-GNRs, and prevents them from settling down in biological media.

The initial cyto-toxicity screening of O-GNR-PEG-DSPE formulations were done with SKBR3, MCF7, and HeLa cells using various assays that allow assessment of its effects on cell anatomy and physiology. These assays provide information on cell metabolism (alamar blue), cell machinery (neutral red), cell membrane integrity (LDH), cell mortality (trypan blue), and cell proliferation (clonogenic assay), which are direct or indirect indicators of cytotoxicity. All these assays require living cells to firmly adhere to the surface of the tissue culture wells. Thus, before these assays were performed, the four cell lines were incubated with 10µg/ml nanoribbons for 48 hours to confirm that the presence of the O-GNR-PEG-DSPEs does not affect the attachment of the cells to the substrate. No significant changes in cell number were observed when compared to untreated or control cells after multiple DPBS washes (Figure 11). Thus, any observed decrease in cell viability cannot be attributed to live cells detaching from the substrates upon exposure to O-GNR-PEG-DSPE formulations. Although there are reports about the interactions of carbon nanotubes with alamar blue and neutral red dyes (Doak et al., 2009), the high solubility of the O-GNR-PEG-DSPE formulations allows them to get easily rinsed via DPBS washes before the commencement of assays. Thus, these assays did not show any nanoparticle interference.

The results of all five assay indicate that the O-GNR-PEG-DSPE have a dose- and time-dependent cytotoxic effect on the MCF7, SKBR3 and HeLa cell lines. In general the cytotoxic effects increased with increase in incubation concentration, and incubation time. However, the degree of cytotoxicity was significantly lower in MCF7 or SKBR3 cells compared to HeLa cells. The results of the Alamar blue (indicator of cellular metabolism) and Neutral red assays (indicator of lysosomal integrity) on the MCF7 or SKBR3 cells taken together show that, upto 48 hours, ~100% of these cells remain viable, when incubated at10µg/ml concentration. There is decrease in cell viability above this concentration, and ~78% are viable at the highest concentration (400µg/ml). These results for the MCF7 and SKBR3 cells are further corroborated by LDH (indicator of cell membrane integrity), and Trypan blue (indicator of cell death) assay. The LDH assay for both these cell lines shows no increase in LDH release at concentration upto 10µg/ml compared to controls, or cells treated with only PEG-DSPE solution, but increase at higher concentrations. The trypan blue assay show no statistically significant increase in cell mortality upto 10µg/ml, and a marginal (upto 13% cell death) increase at higher concentrations. The cell mortality values for the trypan blue assay are approximately half the values observed in other assays because of a media change at the 36 hour time point to avoid cell death due to nutrient depletion which removed the dead, and detached cells at that time point. The results of the four assays taken together indicate that the O-GNR-PEG-DSPE formulations show no toxic effects on the MCF7 and SKBR3 cells upto 10µg/ml, and low cytotoxicity even at higher concentrations (400µg/ml) over a period of 48 hours.

In contrast, the alamar blue, neutral red, trypan blue, and LDH assay results of HeLa cells taken together indicate O-GNR-PEG-DSPE formulation affect the cell viability at all concentrations, and time points. At lowest incubation concentration 10µg/ml, the % cell death was between 5-25% cell (depending on the time point, and the assay), and steeply increased with concentration with the CD_{50} values ≥ 100µg/ml depending on the assay, and time point. This substantially increased cytotoxicity of the O-GNR-PEG-DSPE formulations on HeLa cells compared to other cancer cell lines was further corroborated by the Clonogenic assay.

The Clonogenic assay results (Figure 7) seven days after the treatment of HeLa cells with 1-30µg/ml of O-GNR-PEG-DSPE solution clearly show dose-dependent decrease in the cell colony sizes with no colony formation at the 30µg/ml incubation concentration. No such decrease was observed at these concentrations for the MCF7 cells, or the controls. The decrease in the colony sizes at 1µg/ml compared to the untreated controls suggests that the O-GNR-PEG-DSPE formulations may have a long term adverse effect on atleast a small percentage of HeLa cells even at these low incubation concentration.

The effects of the O-GNR-PEG-DSPE formulations were also investigated on NIH3T3 fibroblasts cells (a normal non-cancer cell line) using the LIVE cell assay. The results (Figure 8) indicate the viability of the NIH3T3 cells is affected in a manner similar to those observed for the MCF7 and SKBR3 cells; no toxic effects at 10µg/ml, and low toxicity at higher concentrations (upto 250µg/ml) over a 24 hour period. The LIVE cells results for the HeLa cells were similar to the results of the other assays; low toxicity at 10µg/ml and steep increase in toxicity with increase in concentration. Thus, the results of the various assays indicate that the O-

GNR-PEG-DSPE formulations show a differential (higher) cytotoxic response on HeLa cells compared other cancer or normal cells investigated in this study.

The significantly higher toxicity exhibited by HeLa cells may be attributed either to greater reactive oxygen species (ROS) generation, depletion of the nutrients in the culture media due to their absorption or adsorption by the nanoparticles, or the greater cellular uptake of the O-GNR-PEG-DSPEs nanoparticles into the HeLa cells (Chang et al., 2011). ROS production in a cell is dependent on its stress levels, and may even induce cell death. HeLa and MCF7 cells incubated 20µg/ml of O-GNR-PEG-DSPE solution for 2 hours (ROS production under stress starts immediately, and can be quantified within 1-2 hours) showed similar ROS production (Figure 12)**.** Thus, ROS generation may not be the major reason for observed differences in cytotoxicity between the HeLa cells, and other cell lines. Depletion of the nutrients in the culture media due to the presence of carbon nanotubes has been shown in some reports to be another reason for the observed cytotoxicity (Guo et al., 2008, Liu et al., 2009a). To test this hypothesis, 100µg/ml of O-GNR-PEG-DSPE solution was added to the cell culture media for 48 hours. O-GNR-PEG-DSPEs were removed by high speed ultra-centrifugation, and the media was used to culture SKBR3, MCF7 and HeLa cells. All the cells showed normal growth without any signs of cytotoxicity (Figure 13). Thus, the observed differences in cytotoxicity for the HeLa cells, and other cell lines cannot be attributed to the depletion of media nutrients

Greater cellular uptake of the O-GNR-PEG-DSPEs nanoparticles into the HeLa cells and their unfavorable interactions with the cell machinery is another possible explanation and TEM results of HeLa or MCF7 cells support this hypothesis. The cellular uptake and localization of the O-

GNR-PEG-DSPEs into HeLa, and MCF7 cells investigated by TEM showed that the HeLa cells (Figure 9) uptake greater amounts of O-GNR-PEG-DSPEs compared to MCF7 cells (Figure 10). MCF7 cells showed little or no uptake (Figure 10 A-B), and similar results were obtained for the other cell types (SKBR3 and NIH3T3 cells; results not shown). It could also be inferred from the TEM images that HeLa cells possibly uptake O-GNR–PEG-DSPEs through both endocytotic, and macropinocytotic pathways (Figure 9 A-B). The images also suggest that larger aggregates of O-GNR-PEG-DSPE were being uptaken by the macropinocytotic pathway, while smaller aggregates were uptaken through the endocytotic pathway. The images also show that vesicular structures similar to early endosomes take up the O-GNR-PEG-DSPEs (Figure 9 C-D). Early endosomes generally mature to form late endosomes which fuse with the lysosome. However, association of the endosomal vesicles containing O-GNR-PEG-DSPE with any organelles (including lysosome) were not observed after 3 hours of incubation. Also, the O-GNR-PEG-DSPE containing vesicles were not observed inside the nucleus. The morphology of the HeLa cells incubated with the O-GNR-PEG-DSPEs (Figure 9E and F) was similar to cells undergoing necrotic cell death; ruptured cell membrane and swollen vesicles. MCF7 cells incubated with the O-GNR-PEG-DSPEs appear healthy (Figure 10D), and do not show any apparent changes in the gross morphology. While the TEM images provide preliminary indications of possible uptake and cell death mechanism in HeLa cells in the presence of the O-GNR-PEG-DSPEs, clearly more thorough investigations are needed, and are currently underway to understand both the mechanism of uptake, and cell death.

Evaluation of the cyto- and bio-compatibility is necessary to develop any new material for *in vivo* biomedical applications.(Williams, 2008) Some of these same considerations will influence

toxicity of these materials if released to the environment. There is now a wide body of research available that documents the toxicity and cell/tissue responses of carbon nanostructures such as fullerenes, metallofullerenes and carbon nanotubes (single-walled and multi-walled carbon nanotubes) (Sitharaman and Wilson, 2007, Liu et al., 2009b, Lacerda et al., 2006, Nakamura and Isobe, 2003). These reports show that the structure (e.g. spherical, tubular), chemical composition (e.g. pristine, functionalized), and synthesis method (e.g. chemical vapor deposition, arc-discharge) are some of key factors that influence the toxicity and tissue response for these carbon nanostructures. For instance, it has been reported that pristine (hydrophobic) fullerenes or carbon nanotubes elicit adverse toxic effects and cell/tissue responses including reactive oxygen stress, inflammation, and immune response while functionalized water-soluble fullerenes and carbon nanotubes mitigate these serious effects.(Lacerda et al., 2006, Sitharaman and Wilson, 2007) In the case of graphene, relatively little work has been done to assess their toxic effects *in vitro* (Singh et al., 2011, Sasidharan et al., 2011, Chang et al., 2011) and *in vivo* (Yang et al., 2010, Wang et al., 2011) compared to other carbon nanostructures. All these reports are on graphene nanoplatelets prepared by the modified Hummer's method (oxidation of graphite by potassium permanganate, and strong acids followed by mechanical exfoliation) or variations of this technique. These reports indicate that graphene nanoparticles, depending on their chemical composition, and synthesis method, show diverse effects on cells and tissues. Sasidharan et al. report that *in vitro* pristine thermally-exfoliated graphene and those functionalized with carboxylic acid groups shows differential toxic effects. Pristine graphene nanoparticles have cell death 50 values (CD_{50}) of ~50µg/ml, and functionalized graphene nanoparticles do not possess any toxicity even at 300µg/ml concentrations. Chang et al. show *in vitro* that graphene oxide nanoparticles show no cytoxicity at dosages up to 300µg/ml, and a slight decrease in cell

viability above this concentration, which is attributed to oxidative stress. Singh et al. show *in vitro* that the graphene oxide prepared from potassium chlorate show strong aggregatory response in platelets at concentrations down to 2µg/ml. Using rodents, Yang et al. and Wang et al. have investigated *in vivo* toxicity at dosages up to 20 mg/kg of pristine graphene oxide nanoparticles, and those functionalized with water-soluble biocompatible polymer polyethylene glycol. Their results show neither pristine nor functional graphene oxide show any toxic effects, nor do they have any adverse reactions on the internal organs at concentrations as high as 20 mg/kg. One should note that it is difficult to compare the cytotoxic effects of O-GNR-PEG-DSPEs with these various *in vitro* studies, as these studies used different graphene synthesis method, different cell types, and different solubilizing agents for dispersing the graphene nanoparticles. Nevertheless, the results of this study suggest that water-solubilized graphene nanoribbons (O-GNR-PEG-DSPE) prepared from carbon nanotubes have a significant different toxicity profile compared to graphene nanoplatets prepared by the modified Hummer's method or its variation. The results should also provide guidelines on the range of non-toxic concentrations that maybe suitable for potential imaging and drug delivery applications. For instance, recent studies show that O-GNRs show promise as advanced contrast agents for magnetic resonance imaging (MRI) [9] such as cellular MRI, wherein cells will be labeled ex vivo with these nanoparticles, and tracked in vivo by MRI. Thus, this study offers insights into the concentration suitable for the *ex vivo* labeling of cells for this, and other similar applications.

2.5 Conclusion

The cytotoxic screening of O-GNRs water-solubilized with PEG-DSPE, using six different assays, in four representative cell lines; HeLa, NIH-3T3, SKBR and MCF7 showed that these cell lines significantly differed in their response to O-GNR-PEG-DSPE formulations; assessed and evaluated using various endpoints (lactate dehydrogenase (LDH) release, cellular metabolism, lysosomal integrity and cell proliferation) for cytotoxicity. In general, all the cells showed a dose-dependent (10-400µg/ml) and time-dependent (12-48 h) decrease in cell viability. However, the degree of cytotoxicity was significantly lower in MCF7 or SKBR3 cells compared to HeLa cells. These cells were 100% viable upto 48 hours, when incubated at 10µg/ml O-GNR-PEG-DSPE concentration, and showed decrease in cell viability above this concentration with ~78% of cells viable at the highest concentration (400µg/ml). In contrast, significant cell death (5-25% cell death depending on the time point, and the assay) was observed for HeLa cells even at a low concentration of 10µg/ml. The decrease in cell viability was steep with increase in concentration with the CD_{50} values $\geq$ 100µg/ml depending on the assay, and time point. Transmission electron microscopy of the various cells treated with the O-GNR solutions show higher uptake of the O-GNR-PEG-DSPEs into HeLa cells compared to other cell types. Additional analysis indicates that this increased uptake is the dominant cause of the significantly higher toxicity exhibited by HeLa cells. The results suggest that water-solubilized O-GNR-PEG-DSPEs have a heterogeneous cell-specific cytotoxicity, and have significantly different cytotoxicity profile compared to graphene nanoparticles prepared by the modified Hummer's method (graphene nanoparticles prepared by oxidation of graphite, and its mechanical exfoliation) or its variations.

2.6 References

Bratosin, D., Mitrofan, L., Palii, C., Estaquier, J. & Montreuil, J. 2005. Novel fluorescence assay using calcein-AM for the determination of human erythrocyte viability and aging. *Cytometry Part A,* 66A**,** 78-84.

Chang, Y., Yang, S.-T., Liu, J.-H., Dong, E., Wang, Y., Cao, A., Liu, Y. & Wang, H. 2011. In vitro toxicity evaluation of graphene oxide on A549 cells. *Toxicology Letters,* 200**,** 201-210.

Clothier, R. H., Beed, M., Samson, R. & Ward, R. 1997. An In Vitro Approach to the Evaluation of Repeat Exposure in the Prediction of Toxicity. *Toxicology in Vitro,* 11**,** 679-682.

Doak, S. H., Griffiths, S. M., Manshian, B., Singh, N., Williams, P. M., Brown, A. P. & Jenkins, G. J. S. 2009. Confounding experimental considerations in nanogenotoxicology. *Mutagenesis,* 24**,** 285-293.

Ferrari, A. C., Meyer, J. C., Scardaci, V., Casiraghi, C., Lazzeri, M., Mauri, F., Piscanec, S., Jiang, D., Novoselov, K. S., Roth, S. & Geim, A. K. 2006. Raman Spectrum of Graphene and Graphene Layers. *Physical Review Letters,* 97**,** 187401.

Franken, N. A. P., Rodermond, H. M., Stap, J., Haveman, J. & Van Bree, C. 2006. Clonogenic assay of cells in vitro. *Nat. Protocols,* 1**,** 2315-2319.

Geim, A. K. & Novoselov, K. S. 2007. The rise of graphene. *Nat Mater,* 6**,** 183-191.

Guo, L., Von dem Bussche, A., Buechner, M., Yan, A., Kane, A. B. & Hurt, R. H. 2008. Adsorption of Essential Micronutrients by Carbon Nanotubes and the Implications for Nanotoxicity Testing. *Small,* 4**,** 721-727.

Huang P, X. C., Lin J, Wang C, Wang X, Zhang C, Zhou X, Guo S, Cui D. 2011. Folic Acid-conjugated Graphene Oxide loaded with Photosensitizers for Targeting Photodynamic Therapy. *Theranostics***,** 240-250.

Hummers, W. & Offeman, R. 1958. Preparation of Graphitic Oxide. *Journal of the American Chemical Society,* 80**,** 1339-1339.

Kosynkin, D. V., Higginbotham, A. L., Sinitskii, A., Lomeda, J. R., Dimiev, A., Price, B. K. & Tour, J. M. 2009. Longitudinal unzipping of carbon nanotubes to form graphene nanoribbons. *Nature,* 458**,** 872-876.

Lacerda, L., Bianco, A., Prato, M. & Kostarelos, K. 2006. Carbon nanotubes as nanomedicines: From toxicology to pharmacology. *Advanced Drug Delivery Reviews,* 58**,** 1460-1470.

Lalwani, G., Henslee, A. M., Farshid, B., Lin, L., Kasper, F. K., Qin, Y.-X., Mikos, A. G. & Sitharaman, B. 2013. Two-dimensional nanostructure-reinforced biodegradable polymeric nanocomposites for bone tissue engineering. *Biomacromolecules,* 14**,** 900-909.

Lewinski, N., Colvin, V. & Drezek, R. 2008. Cytotoxicity of Nanoparticles. *Small,* 4**,** 26-49.

Lin, Y.-M., Valdes-Garcia, A., Han, S.-J., Farmer, D. B., Meric, I., Sun, Y., Wu, Y., Dimitrakopoulos, C., Grill, A., Avouris, P. & Jenkins, K. A. 2011. Wafer-Scale Graphene Integrated Circuit. *Science,* 332**,** 1294-1297.

Liu, J., Yang, L. & Hopfinger, A. J. 2009a. Affinity of Drugs and Small Biologically Active Molecules to Carbon Nanotubes: A Pharmacodynamics and Nanotoxicity Factor? *Molecular Pharmaceutics,* 6**,** 873-882.

Liu, W., Jackson, B. L., Zhu, J., Miao, C.-Q., Chung, C.-H., Park, Y. J., Sun, K., Woo, J. & Xie, Y.-H. 2010. Large Scale Pattern Graphene Electrode for High Performance in Transparent Organic Single Crystal Field-Effect Transistors. *ACS Nano,* 4**,** 3927-3932.

Liu, Z., Tabakman, S., Welsher, K. & Dai, H. 2009b. Carbon Nanotubes in Biology and Medicine: In vitro and in vivo Detection, Imaging and Drug Delivery. *Nano Res,* 2**,** 85-120.

Miyazaki H, O. S., Sato T,Tanaka S,Goto H,Kanda A et al 2008. Inter-Layer Screening Length to Electric Field in Thin Graphite Film. *Appl. Phys. Express,* 1**,** 034007.

Nakamura, E. & Isobe, H. 2003. Functionalized Fullerenes in Water. The First 10 Years of Their Chemistry, Biology, and Nanoscience. *Accounts of Chemical Research,* 36**,** 807-815.

Novoselov, K. S., Geim, A. K., Morozov, S. V., Jiang, D., Zhang, Y., Dubonos, S. V., Grigorieva, I. V. & FIRSOV, A. A. 2004. Electric Field Effect in Atomically Thin Carbon Films. *Science,* 306**,** 666-669.

Paratala, B. S., Jacobson, B. D., Kanakia, S., Francis, L. D. & Sitharaman, B. 2012. Physicochemical Characterization, and Relaxometry Studies of Micro-Graphite Oxide, Graphene Nanoplatelets, and Nanoribbons. *PLOS ONE,* 7**,** e38185.

Repetto, G., Del peso, A. & Zurita, J. L. 2008. Neutral red uptake assay for the estimation of cell viability/cytotoxicity. *Nature Protocols,* 3**,** 1125-1131.

Sasidharan, A., Panchakarla, L. S., Chandran, P., Menon, D., Nair, S., Rao, C. N. R. & Koyakutty, M. 2011. Differential nano-bio interactions and toxicity effects of pristine versus functionalized graphene. *Nanoscale,* 3**,** 2461-2464.

Schedin, F., Geim, A. K., Morozov, S. V., Hill, E. W., Blake, P., Katsnelson, M. I. & Novoselov, K. S. 2007. Detection of individual gas molecules adsorbed on graphene. *Nat Mater,* 6**,** 652-655.

Singh, S. K., Singh, M. K., Nayak, M. K., Kumari, S., Shrivastava, S., Grácio, J. J. A. & Dash, D. 2011. Thrombus Inducing Property of Atomically Thin Graphene Oxide Sheets. *ACS Nano,* 5**,** 4987-4996.

Sitharaman, B. & Wilson, L. J. 2007. Gadofullerenes and Gadonanotubes: A New Paradigm for High-Performance Magnetic Resonance Imaging Contrast Agent Probes. *Journal of Biomedical Nanotechnology,* 3**,** 342-352.

Sordan, R., Traversi, F. & Russo, V. 2009. Logic gates with a single graphene transistor. *Applied Physics Letters,* 94**,** 073305-3.

Sun, X., Liu, Z., Welsher, K., Robinson, J., Goodwin, A., Zaric, S. & Dai, H. 2008. Nano-graphene oxide for cellular imaging and drug delivery. *Nano Research,* 1**,** 203-212.

Wang, K., Ruan, J., Song, H., Zhang, J., Wo, Y., Guo, S. & Cui, D. 2011. Biocompatibility of Graphene Oxide. *Nanoscale Res Lett,* 6**,** 8.

WilliamS, D. F. 2008. On the mechanisms of biocompatibility. *Biomaterials,* 29**,** 2941-2953.

Yang, K., Wan, J., Zhang, S., Zhang, Y., Lee, S.-T. & Liu, Z. 2010. In Vivo Pharmacokinetics, Long-Term Biodistribution, and Toxicology of PEGylated Graphene in Mice. *ACS Nano,* 5**,** 516-522.

Yang, X., Zhang, X., Ma, Y., Huang, Y., Wang, Y. & Chen, Y. 2009. Superparamagnetic graphene oxide-Fe3O4 nanoparticles hybrid for controlled targeted drug carriers. *Journal of Materials Chemistry,* 19**,** 2710-2714.

2.7 Figures

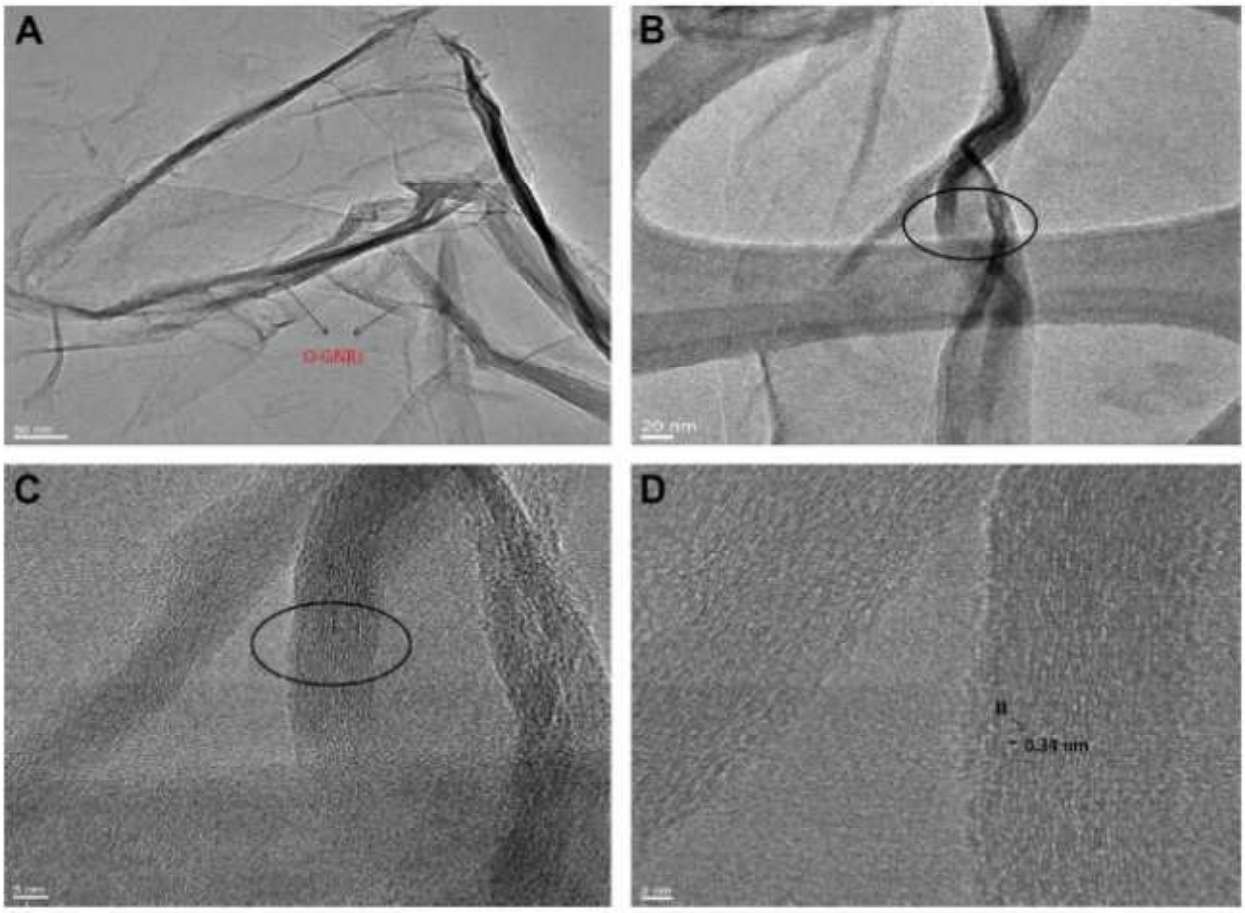

Figure 1: (A) Representative low resolution TEM image showing multiple oxidized graphene nanoribbons (O-GNR). (B-D) High Resolution TEM micrographs of graphene oxide nanoribbons at 200kV. (B) Image depicting unzipping of carbon nanotubes to form O-GNR. (C) Corresponding high resolution image of the highlighted area revealing multiple layers of oxidized graphene nanoribbon. (D) Further high resolution micrograph of image (C) revealing Van-der-Waal thickness of ~ 0.34 nm, corresponding to individual graphene layers. Scale bars: (B) 20 nm, (C) 5 nm and (D) 2 nm.

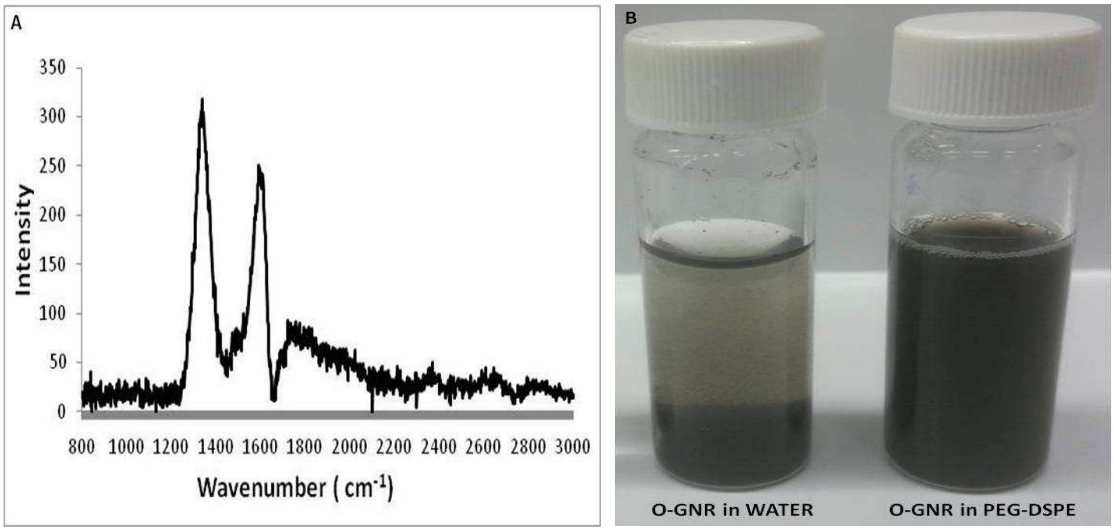

Figure 2: (A) The Raman spectra of O-GNR-PEG-DSPE showing the characteristic D and G peaks of graphene at 1332 cm^{-1}, and 1580 cm^{-1}. (B) Digital photograph of O-GNRs dispersed in water (left image) or PEG-DSPE solution (right image) at a concentration of 1 mg/ml, and kept undisturbed for 3 hours.

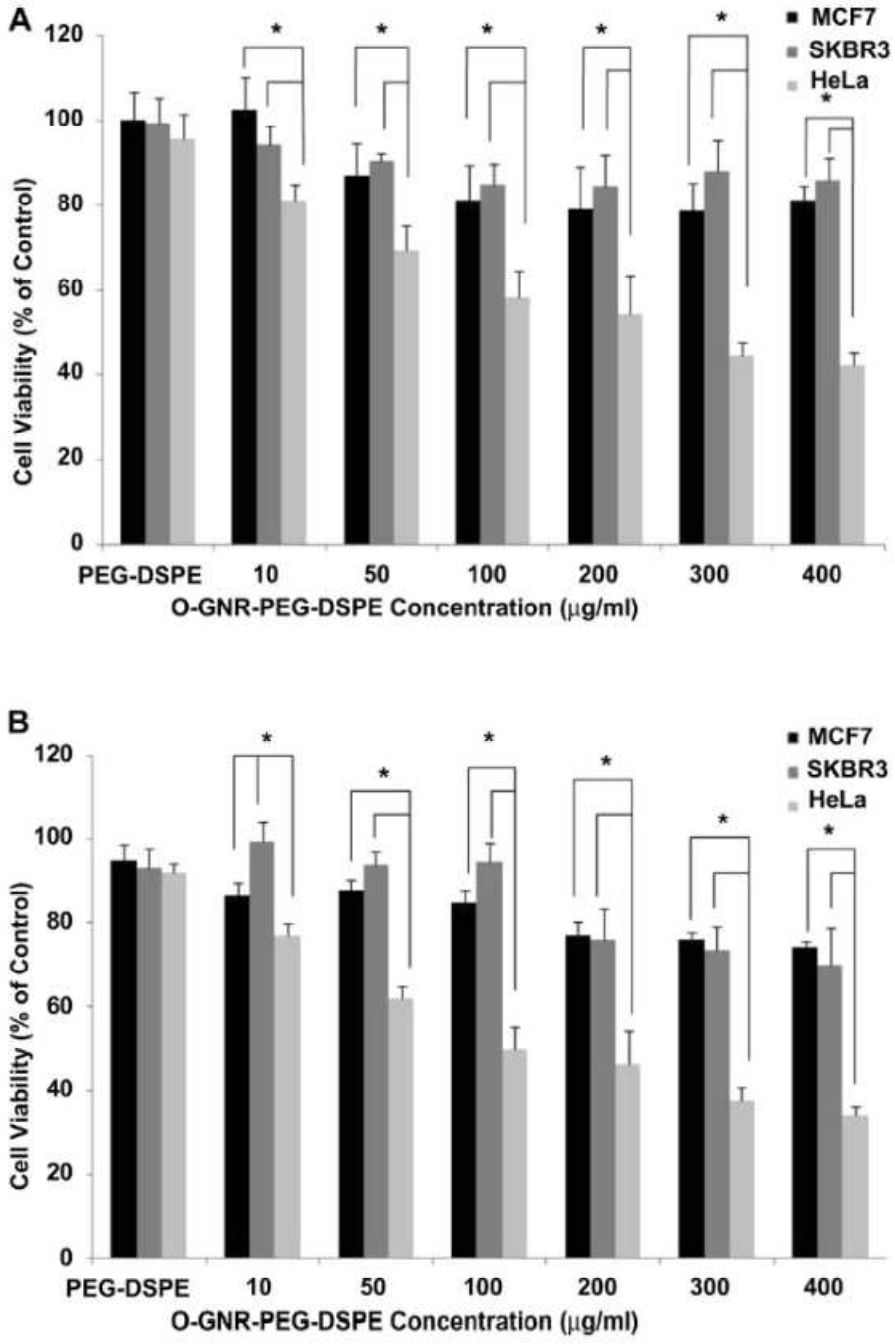

Figure 3: Alamar blue assay to assess the cell viability of HeLa, MCF7 and SKBR3 cells incubated with PEG-DSPE (control) and various O-GNR-PEG-DSPE (10-400μg/ml) concentrations at (A) 24 and (B) 48 hour time points. Data are presented as mean +SD (n = 6 per group). * = $p < 0.05$ between groups at that particular concentration.

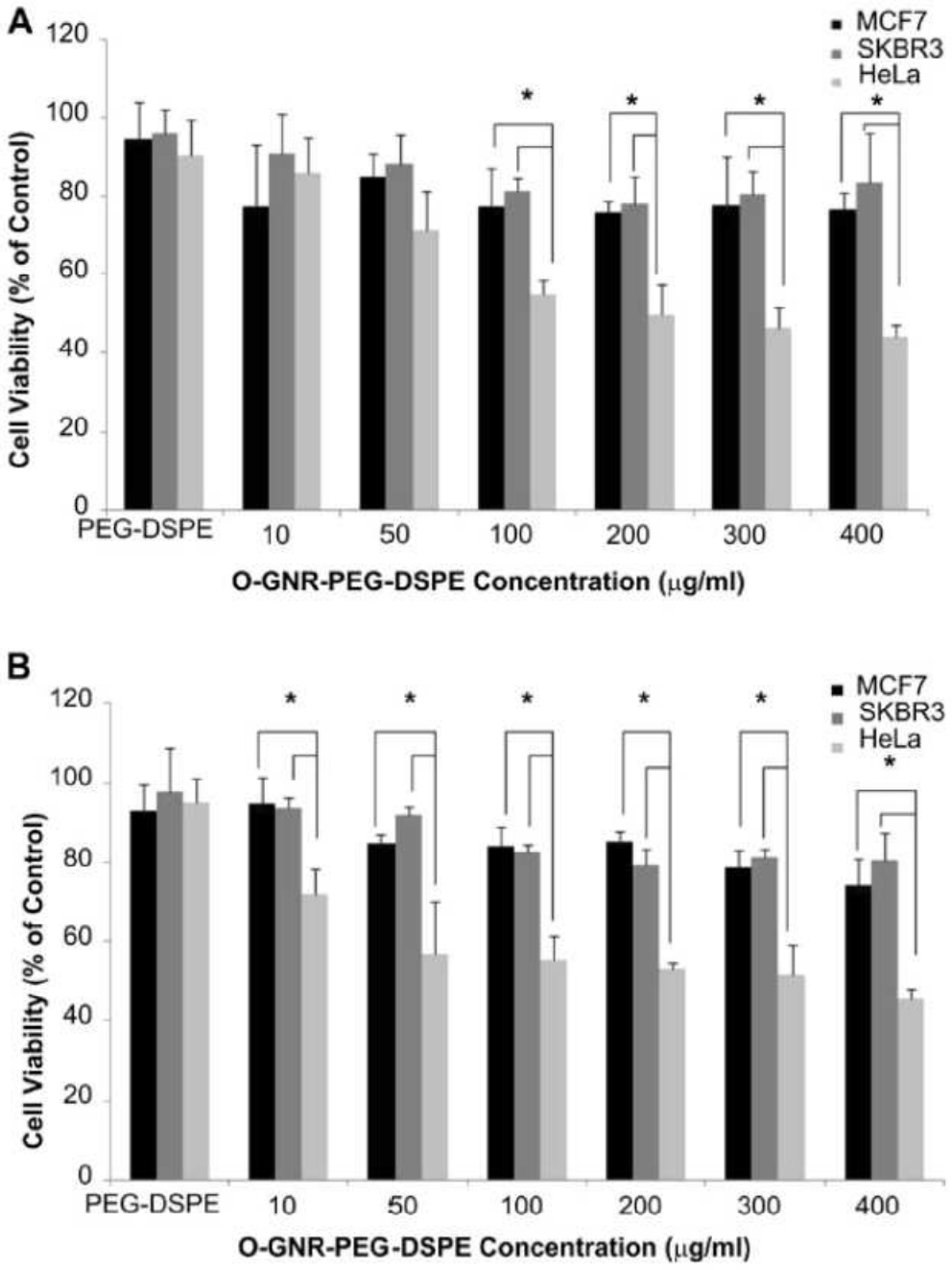

Figure 4: The Neutral red assay to assess the cell viability of HeLa, MCF7 and SKBR3 cells incubated with PEG -DSPE(control) and various O-GNR-PEG-DSPE (10-400 μg/ml) concentrations at (A) 24 and (B) 48 hours. . Data are presented as mean +SD (n = 6 per group). * = $p < 0.05$ between groups at that particular concentration.

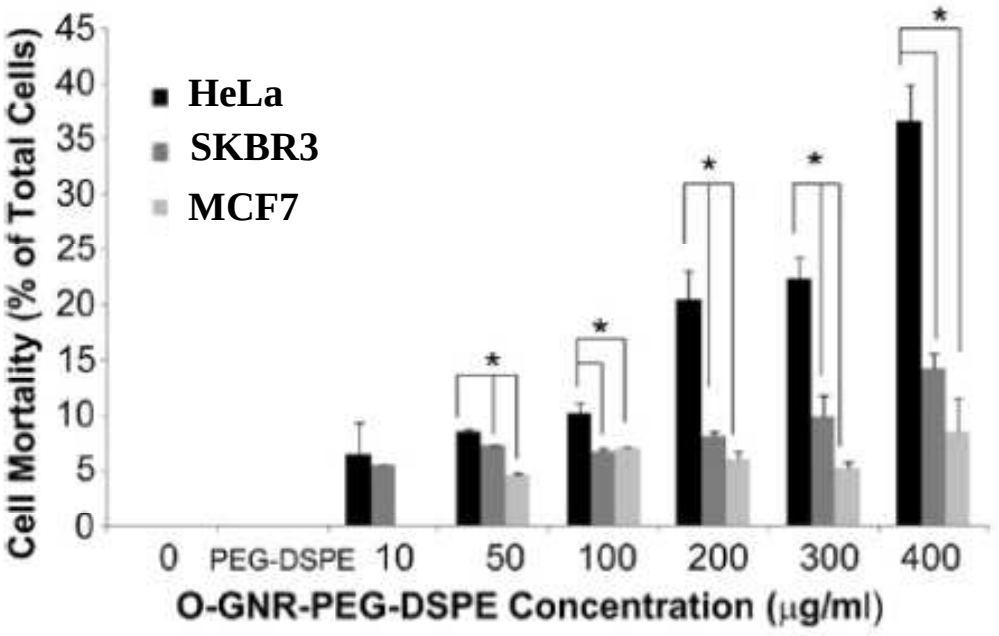

Figure 5: Trypan Blue Assay for assessing cell mortality in HeLa, SKBR and MCF 7 cells incubated with PEG-DSPE (control) and various O-GNR-PEG-DSPE (10-400μg/ml) concentrations for 12 hours. Data are presented as mean +SD (n = 4 per group). * = $p < 0.05$ for two particular groups.

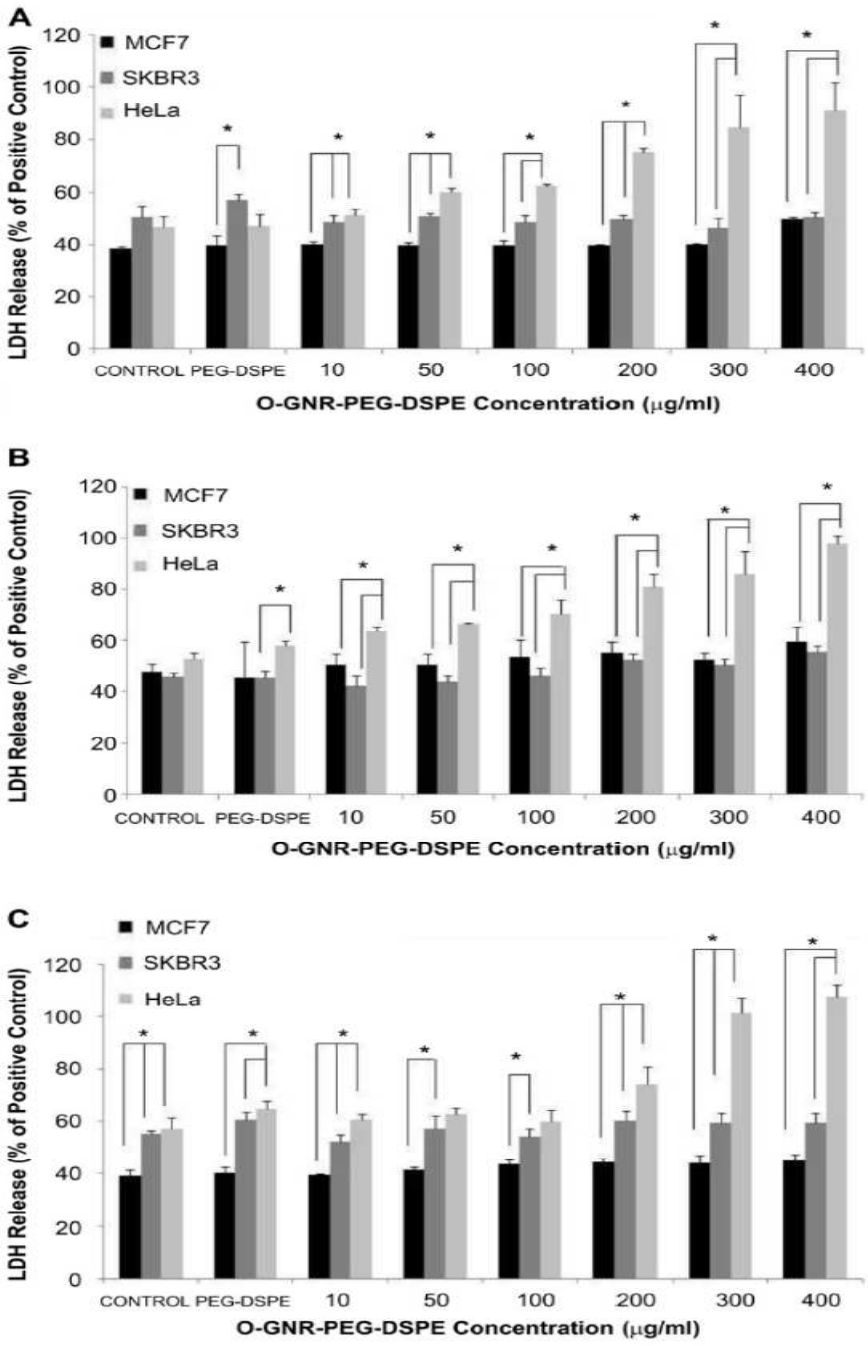

Figure 6: %LDH release (normalized to LDH release from positive control; cells incubated with lysis buffer for 45 min) in HeLa , SKBR and MCF7 cells following incubation with various O-GNR-PEG-DSPE (10-400μg/ml) concentrations at (A) 24, (B) 48 and (C) 72 hours. . Data are presented as mean +SD (n = 6 per group). * = $p < 0.05$ between groups at that particular concentration.

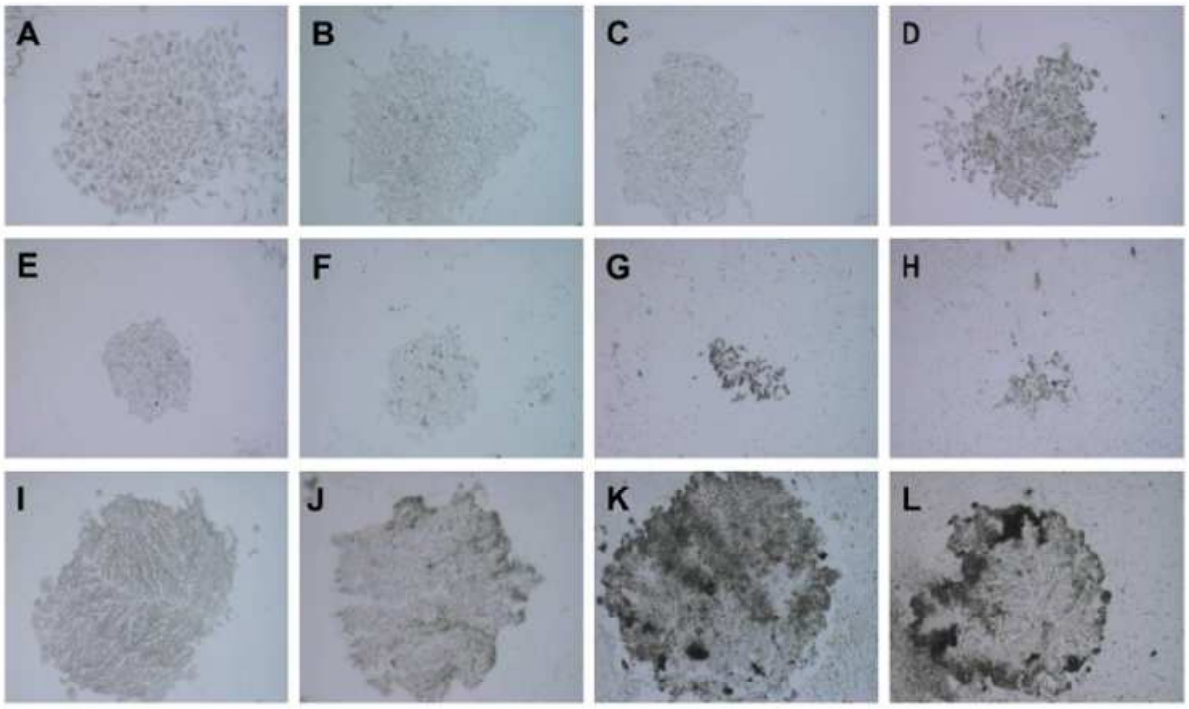
A
B
C
D
E
F
G
H
I
J
K
L

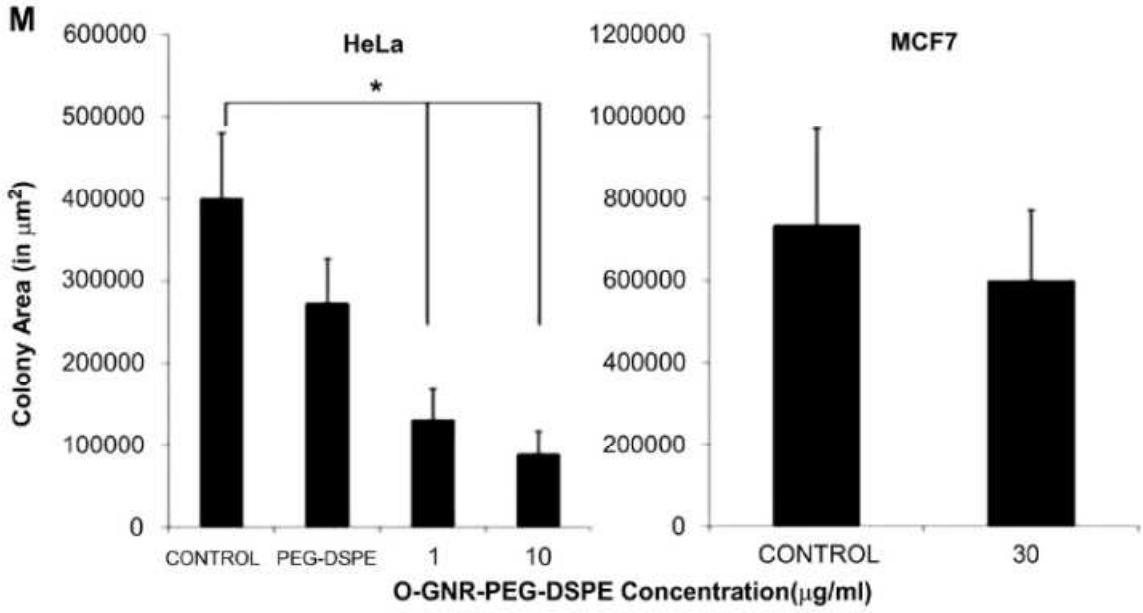
M
HeLa
MCF7
*
Colony Area (in μm²)
600000
500000
400000
300000
200000
100000
0
1200000
1000000
800000
600000
400000
200000
0
CONTROL
PEG-DSPE
1
10
CONTROL
30
O-GNR-PEG-DSPE Concentration(μg/ml)

Figure 7: Representative bright-field optical microscopy images after 7 days of (A-B) HeLa cell colonies formed from control cells (untreated cells) ; (C-D) HeLa cell colonies formed after individual HeLa cells were initially incubated with only PEG-DSPE solution; (E-F) HeLa cell colonies formed after individual HeLa cells were initially incubated with 1µg/ml O-GNR-PEG-DSPE's; (G-H) HeLa cell colonies formed after individual HeLa cells were initially incubated with 10µg/ml O-GNR-PEG-DSPE's; (I-J) MCF7 cell colonies formed from control cells (untreated cells); (K-L) MCF7 cell colonies formed after individual MCF7 cells were initially incubated with to 30µg/ml O-GNR-PEG-DSPE solution. (M) Quantified colony areas for HeLa cells (Control, incubated with to only PEG-DSPE and treated with 1µg/ml and 10µg/ml O-GNR-PEG-DSPE solutions), and MCF7 cells (Control, and treated with 30µg/ml O-GNR-PEG-DSPE solution).Data are presented as mean + SD (n = 6 per group). * = $p < 0.05$ between groups. All the optical images images have a size bar of 200 µm.

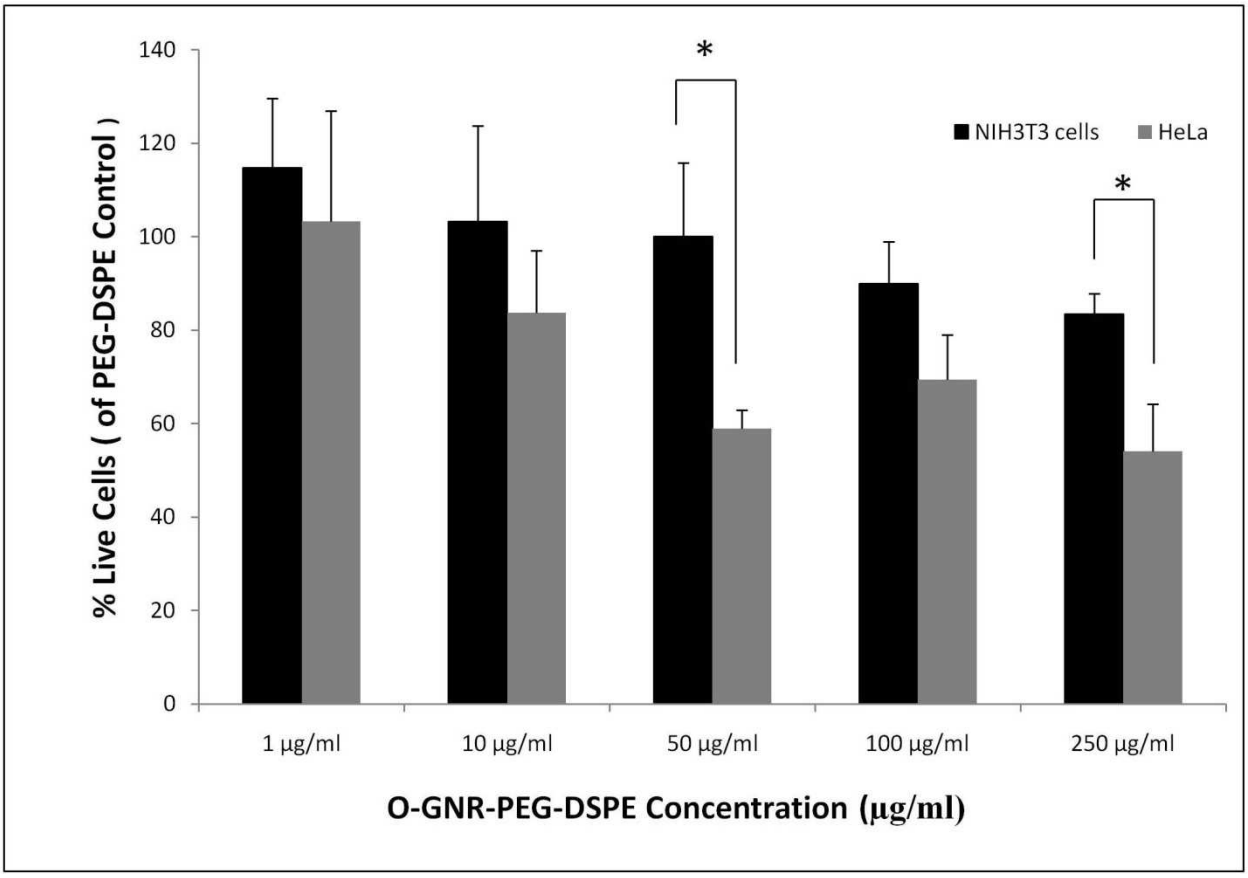

Figure 8: % Cell Viability (normalized to viability of cells exposed to PEG-DSPE) using Live Cell Assay in HeLa and NIH3T3 cells incubated with various O-GNR-PEG-DSPE (1-250µg/ml) concentrations for 24 hours. Data are presented as mean +SD (n = 6 per group). * = $p < 0.05$ for two particular groups.

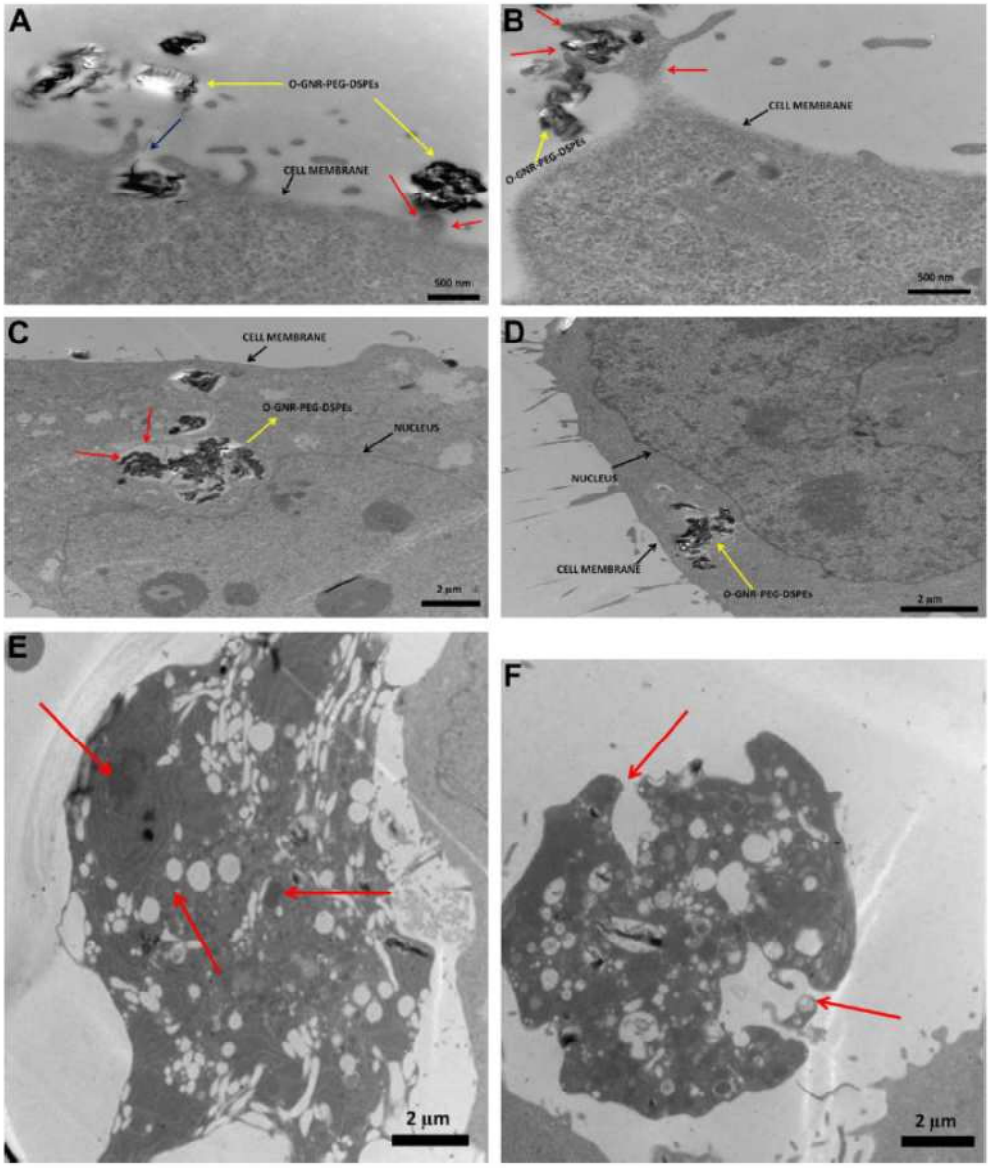

Figure 9: TEM images of a HeLa cell incubated with 20µg/ml O-GNR-PEG-DSPE solution for 3 hours.(A) O-GNR-PEG-DSPE aggregates at the periphery of the cell (blue arrows). (B) Cell membrane protruding towards and engulfing large O-GNR–PEG-DSPE aggregates (red arrows). (C-D) O-GNR-PEG-DSPE aggregates enclosed in large cytoplasmic vesicles similar to endosomes (red arrows). (E-F) HeLa cells after exposure to 20µg/ml O-GNR-PEG-DSPEs (yellow arrow) for 24 hours with (E) swollen vesicles, and (F) ruptured plasma membrane (red

arrows) suggesting the cells are undergoing necrosis. 12 cells per treatment conditions were analyzed.

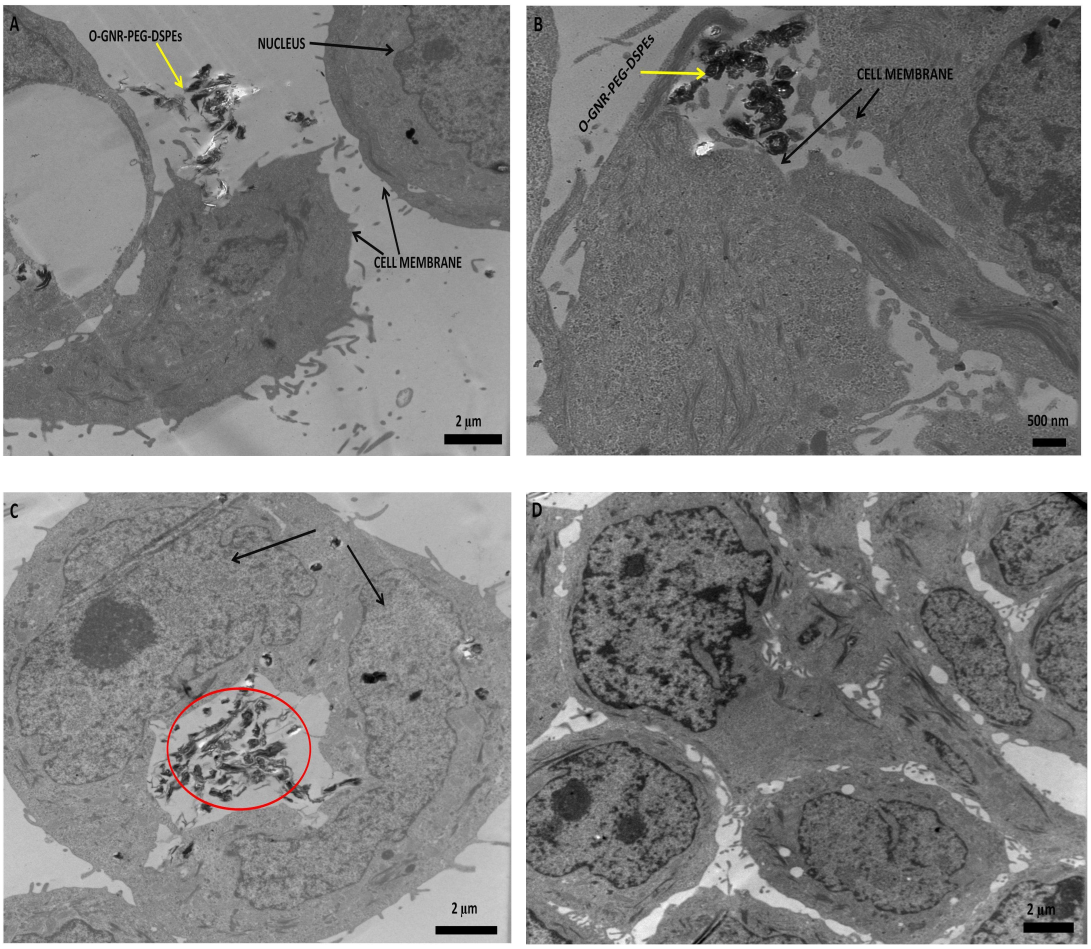

Figure 10: Representative TEM images of MCF-7 cells incubated with 20µg/ml O-GNR-PEG-DSPE solution for 3 hours. (A-C) O-GNR-PEG-DSPE (yellow arrows) aggregates in the periphery of MCF7 cells. (D) MCF7 cells exposed to 20µg/ml O-GNR-PEG-DSPEs for 24 hours show no uptake or changes in the cellular morphology. 12 cells per treatment condition was analyzed

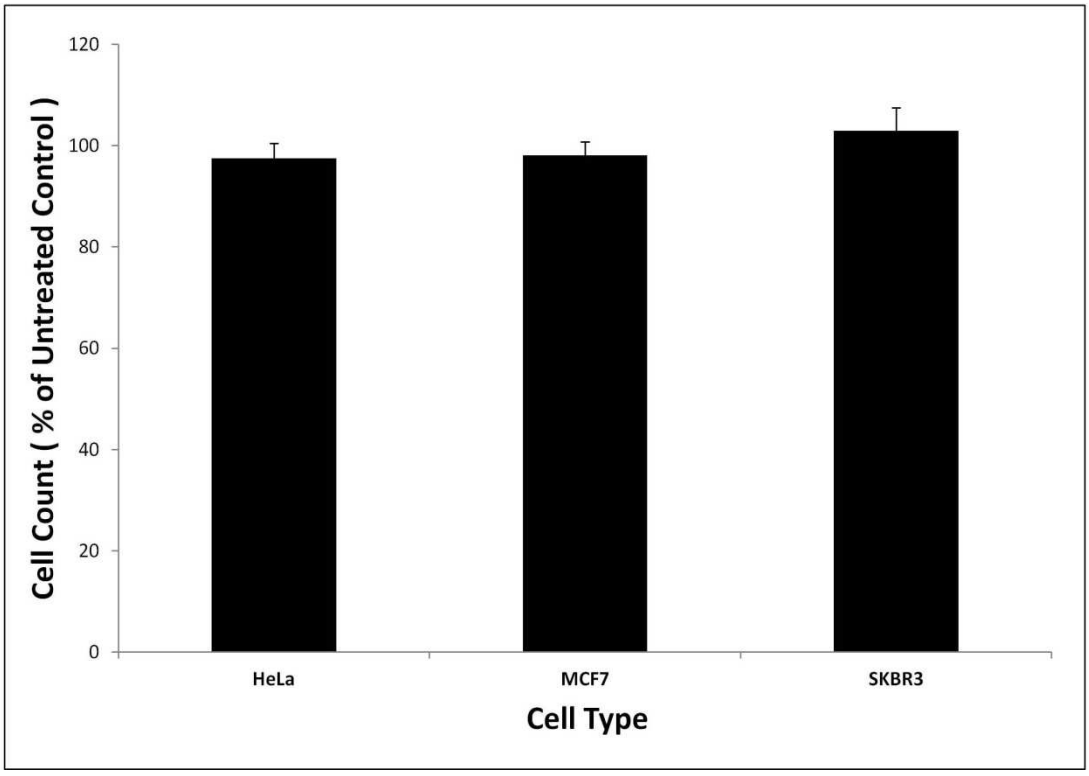

Figure 11: Percentage (%) cell count (normalized to control cells exposed to only PEG-DSPE) of HeLa, MCF7, and SKBR3 cells incubated with a O-GNR-PEG-DSPE concentration of 10µg/ml for 48 hours. Data are presented as mean +SD (n = 3 per group).

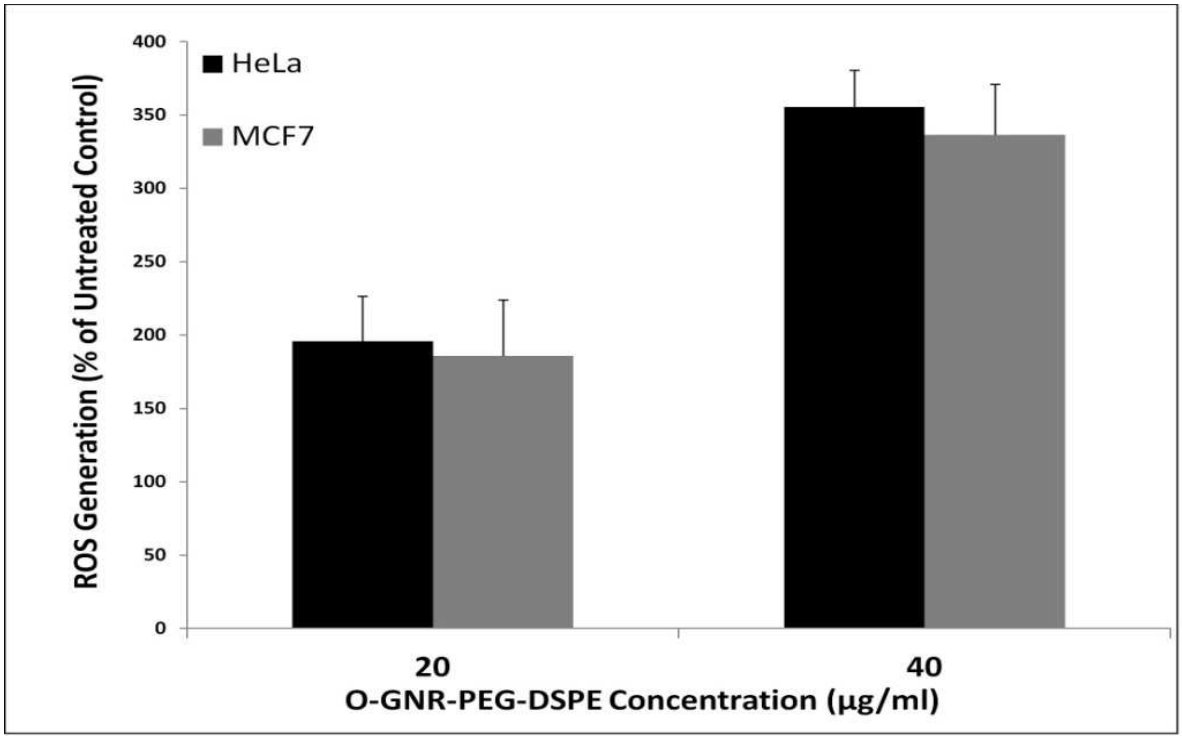

Figure 12: Percentage (%) ROS generation (normalized to ROS production of control cells exposed to only PEG-DSPE) using fluorescence based ROS quantification assay in HeLa and MCF7 cells incubated with 10µg/ml or 20µg/ml of O-GNR-PEG-DSPEs) for 2 hours. Data are presented as mean +SD (n = 6 per group).

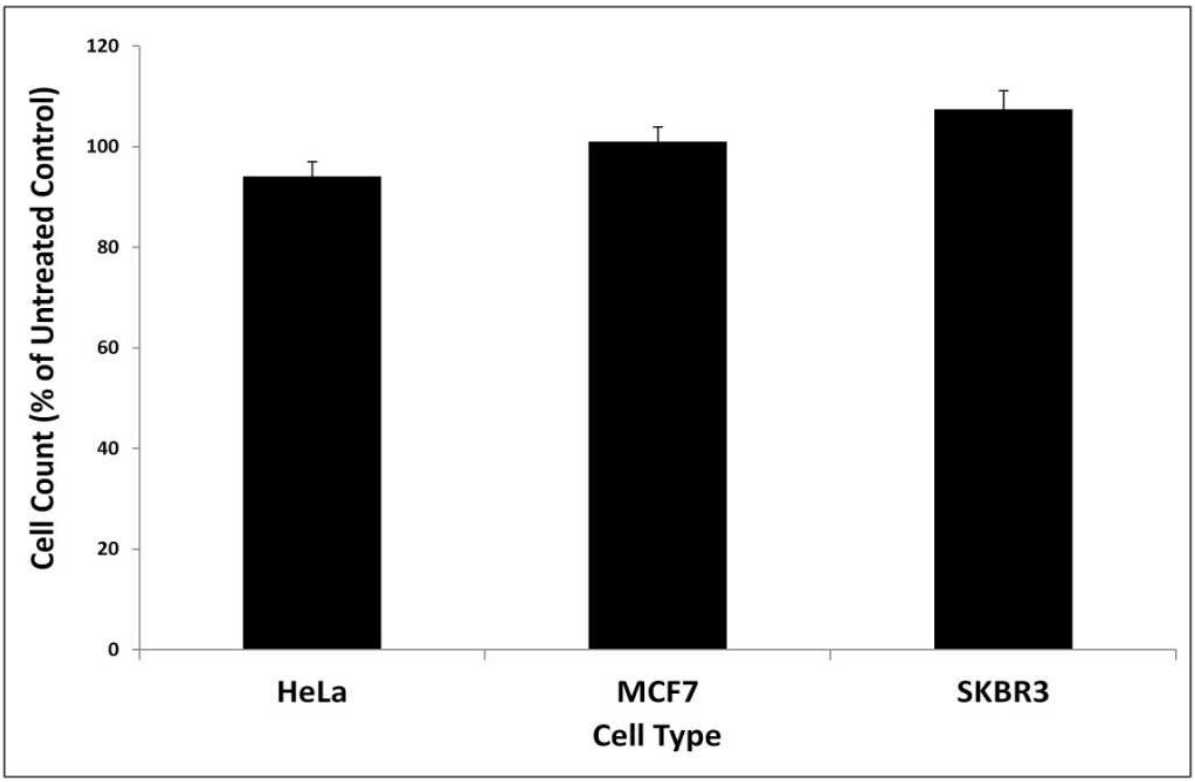

Figure 13 Percentage (%) cell count (normalized to control cells exposed to normal media) of HeLa, MCF7 or SKBR3 cells after incubation with media pre-exposed to an O-GNR-PEG-DSPE concentration of 100µg/ml for 48 hours. Data are presented as mean +SD (n = 3 per group).

Chapter 3

HEMATOLOGICAL TOXICITY OF GRAPHENE NANORIBBONS

3.1 Introduction

Interaction of cells and proteins with nanoparticles in tissues or circulating body fluids (blood, lymph, cerebrospinal fluid) often governs the biological effects of nanoparticles *in-vivo*.(Lynch and Dawson, 2008, Fischer and Chan, 2007) Depending on the route and extent of exposure, nanoparticle-cell interactions can result in unwanted and detrimental effects.(Deng et al., 2010) Such effects are dependent on the size, shape, charge and surface characteristics of nanoparticles (Deng et al., 2010, Lynch et al., 2009, Deng et al., 2009). The type of interaction (i.e. direct cell interaction or indirect interaction after conjugation with other proteins) may also influence the effects observed.(Deng et al., 2010, Lynch et al., 2009) Binding of proteins to nanoparticles may result in disruption of protein structure, unfolding of proteins or aggregation of proteins.(Lynch and Dawson, 2008, Deng et al., 2010) It may also lead to unwarranted activation of cellular receptors, resulting in a variety of responses, depending on the particular nanoparticle-protein interaction.(Deng et al., 2010) Thus, proper characterization of nanoparticle-protein and nanoparticle-cell interactions must be performed before any nanoparticle can be deemed suitable for biomedical use.

The use of nanoparticles for *in-vivo* biomedical applications often involves their intravenous, intramuscular and intra-peritoneal injection. This can result in interaction of the particles with different components of the circulatory system including blood proteins, clotting factors, blood cells and components of the immune and allergy response system. Thus hematological toxicity of

nanoparticles is a very important part of its overall toxicological assessment. Hematological toxicity of nanoparticles has been extensively investigated in recent years. Reports suggest that manifestation of nanoparticle-induced hematological toxicity may vary and include increased or decreased cell counts (red and white blood cells), activation or inhibition of the immune response system, hemolysis, endothelial dysfunction and allergic responses. For example, gold nanoparticles(Zhang et al., 2011), depending on their size elicit an increase or decrease in red and blood cell count(Zhang et al., 2011). Iron oxide, Titanium dioxide, Silica and Carbon black nanoparticles have been shown to induce inflammation and endothelial dysfunction (Zhu et al., 2011, Montiel-Dávalos et al., 2012, Duan et al., 2013, Vesterdal et al., 2012). Zinc oxide nanoparticles have been shown to activate immune response(Adamcakova-Dodd et al., 2014). Polymeric nanoparticles have been shown to decrease histamine release(Tahara et al., 2012). Single walled carbon nanotube (SWCNT) dispersions, depending on their aggregation status, can induce either vaso-constrictory or vaso-dilatory responses in arterioles although exposure to the particles produced endothelial dysfunction in the arterioles(Frame et al., 2014).

Graphene based nanoparticles have shown promise for therapeutic drug delivery and imaging applications. Graphene (a.k.a graphene oxide or graphene nanoplatelets) synthesized from graphite using Hummers method (also known as graphene nanoplatelets) has been extensively investigated in vitro and in vivo. (Sun et al., 2008, Zhang et al., 2010) Studies have examined the *in vitro* cellular as well as hematological toxicity of this particular form of graphene.(Chang et al., 2011, Wang et al., 2011a, Chowdhury et al., 2013) We recently reported that dextran functionalized graphene nanoplatelets decrease histamine release from rat mast cells and shows 12-20% increase in complement activation at high concentrations (>7 mg/ml)(Chowdhury et al., 2013). However, graphene nanoplatelets, unlike SWCNTs, did not cause endothelial

dysfunction(Chowdhury et al., 2013, Frame et al., 2014). These and other studies on other carbon nanoparticles such as fullerenes and metallofullerenes(Lalawani and Sitharaman, 2013), indicate that structure, chemical composition (pristine, functionalized of carbon nanoparticles play an important role in their cellular interactions and associated hematotoxicity. Thus, structurally different carbon nanoparticles should be examined individually to better understand their specific hematotoxic responses.

Graphene nanoribbons (O-GNR) synthesized by oxidative unzipping of multiwalled carbon nanotubes(Kosynkin et al., 2009) have also recently shown promise for bio-imaging and drug delivery applications(Paratala et al., 2012, Chowdhury et al., 2014). These graphene nanoparticles are structurally different from graphene nanoplatelets (O-GNRs are more oxidized compared to graphene nanoplatelets) (Mullick Chowdhury et al., 2012, Mullick Chowdhury et al., 2014, Kosynkin et al., 2009). Also, the structure of O-GNR edges are different from graphene nanoplatelets due to the difference in the starting material.(Kosynkin et al., 2009) In Chapter 2, a detailed analysis of the cellular uptake and toxicity of water solubilized O-GNR (coated by PEG-DSPE and henceforth called O-GNR-PEG-DSPE) showed that they have a cell specific uptake and toxicity effect with high uptake and toxicity specifically in HeLa cells(Mullick Chowdhury et al., 2012). These results were significantly different from those that of graphite derived graphene showing that difference in source, structure and defects results in a difference in how these particles interact with different cells(Mullick Chowdhury et al., 2012). However, before *in vivo* toxicology and pharmacology studies on these nanoparticles are conducted, a thorough *in vitro* hematological toxicity assessment of these particles is necessary.

In this chapter, I report the effects of interaction of O-GNR-PEG-DSPE with red blood cells (RBC's) and other cellular and protein components of blood vascular system like binding to albumin, activation of platelets and complement system proteins, release of histamine from mast cells, cytokine release and interaction with endothelial cells. Knowledge of the specific effects of O-GNR-PEG-DSPE will provide an idea about potential toxicity issues with these particles and will also help choose a safe dose range for future biomedical applications.

3.2 Materials and Methods

3.2.1 O-GNR Synthesis

O-GNRs were synthesized from multi-walled carbon nanotubes (MWCNTs) (Sigma-Aldrich, Length=5-9 μm) using reported previously oxidative longitudinal unzipping method as reported in the last chapter.(Mullick Chowdhury et al., 2012, Kosynkin et al., 2009)
O-GNRs used in this study were characterized using Transmission Electron Microscopy.

3.2.2 Transmission Electron Microscopy

Samples for transmission electron microscopy were prepared by dispersing the O-GNR in 1:1 mixture of water/ethanol by bath sonication for 1 min followed by ultracentrifugation at 5000 rpm for 5 mins. The supernatant was dropped onto on formvar coated copper grids. The grids were then viewed with a Tecnai Bio Twin G transmission electron microscope (FEI, Hillsboro, OR), at 80 kV. Digital images were acquired using an XR-60 CCD digital camera system. (AMT, Woburn, MA)

3.2.3 Cell Culture

RBL-2H3 rat mast cells and Human umbilical vein endothelial cells) were obtained from ATCC (Manassas, VA, USA). RBL-2H3 cells and grown in minimum essential medium with sodium pyruvate, non-essential amino acids and supplemented with 15% fetal bovine serum.1% penicillin-streptomycin was used as antibiotic. Human umbilical vein endothelial cells were grown in F-12K medium supplemented with 10% FBS, 100μg/ml heparin and 30μg/ml endothelial cell growth supplement. Both cell lines were incubated at 37^{o}C in a humidified atmosphere of 5% CO_2, and 95% air.

3.2.4 Protein Binding

Pierce BCA protein assay kit was used to draw a standard curve for different concentrations (0-2 mg/ml) of Human serum albumin (HSA). HSA (2 mg/ml) was incubated with 10μg/ml and 80μg/ml O-GNR (no PEG-DSPE coating) and 10μg/ml and 80μg/ml O-GNR-PEG-DSPE on a shaker for 1 hour at 37 ^{o} C. Following the incubation all four samples were centrifuged at 3000 rpm for 30 minutes to pellet the O-GNR and O-GNR-PEG-DSPE along with any bound protein. The supernatant was collected and the concentration of proteins in the supernatant from each sample was estimated using Pierce BCA protein assay kit (Thermo Scientific, Waltham, MA) and the standard curve using a Evolution 300 UV-Vis spectrophotometer (Thermo Scientific, Waltham, MA).

3.2.5 Interaction with Red blood cells

1 ml human whole blood collected from a non-smoking male individual (obtained from Biochemed, Winchester, VA) and centrifuged at 2500 rpm for 10 minutes to separate red blood cells and plasma. The red blood cells were separated and diluted in 10 ml of phosphate buffered saline. 2 ml of the diluted red blood cells were incubated with 20μg/ml of O-GNR-PEG-DSPE or left untreated (control) on a shaker for 3 hours at 37^{o}C. At the end of three hours, cells were centrifuged at 2500 rpm for 5 minutes and fixed with 2.5% electron microscopy grade glutaraldehyde (Electron Microscopy Sciences, Hatford, PA) in 0.1 M PBS. After fixation, the red blood cells were placed in 2% osmium tetroxide in 0.1 M PBS, dehydrated using ethanol washes, and embedded in durcupan resin (Sigma-Aldrich, St. Louis, USA). The fixed and dehydrated red blood cells were blocked, cut into 80 nm ultra-thin sections using an Ultracut E microtome (Reichert-Jung, Cambridge, UK), and put on formvar-coated copper grids. The sections were then viewed with a Tecnai Bio Twin G transmission electron microscope (FEI, Hillsboro, OR), at 80 kV. Digital images were acquired using an XR-60 CCD digital camera system. (AMT, Woburn, MA)

3.2.6 Blood cell Hemolysis

A. Cell morphology analysis

1 ml whole human blood collected from a non-smoking male (obtained from BioChemed, Winchester, VA) was treated with 20μg/ml, 80μg/ml and 160μg/ml O-GNR-PEG-DSPE formulation or left untreated for 3 hours. The treated or untreated blood was centrifuged at 2500 rpm for 10 minutes to separate the blood cell components. 200μl of the blood cell component was poured into 2 ml of isotonic buffer, and 15 μl of the resultant solution was streaked and

fixed on a microscopic slide for imaging. The obtained slides were viewed under a bright-field microscope (Axiolab Microscope, Carl Zeiss, Thornwood, NY). Polyethyleneimine (PEI), a known hemolytic agent was used as negative positive control, and phosphate buffered saline treated normal blood was used as negative control.

B. Hemoglobin release analysis

Release of hemoglobin from ruptured or lysed red blood cells on exposure to various concentrations of O-GNR-PEG-DSPE was assessed by a method developed by McNeil *et al*(Dobrovolskaia et al., 2008) . Briefly 2 ml of whole blood (Biochemed, Winchester, VA) was centrifuged at 2500 rpm for 15 minutes, and red blood cells were separated out. The red blood cells obtained as a pellet was carefully resuspended in 5 ml of phosphate buffered saline. O-GNR-PEG-DSPE was added to the suspensions to reach concentrations of 20, 40, 80 and 160μg/ml and incubated for 3 hours. Following this step the mixture were centrifuged at 2500 rpm for 15 minutes and the supernatants were removed. Ferricyanide along with bicarbonate was added to the removed supernatant, and incubated for 5 minutes. The absorbance of the resultant mixture was measured at 540 nm using an Evolution 300 UV-VIS Spectrophotometer (Thermo Scientific, West Palm Beach, FL). Cells treated with PEG-DSPE alone were utilized as a negative control and cells treated with a known hemolytic agent Triton X 100 (1%) for 60 minutes were used as positive control.

3.2.7 Histamine release from mast cells

For this assay RBL-2H3 cells (10^4 cells per well in 48 well plates) were sensitized by pre-treatment with anti-2,4 dinitrophenyl (anti-DNP) IgE antibody (0.5 mg/ml) for 1 hour at 37^oC

following which the cells were treated with PEG-DSPE (1.2 mg/ml), O-GNR-PEG-DSPE (10, 20, 40 and 80μg/ml) and DNP-BSA (for inducing histamine release). Quantification of histamine release from RBL-2H3 cells treated with PEG-DSPE, O-GNR-PEG-DSPE and DNP-BSA was done using a histamine-O-pthalaldehyde (OPT) reaction which produces a fluorescent product. This assay procedure has been reported previously in detail by our group(Chowdhury et al., 2013). Briefly, in the first part of the assay, any histamine released from O-GNR-PEG-DSPE treated activated RBL-2H3 cells was collected into an organic phase from cell media treated with 0.4 N $HClO_4$. The histamine collected into the organic phase is then returned to aqueous phase. In the final step histamine in aqueous phase is conjugated with OPT to produce a complex with excitation at 360 nm and emission at 450 nm. The fluorescence intensity produced is directly proportional to the amount of histamine that has been released. The fluorescence of the histamine-OPT conjugate was assessed at 450 nm emission after excitation at 360 nm in a Cytofluor fluorescence multiwell plate reader (Series H4000 PerSeptive Biosystems, Framingham, MA).

3.2.8 Platelet activation

Immunoclone PF_4 (Platelet Factor 4) ELISA kit (American Diagnostic Inc, Stamford, CT) was used to assess platelet activation in terms of PF_4 levels in whole human blood after treatment with 20μg/ml, 40μg/ml and 80μg/ml O-GNR-PEG-DSPE. Briefly, 1 ml human whole blood collected from two non-smoking male individuals (hereafter called Blood sample 1 and Blood sample 2) (obtained from Biochemed, Winchester, VA) was treated with the three concentrations of O-GNR-PEG-DSPE or left untreated (control). The plasma from these untreated and treated samples was collected after centrifugation of the whole blood samples at 2500 rpm for 30 minutes. Plasma samples collected were diluted five times using sample diluents provided with

the kit. 0.2 ml of each plasma sample was incubated for 1 hour in anti-PF_4 coated wells following which each well was washed five times with 0.3 ml wash solution provided in the kit. Post washing 0.2 ml of anti PF4–Horse radish peroxidase (HRP) immunoconjugate was added to each well and incubated for 1 hour. Following this incubation the wells were washed again (5 times, using 0.3 ml wash solution each time). 0.2 ml of TMB substrate /peroxidase substrate (3, 3', 5, 5'-Tetramethylbenzidine) was then added to the wells for 5 minutes at room temperature and 50 µl of 0.45 M H_2SO_4 was added, and incubated for 10 minutes to terminate the reaction. Absorbance of each well was measured at 450 nm using a microwell plate reader (ELx 800, BIOTEK,Winooski, VT).

3.2.9 Activation of complement proteins

Microvue SC5b-9 and Bb plus ELISA kits (Quidel Corporation, San Diego, CA)was used to assess total complement activation and complement activation through the alternate pathway in whole human blood after treatment with 20µg/ml, 40µg/ml and 80µg/ml O-GNR-PEG-DSPE. Briefly, 1 ml human whole blood collected from two non-smoking male individuals (obtained from Biochemed, Winchester, VA) was treated with the three concentrations of O-GNR-PEG-DSPE or left untreated (control). The plasma from these untreated and treated samples was collected after centrifugation of the whole blood samples at 2500 rpm for 30 minutes. Plasma samples from blood sample 1 were diluted five times and from blood sample 2 were diluted 3 times using sample diluents provided with the kit.0.1 ml of diluted treated and control samples were incubated for 1 hour in each well of anti human SC5b 9/Bb coated micro well strip.

Following this step which each well was washed five times with 0.3 ml wash solution provided in the kit and 0.05 ml of anti SC5b9–HRP Immunoconjugate/Bb-HRP immunoconjugate was added to each well and incubated for 30 minutes. The wells were washed again (5 times, using 0.3 ml wash solution each time) and 0.1 ml of TMB substrate /peroxidase substrate (3, 3', 5, 5'-Tetramethylbenzidine) was added to the wells for 15 minutes at room temperature and 0.1ml of 0.45 M H_2SO_4 was added, and incubated for 10 minutes to terminate the reaction. Absorbance of each well was measured at 450 nm using a microwell plate reader (ELx 800, BIOTEK,Winooski, VT).

3.2.10 TNF-Alpha and IL-10 Release

Human TNF-Alpha and IL-10 ELISA kits (Invitrogen, Grand Island, NY) were used to assess cytokine release in terms of Tumor Necrosis Factor-Alpha and Interleukin-10 release in whole human blood after treatment with 20μg/ml, 40μg/ml and 80μg/ml O-GNR-PEG-DSPE. Briefly, 1 ml human whole blood collected from two non-smoking male individuals) (obtained from Biochemed, Winchester, VA) was treated with the three concentrations of O-GNR-PEG-DSPE or left untreated (control) for 1 hour. The whole blood samples and controls were centrifuged at 2500 rpm for 30 minutes and the plasma was collected from each. Wells coated with anti human TNF-Alpha/ Anti IL-10 antibody were prepared by adding 50ul of incubation buffer provided with the kit; 50ul of the plasma samples (from treated and control) were then transferred to the appropriate wells, and incubated at room temp for 2 hours. The wells were then aspirated and washed 4 times with wash buffer provided with the kit (0.3ml per well per wash). 0.1 ml of biotinylated anti-TNF-Alpha/IL-10 was then pipetted into the wells, and mixed. The wells were left to incubate at room temp for 2 hours. The wells were then aspirated and washed 4 times with

wash buffer provided with the kit. 0.1 ml of streptavidin-HRP working solution was added to the wells, and then left to incubate at room temp for 30 minutes. The wells are then aspirated and washed 4 times (0.3ml per well per wash). 0.1 of stabilized chromogen solution provided with the kit was then added to each well, then left to incubate at room temp for 30 minutes in the dark. 0.1ml of stop solution was added to the wells, and the wells were read using an Infinite M200 multiwell plate reader (Tecan Group, Morrisville, NC) at 450nm absorbance.

3.2.11 Effect on endothelial cells

A. TEM of endothelial cells exposed to O-GNR-PEG-DSPE

Six well plates with surfaces covered with ACLAR® film (Electron Microscopy Sciences, Hatford, PA) were plated with cells at a density of 6x 10^5 cells per plate, and exposed to 40 µg/ml O-GNR-PEG-DSPE for 12 hours. At the end of twelve hours, cells were fixed with 2.5% electron microscopy grade glutaraldehyde (Electron Microscopy Sciences, Hatford, PA) in 0.1 M PBS. After fixation, the films containing fixed cells were placed in 2% osmium tetroxide in 0.1 M PBS, dehydrated through graded ethanol washes, and embedded in durcupan resin (Sigma-aldrich, St. Louis, USA). Areas with high cell densities were blocked, cut into 80 nm ultra-thin sections using an Ultracut E microtome (Reichert-Jung, Cambridge, UK), and placed on formvar-coated copper grids. The sections were then viewed with a Tecnai Bio Twin G transmission electron microscope (FEI, Hillsboro, OR), at 80 kV. Digital images were acquired using an XR-60 CCD digital camera system. (AMT, Woburn, MA)

B. Cell Viability using Presto Blue Assay

Cell viability in terms of mitochondrial integrity, and overall cellular metabolism was measured by presto blue assay (Invitrogen, Grand Island, NY). Human umbilical vein endothelial cells were plated at 6 x 10^3 cells per well in 96 well plates, and incubated for 18 hours. Before commencing with the assay, old media was replaced with 150µl of fresh media in each well. 50µl of O-GNR PEG-DSPE stock solutions at various concentrations were added to every well for a final treatment concentration of 100µg/ml, 200µg/ml, 300µg/ml, 400µg/ml, 500µg/ml and 600µg/ml. The cells were incubated at 37^{o}C for 24 hours. After the 24 hr time point, media was removed, and wells were rinsed twice with Dulbecco's phosphate buffer saline (DPBS) before adding 100µl of fresh media, and 10µl of Presto Blue reagent. The plates were again incubated for 2 hours at 37^{o}C. Fluorescence readings of the wells were recorded using a Spectra Max M3 multimode microplate reader (Molecular Devices, Sunnyvale, CA) with excitation at 530 nm, and emission at 580 nm. Fluorescence reading for cells in the culture medium containing only PEG-DSPE was used for baseline correction. The cell viability in terms of % of control cells is expressed as the percentage of $(F_{test} - F_{blank})/(F_{control} - F_{blank})$, where F_{test} is the fluorescence of the cells exposed to nanoribbon sample, $F_{control}$ is the fluorescence of the unexposed control sample and F_{blank} is the fluorescence of the wells without any cells.

3.2.12 Statistical Analysis

All data are presented as mean+standard deviation. Student't' test was used to analyze the differences among groups. All statistical analyses were performed using a 95% confidence interval ($p < 0.05$).

3.3 Results

Characterization

3.3.1 Transmission Electron Microscopy

Figure 1 is a representative TEM image of graphene nanoribbon obtained after complete unzipping of a multi walled carbon nanotube. The size of the obtained nanoribbons varied from 500-1500 nm (n=15 particles).

3.3.2 Protein binding

Figure 2 shows the binding of human serum albumin to O-GNR without PEG-DSPE coating and O-GNR-PEG-DSPE at two different concentrations. Absorbance of the proteins in the supernatant of O-GNR without PEG-DSPE coating two thirds (~67%) lower than unexposed control protein at both 10μg/ml and 80μg/ml concentration. Coating with PEG-DSPE increases the concentration of proteins in the supernatant to ~50% lower than unexposed values for 80μg/ml and ~33% lower than unexposed values for the 10μg/ml concentration.

3.3.3 Interaction with Red blood cells

The effect of interaction of red blood cells with O-GNR-PEG-DSPE was evaluated through transmission electron microscopy images of cells treated with the nanoparticles. Figure 2A-D represents transmission electron microscopy images of red blood cells before and after

incubation with O-GNR-PEG-DSPE. Figure 2 E-H are illustrations representing corresponding TEM image of the RBC's (the red portion in each figure indicates the cross section showed on the corresponding TEM image). Figure 2A and 2E shows the cross section of an untreated blood cell used as control. Figure 2B and F shows a RBC interacting with O-GNR-PEG-DSPE (red arrows). The figure suggests that the RBC has lost its concave shape on the side where it interacts with the membrane. Figure 2C and G shows a RBC interacting with O-GNR-PEG-DSPE (red arrows) on the surface of the cells. The cross section shows complete loss of concave nature on one side and partial loss on the other side. Figure 2D and H shows a RBC interacting with O-GNR-PEG-DSPE on the membrane as well as surface of the cells (red arrows). The cross section shows complete loss in bi-concave nature and formation of circular cross section not characteristic of normal RBC's. Also, visible are protrusions from the red blood cell membrane (red arrows).

Figure 3 are transmission electron microscopy images showing the effects of O-GNR-PEG-DSPE interaction on the surface of RBC's. Figure 3A shows the direct interaction between the edges of O-GNR-PEG-DSPE and cell membrane (black arrows). Figure 3B and 3C also show the direct interaction between the edges of O-GNR-PEG-DSPE and cell membrane (black arrows). Membrane disintegration / ruffling is also observed at the sites (red arrows) in Figure 3B and C. Figure 3D shows direct interaction of multiple O-GNR-PEG-DSPE with the cell membrane (black arrows).A depression in the cell membrane at the site of interaction (red arrows) is observed in the same figure. Figure 3E and F show protrusions from RBC membrane near the sites where it interacts with O-GNR-PEG-DSPE (red arrows).

3.3.4 Blood cell Hemolysis

Figure 4 shows the effect of incubation of O-GNR-PEG-DSPE with RBC's on hemolysis of the cells analysed usingbright field optical microscopy and quantification of total hemoglobin released on treatment. Figure 4A-E are brightfield optical miscroscopy images of red blood cells treated with different concentrations of the nanoparticles. Figure 4A represents the untreated control cells (black arrows) and Figure 4B represents the lysed control cells (lysed with Triton x 100). Figure 4C, representing the RBC's treated with 20μg/ml O-GNR-PEG-DSPE shows mostly structurally unaltered cells (black arrows) with a few cells present that show change in shape (red arrows) (compared to 4A). Figure 4D, representing the RBC's treated with 80μg/ml O-GNR-PEG-DSPE showed presence of more cells with changed shape (red arrows). However, no lysed cells were observed for both concentrations. Figure 4E, which represents the RBC's treated with 160μg/ml O-GNR-PEG-DSPE, had the largest number of cells with changes in cell shape and dimensions (red arrows). Lysed cells were not observed at this concentration either. Figure 4F represents the quantification of hemoglobin released from RBC's exposed to various concentrations (0-160μg/ml) of O-GNR-PEG-DSPE. Results from the quantification of hemoglobin released showed very small increase at all treatment concentrations. The absorbance of the product (at 540 nm) obtained after treatment of released hemoglobin with ferricyannide (in presence of bicarbonate) showed a very small increase (from ~0.048 to ~0.08 for change of O-GNR-PEG-DSPE treatment concentration from 20μg/ml to 160μg/ml) indicating very little hemoglobin was released in the supernatants. In comparison, lysed RBCs (using Triton X 100) showed an absorbance of ~1.4 indicating a large amount of hemoglobin in the supernatant. Figure 4F represents one lysed RBC showing a disrupted membrane (red arrows) and O-GNR-

PEG-DSPE on the surface (black arrows). It should be noted that very few lysed cells were observed in transmission electron microcopy and brightfield images of RBC's treated with O-GNR-PEG-DSPE.

3.3.5 Mechanism of RBC membrane disruption

Figure 5 is a schematic showing the probable progressive steps through which O-GNR-PEG-DSPE induces structural changes in the red blood cells and the fate of the structurally modified cells. The figure shows the entire RBC as well as its cross section for each step. The figure shows that O-GNR-PEG-DSPE interacts with red blood cell membranes (black arrows) to alter their membrane integrity, which can be evidenced by membrane protrusions from the red blood cell membrane (green arrows). Complete disruption of the membrane integrity leads to formation of spherically shaped RBC's that are indentified and taken out of circulation by the reticuloendothelial (RES) system.

3.3.6 Effect on mast cells: Histamine release

Figure 6A shows the effect of O-GNR-PEG-DSPE treatment on histamine release from activated RBL-2H3 rat mast cells evaluated through the release of histamine from activated and induced RBL-2H3 cells and estimated using histamine-OPT reaction that produces a fluorescent conjugate. The results indicate that O-GNR-PEG-DSPE (tested upto 80μg/ml) did not induce an increase in histamine release compared to uninduced control. PEG-DSPE alone did not induce histamine release either. The positive control (i.e. DNP-BSA) treated cells showed a ~40% increase in histamine release compared to untreated control.

3.3.7 Effect on platelets: PF_4 release

Figure 6B represents the effects of O-GNR-PEG-DSPE treatment on platelet activation in two different samples of whole human blood evaluated in terms of PF_4 levels in the blood post nanoparticle treatment. The PF_4, a heparin binding and deactivating protein is the most abundant protein found in platelets. It is released into the plasma once platelets are activated. Hence PF_4 concentration in plasma is an efficient marker for platelet activation in blood. The figure shows that there was no statistically significant change in PF_4 levels on treatment with the three concentrations of O-GNR-PEG-DSPE.

3.3.8 Interaction with complement proteins

Figure 6 C and D represents the total complement activation in terms of SC5b9 protein levels in plasma, and alternate pathway activation in terms of Bb protein levels in plasma, on treatment of whole human blood from two individuals with increasing concentrations of O-GNR-PEG-DSPE. All forms of complement activation lead to formation of SC5b9 and hence it is considered an excellent marker for analysis of total complement activation. Bb protein is an activation product specific for activation of the alternate pathway. Figure 6B shows that there was no significant change in the levels of Bb protein in blood for all the treatment concentrations of O-GNR-PEG-DSPE. Figure 6D shows that concentrations upto 80μg/ml of O-GNR-PEG-DSPE did not significantly alter the levels of SC5b9 in blood of both individuals.

3.3.9 Effect on macrophages and monocytes: TNF-Alpha and IL-10 Release

Figure 6 E and F represents the release of TNF – Alpha and IL-10 respectively from whole human blood of two individuals treated or not treated with O-GNR-PEG-DSPE. Figure 6E shows that there is no significant difference in the release of TNF–Alpha from untreated or

treated cells in both blood samples. Figure 6F shows that there is a decrease in IL-10 release (by ~5-7%) for blood sample 1 and (~8-10%) for blood sample 2 on exposure to all concentrations of O-GNR-PEG-DSPE.

3.3.10 TEM of endothelial cells exposed to O-GNR-PEG-DSPE

Figure 7 A-D are representative transmission electron microscopy images of Human umbilical vein endothelial cells treated with O-GNR-PEG-DSPE for 12 hours. Figure 7A shows O-GNR-PEG-DSPE aggregates (red arrow) near the cell membrane (yellow arrow). Membrane protrusions (blue arrow) from the cells can also be observed. Figure 7B shows O-GNR-PEG-DSPE aggregates (red arrow) being uptaken through membrane protrusions (cell membrane indicated with yellow arrows and protrusions indicated with blue arrows). Figure 7C and D shows Human umbilical vein endothelial cells with vesicles (black arrows) containing uptaken O-GNR-PEG-DSPE aggregates (red arrows). The cell membrane is indicated with yellow arrow.

3.3.11 Cell Viability using Presto Blue Assay

Figure 7E shows the viability of Human umbilical vein endothelial cells treated with different concentrations of O-GNR-PEG-DSPE (0-600µg/ml) evaluated using the presto blue assay. The results obtained show a concentration dependent decrease in cell viability. Treatment of Human umbilical vein endothelial cells with the two lowest concentrations of O-GNR-PEG-DSPE tested (100-200µg/ml) resulted in a decrease in viability by 15-18%. Treatment of Human umbilical vein endothelial cells with the two highest concentration of O-GNR-PEG-DSPE tested (500-600µg/ml) resulted in a decrease in cell viability by 32-40%.

3.4 Discussion

The aim of this study was to investigate the interaction between graphene nanoribbons and the cellular and protein components of the blood vascular system. Graphene nanoribbons, synthesized from MWCNT vary in dimensions depending on the size of the starting material (i.e. MWCNT) and the time of oxidation(Kosynkin et al., 2009). Our group has previously shown that graphene nanoribbons can vary in size between 500-1500 nm(Mullick Chowdhury et al., 2012). Representative TEM images (Figure 1) shows graphene nanoribbons of size ~1.5 µm obtained from unzipping of MWCNT varying in size between 5-9 µm. Figure 1A also shows the ribbon like morphology of the unzipped nanotubes.

Graphene nanoparticles, due to their inherent hydrophobicity have been difficult to get into aqueous suspension. Also, graphene particles have been shown to interact with and attach to proteins, making it difficult for use in biomedical applications involving intravenous injections(Tan et al., 2013). As such, researchers have used hydrophilic groups to functionalize graphene particles before using them for biomedical applications (Tan et al., 2013, Sun et al., 2008, Wang et al., 2011b, Liu et al., 2008). Recently, our group has shown that non-covalent functionalization of graphene nanoribbons with DSPE-PEG (forming O-GNR-PEG-DSPE) increases their stability in aqueous suspensions(Mullick Chowdhury et al., 2012).

Almost immediately after injection into the blood stream, nanoparticles come in contact with the repertoire of proteins in blood resulting in the formation of a “corona” of proteins around the particles. Reports also show that proteins bound on nanoparticle surface influence their biodistribution and uptake into immune competent and phagocytotic cells. Thus, the protein composition of the corona will influence the toxicological effects observed. To neutralize the

protein binding, (especially in charged nanoparticles which bind more proteins compared to neutral nanoparticles) nanoparticles are often functionalized with hydrophilic polymers like PEG.

The PEG-DSPE functionalization of O-GNR showed a concentration dependent decrease in interactions between albumin (the most abundant protein in blood) and nanoribbons (Figure 1B). However, on PEG-DSPE functionalization the protein-O-GNR binding could be decreased, but not completely eliminated (Figure 1B).

Due to the dynamics of blood flow, O-GNR-PEG-DSPE, once injected intravenously will come in contact with the red blood cells (RBC) (which are the most abundant cells in blood). RBC's are devoid of nucleus and are characterized by their bi-concave shape(Zarda et al., 1977). Maintenance of the bi-concave shape is essential for movement of red blood cells through blood vessels and capillaries(Zarda et al., 1977). The RBC membrane is supported by a cytoskeleton made up of spectrin, actin and ancillary proteins (ankyrin, protein 4.1 etc) that support the bi-concave shape(Agre and Parker, 1989). Analysis of cross section of RBC's using TEM before and after interaction of the cells with O-GNR-PEG-DSPE showed that the particles can deform the RBC biconcave structure (Figure 2). Post 3 hour incubation with the O-GNR-PEG-DSPE particles, red blood cells, which interacted with the particles (evidenced by presence of O-GNR-PEG-DSPE on the membrane or inside the cells) showed either loss of biconcave structure on one side (Figure 2B and Figure 2C) or complete loss of biconcave structure (Figure 2D). On loss of biconcave structure the RBC's formed cells which are similar to spherocytes i.e spherical red blood cells(Peters and Lux, 1993). Spherocytes are considered abnormal cells and removed from circulation by the reticulo endothelial system(Wiley, 1970). Detailed analysis of the interaction between the RBC membrane and O-GNR-PEG-DSPE showed that most interactions took place

on the cell membrane with sharp edges interacting with the membrane directly (Figure 3A). It is possible that the sharp edges from O-GNR-PEG-DSPE interact directly with the cytoskeleton and disrupt its structure. This can be evidenced from the observation of ruffling/disintegration around the area in the membrane where O-GNR-PEG-DSPE interacts with the cell (Figure 3B-C). Also, in some cases depression of the cell membrane was observed at the site of interaction (Figure 3D). Disruption of the cellular cyto-skeletal architecture may take place by several other mechanisms also. For example, graphene nanoparticles are hydrophobic in nature and recently polymer nanoparticles have been shown to disrupt RBC structure due to their hydrophobicity (Shima et al., 2014). Recently, our group has also shown that O-GNR-PEG-DSPE can interact with and activate EGF receptors(Mullick Chowdhury et al., 2014). Although RBC's do not express EGFR, it is possible that O-GNR-PEG-DSPE is interacting with some essential proteins in the cytoskeleton (like protein 4.1, spectrin, actin or ankyrin) and modulating its activity (through modifications like phosphorylation) to show the effects observed(Manno et al., 2005, Eder et al., 1986). The membrane dynamics of RBC's are usually very tightly regulated and extensions from /fragementation of the membrane surface is not observed due to the rigid cyto-skeletal structure(Banerjee et al., 1998). As such membrane extensions from RBC's imply a breakdown in cyto-skeletal structure. Such extensions were observed near the area of the membrane where RBC's interacted with O-GNR-PEG-DSPE (Figure 3E-F), implying cyto-skeletal disruption or membrane fragmentation characteristic of spherocyte formation (Jacob, 1969).

Membrane penetration and cyto-skeletal disruption can lead to hemolysis (Barshtein et al., 2011). In two recent studies, graphene nanoparticles and MWCNT's have been shown to induce hemolysis by disrupting the cell membrane(Meng et al., 2012, Liao et al., 2011). Our group has

previously shown that functionalization of graphene nanoplatelets with dextran can mitigate the observed hemolysis in graphene(Chowdhury et al., 2013). Brightfield images of RBC's exposed to O-GNR-PEG-DSPE showed a concentration dependent increase in the number of deformed cells, further proving that interaction with O-GNR-PEG-DSPE leads to disruption in RBC structure (Figure 4A-E). However, very few lysed cells were observed (on comparison with Triton x 100 treated cells) showing that although cells change in shape there is no cell lysis (Figure 4A-E). This was further proved by quantification of hemoglobin released on treatment of cells with O-GNR-PEG-DSPE. Very small increase in hemoglobin release was observed, even for cells treated with upto 160µg/ml O-GNR-PEG-DSPE (Figure 4F). Although rare, TEM of cells exposed to O-GNR-PEG-DSPE showed evidence of a few hemolysed cells (Figure 4G is provided as a representative).

From the data obtained through TEM and hemolysis studies it can be predicted that binding of O-GNR-PEG-DSPE to RBC's leads to cyto-skeletal disruption either due to the hydrophobic interactions of the particles with membrane, direct rupture of cyto-skeletal elements or changes in molecular level (e.g. unwanted phosphorylation of proteins that lead to structural disintegration of the cytoskeleton). The cyto-skeletal disruption leads to loss of biconcave shape of the RBC's leading to the gradual formation of spherocyte like structures (Figure 5) Also, membrane extensions from RBC's can be observed due to the disrupted cytoskeleton or membrane fragmentation. Cross section of RBC's shows the change from biconcave to round spherocyte structures (Figure 5). However, lysis of the spherocytes does not take place. Sperocytes are considered unfit for circulation and are generally removed by macrophages of the the reticulo-endothelial system. We assume the round cells produced after interaction of RBC's

with O-GNR-PEG-DSPE is removed by a similar mechanism without lysis in circulation (Figure 5).

Since interaction of red blood cells with O-GNR-PEG-DSPE causes changes in the structure of RBC's it was essential to see if interaction with other blood cells and proteins could cause any detrimental effects. Although, the chances of interaction of O-GNR-PEG-DSPE with other blood cells (white blood cells, platelets) and proteins (complement proteins) would be lower than RBC's (as total volume of RBC's in blood is much higher compared to the other cells and proteins), these cells dictate functioning of the immunity and allergen response system.

Release of histamine is the major allergen response system in the human body(Akdis and Blaser, 2003). It is a bioactive amine that once released can interact with receptors on cells of different tissues to produce different physiological and pathological effects(Weiss et al., 1932). Histamine is stored as granules in circulating basophils and mast cells that need to be activated (through immunoglobulin E) and induced by an allergen before they can release the stored histamine through de-granulation(Dvorak and Galli, 1987). Interaction of some nanoparticles with mast cells has been reported to activate histamine release leading to an allergen response(Chen et al., 2012). Very few studies have studied the effects of graphene structures on histamine release. Recently, it has been reported by our group that exposure of dextran coated graphene oxide nano-platelets to both mast cells and human blood results in decreased histamine release compared to unexposed controls(Chowdhury et al., 2013). Since structurally O-GNR-PEG-DSPE is significantly different from nanoplatelets it is essential to understand the effects of O-GNR-PEG-DSPE interaction on histamine release from mast cells. Our results show that upto 80μg/ml O-GNR-PEG-DPE does not induce histamine release on exposure to rat mast cells. This result

indicates that different graphene structures can produce different effects on exposure to the same cells or tissues.

Platelets in blood circulate in their inactive form and are activated through breakage or disruption in the endothelium of blood vessels(Gresele et al., 2003). Activation of platelets ultimately leads to the clotting of blood at the site of endothelium breakage(Gresele et al., 2003). Foreign particles in blood might lead to activation as well by interacting directly with the platelets and inducing their activation cascade(Radomski et al., 2005). Carbon based nanoparticles like single and multiwalled carbon nanotubes and graphene nanoplatelets have been previously shown to activate blood platelets leading to platelet aggregation and formation on clots(Meng et al., 2012, Semberova et al., 2009, Singh et al., 2011). Clots formed without breakage in endothelium might result in blockage of blood flow through the vessel and hence may prove fatal(WU and HOAK, 1975). However, exposure of O-GNR-PEG-DSPE concentrations (upto 80µg/ml) did not significantly alter the level of activation of platelets in whole human blood. This indicates that interaction of platelets does not induce the activation cascade in platelets.

Activation of the complement proteins in blood is an important biocompatibility test for most materials to be used for biomedical applications(Nilsson et al., 2007). The complement system represents a set of multiple proteins that are involved in the immunological response to foreign bodies or antigens(Nilsson et al., 2007). The three main pathways involved in complement activation are the classical pathway (where antigen antibody complexes are formed that lead to a cascade of protein cleavage reactions resulting in the activation of the complement system), alternate pathway (which does not involve formation of antigen antibody complex but spontaneous activation of the protein cleavage reactions in response to the antigen) and the lectin pathway (which is initiated by mannose binding lectin binding to antigens)(Nilsson et al., 2007).

Biomaterials once injected *in-vivo* usually trigger the alternate or lectin pathway but do not usually affect the classical pathway(Nilsson et al., 2007). Multiple nanoparticles have been shown to activate the complement system, resulting in hypersensitivity reactions that are common in case of unwanted activation of complement system. For example, pegylated single walled carbon nanotubes have been reported to activate the complement system through the lectin pathway(Hamad et al., 2008) and pegylated Doxil® liposomal nanoparticles activate the alternate pathway(Chanan-Khan et al., 2003). This indicates that irrespective of biocompatible coating, different nanoparticles may activate the complement pathway through different mechanisms depending on their structure. Recently, our group has shown that dextran functionalized graphene nanoplatelets shows small increase in complement activation (12-20%). Our results show that O-GNR-PEG-DSPE does not induce activation of any form of the complement system in the two blood samples tested. This indicates that interaction of the O-GNR-PEG-DSPE particles with the complement proteins does not result in induction of the protein cleavage cascade. This is probably due to the PEG-DSPE coating present which decreases such activation inducing interactions.

Macrophages and monocytes are part of the immune system that along with their role of phagocytosis also regulate the release of pro-inflammatory or anti-inflammatory cytokines in response to a pathogen or irritant(Schutte et al., 2009). Normally, a balance between pro and anti-inflammatory cytokines is maintained in the body(Barton, 2008). On encountering an antigen, the balance is shifted either towards pro-inflammatory or anti-inflammatory cytokines depending on the type of antigen encountered with a simultaneous decrease in the other kind of cytokine(Barton, 2008). Thus, a change in the equilibrium would mean the macrophages or monocytes have been activated to release these cytokines. Incubation with O-GNR-PEG-DSPE

did not lead to an increase in TNF-Alpha release (a pro-inflammatory cytokine) in whole blood (Figure 6E). However, a small decrease in IL-10 (an anti-inflammatory cytokine) release (by 5-10%) was observed (Figure 6F). However, calculation of total protein content from absorbance readings and standard curve provided with the kit showed that the concentration of IL-10 (~1 pg/ml) for both control and treated blood samples was within the normal limits (< 3 pg/ml).

Intravenous injection of O-GNR-PEG-DSPE would mean that injected particles will come in contact with endothelial cells lining the blood vessels. Once injected, the endothelial cells at the site of injection would be subject to several times higher concentration of O-GNR-PEG-DSPE compared to the steady state concentration in blood achieved after several passes through the circulatory system.(Frame et al., 2014, Chowdhury et al., 2013) Thus, it is essential to evaluate the toxicity of these particles on endothelial cells. To this end, we treated Human Umbilical Vein Endothelial cells with O-GNR-PEG-DSPE. Direct exposure of particles does not mimic the actual situation where O-GNR-PEG-DSPE will flow (along with the blood) over these cells. However, it would give us an idea about endothelial cell-GNR-PEG-DSPE interaction, and the concentration of the particles that is toxic to endothelial cells. Results showed that the endothelial cells can take up large amounts these O-GNR-PEG-DSPE aggregates into vesicular structures by producing cell membrane protrusions (Figure 7 A-D). Also, a concentration of treatment dependent decrease in cell viability was observed (Figure 7E). The toxicity observed might be due to the high uptake of O-GNR-PEG-DSPE. Formation of large number of uptake vesicles (as seen in the TEM images) might affect the regular functioning of cell organelles resulting in the observed concentration depend toxicity. However, the CD_{50} of O-GNR-PEG-DSPE was much higher than the largest concentration of O-GNR-PEG-DSPE tested (600µg/ml) (Figure 7E). Although, the lowest concentration tested (100µg/ml) produced a ~15% decrease in

viability treatment of the cells compared to untreated controls increasing the treatment concentration by 500µg/ml decreased the cell viability by ~25% more only.

3.5 Conclusion

In conclusion, results from this study suggest that O-GNR-PEG-DSPE can interact with red blood cells in circulation to alter their structural integrity. However, this change in structural integrity does not cause red blood cell hemolysis under non flow conditions. Hemolysis of the structurally altered RBC's under flow conditions after treatment with the nanoparticles will require further investigation. O-GNR-PEG-DSPE does not affect histamine release from mast cells, PF4 activation in platelets and does not induce complement activation. However, a small decrease in anti-inflammatory cytokine levels was observed. Treatment of endothelial cells with O-GNR-PEG-DSPE showed high uptake of these particles in endothelial cells. This opens avenues for development of these particles as agents for drug or gene delivery to endothelial cells. However, with increasing concentration, a decrease in endothelial cell viability was observed probably due to the inhibition of the normal cell processes by uptaken O-GNR-PEG-DSPE.

Contribution: Justin Fang has contribution in the data presented in this chapter.

3.6 References

Adamcakova-Dodd, A., Stebounova, L. V., Kim, J. S., Vorrink, S. U., Ault, A. P., T O'Shaughnessy, P., Grassian, V. H. & Thorne, P. S. 2014. Toxicity assessment of zinc oxide nanoparticles using sub-acute and sub-chronic murine inhalation models. *Particle and fibre toxicology,* 11**,** 15.

Agre, P. & Parker, J. C. 1989. *Red blood cell membranes: structure, function, clinical implications*, CRC Press.

Akdis, C. A. & Blaser, K. 2003. Histamine in the immune regulation of allergic inflammation. *Journal of allergy and clinical immunology,* 112**,** 15-22.

Banerjee, R., Nageshwari, K. & Puniyani, R. 1998. The diagnostic relevance of red cell rigidity. *Clinical hemorheology and microcirculation,* 19**,** 21-24.

Barshtein, G., Arbell, D. & Yedgar, S. 2011. Hemolytic Effect of Polymeric Nanoparticles: Role of Albumin. *NanoBioscience, IEEE Transactions on,* 10**,** 259-261.

Barton, G. M. 2008. A calculated response: control of inflammation by the innate immune system. *The Journal of clinical investigation,* 118**,** 413.

Chanan-Khan, A., Szebeni, J., Savay, S., Liebes, L., Rafique, N., Alving, C. & Muggia, F. 2003. Complement activation following first exposure to pegylated liposomal doxorubicin (Doxil®): possible role in hypersensitivity reactions. *Annals of oncology,* 14**,** 1430-1437.

Chang, Y., Yang, S.-T., Liu, J.-H., Dong, E., Wang, Y., Cao, A., Liu, Y. & Wang, H. 2011. In vitro toxicity evaluation of graphene oxide on A549 cells. *Toxicology letters,* 200**,** 201-210.

Chen, E. Y., Garnica, M., Wang, Y.-C., Mintz, A. J., Chen, C.-S. & Chin, W.-C. 2012. A mixture of anatase and rutile TiO 2 nanoparticles induces histamine secretion in mast cells. *Particle and fibre toxicology,* 9**,** 2-2.

Chowdhury, S. M., Kanakia, S., Toussaint, J. D., Frame, M. D., Dewar, A. M., Shroyer, K. R., Moore, W. & Sitharaman, B. 2013. In Vitro Hematological and In Vivo Vasoactivity Assessment of Dextran Functionalized Graphene. *Scientific reports,* 3.

Chowdhury, S. M., Mannepalli, P. & Sitharaman, B. 2014. Graphene Nanoribbons Elicit Cell Specific Uptake and Delivery Via Activation of Epidermal Growth Factor Receptor Enhanced by Human PapillomaVirus E5 Protein. *Acta Biomaterialia*.

Deng, Z. J., Liang, M., Monteiro, M., Toth, I. & Minchin, R. F. 2010. Nanoparticle-induced unfolding of fibrinogen promotes Mac-1 receptor activation and inflammation. *Nature nanotechnology,* 6**,** 39-44.

Deng, Z. J., Mortimer, G., Schiller, T., Musumeci, A., MARTIN, D. & MINCHIN, R. F. 2009. Differential plasma protein binding to metal oxide nanoparticles. *Nanotechnology,* 20**,** 455101.

Dobrovolskaia, M. A., Clogston, J. D., Neun, B. W., Hall, J. B., Patri, A. K. & McNeil, S. E. 2008. Method for analysis of nanoparticle hemolytic properties in vitro. *Nano letters,* 8**,** 2180-2187.

Duan, J., Yu, Y., LI, Y., YU, Y., LI, Y., Zhou, X., Huang, P. & Sun, Z. 2013. Toxic effect of silica nanoparticles on endothelial cells through DNA damage response via Chk1-dependent G2/M checkpoint. *PloS one,* 8**,** e62087.

Dvorak, A. & Galli, S. 1987. Antigen-induced, IgE-mediated degranulation of cloned immature mast cells derived from normal mice. *The American journal of pathology,* 126**,** 535.

Eder, P. S., Soong, C. J. & Tao, M. 1986. Phosphorylation reduces the affinity of protein 4.1 for spectrin. *Biochemistry,* 25**,** 1764-1770.

Fischer, H. C. & Chan, W. C. 2007. Nanotoxicity: the growing need for< i> in vivo</i> study. *Current opinion in Biotechnology,* 18**,** 565-571.

Frame, M. D., Dewar, A. M., Mullick Chowdhury, S. & Sitharaman, B. 2014. Vasoactive effects of stable aqueous suspensions of single walled carbon nanotubes in hamsters and mice. *Nanotoxicology,* 8**,** 867-875.

Gresele, P., Page, C., Fuster, V. & Vermylen, J. 2003. Platelets in Thrombotic and Non-Thrombotic Disorders. *Transfusion Medicine,* 13**,** 57-58.

Hamad, I., Christy Hunter, A., Rutt, K. J., Liu, Z., Dai, H. & Moein MoghimI, S. 2008. Complement activation by PEGylated single-walled carbon nanotubes is independent of C1q and alternative pathway turnover. *Molecular immunology,* 45**,** 3797-3803.

Jacob, H. S. 1969. The defective red blood cell in hereditary spherocytosis. *Annual review of medicine,* 20**,** 41-61.

Kosynkin, D. V., Higginbotham, A. L., Sinitskii, A., Lomeda, J. R., Dimiev, A., Price, B. K. & Tour, J. M. 2009. Longitudinal unzipping of carbon nanotubes to form graphene nanoribbons. *Nature,* 458**,** 872-876.

Lalwani, G. & Sitharaman, B. 2013. Multifunctional fullerene-and metallofullerene-based nanobiomaterials. *Nano Life,* 3.

Liao, K.-H., Lin, Y.-S., Macosko, C. W. & Haynes, C. L. 2011. Cytotoxicity of graphene oxide and graphene in human erythrocytes and skin fibroblasts. *ACS applied materials & interfaces,* 3**,** 2607-2615.

Liu, Z., Robinson, J. T., Sun, X. & Dai, H. 2008. PEGylated nanographene oxide for delivery of water-insoluble cancer drugs. *Journal of the American Chemical Society,* 130**,** 10876-10877.

Lynch, I. & Dawson, K. A. 2008. Protein-nanoparticle interactions. *Nano Today,* 3**,** 40-47.

Lynch, I., Salvati, A. & Dawson, K. A. 2009. Protein-nanoparticle interactions: what does the cell see? *Nature nanotechnology,* 4**,** 546-547.

Manno, S., Takakuwa, Y. & Mohandas, N. 2005. Modulation of erythrocyte membrane mechanical function by protein 4.1 phosphorylation. *Journal of Biological Chemistry,* 280**,** 7581-7587.

Meng, J., Cheng, X., Liu, J., Zhang, W., Li, X., Kong, H. & Xu, H. 2012. Effects of Long and Short Carboxylated or Aminated Multiwalled Carbon Nanotubes on Blood Coagulation. *PloS one,* 7**,** e38995.

Montiel-Dávalos, A. L., Ventura-Gallegos, J. L., Alfaro-Moreno, E., Soria-Castro, E., García-Latorre, E., Cabañas-Moreno, J. G., Ramos-Godinez, M. A. D. P. & López-Marure, R. 2012. TiO2 nanoparticles induce dysfunction and activation of human endothelial cells. *Chemical research in toxicology,* 25**,** 920-930.

Mullick Chowdhury, S., Lalwani, G., Zhang, K., Yang, J. Y., Neville, K. & Sitharaman, B. 2012. Cell specific cytotoxicity and uptake of graphene nanoribbons. *Biomaterials.*

Mullick Chowdhury, S., Manepalli, P. & Sitharaman, B. 2014. Graphene Nanoribbons Elicit Cell Specific Uptake and Delivery Via Activation of EGFR Enhanced by HPVE5 *Acta Biomaterialia,* (under review).

Nilsson, B., Ekdahl, K. N., Mollnes, T. E. & Lambris, J. D. 2007. The role of complement in biomaterial-induced inflammation. *Molecular immunology,* 44**,** 82-94.

Paratala, B. S., Jacobson, B. D., Kanakia, S., Francis, L. D. & Sitharaman, B. 2012. Physicochemical characterization, and relaxometry studies of micro-graphite oxide, graphene nanoplatelets, and nanoribbons. *PloS one,* 7**,** e38185.

Peters, L. & Lux, S. Ankyrins: structure and function in normal cells and hereditary spherocytes. Seminars in hematology, 1993. 85.

Radomski, A., Jurasz, P., Alonso-Escolano, D., Drews, M., Morandi, M., Malinski, T. & Radomski, M. W. 2005. Nanoparticle-induced platelet aggregation and vascular thrombosis. *British journal of pharmacology,* 146**,** 882-893.

Schutte, R. J., Parisi-Amon, A. & Reichert, W. M. 2009. Cytokine profiling using monocytes/macrophages cultured on common biomaterials with a range of surface chemistries. *Journal of Biomedical Materials Research Part A,* 88**,** 128-139.

Semberova, J., De Paoli Lacerda, S. H., Simakova, O., Holada, K., Gelderman, M. P. & Simak, J. 2009. Carbon nanotubes activate blood platelets by inducing extracellular Ca2+ influx sensitive to calcium entry inhibitors. *Nano letters,* 9**,** 3312-3317.

Shima, F., Akagi, T. & Akashi, M. 2014. The role of hydrophobicity in the disruption of erythrocyte membrane by nanoparticles composed of hydrophobically modified poly (γ-glutamic acid). *Journal of Biomaterials Science, Polymer Edition,* 25**,** 203-210.

Singh, S. K., Singh, M. K., Nayak, M. K., Kumari, S., Shrivastava, S., Grácio, J. J. & Dash, D. 2011. Thrombus inducing property of atomically thin graphene oxide sheets. *ACS nano,* 5**,** 4987-4996.

Sun, X., Liu, Z., Welsher, K., Robinson, J. T., Goodwin, A., Zaric, S. & Dai, H. 2008. Nano-graphene oxide for cellular imaging and drug delivery. *Nano research,* 1**,** 203-212.

Tahara, K., Tadokoro, S., Yamamoto, H., Kawashima, Y. & Hirashima, N. 2012. The suppression of IgE-mediated histamine release from mast cells following exocytic exclusion of biodegradable polymeric nanoparticles. *Biomaterials,* 33**,** 343-351.

Tan, X., Feng, L., Zhang, J., Yang, K., Zhang, S., Liu, Z. & Peng, R. 2013. Functionalization of Graphene Oxide Generates a Unique Interface for Selective Serum Protein Interactions. *ACS applied materials & interfaces,* 5**,** 1370-1377.

VesterdaL, L. K., Mikkelsen, L., Folkmann, J. K., Sheykhzade, M., Cao, Y., RoursgaarD, M., Loft, S. & Møller, P. 2012. Carbon black nanoparticles and vascular dysfunction in cultured endothelial cells and artery segments. *Toxicology letters,* 214**,** 19-26.

Wang, K., Ruan, J., Song, H., Zhang, J., Wo, Y., Guo, S. & Cui, D. 2011a. Biocompatibility of graphene oxide. *Nanoscale Res Lett,* 6.

Wang, Y., Li, Z., Wang, J., Li, J. & Lin, Y. 2011b. Graphene and graphene oxide: biofunctionalization and applications in biotechnology. *Trends in biotechnology,* 29**,** 205-212.

Weiss, S., Robb, G. P. & Ellis, L. B. 1932. The systemic effects of histamine in man: with special reference to the responses of the cardiovascular system. *Archives of Internal Medicine,* 49**,** 360.

Wiley, J. S. 1970. Red cell survival studies in hereditary spherocytosis. *Journal of Clinical Investigation,* 49**,** 666.

Wu, K. K. & Hoak, J. C. 1975. Increased platelet aggregates in patients with transient ischemic attacks. *Stroke,* 6**,** 521-524.

Zarda, P., Chien, S. & Skalak, R. 1977. Elastic deformations of red blood cells. *Journal of biomechanics,* 10**,** 211-221.

Zhang, L., Xia, J., Zhao, Q., Liu, L. & Zhang, Z. 2010. Functional graphene oxide as a nanocarrier for controlled loading and targeted delivery of mixed anticancer drugs. *Small,* 6**,** 537-544.

Zhang, X.-D., Wu, D., Shen, X., Liu, P.-X., Yang, N., Zhao, B., Zhang, H., Sun, Y.-M., Zhang, L.-A. & Fan, F.-Y. 2011. Size-dependent in vivo toxicity of PEG-coated gold nanoparticles. *International journal of nanomedicine,* 6**,** 2071.

Zhu, M.-T., Wang, B., Wang, Y., Yuan, L., Wang, H.-J., Wang, M., Ouyang, H., Chai, Z.-F., Feng, W.-Y. & Zhao, Y.-L. 2011. Endothelial dysfunction and inflammation induced by iron oxide nanoparticle exposure: Risk factors for early atherosclerosis. *Toxicology letters,* 203**,** 162-171.

3.6 Figures

Figure 1

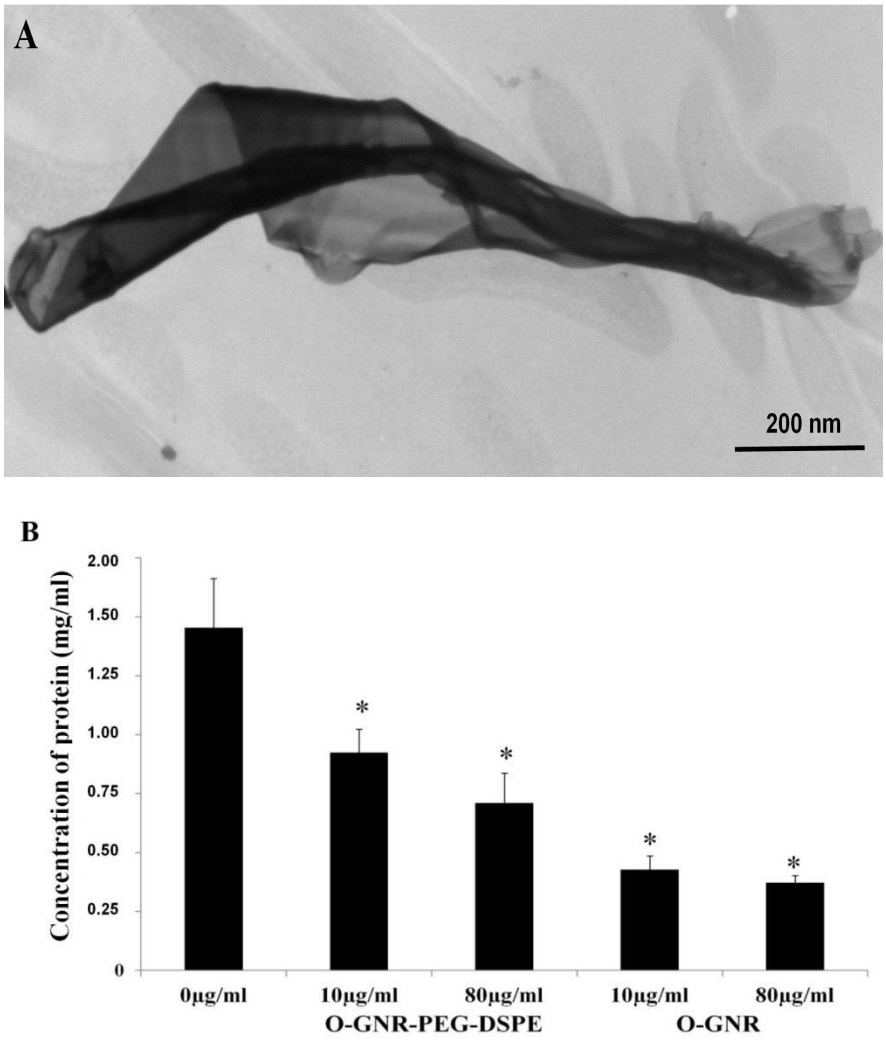

Figure 1 (A) Representative image of GNR-PEG-DSPE nanoparticle formed on unzipping of a MWCNT **(B)** Concentration of human serum albumin in the supernatant of O-GNR and O-GNR-PEG-DSPE (at 10µg/ml and 80µg/ml) treated protein solution centrifuged for 30 minutes at 3000 rpm. Concentration of the untreated but centrifuged control protein solution is provided as a reference.

Figure 2

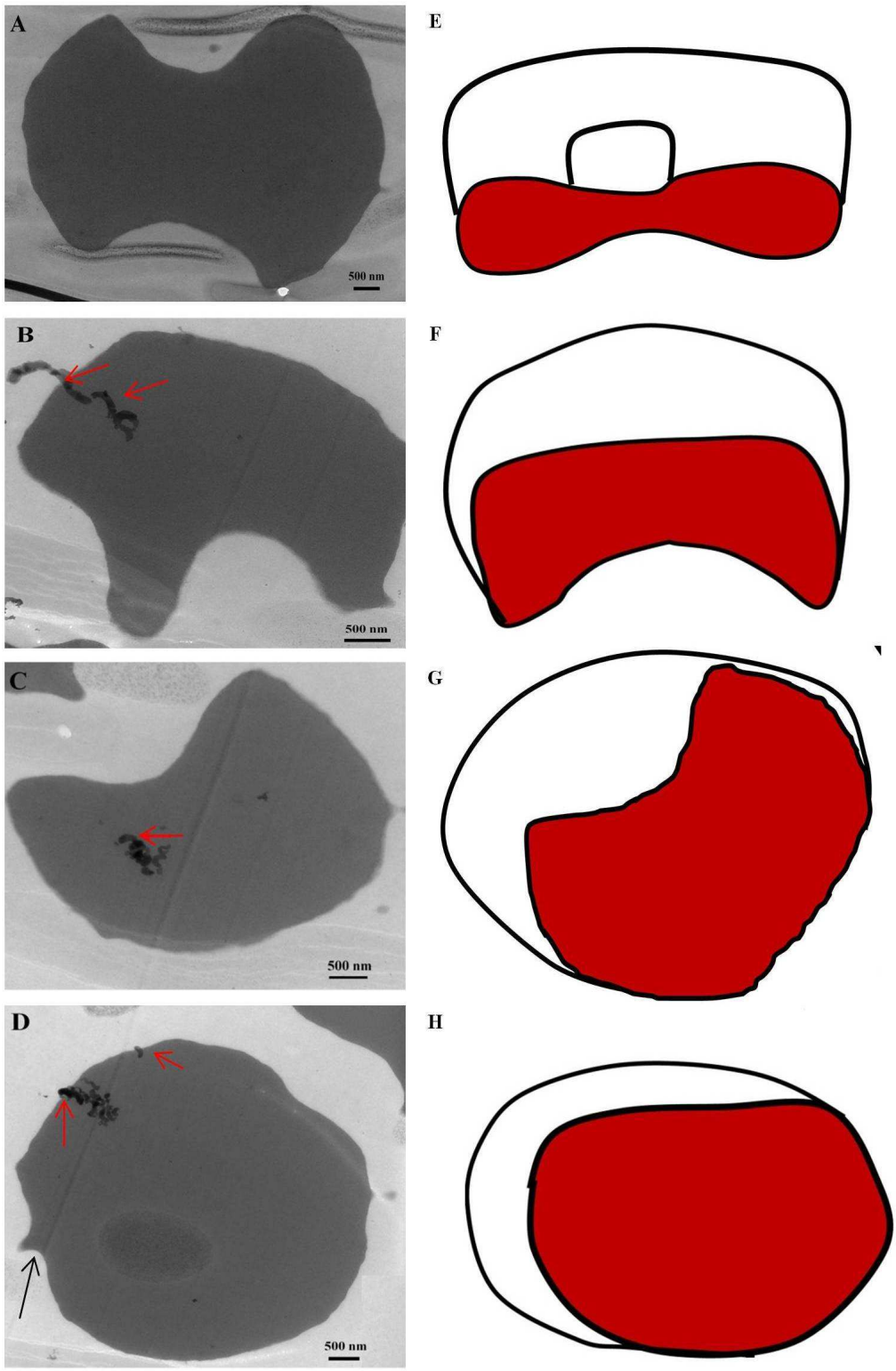

Figure 2 Representative TEM images and illustration of red blood cells treated or untreated with O-GNR-PEG-DSPE. (A and E) Representative TEM images and illustration of cross section of red blood cells not treated with O-GNR-PEG-DSPE. (B and F) Representative TEM image and illustration of cross section of a red blood cell treated with PEG-DSPE showing loss of concave shape on one side. (C and G) Representative TEM image and illustration of cross section of a red blood cell treated with PEG-DSPE showing loss of concave shape on both sides. (D and H) Representative TEM image and illustration of cross section of a red blood cell treated with PEG-DSPE showing formation of a spherical cross section due to loss of structural integrity of the cells. O-GNR-PEG-DSPE particles are indicated with red arrows whereas protrusions/ fragmentation from the membrane are indicated with black arrows.

Figure3

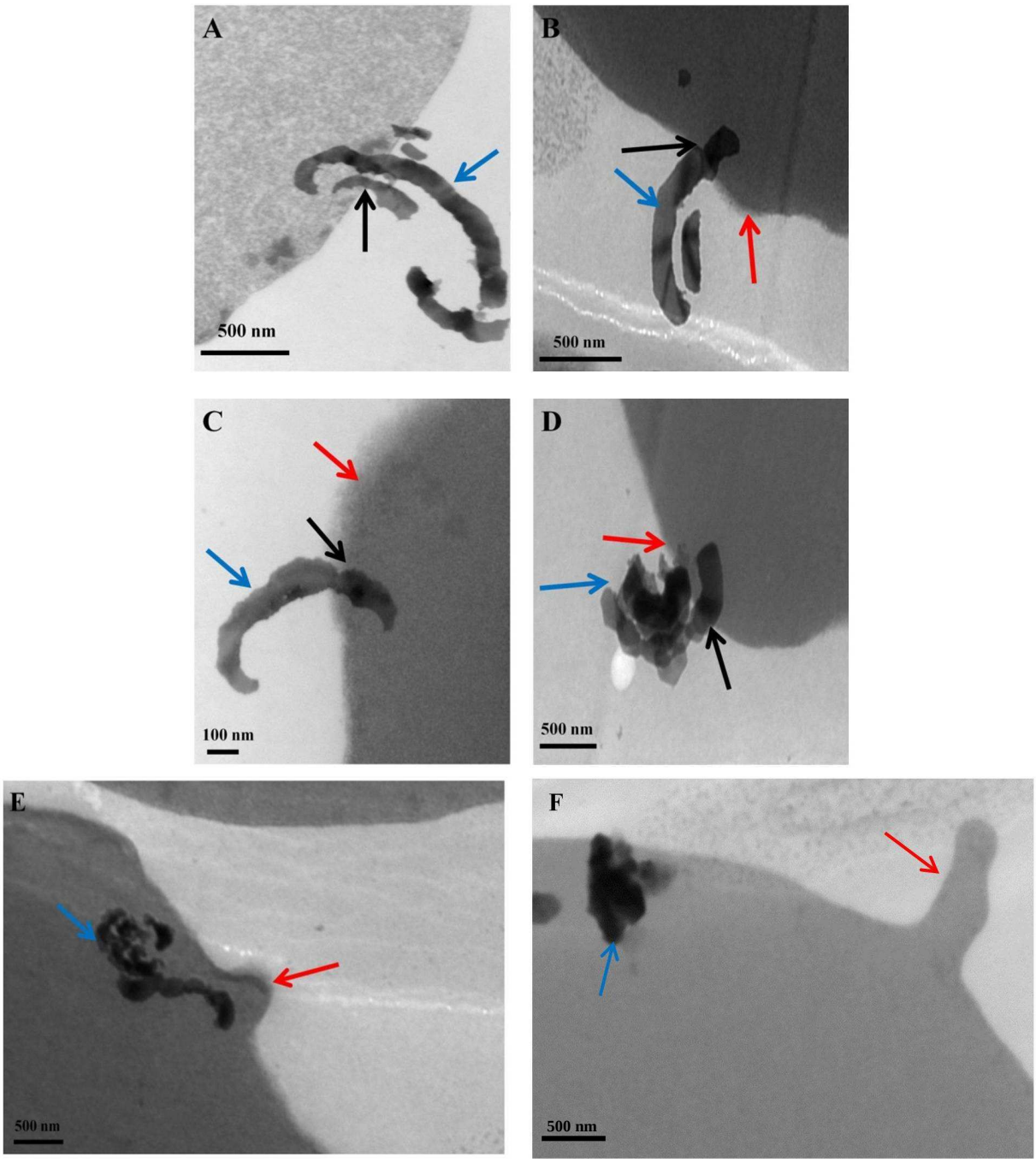

Figure 3 Representative TEM images of red blood cells showing interaction of RBC membrane with O-GNR-PEG-DSPE. (A) Representative TEM image of a red blood cell showing edges of O-GNR-PEG-DSPE interact with RBC membrane. (B-C) Representative TEM images of red blood cells showing membrane disintegration/ruffling (red arrows) at the site of surface interaction (D) Representative TEM images of red blood cells showing membrane depression (red arrows) at the site to interaction. (E-F) Representative TEM images of red blood cells showing membrane protrusions/fragmentations near the sites where cell membrane interacts with O-GNR-PEG-DSPE. O-GNR-PEG-DSPE particles are indicated with blue arrows whereas protrusions/ fragmentation from the membrane are indicated with red arrows. The site of interaction of RBC membrane with O-GNR-PEG-DSPE particles is indicated with black arrows.

Figure 4

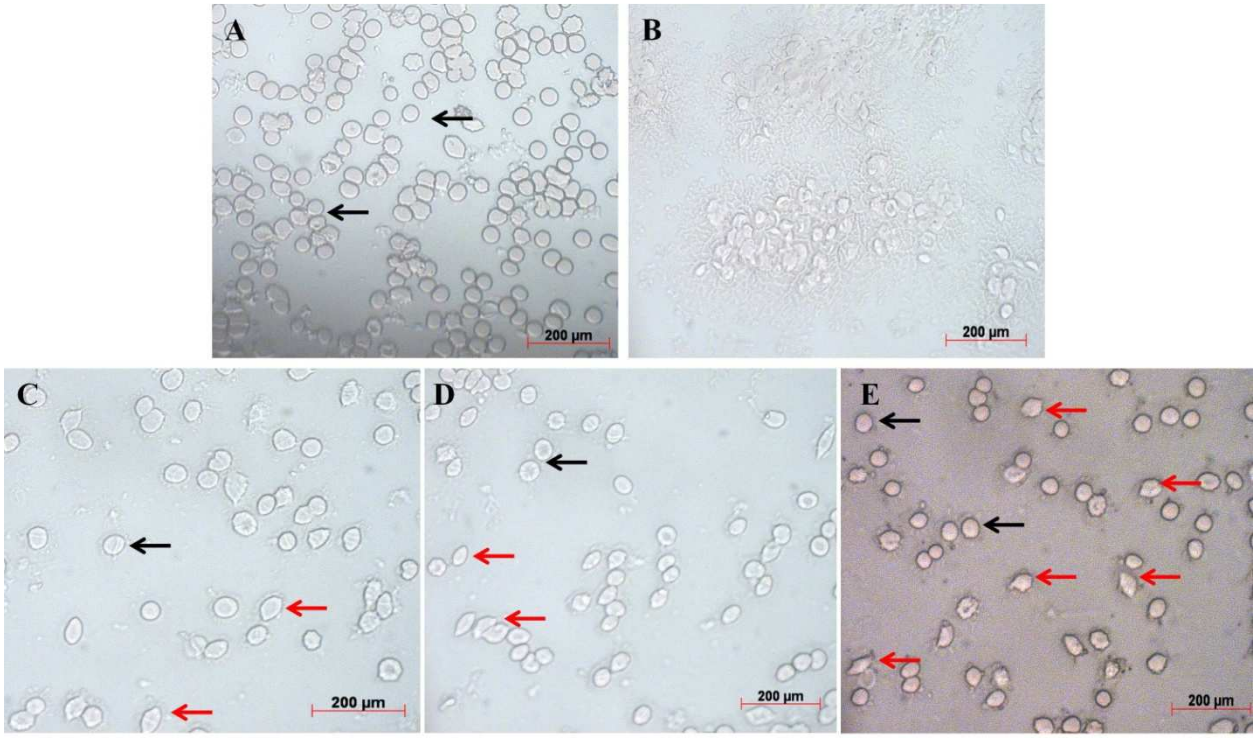
A
200 μm
B
200 μm
C
200 μm
D
200 μm
E
200 μm

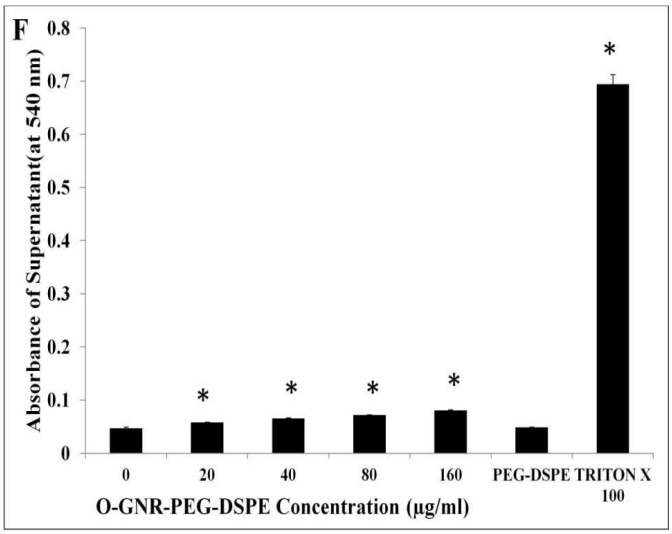
F
Absorbance of Supernatant(at 540 nm)
0.8
0.7
0.6
0.5
0.4
0.3
0.2
0.1
0
*
*
*
*
*
0
20
40
80
160
PEG-DSPE
TRITON X 100
O-GNR-PEG-DSPE Concentration (μg/ml)

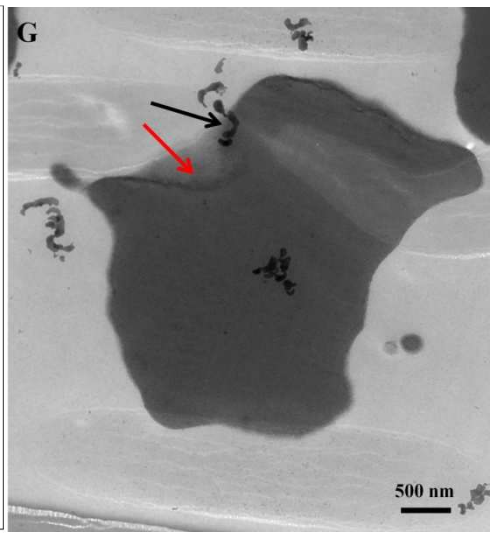
G
500 nm

Figure 4. (A) Representative image of untreated control red blood cells. (B) Representative image showing hemolysed cells treated with poly ethylene imine. (C-E) Representative images of blood cells treated with 0-160μg/ml GNR-PEG-DSPE, respectively. (F) Supernatants obtained after centrifuging red blood cell suspensions treated with GNR-PEG-DSPE formulations, or Triton X 100 for 45 minutes. (G) Absorbance values of the supernatants at 540 nm obtained after conversion of the hemoglobin present to cyanomethemoglobin. Scale bar (A-E) = 200 μm for image (H)Representative Transmission Electron Microscopy image of a hemolysed red blood cell treated with O-GNR-PEG-DSPE

Figure 5

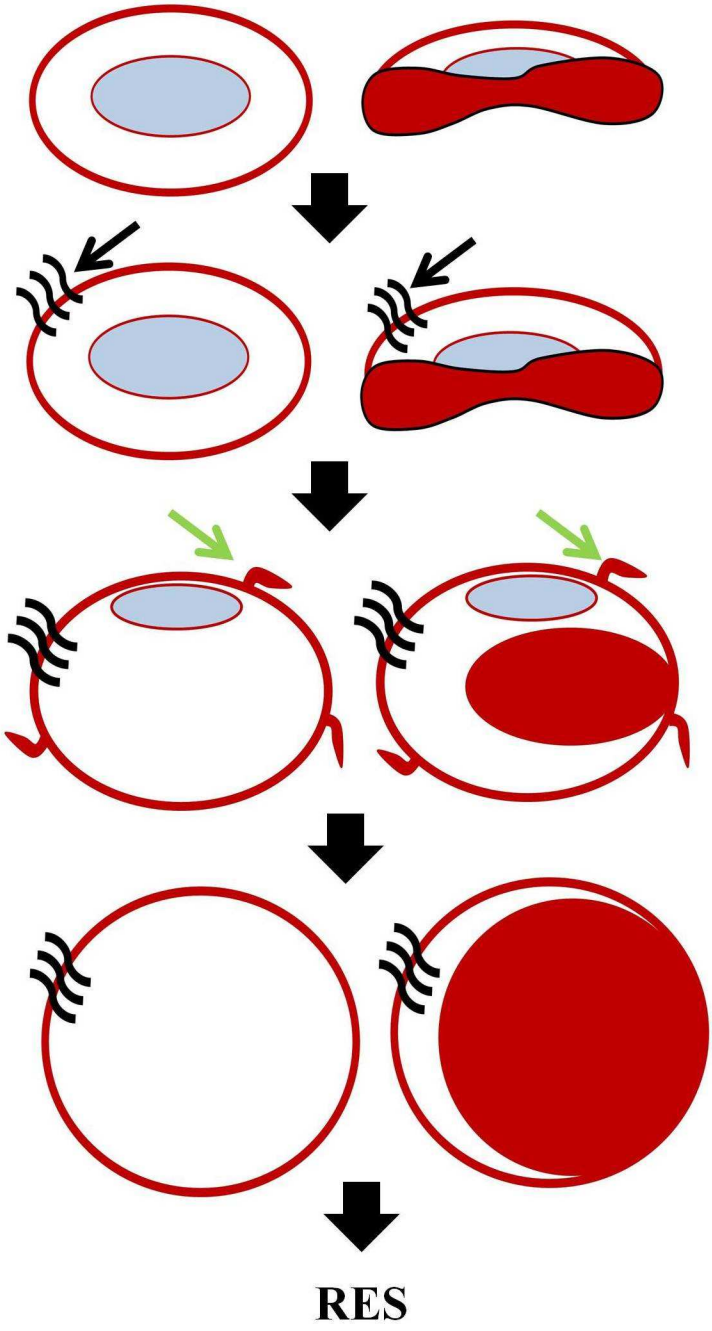

Figure 5 Schematic showing probable mechanism of RBC membrane disruption and formation of spherocyte like structures**.** Fragmentation from disrupted RBC's is indicated with green arrows and O-GNR-PEG-DSPE is indicated with black arrows.

Figure 6

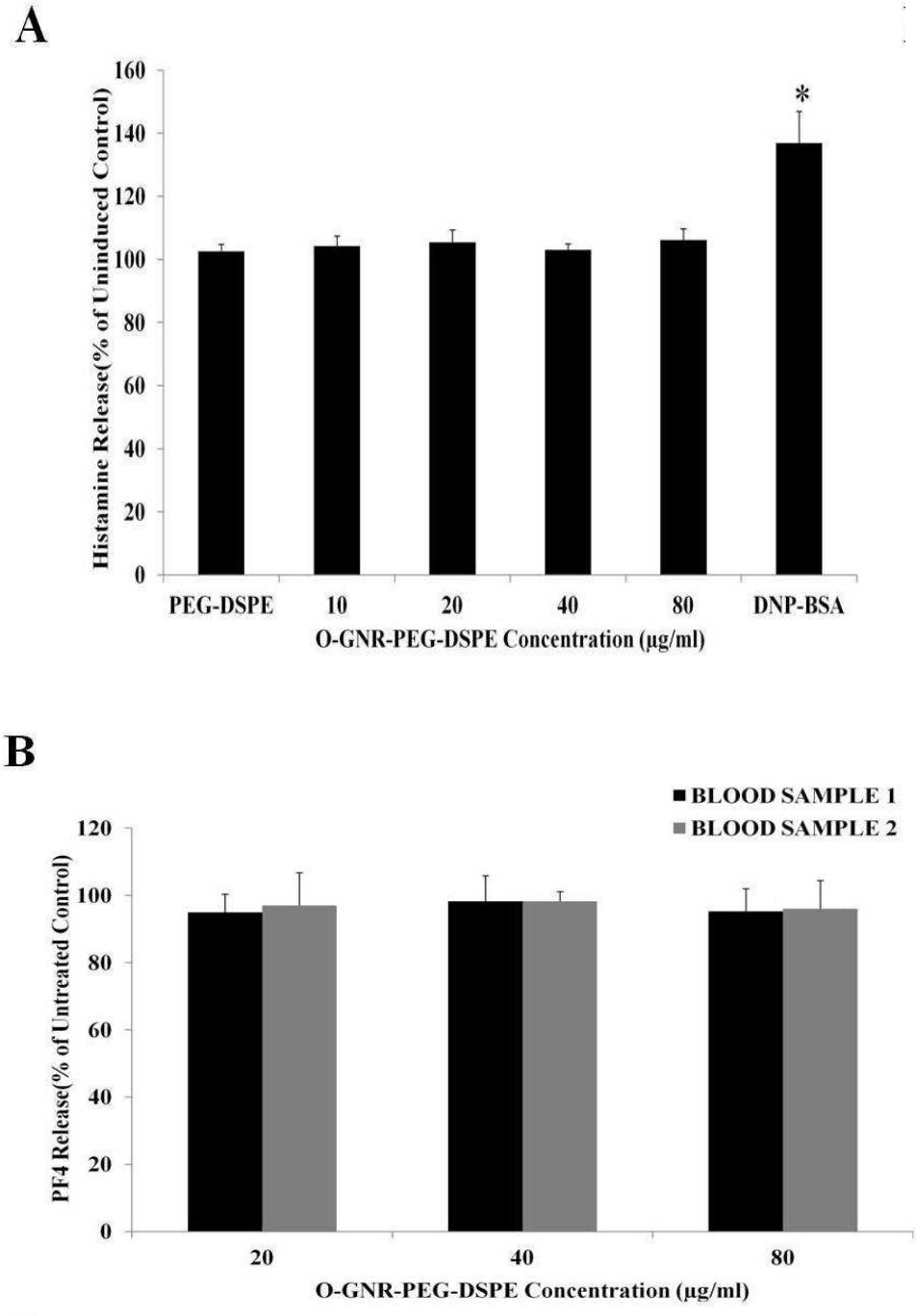
A
Histamine Release(% of Uninduced Control)
160
140
120
100
80
60
40
20
0
*
PEG-DSPE
10
20
40
80
DNP-BSA
O-GNR-PEG-DSPE Concentration (µg/ml)
B
BLOOD SAMPLE 1
BLOOD SAMPLE 2
PF4 Release(% of Untreated Control)
120
100
80
60
40
20
0
20
40
80
O-GNR-PEG-DSPE Concentration (µg/ml)

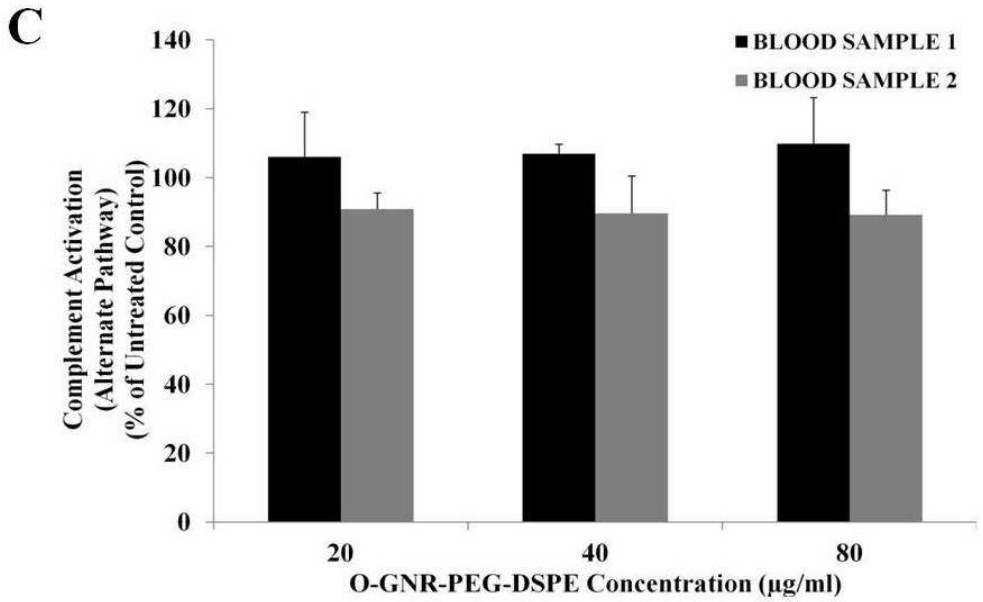
C
140
120
100
80
60
40
20
0
Complement Activation
(Alternate Pathway)
(% of Untreated Control)
BLOOD SAMPLE 1
BLOOD SAMPLE 2
20
40
80
O-GNR-PEG-DSPE Concentration (µg/ml)

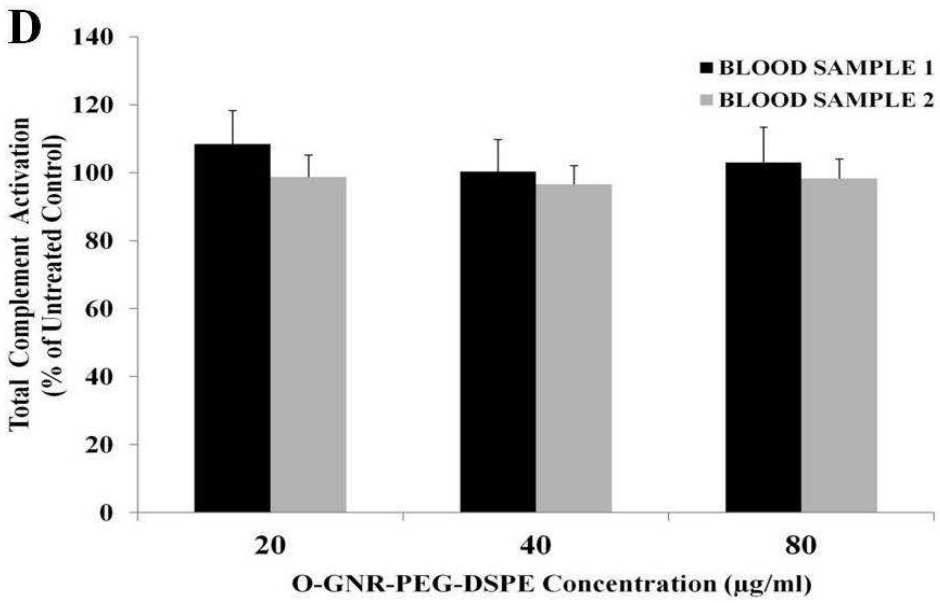
D
140
120
100
80
60
40
20
0
Total Complement Activation
(% of Untreated Control)
BLOOD SAMPLE 1
BLOOD SAMPLE 2
20
40
80
O-GNR-PEG-DSPE Concentration (µg/ml)

E

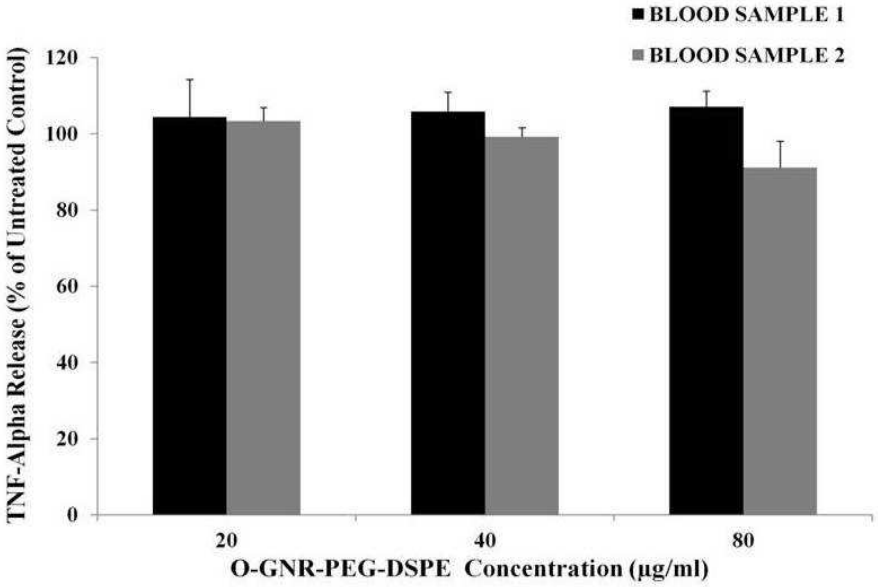
BLOOD SAMPLE 1
BLOOD SAMPLE 2
TNF-Alpha Release (% of Untreated Control)
120
100
80
60
40
20
0
20
40
80
O-GNR-PEG-DSPE Concentration (µg/ml)

F

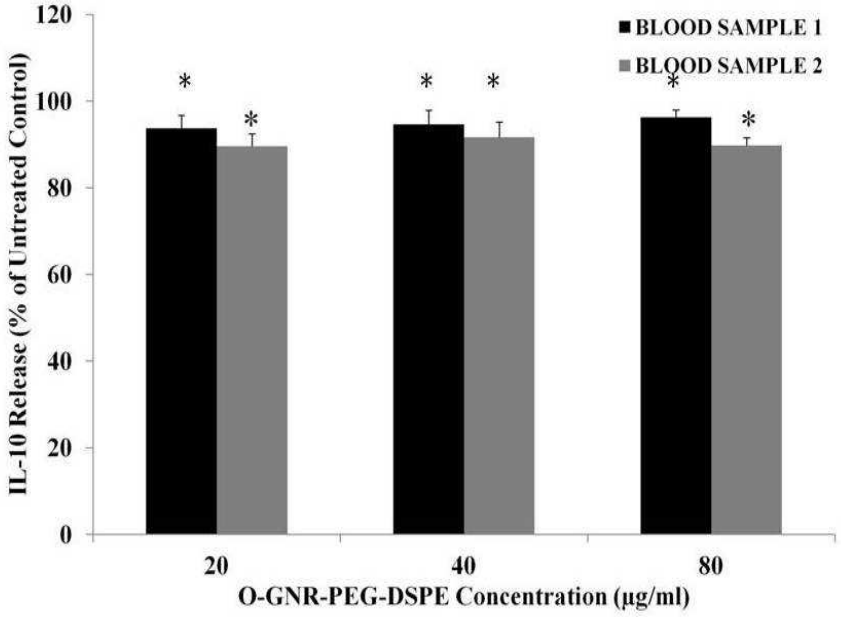
BLOOD SAMPLE 1
BLOOD SAMPLE 2
IL-10 Release (% of Untreated Control)
120
100
80
60
40
20
0
*
20
40
80
O-GNR-PEG-DSPE Concentration (µg/ml)

Figure 6 (A) Histamine release from activated and induced RBL-2H3cells treated O-GNR-PEG-DSPE (0-80μg/ml) formulations for 45 min. **(B)** Platelet activation assay presented in terms of PF_4 production in whole human blood from two individuals incubated at 0-80μg/ml GNR-PEG-DSPE concentrations for 45 min. **(C)** Total complement activation assay presented in terms of Sc5b-9 protein production in human whole blood from two individuals treated with various O-GNR-PEG-DSPE (0-80μg/ml) concentrations.**(D)** Alternate complement pathway activation in terms of Bb protein production in two human whole blood samples treated with various concentrations of O-GNR-PEG-DSPE (0-80μg/ml). **(E)** Pro-inflammatory cytokine release assay presented in terms of TNF-Alpha release in whole human whole blood from two individuals treated with various O-GNR-PEG-DSPE (0–80μg/ml) concentrations. **(F)** Anti-inflammatory cytokine release assay presented in terms of IL-10 release in whole human blood from two individuals treated with various O-GNR-PEG-DSPE (0–80μg/ml) concentrations. Data are presented as mean +SD (n = 4 per group). * = $p < 0.05$ between untreated control and particular treatment group.

Figure 7

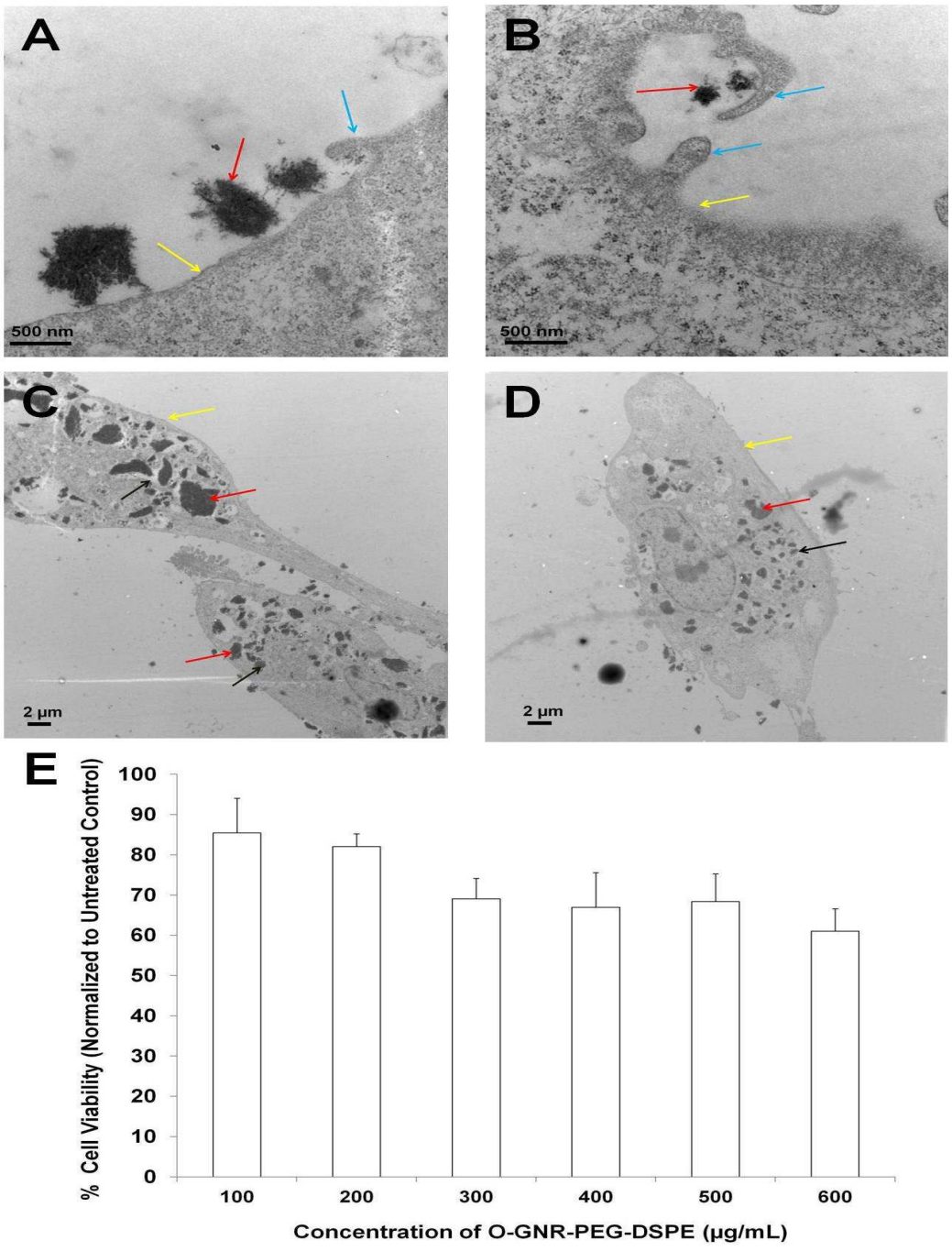
A
500 nm
B
500 nm
C
2 µm
D
2 µm
E
% Cell Viability (Normalized to Untreated Control)
100
90
80
70
60
50
40
30
20
10
0
100
200
300
400
500
600
Concentration of O-GNR-PEG-DSPE (µg/mL)

Figure 7

Representative TEM images of human umbilical vein endothelial cells treated with 40µg/ml O-GNR-PEG-DSPE for 12 hours showing .(A) O-GNR-PEG-DSPE aggregates (red arrows) at the periphery of the cell (yellow arrows). (B) Cell membrane protrusions (blue arrows) moving towards and engulfing large O-GNR–PEG-DSPE aggregates (red arrows). (C-D) O-GNR-PEG-DSPE aggregates (red arrow) enclosed in large cytoplasmic vesicles (black arrows). Yellow arrows in all the images represent the cell membrane. (E) % Cell Viability (normalized to viability of untreated cells) using Presto Blue Assay in human umbilical vein endothelial cells incubated with various O-GNR-PEG-DSPE (0-600µg/ml) concentrations for 24 hours. Data are presented as mean +SD (n = 5 per group). All treatment groups showed $p < 0.05$ when compared to untreated control.

Chapter 4

MECHANISM OF UPTAKE AND *IN VITRO* DRUG DELIVERY STUDIES WITH GRAPHENE NANORIBBONS

Preface

Portions of this chapter have been reproduced from

> **Mullick Chowdhury, S**., Mannepalli, P. & Sitharaman, B. Graphene Nanoribbons Elicit Cell Specific Uptake and Delivery Via Activation of Epidermal Growth Factor Receptor Enhanced by Human PapillomaVirus E5 Protein. *Acta Biomaterialia* (2014) with permission from Elsevier publishing.

The authors listed in the above manucript have contributions towards the data reported in this chapter.

4.1 Introduction

Many pharmaceutical formulations of drugs, genes and imaging agents show significant limitations that result in low therapeutic indices (ratio of therapeutic to toxic dose). These limitations stimulate the development of pharmaceutical delivery agents. There is now a large body of work that documents the tremendous progress in research and development of drug delivery agents (Sant et al., 2012, Hubbell and Langer, 2013, Bae and Park, 2011). A variety of micro- and nano-particles have been explored as delivery systems, including particles synthesized from carbon (fullerenes, metallofullerenes, carbon nanotubes and recently graphene(Lalwani and Sitharaman, 2013, Liu et al., 2009, Bitounis et al., 2013, Frame et al., 2014)), ceramics, polymers, lipids, or metals and formed in a variety of configurations (i.e., spheres, tubes, branched structures, and shells)(Haley and Frenkel, 2008). These systems serve as the scaffold onto which the active pharmaceutical ingredient (API) is covalently or non-covalently loaded. Multi-component targeted delivery systems have also been developed, in which targeting moieties (e.g. antibodies or peptides) are covalently or non-covalently appended onto APIs, or API- loaded micro- or nano-particles. These systems typically target specific antigens on the cell surface to enhance the uptake of delivery systems into specific tumor cells to improve treatment efficacy. 'Antibody mimics' synthesized via imprinting of specific antigens onto polymeric scaffolds are used mainly in competitive binding assays(Vlatakis et al., 1993). Identification of materials that serve not only as scaffolds that efficiently load and deliver drugs, but also activate specific cell receptors without additional presence or functionalization of amino acid sequences or other epitopes would constitute a significant advance in targeted delivery system design.

In chapter 2, we had evaluated the cytotoxicity of oxidized graphene nanoribbon (O-GNR)-based formulations(Mullick Chowdhury et al., 2013). In that chapter O-GNRs were synthesized in macroscopic amounts using an oxidative method pioneered by Kosynkin, Tour, and co-workers that longitudinally "unzips" carbon nanotubes(Kosynkin et al., 2009). O-GNR morphology is distinctly different from graphene oxide nanoplatelets, which are synthesized using graphite and are widely used in graphene-based cellular uptake and delivery studies (Bitounis et al., 2013, Kanakia et al., 2013, Chowdhury et al., 2013). Results from the in vitro toxicity study reported in Chapter 2 had shown that O-GNRs (**Figure 1A and B**) water-solubilized with the amphiphilic polymer PEG-DSPE to form a supramolecular complex (O-GNR-PEG-DSPE) when incubated at various concentrations (0-400µg/ml) and time points (24-72 hours) in four different cell lines (HeLa, MCF7, SKBR 3 and NIH3T3) were more cytotoxic to HeLa cells compared to other cell lines(Mullick Chowdhury et al., 2013). These studies provided preliminary indication that enhanced uptake of O-GNR-PEG-DSPEs into HeLa cells was an important reason for the observed differences in cytotoxicity. In this chapter, we further investigate the O-GNR-PEG-DSPEs uptake mechanism, and report two surprising yet related phenomena. (1) O-GNR-PEG-DSPEs activate epidermal growth factor receptors (EGFRs) and are taken up in significant amounts in cells with high EGFR expression. (2) Cells with integrated human papilloma virus (HPV) genomes, which express EGFR (at normal or elevated levels), elicit enhanced O-GNR-PEG-DSPE uptake via the modulation of EFGR by the viral protein E5. We further demonstrate that these phenomena lead to differential and increased intracellular drug delivery efficacy even in drug resistant cells.

4.2. Materials and Methods

4.2.1Synthesis and Characterization of O-GNR-DSPE-PEG formulations:

Previously reported procedures were employed for the O-GNR synthesis from multi walled carbon nanotubes (Sigma-Aldrich, St Louis, MO) and preparation of O-GNR-DSPE-PEG dispersions [9, 10]. For atomic force microscopy (AFM) and TEM characterization, O-GNR-PEG-DSPE samples diluted to 5µg/ml using a 1:1 ethanol water mixture were probe sonicated, (Cole Parmer Ultrasonicator LPX 750) and centrifuged at 2000 rpm for 30 minutes. The supernatant was collected and drop cast onto silicon wafers (AFM samples) or copper grids (Ted Pella) (TEM samples) and dried overnight. AFM was performed using a Nano Surf Easy Scan 2 AF microscope (NanoScience Instruments Inc, Phoenix, AZ), operating in tapping mode with a V-shaped cantilever. TEM was performed on a Tecnai Bio Twin G transmission electron microscope (FEI, Hillsboro, OR), at 80 kV. Digital images were acquired using an XR-60 CCD digital camera system (AMT, Woburn, MA).

4. 2.2 Cell Culture:

Eleven cell lines were used for the various experiments based on their EGFR expression. All cell lines were obtained from ATCC (Manassas, VA, USA). HeLa, A549,MRC5,U251, A431 cells were grown in Dulbecco's Modified Eagle medium, SKBR3 cells were grown in McCoy's medium, MCF7 and CaSki cells were grown in RPMI 1600 medium. SiHa, C33A and U87MG cells were grown in Minimum Essential medium (MEM). All the media were supplemented with 10% fetal bovine serum and 1 % penicillin-streptomycin. Cells were incubated at 37^{o}C in a humidified atmosphere of 5% CO_2, and 95% air.

4.2.3 TEM of Cell Specimens

Six well plates with surfaces covered with ACLAR® film (Electron Microscopy Sciences, Hatford, PA) were plated with HeLa, C33A and A431 cells at a density of 5x 10^5 cells per plate, and exposed to O-GNR-PEG-DSPEs for 15 minutes, 30 minutes or 3 hours according to the specific assay. For inhibitor studies, cells were first incubated with 80 µM dynasore, 3µg/ml filipin, 50 mM EIPA or 1µM Gefitinib for 30 minutes. Next, cells were treated with O-GNR-PEG-DSPE at 50µg/ml concentrations for 15 minutes, 30 minutes or 3 hours. After 15 minutes, 30 minutes or 3 hours as per specific experiments, cells were fixed with 2.5% electron microscopy grade glutaraldehyde (Electron Microscopy Sciences, Hatford, PA) in 0.1 M PBS. After fixation, films containing fixed cells were placed in 2% osmium tetroxide in 0.1 M PBS, dehydrated through graded ethanol washes, and embedded in durcupan resin (Sigma-aldrich, St. Louis, USA). Areas with high cell densities were blocked, cut into 80 nm ultrathin sections using an Ultracut E microtome (Reichert-Jung, Cambridge, UK), and placed on formvar-coated copper grids. The sections were then viewed with a Tecnai Bio Twin G transmission electron microscope (FEI, Hillsboro, OR) at 80 kV. Digital images were acquired using an XR-60 CCD digital camera system. (AMT, Woburn, MA). 15 cells of each cell line treated with O-GNR-PEG-DSPE was observed to come to a conclusion about uptake of O-GNR-PEG-DSPE in these cell lines

4.2.4 Confocal Microscopy

5x 10^5 cells were plated in glass bottom 35 mm plates and incubated for 18 hours. Following incubation, media was removed and replaced with serum-free media and cells were further incubated for 24 hours. Post-incubation, cells were treated with 50µg/ml O-GNR-PEG-DSPE for 15 minutes or 30 minutes. This step was followed by three washes with phosphate buffered

saline and fixation for 30 minutes with 2.5% glutaraldehyde. Then, the fixed cells were treated with 0.5% Triton X-100, and washed 3 times with PBS; this was followed by incubation with either phallodin rhodamine (for actin) (Invitrogen) or anti-phospho EGFR antibody with attached Alexa fluor 488(Millipore, Billerica, MA). Cells treated with gefitinib before O-GNR-PEG-DSPE treatment, EGF treated cells, and untreated cells were used as controls.

4.2.5 Doxorubicin loading on O-GNR-PEG-DSPE

The protocol used to load doxorubicin (Dox) onto O-GNR-PEG-DSPEs was adapted from the literature available for drug-loading for graphene. Briefly, 10 mg of Dox was mixed with 20 ml of 200µg/ml O-GNR-PEG-DSPE, bath sonicated for 60 minutes, and stirred for 24 hours. After 24 hours, the mixture was centrifuged at 13000 rpm for 60 minutes. The supernatant containing unloaded Dox was separated from the pelleted O-GNR-PEG-DSPEs containing loaded Dox by decantation. The amount of drug in the supernatant (i.e. drug not loaded) was calculated using the Dox absorbance spectra from the supernatant at 490 nm and the absorbance vs. Dox concentration standard curve. The amount of drug loaded on O-GNR-PEG-DSPEs was calculated by subtracting the drug in the supernatant from the starting amount of Dox (i.e., 1 mg). Drug loading efficiency (DLE) was calculated using the following formula: DLE = [(Drug Loaded in mg) / (Weight of O-GNR-PEG-DSPE in mg)]*100. The drug-loaded O-GNR-PEG-DSPE was resuspended in PEG-DSPE at 200µg/ml and 120µg/ml (of O-GNR-PEG-DSPE) before being used as stock solutions for drug delivery and drug release experiments respectively.

4. 2.6 Doxorubicin release from O-GNR-PEG-DSPE

Bipthalate buffer (pH 4), phosphate buffered saline (pH 7), and borate buffered saline (pH 10) were used to assess drug release from Dox-loaded O-GNR-PEG-DSPEs. One ml of a 120µg/ml Dox-loaded O-GNR-PEG-DSPE solution was re-suspended in 10 ml of the three different

buffers to produce ~60 µg of Dox-loaded onto O-GNR-PEG-DSPE in each buffer solution. This solution was incubated at 37^{o}C in a water bath placed on a horizontal shaker for 60 hours. One ml of buffer was collected every 12 hours, and the amount of Dox released was calculated using the absorbance of the collected buffer at 490 nm and the standard Dox absorbance vs. concentration standard curve.

4.2.7 Lactate Dehydrogenase (LDH) Assay

This assay was conducted using a LDH release TOX-7 assay kit (Sigma-Aldrich, St Louis, MO). Cells were plated, at a density of 5 x 10^3 cells per well, in 96 well cell culture plates, and incubated for 18 hours. Following media changes, and cell treatment with Dox-loaded O-GNR-PEG-DSPE (50µg/ml), cells were incubated at 37^{o}C for 24 hours. After 24 hours, media was collected from individual wells, and centrifuged at 1200 rpm for 5 minutes. Fifty µl of the media supernatant was added to a fresh 96 well plate along with LDH assay reagent, and incubated for 45 minutes. Absorbance values were recorded at 490 nm. The positive control was prepared by adding 10 µl of lysis solution to control cells, 45 min before centrifugation. LDH secretion (% of positive control) was calculated using the formula $(OD_{test} - OD_{blank})/(OD_{positive} - OD_{blank})$, where OD_{test} is the optical density of control cells or cells exposed to O-GNR-PEG-DSPE, and $OD_{positive}$ is the optical density of the positive control cells, and OD_{blank} is the optical density of the wells without cells. Absorbance of culture media containing PEG-DSPE was used for baseline correction in all groups. LDH secretion (% of Dox-loaded O-GNR-PEG-DSPE treated cells) was calculated using the formula $(OD_{test} - OD_{blank})/(OD_{treatment} - OD_{blank})$, where OD_{test} is the optical density of the inhibited cells exposed to Dox-loaded O-GNR-PEG-DSPE, $OD_{treatment}$ is the optical density of the cells treated with only Dox-loaded O-GNR-PEG-DSPE,

and OD_{blank} is the optical density of the wells without cells. Absorbance of culture media containing PEG-DSPE was used for baseline correction in all groups.

4.2.8 Western Blots

HeLa, A431 cells and C33A cells were plated at cell density of 1 $x10^5$ or 5 $x10^5$ in six well plates and grown for 18 hours. Five $x10^5$ A431 and C33A cells transfected with MSCV- FLAG - HPV16 E5 plasmid (Addgene, Cambridge,MA) in six well plates were also used. Cell lines were either left untreated or treated with O-GNR-PEG-DSPEs (50µg/ml) for 15 minutes. Next, cells were lysed, and whole cell protein lysates were collected. Western blot analysis for EGFR expression before and after treatment with O-GNR-PEG-DSPEs was conducted using rabbit anti-EGFR primary antibody (Santa Cruz Biotechnology), and anti rabbit-HRP secondary antibody (Santa Cruz Biotechnology). Western blot analysis for activated EGFR expression before and after treatment with O-GNR-PEG-DSPE (and before and after gefitinib and O-GNR-PEG-DSPE treatment) was performed using mouse anti-phospho EGFR antibody (Millipore, Billerica, MA), and anti-mouse -HRP (Santa Cruz Biotechnology Santa Cruz, CA). 4 different blots for each experiment were used for densitometry analysis using Image J and subsequent statistical analysis. Data obtained from densitometry analysis is represented as ratio of EGFR or p-EGFR band density and corresponding beta actin band density.

4.2.9 Presto Blue Assay for Cell Viability

Cell viability of HeLa cells exposed to different concentrations of the four inhibitors Dynasore, Fillipin, EIPA and Gefitinib was measured by presto blue assay using a method discussed in the previous chapter (Invitrogen, Grand Island, NY). Briefly, HeLa cells were plated at 6 x 10^3 cells per well in 96 well plates, and incubated for 24 hours. Before commencing with the assay, old

media was replaced with 180µl of fresh media in each well. 20µl of inhibitor solutions at different concentrations were added to every well so as to reach the target concentration when diluted in the media. The concentrations tested ranged from 0-100 µM for dynasore, 0-5µg/ml for fillipin, 0-1 mM for EIPA and 0-2 µM for gefitinib. The cells were incubated at 37^{o}C for 24 hours. After 24 hours, media was removed, and wells were rinsed twice with Dulbecco's phosphate buffer saline (DPBS) before adding 200µl of fresh media, and 20µl of Presto Blue reagent. The plates were then incubated for 2 hours at 37^{o}C. Fluorescence readings of the wells were recorded using a Spectra Max M3 multimode microplate reader (Molecular Devices, Sunnyvale, CA) with excitation at 530 nm, and emission at 580 nm. Fluorescence reading for cells in the culture medium containing only PEG-DSPE was used for baseline correction. The cell viability in terms of % of untreated control cells is expressed as the percentage of $(F_{test} - F_{blank})/(F_{control} - F_{blank})$,where F_{test} is the fluorescence of the cells exposed to nanoribbon sample, $F_{control}$ is the fluorescence of the unexposed control sample and F_{blank} is the fluorescence of the wells without any cells.

4.2.10 siRNA transfection of HeLa cells

One x10^5 or 5 x10^5 HeLa cells were plated in 96-well and 6-well plates and incubated for 18 hours. Cells were transfected with siRNA against EGFR (Santa Cruz Biotechnology, Santa Cruz, CA) and siRNA against HPV18E5 (Qiagen) using the Fugene 6 transfection reagent. Briefly, 1 µl of each siRNA against EGFR and siRNA against HPV18E5 were added to 489 µl of OPTI-MEM media and 10 µl of transfection reagent to prepare 500 µl of transfection reagent-DNA complex. One hundred µl of this complex was added to each well of 96 well plates and 500 µl of this complex was added to each well in 6 well plates. Transfection was allowed to proceed for 12 hours after which EGFR activation in the transfected cells was checked with confocal

miscroscopy and flow cytometry using mouse anti-phospho EGFR primary and anti-mouse rhodamine as secondary antibody after exposing cells to 10 ng EGF per well. Drug delivery studies in siRNA transfected cells were conducted according to the method described in the LDH assay section. Ambion® *Silencer*® Negative Control #1 siRNA was used as the negative control and untreated cells (with and without siRNA treatment) were used as controls.

4.2.11 Transfection of HPV 16-E5 plasmid into A431 and C33A cells and wt EGFR plasmid into C33A cells

MSCV-FLAG-HPV16-E5 plasmid and wt EGFR expressing plasmid (plasmid 11011) was obtained from Addgene (Cambridge,MA), and transiently transfected into A431 and C33A cells using the Fugene 6 transfection reagent. Briefly, 2µg of the plasmid was mixed with 6 µl of Fugene 6 reagent and 94 µl of OPTI-MEM media to form 100 µl of transfection agent-plasmid mixture.10 µl and 50 µl of this mixture was added to each well in 96 well plates containing 90 µl OPTI-MEM and cells and 6 well plates containing 450 µl OPTI-MEM reduced serum media (Life Technologies, Carlsbad, CA) and cells respectively. The transfection was allowed to proceed for 12 hours following which successful transfection was confirmed by fluorescence microscopy and flow cytometry. Mouse anti-flag and Mouse anti-EGFR primary antibodies (Sigma-Aldrich,St Louis, MO) and anti-mouse-rhodamine (Sigma-Aldrich, St Louis, MO) secondary were used for fluorescence microcopy and flow cytometry. Drug delivery studies in the MSCV-FLAG-HPV16E5 and EGFR transfected cells were conducted according to the method described under LDH assay. Untreated cells (transfected and untransfected) were used as controls.

4.2.12 Cell Counting

Cell proliferation of normal C33A cells and wt EGFR plasmid transfected C33A cells after 24 hours was compared by cell counting. Briefly, $15x10^4$ transfected and non –transfected cells were plated in 10 cm cell culture plates and allowed to grow for 4 hours. After 4 hours the media was changed with fresh media and the cells were allowed to grow undisturbed for 24 hours. After this period the cells were trypsinized and cell numbers were counted using a hemocytometer.

4.2.13 Flow Cytometry

Flow cytometry was used for quantification of activated EGFR expression before and after siRNA transfection (against EGFR and HPV18 E5) as well as to quantify transfection efficiency and expression of the MSCV-FLAG-HPV16 E5 and wt EGFR plasmid in transfected A431 and C33A cells. To prepare for flow cytometry, the cells were fixed using 2.5% glutaraldehyde and excess glutaraldehyde was washed away , treated with 0.1% Triton X 100 for 5 minutes followed by treatment with appropriate antibodies, trypsinized, and resuspended in FACS buffer (Phosphate buffered saline containing 20% fetal bovine serum). Flow cytometry was performed immediately after all samples were prepared using a FACS Calibur Cell Sorter (BD Biosciences, San Jose, CA). BD FACS Diva 8.0 software was used for data analysis.

2.12 Statistics

All data are presented as mean ± standard deviation. Student's' test was used to analyze the differences among groups. Each independent experiment (n=1) was an average of three wells done in parallel. One-way ANOVA followed by Tukey Kramer post hoc analysis was used for

multiple comparisons between groups. All statistical analyses were performed using a 95% confidence interval ($p < 0.05$).

4.3. Results

4.3.1. Water dispersed graphene nanoribbons activate epidermal growth factor receptors

We first conducted qualitative analysis of O-GNR-PEG-DSPE uptake into HeLa and three other cell lines (MCF7, A549 and MRC5) using transmission electron microscopy (TEM). These results suggest that HeLa cells take up O-GNR-PEG-DSPE aggregates into large vesicular cytoplasmic structures (resembling macropinosomes) (**Figure 1C and D**). Uptake seemed to be mediated through extensions from the plasma membrane, which engulfed O-GNR-PEG-DSPE on the cell surface (**Figure 1 C and D,** white arrows). We also observed large and small perinuclear vesicular structures within O-GNR-PEG-DSPE aggregates after 30 min of incubation (**Figure 1 E and F**) as well as a few endocytic vesicles, which formed before the macropinocytosis-like response, (**Figure 1D**, yellow arrows). In comparison, other cell lines (MCF7, MRC5 and A549) showed only small aggregates or O-GNR-PEG-DSPE uptake (**Figure 2 A, B and C**).

Next, we conducted inhibitor studies in HeLa cells to investigate the uptake mechanism at potentially safe concentrations of O-GNR-PEG-DSPE and inhibitors. Cellular analyses using TEM indicated that, although, both macropinocytotic and endocytic vesicles were observed in non-inhibited HeLa cells treated with O-GNR-PEG-DSPE, dynasore (a dynamin inhibitor that prevents clathrin-mediated endocytosis) could completely prevent O-GNR-PEG-DSPE uptake (**Figure 3 A and B**) whereas filipin (a caveolae-mediated endocytosis inhibitor) did not show the same effect (**Figure 3 C and D**). Ethyl-isopropyl amiloride (EIPA), a macropinocytosis inhibitor

largely prevented the uptake of larger aggregates, but in a few cases, smaller aggregates were found in endosomal vesicles even with EIPA inhibition (**Figure 3 E and F).** Based on these results, we hypothesized that the uptake mechanism for O-GNR-PEG-DSPE into HeLa cells is predominantly a dynamin-dependent macropinocytosis-like response although dynamin-dependent clathrin-mediated endocytosis may play a smaller role.

Investigation of actin polymerization of HeLa cells exposed to O-GNR-PEG-DSPE revealed the presence of circular ruffles 15 min post exposure (**Figure 4 B and C**, white arrows). O-GNR-PEG-DSPE uptake was observed along ruffle margins (**Figure 4 C**, red arrows). Several reports demonstrated dynamin-dependent ruffle formation, and a macropinocytosis-like uptake mechanism during activation and internalization of epidermal growth factor receptors (EGFRs),(Orth, 2006) involving plasma membrane protrusions that sequester a large number of ligand-bound (i.e., activated) EGFRs in large vesicular cytoplasmic structures. We observed similar protrusions in HeLa specimens treated with O-GNR-PEG-DSPE (**Figure 1C and D**). Activated EGFR uptake occurs via a complex network of connected vesicles unlike the spherical vesicles observed in classical macropinocytosis; localization of these vesicles is mainly perinuclear(Orth, 2006). We noted O-GNR-PEG-DSPE in structures with similar features, such as connected vesicles with perinuclear localization (**Figure 1E and F**, blue arrows, black arrows point to nucleus). Thus, we performed additional inhibitory studies in HeLa cells with gefitinib (an EGFR kinase inhibitor) to ascertain whether O-GNR-PEG-DSPE uptake is dependent on EGFR activation and sequestration(Kitazaki et al., 2005). TEM results showed no observable nanoparticles inside the cells in cytoplasmic vesicles even after 3-hours exposure to the cells (**Figure 1 G**). O-GNR-PEG-DSPE aggregates were present on the membrane (**Figure 1 H**), but

not ruffles (**Figure 4D**). Taken together, these results taken together indicated that gefitinib prevents cellular uptake of these nanoparticles (**Figure 1 E**).

We next employed fluorescently tagged anti-phospho EGFR antibodies, and investigated whether O-GNR-PEG-DSPE activates EGFR in HeLa cells, and subsequently leads to O-GNR-PEG-DSPE uptake. HeLa cells grown in serum free media and treated with O-GNR-PEG-DSPE showed increased green fluorescence, which is indicative of increased EGFR activation (i.e. increased EGFR phosphorylation; **Figure 5 A, B and C**). O-GNR-PEG-DSPE activated cell surface EGFR (**Figure 5 D, E and F**, red arrows). Our results also indicated that O-GNR-PEG-DSPE aggregates co-localize with activated EGFR receptors in vesicles (**Figure 5 D-I).** HeLa cells exposed to gefitinib prior to O-GNR-PEG-DSPE treatment failed to show significant EGFR activation (**Figure 5 J, K and L**). A431 cells, which also over express EGFR showed activation, albeit at lower levels (**Figure 6**). MCF7 cells, which have low EGFR expression showed insignificant EGFR activation (**Figure 6**). Western blot analysis of unexposed and exposed HeLa cells showed that the number of activated EGFR receptors increased post exposure to O-GNR-PEG-DSPE. However, total EGFR content remained the same (**Figure 5S**). Gefitinib pre-treatment could decrease this phosphorylation (**Figure 5T**). These results provided additional corroboration that O-GNR-PEG-DSPE uptake is dependent on EGFR activation and sequestration.

4.3.2 Differential intracellular drug delivery and enhanced drug efficacies

We next performed drug delivery studies using O-GNR-PEG-DSPEs. The primary goals of these studies were twofold: 1) to further corroborate that O-GNR-PEG-DSPE uptake of into cells occurs via EGFR activation; 2) to determine possible reasons for higher O-GNR-PEG-DSPE uptake by HeLa cells. An ancillary goal was to investigate the capabilities of O-GNR-PEG-

DSPEs as cell specific delivery agents. The FDA-approved anti-cancer drug doxorubicin (Dox) was chosen for these studies because it only enters cells through passive diffusion, and thus at low concentrations shows poor uptake into many cancer cells;(Arora et al., 2012) Dox typically requires a delivery agent to increase efficacy. Once inside the cell, membrane-bound p-glycoprotein (P-gp), expressed in certain cells (see **Table 1**), can 'pump' Dox out of the cells, (Arora et al., 2012) which may in turn lead to drug resistance. Cell clones resistant to low concentrations (treatment of cells with 20µg/ml Dox for 24 hours of Dox) were chosen. Thus, any increase in cytotoxic effects of similar concentration (20µg/ml) of Dox loaded onto O-GNR-PEG-DSPEs would imply increased delivery of Dox by O-GNR-PEG-DSPEs.

Dox was non-covalently loaded onto O-GNR-PEG-DSPE through simple pi-pi stacking interactions (**Figure 7A**)(Liu et al., 2009). The optimum drug loading efficiency of the O-GNR-PEG-DSPE formulation was 40%, i.e., 0.4 mg of Dox could be loaded on 1 mg of O-GNR-PEG-DSPE (**Figure 7 B**). Dox release from O-GNR-PEG-DSPE took place mainly in an acidic environment (pH, 4 to 6, 100% release in 3 days) with minimal drug release in a neutral or basic environment (pH $\geq$ 7, 10% release in 3 days). Drug release at acidic pH followed first order kinetics. Such a drug release profile is ideal for tumor drug delivery agents as the pH of tumors is predominantly acidic (**Figure 7D**)(Gerweck et al., 2006).

In vitro drug delivery studies were conducted using 50 µl of O-GNR-PEG-DSPE solution at a potential therapeutic dosage of 50µg/ml (determined from previous cytotoxicity studies for O-GNR-PEG-DSPE(Mullick Chowdhury et al., 2013)) loaded with 40% Dox by weight (20 µg/ml); treatment duration was 24 hours and the solution was studied in 11 cell lines (**Table 1**, cell line selection criteria for these studies were based on previous results). Since HeLa is a cervical cancer cell line with an integrated HPV genome, we chose cell lines comprised of

cervical cancers cells with or without an HPV genome, and non-cervical cancer cells with low, normal or high EGFR expression(Bachran et al., 2010, Home, 2012, Berkers et al., 1991, Defize et al., 1988, Stea et al., 2003, Bonavia et al., 2010, Sirotnak et al., 2000, Abourbeh et al., 2012, Meira et al., 2011, Wong, 2005, Cai et al., 2008). Expression capability of P-gp, also known as multidrug resistant protein 1 (MDR1) expression status of the cell lines is also provided since it can also influence accumulation and efficacy of Dox inside the cells (De Rosa et al., 2004, Biing et al., 1994, Li et al., 2006, Zhou et al., 2011, Mechetner et al., 1998, Jacobs et al., 2011, Villar et al., 2012, Lutterbach et al., 1998, Mutoh et al., 2006). We used a lactate dehydrogenease (LDH) assay to assess cytotoxicity due to cellular delivery of Dox. LDH, a cytoplasmic marker for membrane integrity, provides an indirect means of assessing cytotoxicity(Mullick Chowdhury et al., 2013). Leaky membranes of damaged or dead cells show increased LDH release into surrounding media compared to normal intact cells. Our previous results validated this assay as a robust assessment of cytotoxicity without any interference from O-GNR-PEG-DSPE(Mullick Chowdhury et al., 2013). Under the same conditions, HeLa and CaSki cells showed ~100% greater LDH release, and SiHa cells showed ~75% greater LDH release when both were compared to cells treated with free Dox dispersed in PEG-DSPE (F**igures 8 B-F)**. HeLa and SiHa express normal levels of EGFR while CaSki cells over-express EGFR. At the same loading concentration, three cell types with high EGFR expression MDA-MB-231, A431 cells (a non cervical cancer squamous cell carcinoma cell line of the vulva) and U251 cells (a glioblastoma cell line) showed ~20% and ~15% higher LDH release respectively compared to cells treated with free Dox dispersed in PEG-DSPE. C33a, a cervical cancer cell line without the HPV genome, and other cell lines (U87MG, MCF7, A549 and MRC5 cells) did not show a statistically significant decrease in viability compared to free Dox (**Table 1** and **Figures 9A-F**). Six cell

lines that showed increased LDH release (HeLa, CaSki, SiHa, MDA-MB-231, A431 and U251 cells) either over-express EGFR on their surface and/or have integrated HPV genome/genomes(Bachran et al., 2010, Berkers et al., 1991, Defize et al., 1988, Stea et al., 2003, Cai et al., 2008). The other cell lines show low or normal EGFR expression (Home, 2012, Bonavia et al., 2010, Sirotnak et al., 2000, Abourbeh et al., 2012, Meira et al., 2011). HeLa,CaSki and MDA-MB-231 cells, that either possess integarted HPV genome/s or over express EGFR or both, and do not express P-gp, exhibited the highest LDH release. Cell lines with an integrated HPV genome (SiHa) or high EGFR expression (A431and U251 cells) which also express P-gp, exhibited higher LDH release compared to free drug as well. However, other cell lines with low or normal EGFR expression, but do not express P-gp (MRC5, U87MG, A549, MCF7, C33A), did not show a similar increase in LDH levels. These results indicate that cells with an HPV genome or EGFR over expression exhibit increased drug efficacy, even in those with p-glycoprotein expression.

Next, drug delivery studies were performed on HeLa and CaSki cell lines after treatment with endocytosis and macropinocytosis inhibitors. We used very low non-toxic concentrations of cell inhibitors to ensure that any observed cell death was mainly due to Dox-loaded O-GNR-PEG-DSPE uptake **(Figure 11). Figure 12 A-D and Figure 13 A-D** shows the salient results of these studies for HeLa cells and CaSki cells, respectively. In HeLa cells, unexposed control cells showed approximately 33% LDH release compared to the lysed control cells. HeLa cells treated with dynasore at 20µM showed no difference in LDH release from the non-inhibited cells treated with dox loaded O-GNR-PEG-DSPE (**shown in Figure 9E**, **~75% of lysed control cells**). However, when HeLa cells were treated with dynasore at 80µM, LDH release decreased to ~65% of cells exposed to the drug loaded nanoparticle (**Figure 12 A**). HeLa cells treated with

filipin at various concentrations (1-3µg/ml) did not show a significant decrease in LDH levels (**Figure 12B**). HeLa cells treated with EIPA, at 0.25mM and 0.5mM concentrations, showed a decrease to ~80% and ~72% LDH release, respectively (**Figure 12C**). HeLa cells treated with gefitinib, at 0.5µM concentration, decreased LDH release to ~ 76% and at 1µM to ~50% (**Figure12D**)

Dynasore inhibition of dynamin prevented O-GNR-PEG-DSPE uptake by both clathrin-mediated endocytosis and ruffle-mediated vesicle formation. EIPA inhibits only macropinocytosis-like processes (ruffle-mediated vesicle formation in this case). EIPA inhibition decreased LDH Release to ~72% of non-inhibited cells, similar to the ~65% LDH release observed after dynasore inhibition. This comparison provided additional indication that dynamin-dependent endocytosis might play a minor role in drug-loaded nanoparticle uptake. Filipin, which prevents caveolae-mediated endocytosis, did not show such an effect, thus ruling it out as an uptake mechanism. Gefitinib, a tyrosine kinase inhibitor also decreases LDH release in response to drug-loaded O-GNR-PEG-DSPEs to ~50% that of uninhibited cells. CaSki cells produced similar results indicating that the mechanism of O-GNR-PEG-DSPE uptake in both cell lines was similar although CaSki cells expressed more EGFR compared to HeLa cells (**Figure 9 A-D**). Further, transfection of small interfering ribonucleic acid (siRNA) against EGFR (**Figure 15**) into HeLa cells also significantly decreased cell death due to drug delivery, and corroborated the EGFR-mediated uptake mechanism of O-GNR-PEG-DSPEs (**Figure 12E**). Efficiency of EGFR inhibition in HeLa cells was confirmed by confocal microscopy and flow cytometry (**Figure 15**). Flow cytometry results indicated that si RNA transfected cells produced ~5 times less activated EGFR compared to uninhibited cells treated with EGF (activation evidenced by increase in fluorescence intensity from untreated control cells). Drug delivery experiments with C33A cells

transfected with a plasmid expressing wt EGFR showed a small increase in drug delivery efficiency compared to untransfected cells showing that the EGFR expression might play a role in the slightly higher delivery response in the transfected cells. Transfection in these cells was confirmed by flow cytometry (**Figure 10 A**). Cell count analysis showed that the higher LDH release was not due to higher growth rate of the C33A cells transfected with EGFR as both cell lines showed similar growth after 24 hours (**Figure 10B**).

Similar drug delivery experiments on HeLa cells performed with Dox-loaded PEG-DSPE-coated multi-walled carbon nanotubes and graphene nanoplatelets as well as Dox-loaded Dextran or Pluronic F127 (routinely used to improve water dispersibility of carbon nanotube and graphene nanoparticles)-coated O-GNRs failed to show the same drug delivery response (**Figure 14 A-D**). O-GNRs themselves could not be used an experimental group due to poor dispersibility and stability in buffer and media solutions.

4.3.3 Role of human papillomavirus E5 protein

HeLa, CaSki and SiHa cells, which showed the highest cytotoxicity during drug delivery experiments are all squamous cervical carcinoma (SCC) cells with integrated human papillomavirus (HPV16 or HPV18) genomes(Bachran et al., 2010). Thus, we investigated the role of the HPV genome in mediating enhanced uptake of Dox-loaded O-GNR-PEG-DSPEs. HPV viral proteins E5, E6 and E7 are associated with major oncogenic factors in high-risk HPV (Boulenouar et al., 2010). E5, a transmembrane protein, increases ligand-dependent EGFR activation and signaling (DiMaio and Mattoon, 2001). E5 functions by preventing acidification of endosomes containing internalized EGFR, which in turn prevents EGFR degradation, and results in recycling of activated EGFR back to the cell surface. The number of times that

activated EGFRs are recycled by E5 before being degraded is still not known. Among the above three cell lines (HeLa, CaSki and SiHa), HPV genome incorporation is high in CaSki cells (500-600 copies), lower in SiHa cells (1-2 copies) and moderate in HeLa cells (40-50 copies)(Samama et al., 2002). E5 expression in these cell lines is not proportional to the number of incorporated HPV genomes; HPV genome incorporation is random, and often results in loss of viral genome fragments encoding E5 (Tsai, 2003). Although, several studies showed the presence of E5 open reading frames or E5 encoding mRNA transcripts in all three cell lines (Baker et al., 1987, Bauer-Hofmann et al., 1996, Sherman et al., 1992) very few studies successfully quantified E5 protein expression in the three cell lines.

To investigate the role of E5 in O-GNR-PEG-DSPE uptake, we transiently transfected a plasmid containing a FLAG tagged HPV16E5 gene into A431 cells (which show high EGFR expression) and C33A cells (which show low EGFR expression); we conducted drug delivery experiments on these transfected cells and confirmed E5 expression and localization using confocal microscopy (with anti-FLAG antibodies) and quantification using flow cytometry (**Figure 16**). The transfection resulted in ~99.8% transfection efficiency in A431 cells and ~62% transfection efficiency in C33A cells (calculated from flow cytometry data shown in Figure 16). Results indicated that E5 over-expression in A431 cells increased the drug delivery response (i.e., increased LDH release) by approximately 52 % (**Figure 17A**). We also observed a small increase in activated EGFR in EGF-treated and HPV16E5-transfected A431 cells (**Figure 17D**). C33A cells transfected with FLAG tagged HPV16E5 did not show the same response although we did see a small increase in LDH release (**Figure 17B**). This difference is probably due to low EGFR expression in C33A cells compared to A431 cells. We did not observe increased EGFR expression or activation in transfected C33A cells **(Figure 17E)**. TEM images qualitatively

confirmed that over-expression of HPV16E5 increased uptake of O-GNR-PEG-DSPEs in A431 cells but not in C33A cells (**Figure 18A-D**). TEM images of HPV16E5 transfected A431 cells also showed evidence of interconnected vesciles containing the O-GNR-PEG-DSPE. siRNA transfection against E5 in HeLa cells (**Figure 15**) decreased the cytotoxic response upon treatment with Dox loaded O-GNR-PEG-DSPEs (**Figure 17C**). Flow cytometry results for quantification of EGFR inhibition in response to transfection of siRNA against HPV 18 E5 showed that transfected cells showed ~ 4.5 times less activated EGFR compared to uninhibited cells when treated with EGF (activation evidenced by increase in fluorescence intensity from untreated control cells) (**Figure 15**) Taken together, results shown in Figure 17 indicate that presence E5 protein by itself is insufficient for high uptake of O-GNR-PEG-DSPE. Normal or high EGFR expression is necessary to achieve significantly increased drug efficacy. These results corroborated our hypothesis that the E5 is involved in the increased uptake of Dox loaded O-GNR-PEG-DSPEs into HPV-mediated cells.

4.4 Discussion

Based on above results and existing literature regarding EGFRs,(Abulrob et al., 2010) and HPV E5 protein(DiMaio and Mattoon, 2001, Tsai, 2003), we propose the following two models to explain O-GNR-PEG-DSPE uptake and drug delivery processes (**Figure 19**). For non-HPV cells (**Figure 19A**), the O-GNR-PEG-DSPEs activate dense EGFR clusters present at different locations on cell membrane surface. Simultaneous activation of these EGFRs results in a predominantly macropinocytotic response leading to O-GNR-PEG-DSPE uptake along with these receptors. Cell with high EGFR expression should contain a greater number of these EGFR clusters. In these cells, O-GNR-PEG-DSPEs are more likely to interact with and activate these EGFRs clusters on the membrane surface; thus, these cells show higher O-GNR-PEG-DSPE

uptake and consequently increased drug delivery and efficacy compared to cells with normal or low EGFR expression. For cells with the HPV genome (**Figure 19B**), E5 prevents degradation of activated EGFR receptors, and recycles them onto the cell surface, which results in repetition of the uptake mechanism for nanoparticles on the cell surface or surrounding the cells without further EGFR activation. Consequently, these cells with normal or high EGFR expression have higher uptake capacity for Dox-loaded O-GNR-PEG-DSPEs, and show increased cell death compared to cells with only high EGFR expression.

The exact mechanism by which O-GNR-PEG-DSPE activates EGFR requires further study. Interaction of nanoparticles with cell surface proteins could be influenced by a variety of physicochemical attributes including size, morphology including surface, and charge (Deng et al., 2010). Certain nanoparticles interact with extracellular matrix components and these interactions, in turn, activate cell receptors (Deng et al., 2010). Recently synthetic heteropolymers, comprising of PEG blocks non-covalently functionalized onto single walled carbon nanotubes, have also been reported to facilitate biomolecular recognition (Zhang et al., 2013). The 'normal' activators for EGFRs are EGF and transforming growth factor alpha (TGF-α),(Henriksen et al., 2013) EGFRs can also be activated by other mechanisms such as reactive oxygen species (ROS) generation, cellular stress and membrane depolarization (Chen et al., 2006). Thus, additional experiments are underway to elucidate potential EFGR activation mechanism(s) by O-GNR-PEG-DSPEs. Further our results suggest that EGFR activation depends on yet to be determined physicochemical characteristic(s) of the O-GNR-PEG-DSPE complex and that O-GNRs are a critical component. Further investigation is needed to determine whether our results are unique to PEG-DSPE-coated O-GNRs(Kosynkin et al., 2009) used in this study, or can be generalized to nanoribbons prepared by other methods (Jiao et al., 2010).

4.5 Conclusions

O-GNR-PEG-DSPEs activate epidermal growth factor receptors (EGFRs) and are taken up in significant amounts in cells with high EGFR expression. This phenomena leads to differential and increased intracellular drug delivery efficacy. For cells with high EGFR expression, or with HPV genome, the intracellular delivery of the drug doxorubicin by O-GNR-PEG-DSPE increases its efficacy by 100% greater compared to drug alone. Even in cells with high EGFR expression, or with HPV genome, that express the multidrug resistant protein 1 (MDR1), the drug efficacies increase upto 75% compared to drug alone. Drug alone dispersed in PEG-DSPE at the same or twice the concentration loaded onto O-GNR-PEG-DSPEs did not show any statistically significant increase in its efficacy compared to untreated cells. Cells with integrated human papilloma virus (HPV) genomes, which express EGFR (at normal or elevated levels), elicit enhanced O-GNR-PEG-DSPE uptake via the modulation of EFGR by the viral protein E5. This cell specific uptake of O-GNR-PEG-DSPEs and other factors like high drug loading capacity, acidic pH dependent release kinetics, and unique nanoscopic properties that allow it to enter and stay inside tumors due to the enhanced permeability-and-retention (EPR) effect(Haley and Frenkel, 2008)) indicate that these particles can be highly potent as a delivery agent for cancers that over express EGFR or are mediated by HPV (Siddiqui et al., 2012). O-GNR-PEG-DSPE has the potential to be developed as an agent that can mitigate common problems of chemotherapy like non specific toxicity and resistance to drug treatment (Ogino et al., 2007, Lynch et al., 2007).

4.6 References

Abourbeh, G., Shir, A., Mishani, E., Ogris, M., Rödl, W., Wagner, E. & Levitzki, A. 2012. PolyIC GE11 polyplex inhibits EGFR-overexpressing tumors. *IUBMB life,* 64**,** 324-330.

Abulrob, A., Lu, Z., Baumann, E., Vobornik, D., Taylor, R., Stanimirovic, D. & Johnston, L. J. 2010. Nanoscale imaging of epidermal growth factor receptor clustering effects of inhibitors. *Journal of Biological Chemistry,* 285**,** 3145-3156.

Arora, H. C., Jensen, M. P., Yuan, Y., Wu, A., Vogt, S., Paunesku, T. & Woloschak, G. E. 2012. Nanocarriers enhance doxorubicin uptake in drug-resistant ovarian cancer cells. *Cancer Research,* 72**,** 769-778.

Bachran, D., Schneider, S., Bachran, C., Urban, R., Weng, A., Melzig, M. F., Hoffmann, C., Kaufmann, A. M. & Fuchs, H. 2010. Epidermal growth factor receptor expression affects the efficacy of the combined application of saponin and a targeted toxin on human cervical carcinoma cells. *International Journal of Cancer,* 127**,** 1453-1461.

Bae, Y. H. & Park, K. 2011. Targeted drug delivery to tumors: myths, reality and possibility. *Journal of controlled release,* 153**,** 198.

Baker, C. C., Phelps, W. C., Lindgren, V., Braun, M. J., Gonda, M. A. & Howley, P. M. 1987. Structural and transcriptional analysis of human papillomavirus type 16 sequences in cervical carcinoma cell lines. *Journal of virology,* 61**,** 962-971.

Bauer-Hofmann, R., Borghouts, C., Auvinen, E., Bourda, E., Rösl, F. & Alonso, A. 1996. Genomic cloning and characterization of the nonoccupied allele corresponding to the integration site of human papillomavirus type 16 DNA in the cervical cancer cell line SiHa. *Virology,* 217**,** 33-41.

Berkers, J., En Henegouwen, P. V. B. & Boonstra, J. 1991. Three classes of epidermal growth factor receptors on HeLa cells. *Journal of Biological Chemistry,* 266**,** 922-927.

Biing, J., Yang, Y., Liu, H., Ye, C. & Chao, C. 1994. The induction of multidrug resistance in human cervical carcinoma cell lines by estrogenic hormones. *Proceedings of the National Science Council, Republic of China. Part B, Life sciences,* 18**,** 64.

Bitounis, D., Ali-Boucetta, H., Hong, B. H., Min, D.-H. & Kostarelos, K. 2013. Prospects and Challenges of Graphene in Biomedical Applications. *Advanced Materials,* 25**,** 2258-2268.

Bonavia, R., Mukasa, A., Narita, Y., Sah, D. W., VandenberG, S., Brennan, C., Johns, T. G., Bachoo, R., Hadwiger, P. & Tan, P. 2010. Tumor heterogeneity is an active process maintained by a mutant EGFR-induced cytokine circuit in glioblastoma. *Genes & development,* 24**,** 1731-1745.

Boulenouar, S., Weyn, C., Van Noppen, M., Ali, M. M., Favre, M., Delvenne, P. O., Bex, F., Noël, A., Englert, Y. & Fontaine, V. 2010. Effects of HPV-16 E5, E6 and E7 proteins on survival, adhesion, migration and invasion of trophoblastic cells. *Carcinogenesis,* 31**,** 473-480.

Cai, Z., Chen, Z., Bailey, K. E., Scollard, D. A., Reilly, R. M. & Vallis, K. A. 2008. Relationship between induction of phosphorylated H2AX and survival in breast cancer cells exposed to 111In-DTPA-hEGF. *Journal of Nuclear Medicine,* 49**,** 1353-1361.

Chen, C.-H., Cheng, T.-H., Lin, H., Shih, N.-L., Chen, Y.-L., Chen, Y.-S., Cheng, C.-F., Lian, W.-S., Meng, T.-C. & Chiu, W.-T. 2006. Reactive oxygen species generation is involved in epidermal growth factor receptor transactivation through the transient oxidization of

Src homology 2-containing tyrosine phosphatase in endothelin-1 signaling pathway in rat cardiac fibroblasts. *Molecular pharmacology,* 69**,** 1347-1355.
Chowdhury, S. M., Kanakia, S., Toussaint, J. D., Frame, M. D., Dewar, A. M., Shroyer, K. R., Moore, W. & Sitharaman, B. 2013. In Vitro Hematological and In Vivo Vasoactivity Assessment of Dextran Functionalized Graphene. *Scientific reports,* 3.
De Rosa, M. F., Sillence, D., Ackerley, C. & Lingwood, C. 2004. Role of multiple drug resistance protein 1 in neutral but not acidic glycosphingolipid biosynthesis. *Journal of Biological Chemistry,* 279**,** 7867-7876.
Defize, L., Arndt-Jovin, D., Jovin, T., Boonstra, J., Meisenhelder, J., Hunter, T., De Hey, H. & De Laat, S. 1988. A431 cell variants lacking the blood group A antigen display increased high affinity epidermal growth factor-receptor number, protein-tyrosine kinase activity, and receptor turnover. *The Journal of cell biology,* 107**,** 939-949.
Deng, Z. J., Liang, M., Monteiro, M., Toth, I. & Minchin, R. F. 2010. Nanoparticle-induced unfolding of fibrinogen promotes Mac-1 receptor activation and inflammation. *Nature Nanotechnology,* 6**,** 39-44.
DiMaio, D. & Mattoon, D. 2001. Mechanisms of cell transformation by papillomavirus E5 proteins. *Oncogene,* 20**,** 7866-7873.
Frame, M. D., Dewar, A. M., Mullick Chowdhury, S. & Sitharaman, B. 2014. Vasoactive effects of stable aqueous suspensions of single walled carbon nanotubes in hamsters and mice. *Nanotoxicology,* 8**,** 867-875.
Gerweck, L. E., Vijayappa, S. & Kozin, S. 2006. Tumor pH controls the in vivo efficacy of weak acid and base chemotherapeutics. *Molecular Cancer Therapeutics,* 5**,** 1275-1279.
Haley, B. & Frenkel, E. 2008. Nanoparticles for drug delivery in cancer treatment. *Urologic Oncology: Seminars and Original Investigations,* 26**,** 57-64.
Henriksen, L., Grandal, M. V., Knudsen, S. L. J., Van Deurs, B. & Grøvdal, L. M. 2013. Internalization Mechanisms of the Epidermal Growth Factor Receptor after Activation with Different Ligands. *PLoS ONE,* 8**,** e58148.
Home, N. 2012. Wild type EGFR is stabilized by direct interaction with HSP90 in cancer cells and tumors.
Hubbell, J. A. & Langer, r. 2013. Translating materials design to the clinic. *Nat Mater,* 12**,** 963-966.
Jacobs, V. L., Valdes, P. A., Hickey, W. F. & De Leo, J. A. 2011. Current review of in vivo GBM rodent models: emphasis on the CNS-1 tumour model. *ASN neuro,* 3**,** 171-181.
Jiao, L., Wang, X., Diankov, G., Wang, H. & Dai, H. 2010. Facile synthesis of high-quality graphene nanoribbons. *Nature Nanotechnology,* 5**,** 321-325.
Kanakia, S., Toussaint, J. D., Chowdhury, S. M., Lalwani, G., Tembulkar, T., Button, T., Shroyer, K. R., Moore, W. & Sitharaman, B. 2013. Physicochemical characterization of a novel graphene-based magnetic resonance imaging contrast agent. *International journal of nanomedicine,* 8**,** 2821.
Kitazaki, T., Oka, M., Nakamura, Y., Tsurutani, J., Doi, S., Yasunaga, M., Takemura, M., Yabuuchi, H., SODA, H. & KOHNO, S. 2005. Gefitinib, an EGFR tyrosine kinase inhibitor, directly inhibits the function of P-glycoprotein in multidrug resistant cancer cells. *Lung Cancer,* 49**,** 337-43.
Kosynkin, D. V., Higginbotham, A. L., Sinitskii, A., Lomeda, J. R., Dimiev, A., Price, B. K. & Tour, J. M. 2009. Longitudinal unzipping of carbon nanotubes to form graphene nanoribbons. *Nature Nanotechnology,* 458**,** 872-876.

Lalwani, G. & Sitharaman, B. 2013. Multifunctional Fullerene-and metallofullerene-based nanobiomaterials. *Nano LIFE*.

Li, L., Xu, J., Min, T. & Huang, W. 2006. Up-regulation of P-glycoprotein expression by catalase via JNK activation in HepG2 cells. *Redox Report,* 11**,** 173-178.

Liu, Z., Tabakman, S., Welsher, K. & Dai, H. 2009. Carbon nanotubes in biology and medicine: in vitro and in vivo detection, imaging and drug delivery. *Nano Research,* 2**,** 85-120.

Lutterbach, B., Sun, D., Schuetz, J. & Hiebert, S. W. 1998. The MYND motif is required for repression of basal transcription from the multidrug resistance 1 promoter by the t (8; 21) fusion protein. *Molecular and cellular biology,* 18**,** 3604-3611.

Lynch, T. J., Kim, E. S., Eaby, B., Garey, J., West, D. P. & Lacouture, M. E. 2007. Epidermal growth factor receptor inhibitor–associated cutaneous toxicities: an evolving paradigm in clinical management. *The Oncologist,* 12**,** 610-621.

Mechetner, E., Kyshtoobayeva, A., Zonis, S., KIm, H., Stroup, R., Garcia, R., Parker, R. J. & Fruehauf, J. P. 1998. Levels of multidrug resistance (MDR1) P-glycoprotein expression by human breast cancer correlate with in vitro resistance to taxol and doxorubicin. *Clinical Cancer Research,* 4**,** 389-398.

Meira, D. D., Almeida, V. H., Mororó, J. S., Caetano, M. S., Nóbrega, I. P., Batista, D., Sternberg, C. & Ferreira, C. G. 2011. Efficient Blockade of Akt signaling is a determinant factor to overcome resistance to Matuzumab. *Molecular cancer,* 10**,** 151.

Mullick Chowdhury, S., LalwanI, G., Zhang, K., Yang, J. Y., Neville, K. & Sitharaman, B. 2013. Cell specific cytotoxicity and uptake of graphene nanoribbons. *Biomaterials,* 34**,** 283-293.

Mutoh, K., TsukaharA, S., Mitsuhashi, J., Katayama, K. & Sugimoto, Y. 2006. Estrogen-mediated post transcriptional down-regulation of P-glycoprotein in MDR1-transduced human breast cancer cells. *Cancer science,* 97**,** 1198-1204.

Ogino, A., Kitao, H., Hirano, S., Uchida, A., Ishiai, M., Kozuki, T., Takigawa, N., Takata, M., Kiura, K. & Tanimoto, M. 2007. Emergence of epidermal growth factor receptor T790M mutation during chronic exposure to gefitinib in a non–small cell lung cancer cell line. *Cancer Research,* 67**,** 7807-7814.

Orth, J. D., Krueger,E.W., Weller,S.G, McNiven, M.A. 2006. A novel endocytic mechanism of epidermal growth factor receptor sequestration and internalization. . *Cancer Res.,* 66**,** 3603–3610.

Samama, B., Plas-Roser, S., Schaeffer, C., Chateau, D., Fabre, M. & Boehm, N. 2002. HPV DNA detection by in situ hybridization with catalyzed signal amplification on thin-layer cervical smears. *Journal of Histochemistry & Cytochemistry,* 50**,** 1417-1420.

Sant, S., Tao, S. L., Fisher, O. Z., Xu, Q., Peppas, N. A. & Khademhosseini, A. 2012. Microfabrication technologies for oral drug delivery. *Advanced Drug Delivery Reviews,* 64**,** 496-507.

Sherman, L., Alloul, N., Golan, I., Durst, M. & Baram, A. 1992. Expression and splicing patterns of human papillomavirus type-16 mrnas in pre-cancerous lesions and carcinomas of the cervix, in human keratinocytes immortalized by HPV 16, and in cell lines established from cervical cancers. *International Journal of Cancer,* 50**,** 356-364.

Siddiqui, S., Fang, M., Ni, B., Lu, D., Martin, B. & Maudsley, S. 2012. Central role of the EGF receptor in neurometabolic aging. *International Journal of Endocrinology,* 2012.

Sirotnak, F. M., Zakowski, M. F., Miller, V. A., Scher, H. I. & Kris, M. G. 2000. Efficacy of cytotoxic agents against human tumor xenografts is markedly enhanced by

coadministration of ZD1839 (Iressa), an inhibitor of EGFR tyrosine kinase. *Clinical Cancer Research,* 6**,** 4885-4892.

Stea, B., Falsey, R., Kislin, K., Patel, J., Glanzberg, H., Carey, S., Ambrad, A. A., Meuillet, E. J. & Martinez, J. D. 2003. Time and dose-dependent radiosensitization of the glioblastoma multiforme U251 cells by the EGF receptor tyrosine kinase inhibitor ZD1839 ('Iressa'). *Cancer letters,* 202**,** 43-51.

Tsai, T. C. C., S. L 2003. The biochemical and biological functions of human papillomavirus type 16 E5 protein. *Arch Virol,* 148**,** 1445-1453.

Villar, V. H., Vögler, O., Martínez-Serra, J., Ramos, R., Calabuig-Fariñas, S., Gutiérrez, A., Barceló, F., Martín-Broto, J. & AlemanY, R. 2012. Nilotinib counteracts P-glycoprotein-mediated multidrug resistance and synergizes the antitumoral effect of doxorubicin in soft tissue sarcomas. *PLoS ONE,* 7**,** e37735.

Vlatakis, G., Andersson, L. I., Müller, R. & Mosbach, K. 1993. Drug assay using antibody mimics made by molecular imprinting. *Nature,* 361**,** 645 - 647.

Wong, S.-F. 2005. Cetuximab: an epidermal growth factor receptor monoclonal antibody for the treatment of colorectal cancer. *Clinical therapeutics,* 27**,** 684-694.

Zhang, J., Landry, M. P., Barone, P. W., Kim, J.-H., Lin, S., Ulissi, Z. W., Lin, D., Mu, B., Boghossian, A. A. & Hilmer, A. J. 2013. Molecular recognition using corona phase complexes made of synthetic polymers adsorbed on carbon nanotubes. *Nature Nanotechnology*.

Zhou, Y., Kim, Y.-S., Yan, X., Jacobson, O., Chen, X. & Liu, S. 2011. 64Cu-labeled Lissamine Rhodamine B: a promising PET radiotracer targeting tumor mitochondria. *Molecular pharmaceutics,* 8**,** 1198-1208.

4.7 Tables

Table 1

Cell Line	Type	EGFR Expression	Cytotoxic Activity	P-glycoprotein expression
HeLa	HPV 18 infected cervical carcinoma	Normal[17]	100% more than free drug	Negative[26]
CaSki	HPV 16 infected cervical carcinoma	Over-expressed[15]	100% more than free drug	Negative[27]
SiHa	HPV 16 infected cervical carcinoma	Normal[15]	75% more than free drug	Positive[27]
MDA-MB-231	Breast Adenocarcinoma	Over-expressed[25]	100% more than free drug	Negative[34]
A431	Squamous Carcinoma of vulva	Over-expressed[18]	20% more than free drug	Positive[28]
U251	Glioblastoma	Over-expressed[19]	15% more than free drug	Positive[31]
U87MG	Glioblastoma	Normal[20]	Same as free drug	Negative[29]
MRC5	Fibroblast cell line from fetal lung	Normal[16]	Same as free drug	Negative[32]

A549	**Adenocarcinoma of alveolar epithelia**	**Low-normal[21]**	**Same as free drug**	**Positive[30]**
MCF7	**Breast Adenocarcinoma**	**Low[22]**	**Same as free drug**	**Positive[30]**
C33A	**Cervical carcinoma not infected by HPV**	**Low[23]**	**Same as free drug**	**Positive[33]**

EGFR expression per cell: Low=less than 40000, Normal=40000-100000 [24], Overexpressed=greater than 1000000

Table 1: Summary of cell lines used, their EGFR and P-gp expression and drug delivery efficiency observed compared to free drug.

4.7 Figures

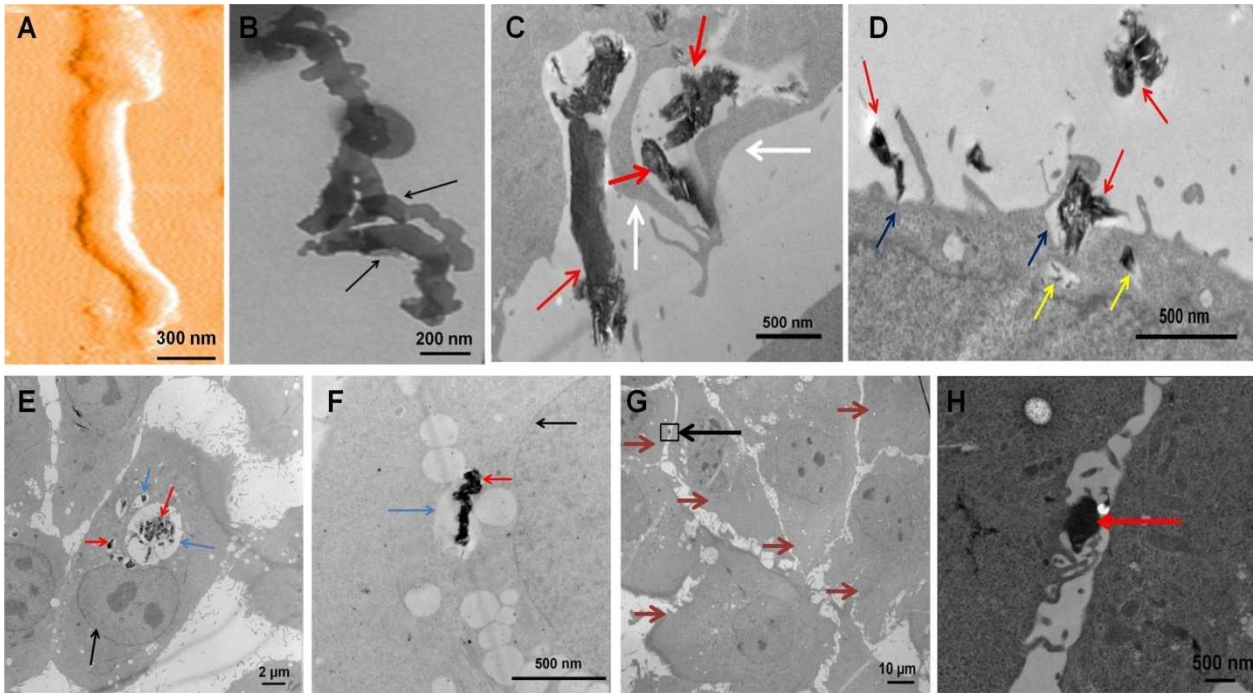

Figure 1. (A) Representative atomic force microscopy (AFM) image of an O-GNR (Oxidized Graphene Nanoribbon); **(B-H)** Representative transmission electron microscopy (TEM) images. **(B)** O-GNR morphology (black arrows). **(C)** HeLa cell with membrane protrusions (white arrows) around O-GNR-PEG-DSPE DSPE (Oxidized Graphene Nanoribbons-1, 2-distearoyl-*sn*-glycero-3-phosphoethanolamine-N [amino (polyethylene glycol)]) aggregates (red arrows) after 15 minutes of incubation with O-GNR-PEG-DSPEs. **(D)** HeLa cell showing O-GNR-PEG-DSPE aggregates (red arrows) on the cell surface (blue arrows) and formation of membrane protrusions (white arrows) after 15 minutes of incubation with O-GNR-PEG-DSPEs. The image also shows smaller endosomal structures (yellow arrows). **(E)** HeLa cell showing significant uptake of O-GNR-PEG-DSPE aggregates (red arrows) into vesicular structures (blue arrows) localized around the nucleus (black arrow) after 30 minutes of incubation with O-GNR-PEG-DSPEs. **(F)** HeLa cell showing uptake of O-GNR-PEG-DSPE aggregates (red arrows) into large and small

perinuclear vesicular structures (blue arrows; black arrow point to the nucleus) after 30 minutes of incubation with O-GNR-PEG-DSPEs. **(G)** HeLa cells, exposed to 1 µM gefitinib followed by O-GNR-PEG-DSPE treatment for 3 hours. Cells show no O-GNR-PEG-DSPE uptake (Brown arrows indicate individual cells). **(H)** Higher magnification of area within the black box in Panel (G) Large O-GNR-PEG-DSPE aggregates (red arrow) on surface of cells.

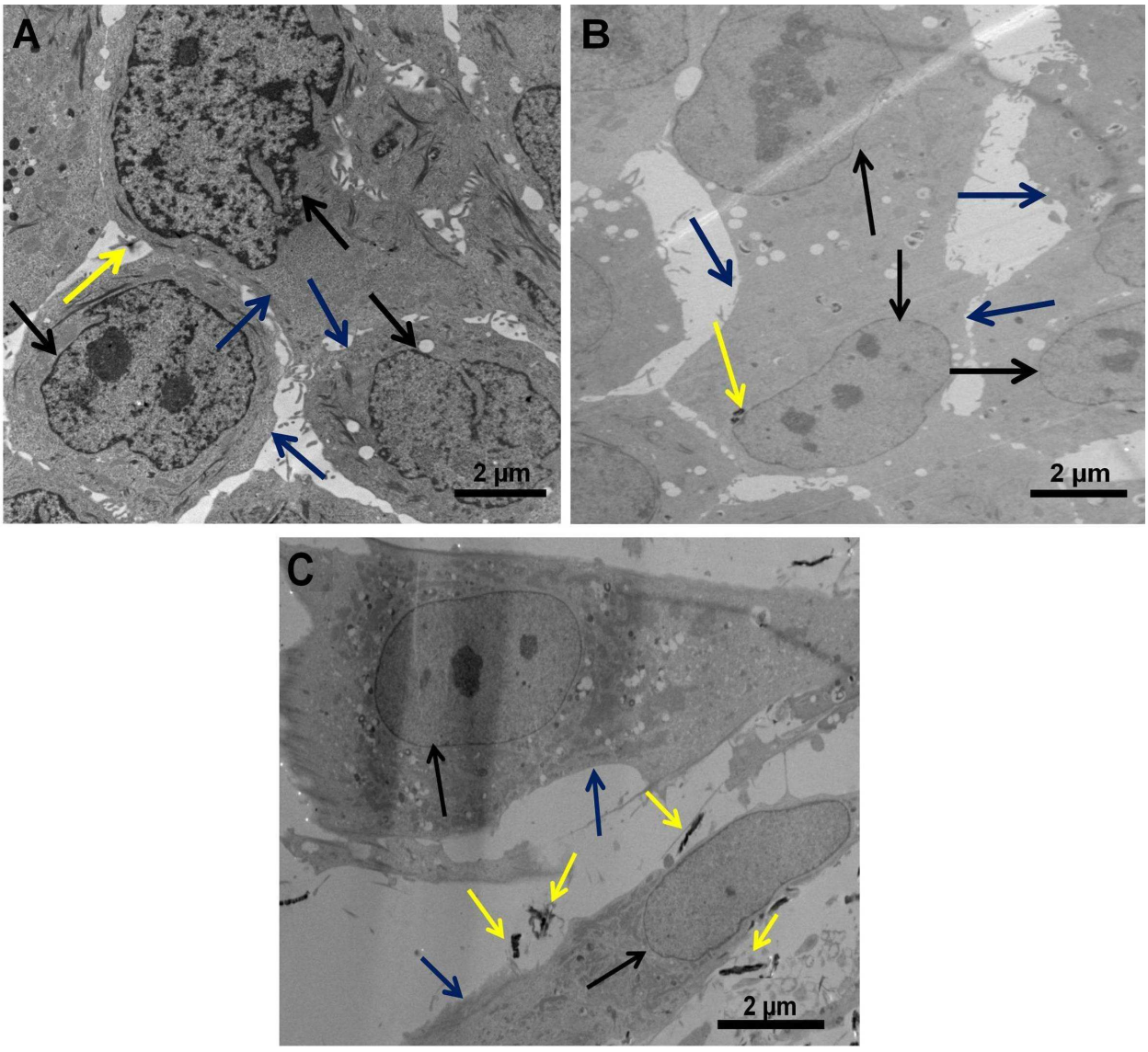

Figure 2. Representative transmission electron microscopy (TEM) images. All cells were treated with 40µg/ml O-GNR-PEG-DSPE (Oxidized Graphene Nanoribbons-1, 2-distearoyl-*sn*-glycero-3-phosphoethanolamine-N[amino(polyethylene glycol)]) for 30 minutes. **(A)** MCF 7 cells show no uptake of O-GNR-PEG-DSPE. **(B)** A549 cells show uptake of small O-GNR-PEG-DSPE aggregates (yellow arrow). **(C)** MRC5 cells show no uptake of O-GNR-PEG-DSPEs (yellow arrows). Black arrows point to the cell nucleus, and blue arrows to the cell membrane. 12 cells for each cell line were analyzed for uptake.

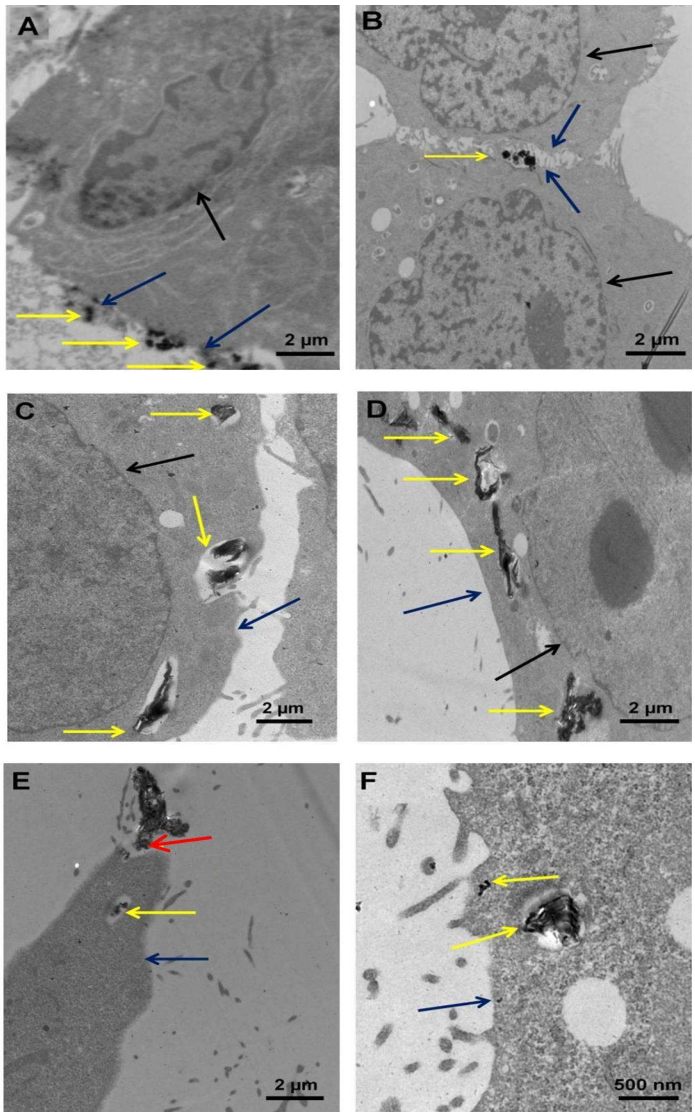

Figure 3. Representative TEM images. All cells were treated with 40µg/ml O-GNR-PEG-DSPE for 30 minutes. **(A & B)** Dynasore treated HeLa cells showing particles on the surface of the cells, with no evidence of macropinocytosis or endocytosis-like responses. **(C & D)** Filipin treated HeLa cells show O-GNR-PEG-DSPE uptake (yellow arrows). **(E and F**) EIPA treated cells that show uptake of smaller particles in endosomes (yellow arrow), and exclusion of larger particles (red arrow). Black arrows point to the cell nucleus while blue arrows indicate the cell membrane. . 12 cells per inhibitor were analyzed for uptake.

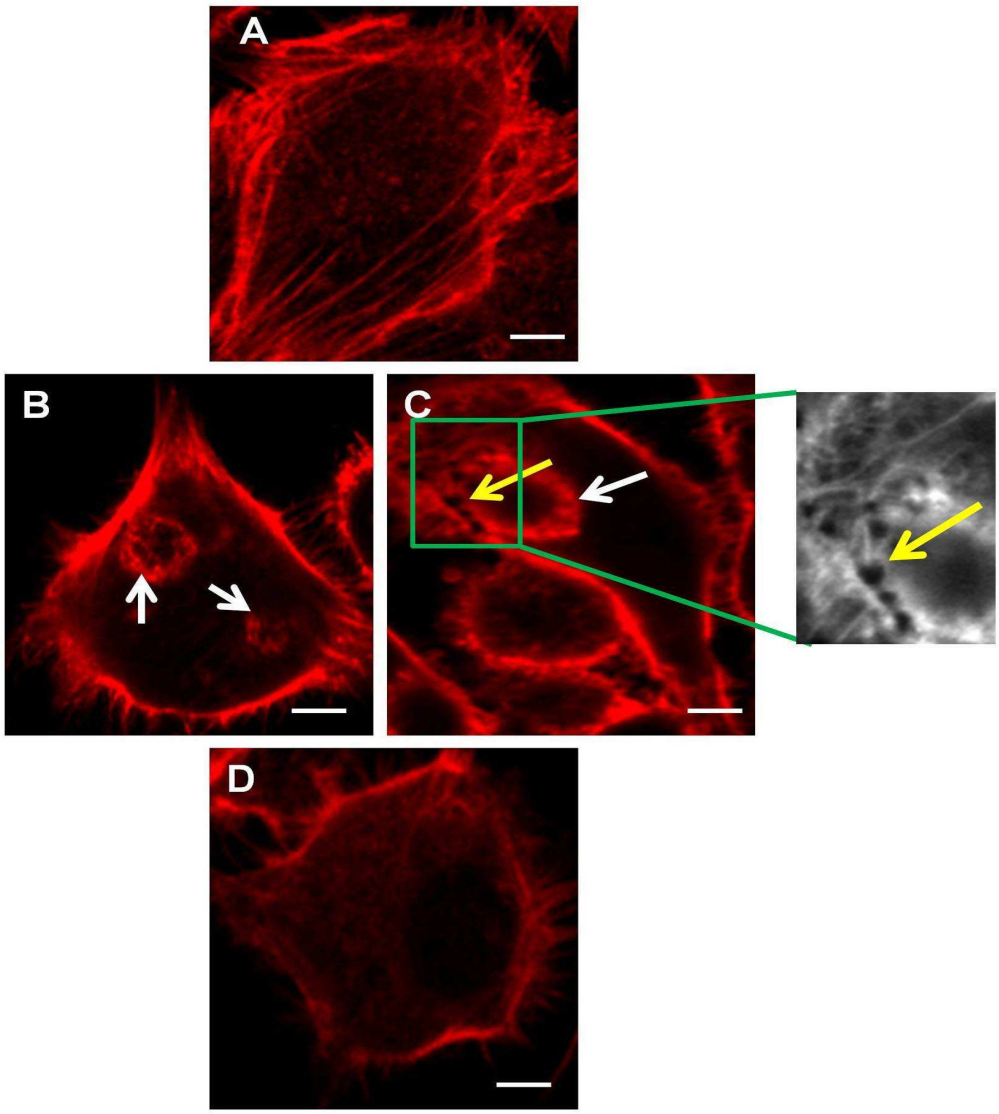

Figure 4. Representative fluorescence microscopy images showing actin microtubules. O-GNR-PEG-DSPE incubation concentration in all the studies was = 50µg/ml **(A)** Phalloidin staining of actin microtubules shows no ruffling in unexposed HeLa cells. **(B)** Circular ruffles (white arrows) in HeLa cells after O-GNR-PEG-DSPE exposure (30 minutes). **(C)** Presence of O-GNR-PEG-DSPE (yellow arrows) along the margin of the ruffles (white arrows). **(D)** Absence of ruffles in HeLa cells, which were pretreated with gefitinib, after O-GNR-PEG-DSPE exposure (30 minutes). 10 cells were analyzed per treatment condition.

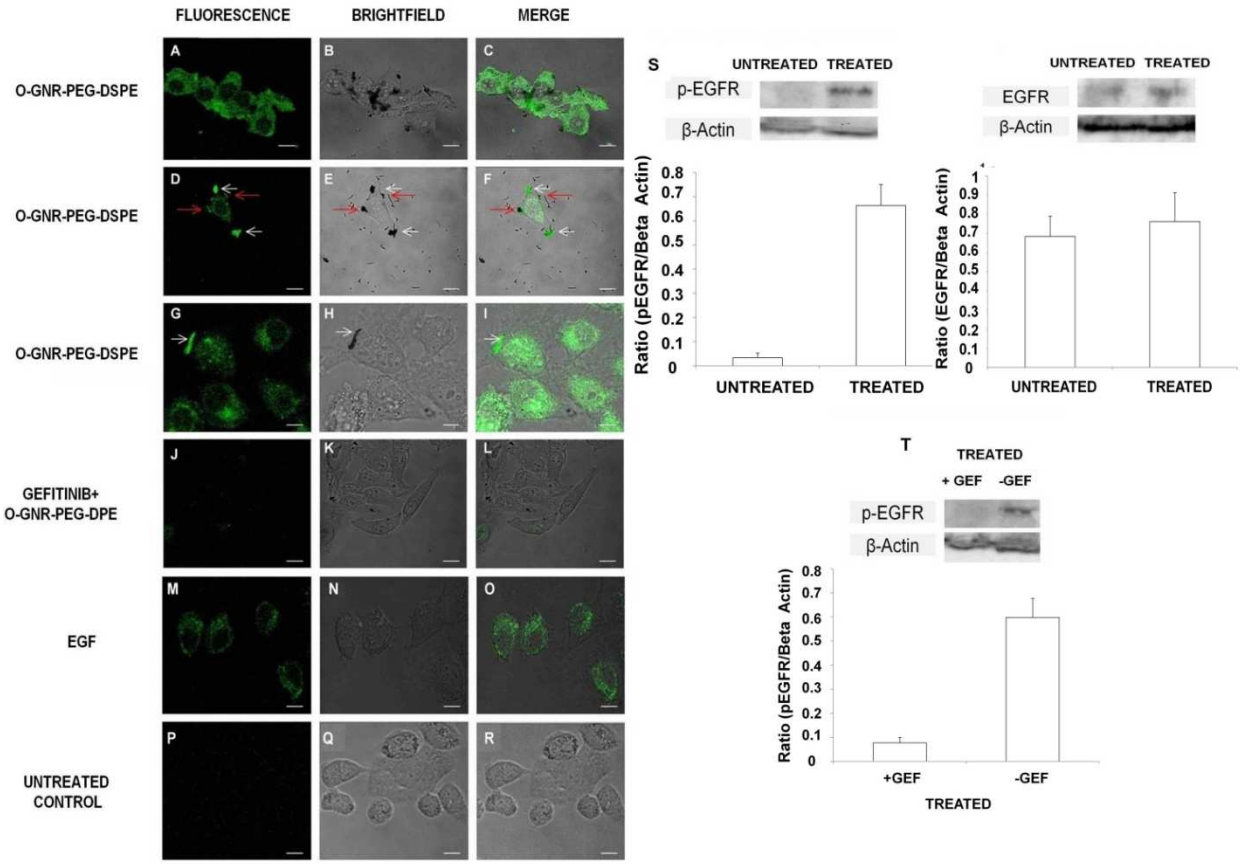

Figure 5. Representative fluorescence, bright field microscopy and merge images. All cells were exposed to 50µg/ml O-GNR-PEG-DSPE for 30 minutes. **(A-C)** Serum deprived HeLa cells exposed to O-GNR-PEG-DSPEs and anti-phospho epidermal growth factor receptor (EGFR) antibody that exhibit activated EGFR receptors (green fluorescence). **(D-F)** Activated surface EGFR receptors co-localized with O-GNR-PEG-DSPEs (red arrows), and activated receptors co-localized with O-GNR-PEG-DSPEs (white arrows) in vesicles. **(G-I)** activated receptors in vesicles co localized with O-GNR-PEG-DSPEs (white arrows). **(J-L)** Gefitinib-pretreated HeLa cells show no significant EGFR activation. **(M-O)** HeLa cells exposed to EGF and anti-phospho EGFR antibody show activated EGFR (positive control). **(P-R)** Unexposed serum-deprived

HeLa cells exposed to anti-phospho EGFR antibody show low activation of EGFR (baseline control). **(S)** Western blot and densitometry quantification for EGFR activation and total EGFR before and after treatment with O-GNR-PEG-DSPEs **(T)** Western blot and densitometry quantification for EGFR activation with and without gefitinib treatment and treatment with O-GNR-PEG-DSPEs (Scale bar=20 µm for microscopy images).

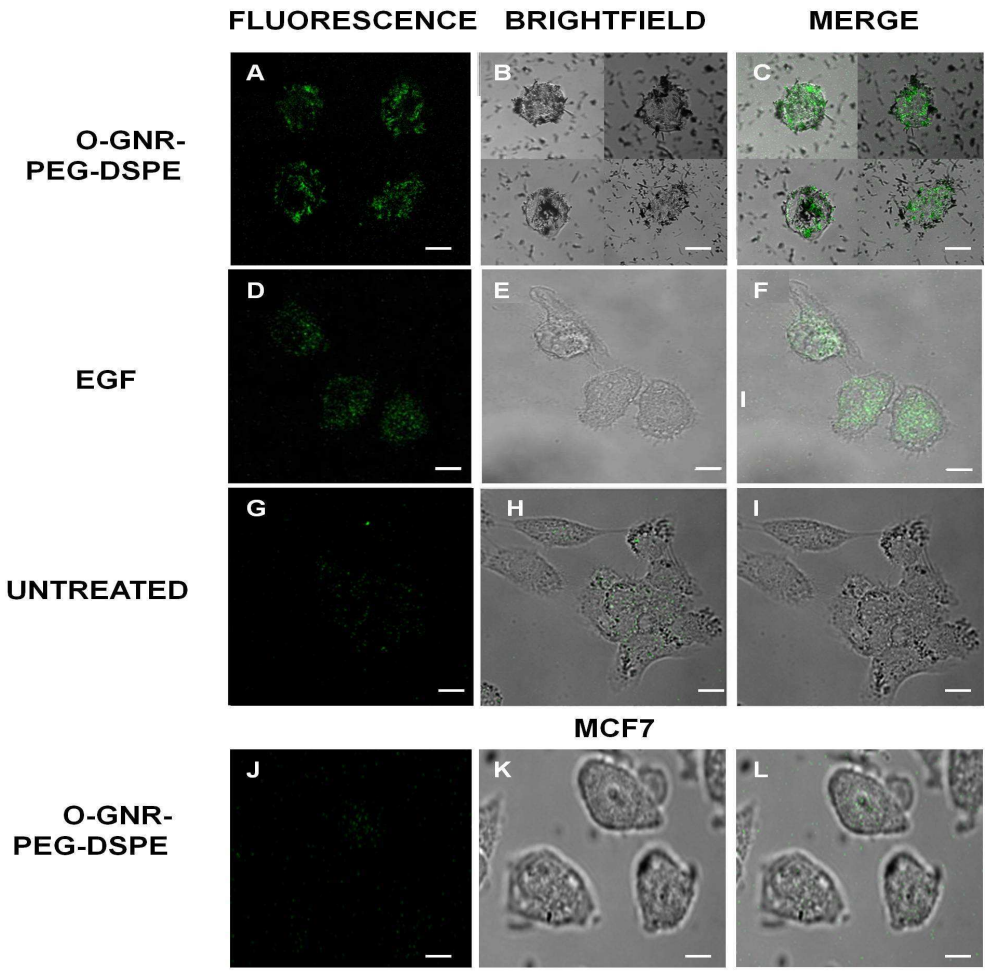

Figure 6. Representative fluorescence, bright field and merged microscopy images. All cells were treated with 50μg/ml O-GNR-PEG-DSPE for 15 minutes **(A-C)** Serum deprived A431 cells were exposed to O-GNR-PEG-DSPEs and anti-phospho epidermal growth factor receptor (EGFR) antibody that exhibit activated EGFRs (green fluorescence). Each figure shows 4 panels with individual cells. **(D-F)** Serum deprived A431 cells treated with EGF showing activated EGF receptors. **(G-I)** Serum deprived untreated A431 cells showing no EGFR activation. **(J-I)** EGF deprived MCF7 cells exposed to O-GNR-PEG-DSPE showing minimal EGFR activation. Size bar=20 μm.

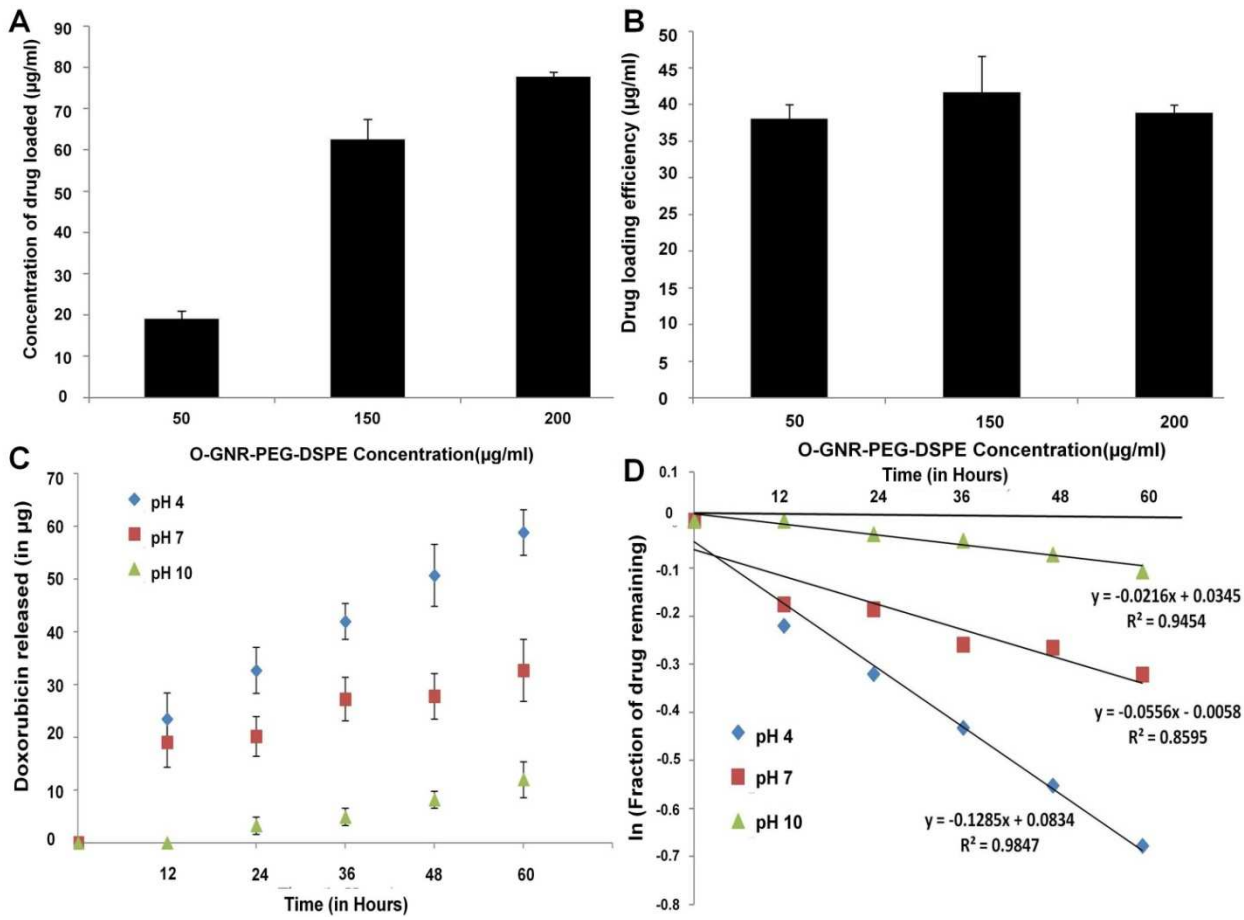

Figure 7. (A) Concentration of drug loaded onto three different concentrations of O-GNR-PEG-DSPE. **(B)** Drug loading efficiency of three different concentrations of O-GNR-PEG-DSPE. **(C)** Drug release profile of O-GNR-PEG-DSPEs. The release of doxorubicin (Dox) from O-GNR-PEG-DSPEs was assessed by suspending a 500 µl solution of 120µg/ml Dox loaded O-GNR-PEG-DSPE in buffers of varying pH (4, 7 and 10) in a 37^{o}C water bath. **(D)** First order fits for drug release from O-GNR-PEG-DSPE.

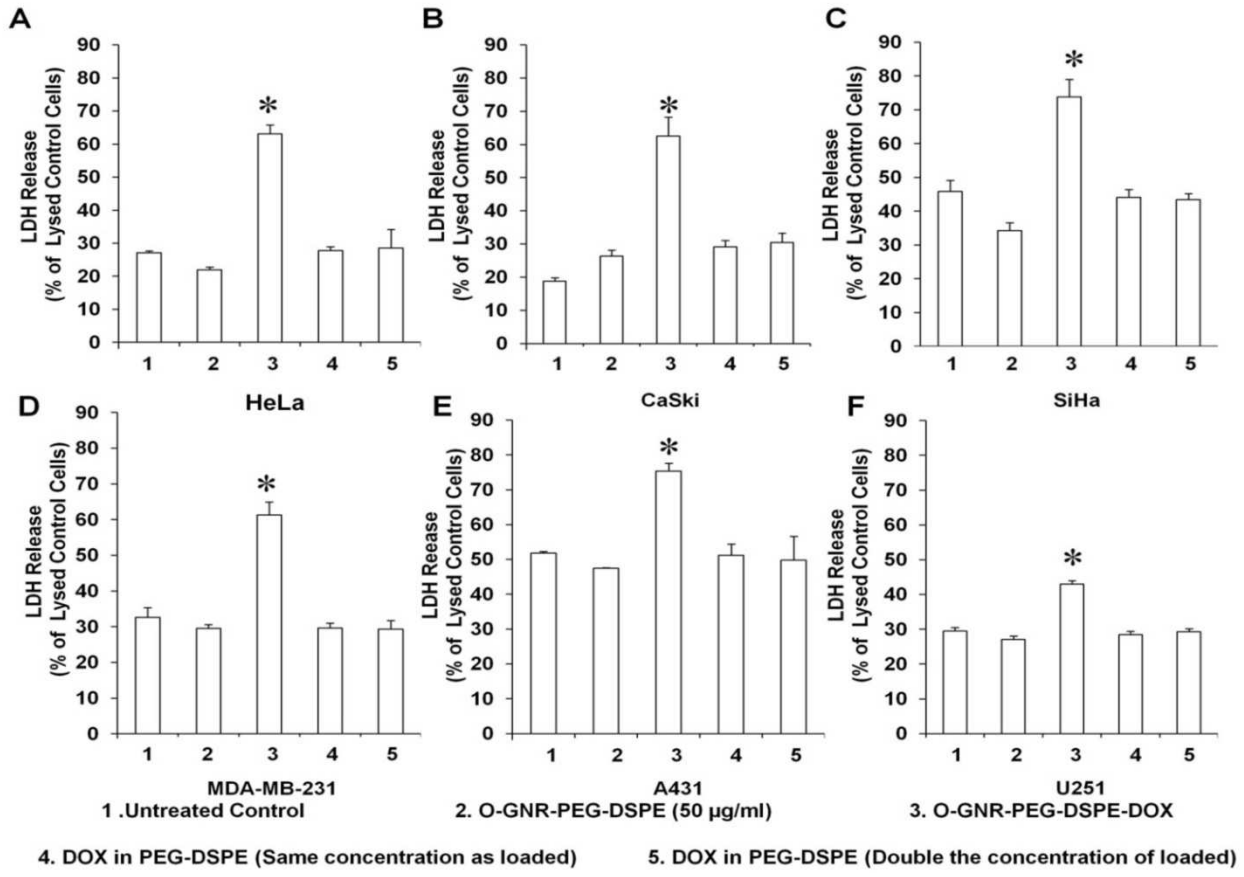

Figure 8. (A-F) Lactic dehydrogenase (LDH) release after treatment with doxorubin (Dox)-loaded O-GNR-PEG-DSPEs in the following cells: **(A)** HeLa. **(B)** CaSki. **(C)**SiHa **(D)** MDA-MB-231 **(E)** A431. **(F)** U251 cells. Untreated cells, cells treated with free dox in PEG-DSPE, and lysed cells were additional controls. All data are normalized to LDH released from lysed control cells. Data are presented as mean ± SD (n = 6 per group). * indicates significant increase ($p < 0.05$) in LDH release compared to cells exposed to Dox in PEG-DSPE at the same concentration as loaded onto O-GNR-PEG-DSPEs. 1= Untreated Control 2= O-GNR-PEG-DSPE (50µg/ml) 3= O-GNR-PEG-DSPE-Dox 4= Dox in PEG-DSPE (Same concentration as loaded) 5= Dox in PEG-DSPE (Double concentration as loaded)

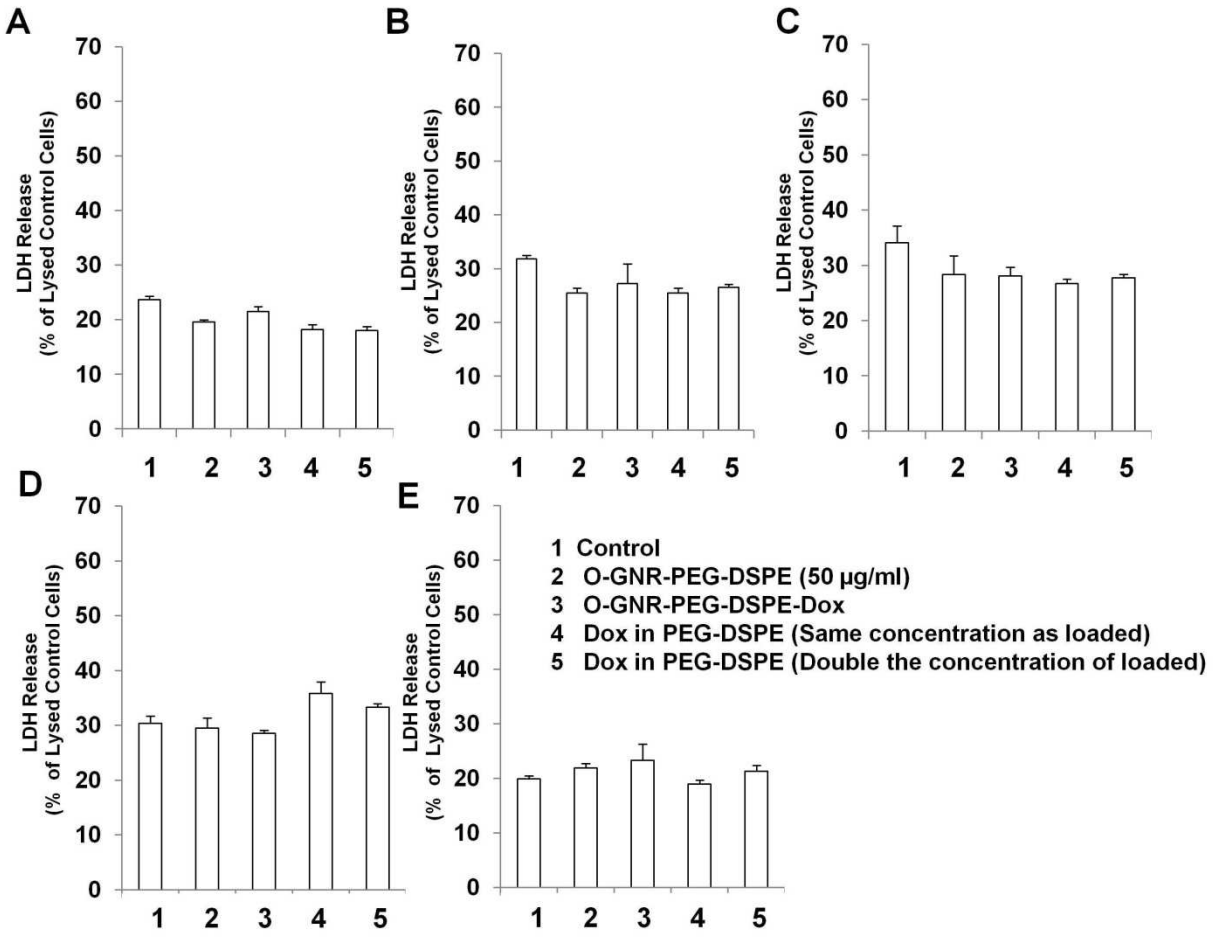

Figure 9. LDH release from the following cell lines treated with Dox-loaded O-GNR-PEG-DSPE and controls (unexposed O-GNR-PEG-DSPE, Dox-loaded O-GNR-PEG-DSPE and free Dox in PEG-DSPE exposed): **(A)** MCF7. **(B)** A549. **(C)** MRC5. **(D)** U87MG. **(E)** C33A. Data are presented as mean + SD (n = 6 per group).

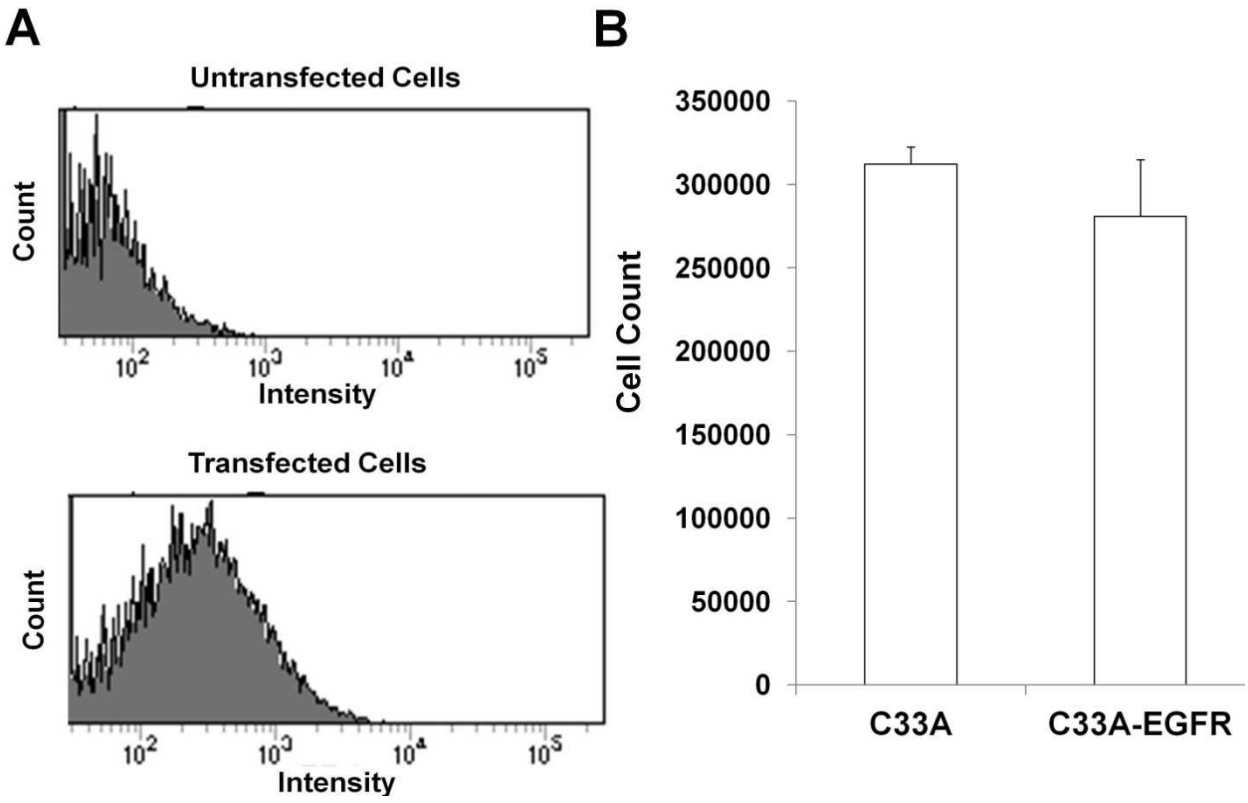

Figure 10 **(A)** Flow cytometry mediated quantitative analysis of EGFR expression in untransfected cells and cells transfected with an EGFR expressing plasmid. Plasmid expression was assessed using a mouse anti- EGFR antibody and a rhodmine tagged goat-anti mouse secondary antibody. (B) Cell count of C33A and EGFR transfected C33A cells after 24 hours (n=6).Data represented as Mean+SD.

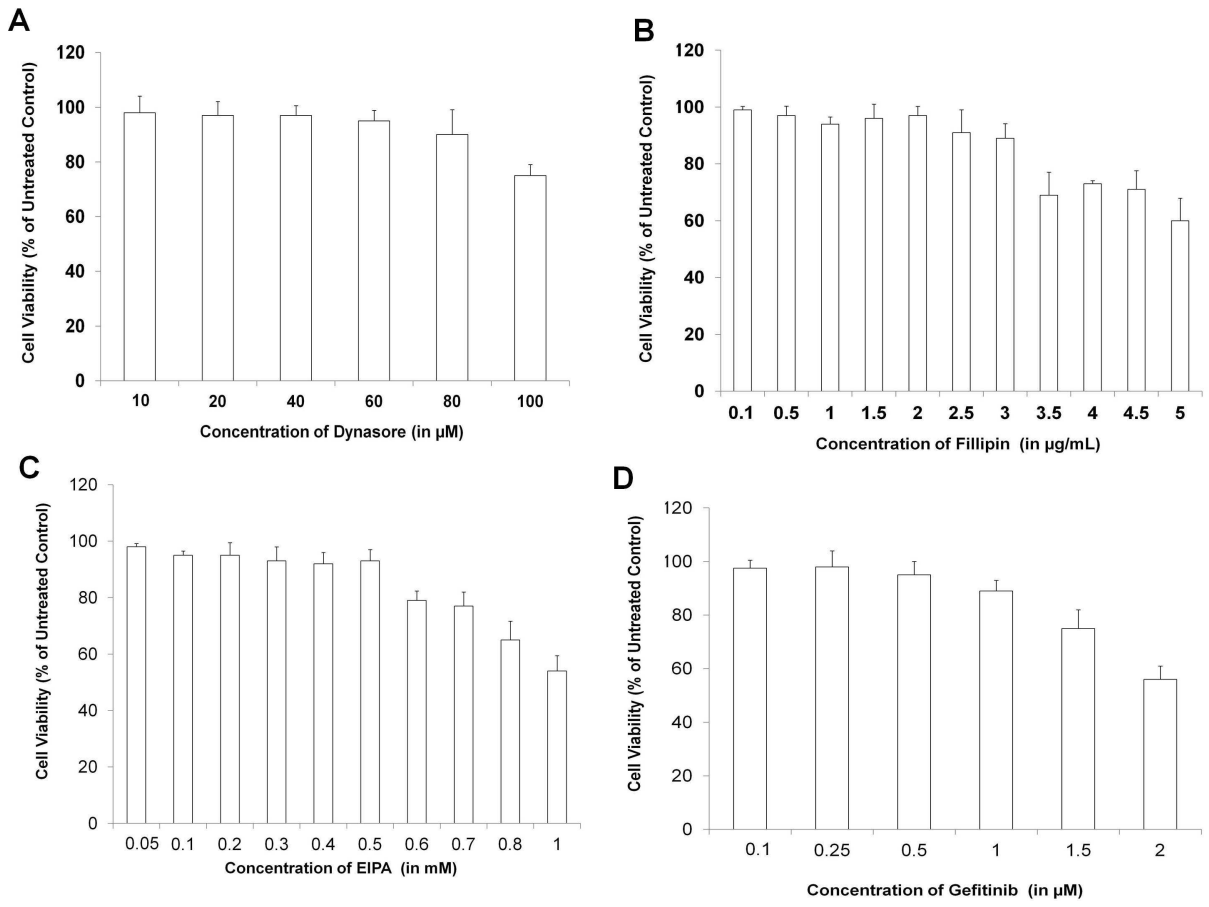

Figure 11 Presto blue assay to assess the cell viability of HeLa cells incubated with different concentrations of (A) Dynasore (B) Filipin (C) EIPA (D) Gefitinib for 24 hours. Data are presented as mean + SD (n = 3 per group).

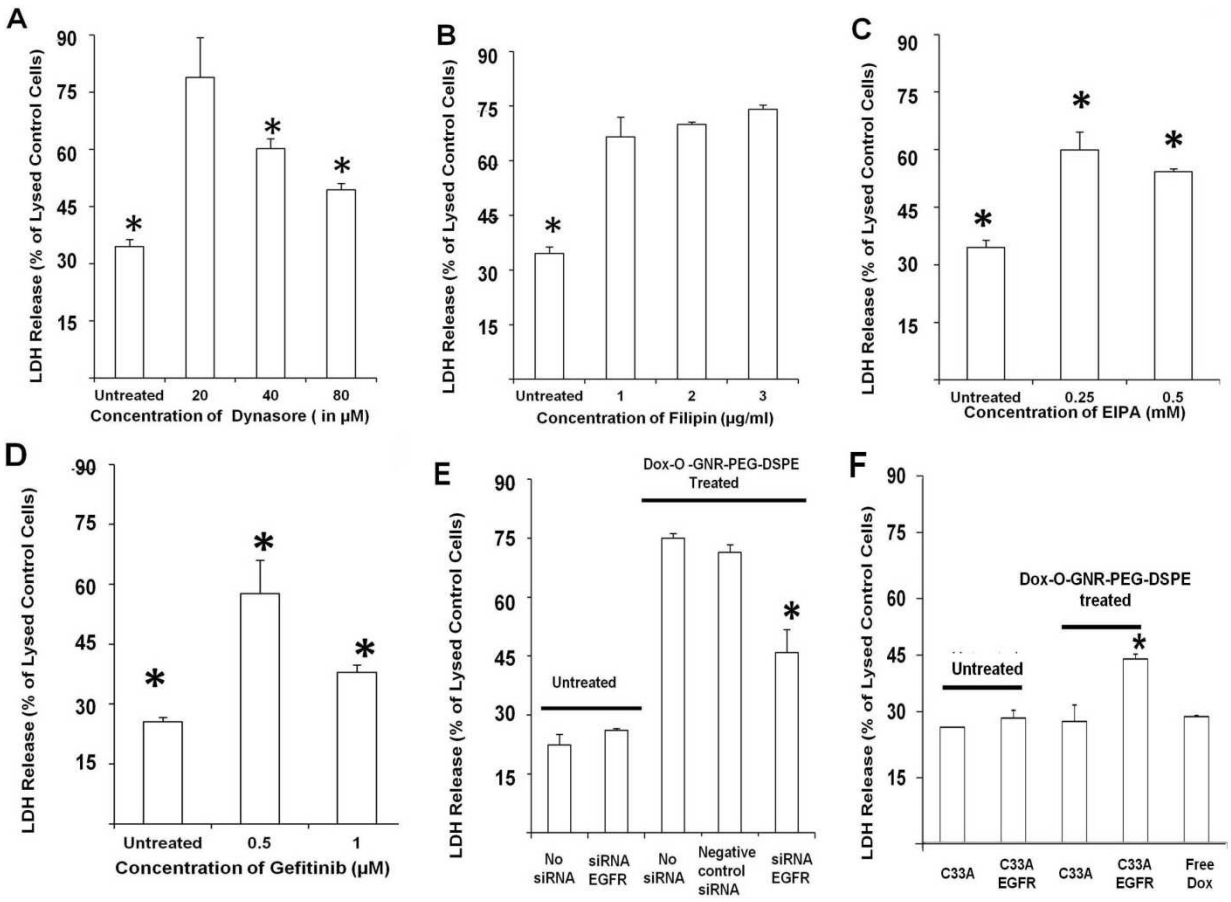

Figure 12. LDH Release from Dox-loaded O-GNR-PEG-DSPE treated HeLa cells exposed to the following: **(A)** Dynasore. **(B)** Fillipin. **(C)** EIPA. **(D)** Gefitinib. **(E)** si RNA against EGFR. Data are presented as mean + SD (n = 3 per group). **(F)** LDH Release from Dox-loaded O-GNR-PEG-DSPE treated C33A cells untransfected or transfected with a EGFR plasmid. * indicates significant decrease ($p < 0.05$) in LDH release compared to uninhibited cells exposed to Dox-O-GNR-PEG-DSPEs. All data are normalized to LDH release from lysed control cells.

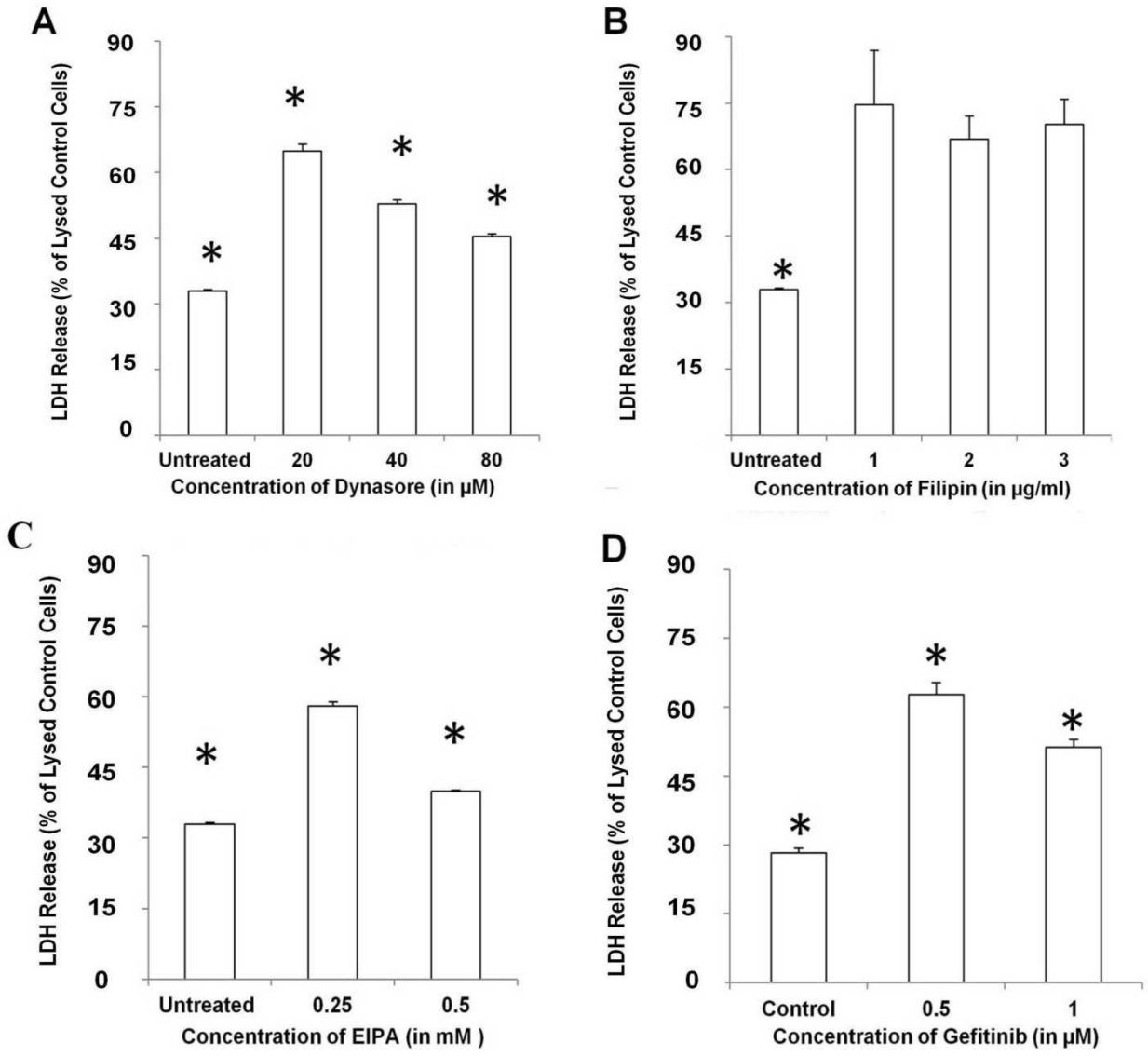

Figure 13. LDH Release from Dox-loaded O-GNR-PEG-DSPEs treated CaSki cells exposed to the following: **(A)** Dynasore. **(B)** Fillipin. **(C)** EIPA. **(D)** Gefitinib. Data are presented as mean ± SD (n = 3 per group). * indicates significant decrease ($p < 0.05$) in LDH release compared to uninhibited cells exposed to Dox-O-GNR-PEG-DSPEs. All data are normalized to LDH released from lysed control cells.

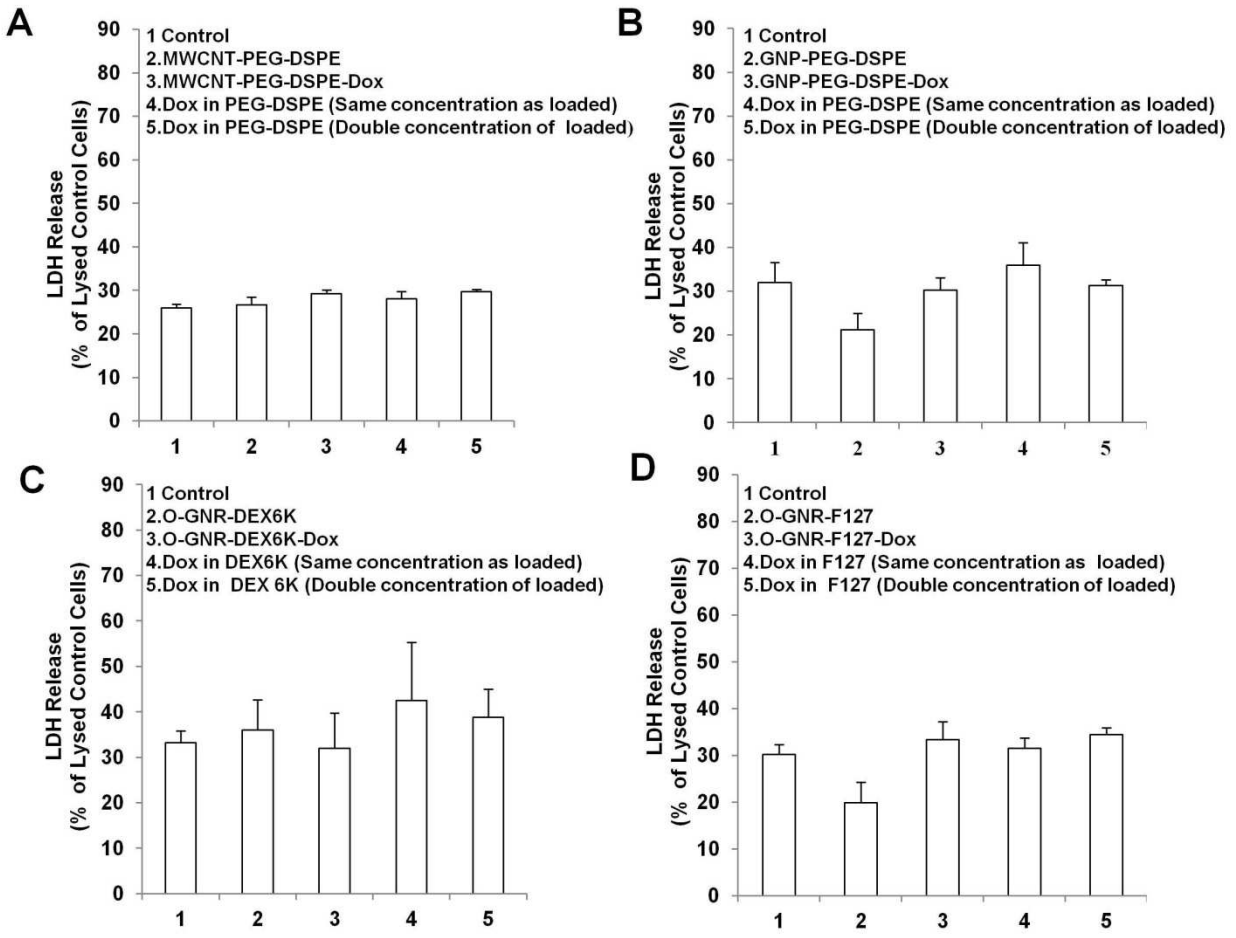

Figure 14. LDH release from HeLa cells treated with the Dox-loaded nanoparticles under the following conditions: **A)** Multiwalled Carbon Nanotubes-PEG-DSPE. **(B)** Graphene Nanoplatelets in PEG-DSPE **(C)** Graphene nanoribbons in Dextran. **(D)** Graphene nanoribbons in pluronic F127 and controls (unexposed O-GNR-PEG-DSPE, Dox–loaded O-GNR-PEG-DSPE and free Dox in PEG-DSPE exposed). Data are presented as mean +SD (n = 6 per group). All data are normalized to the LDH released from lysed control cells.

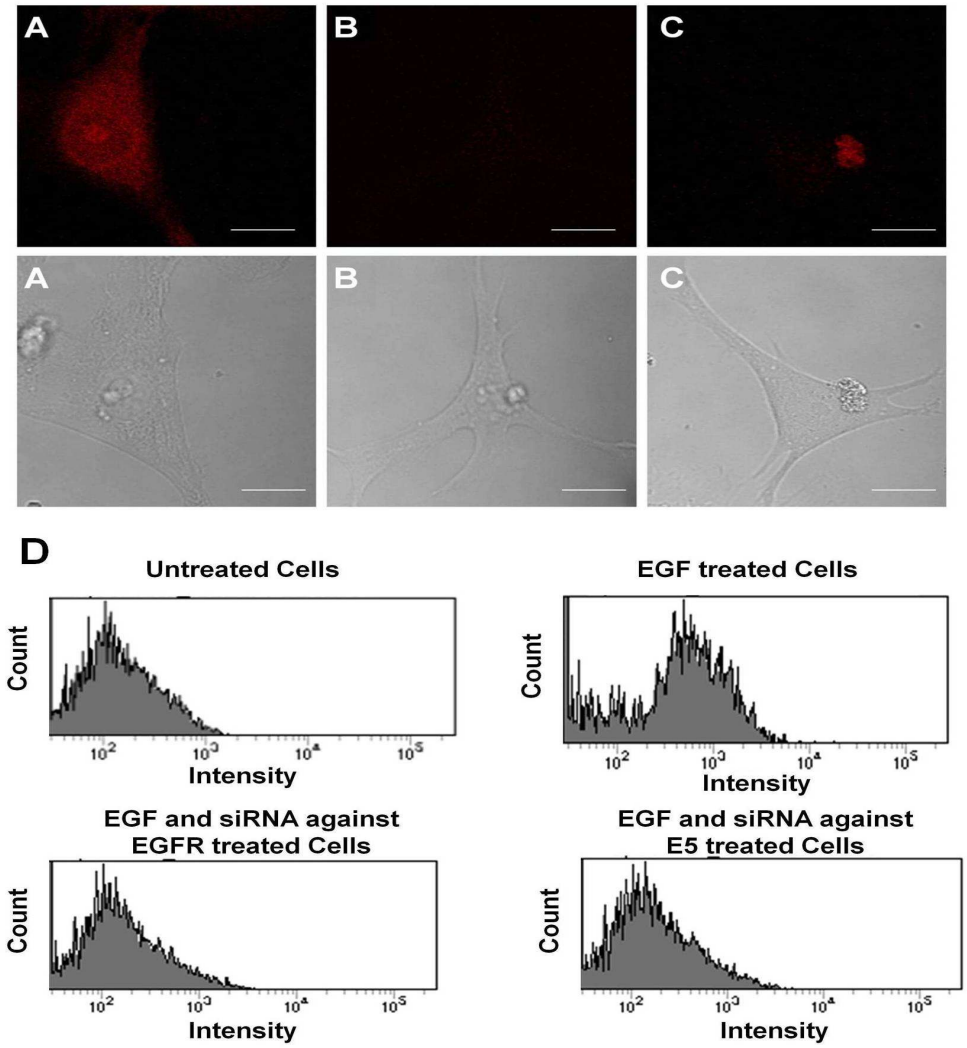

Figure 15. Representative bright field and fluorescence microscopy images depicting EGFR activation in EGF treated HeLa cells transfected with the following: **(A)** Phosphate buffered saline (control). **(B)** siRNA against EGFR. **(C)** siRNA against E5. Size bar=20 μm. **(D)** Flow cytometry mediated quantitative analysis of activated EGFR in Untreated cells, only EGF treated cells, EGF treated cells transfected with siRNA against EGFR and EGF treated cells transfected with siRNA against HPV18 E5. Plasmid expression was assessed using a mouse anti-phospho EGFR antibody and a rhodmine tagged goat-anti mouse secondary antibody.

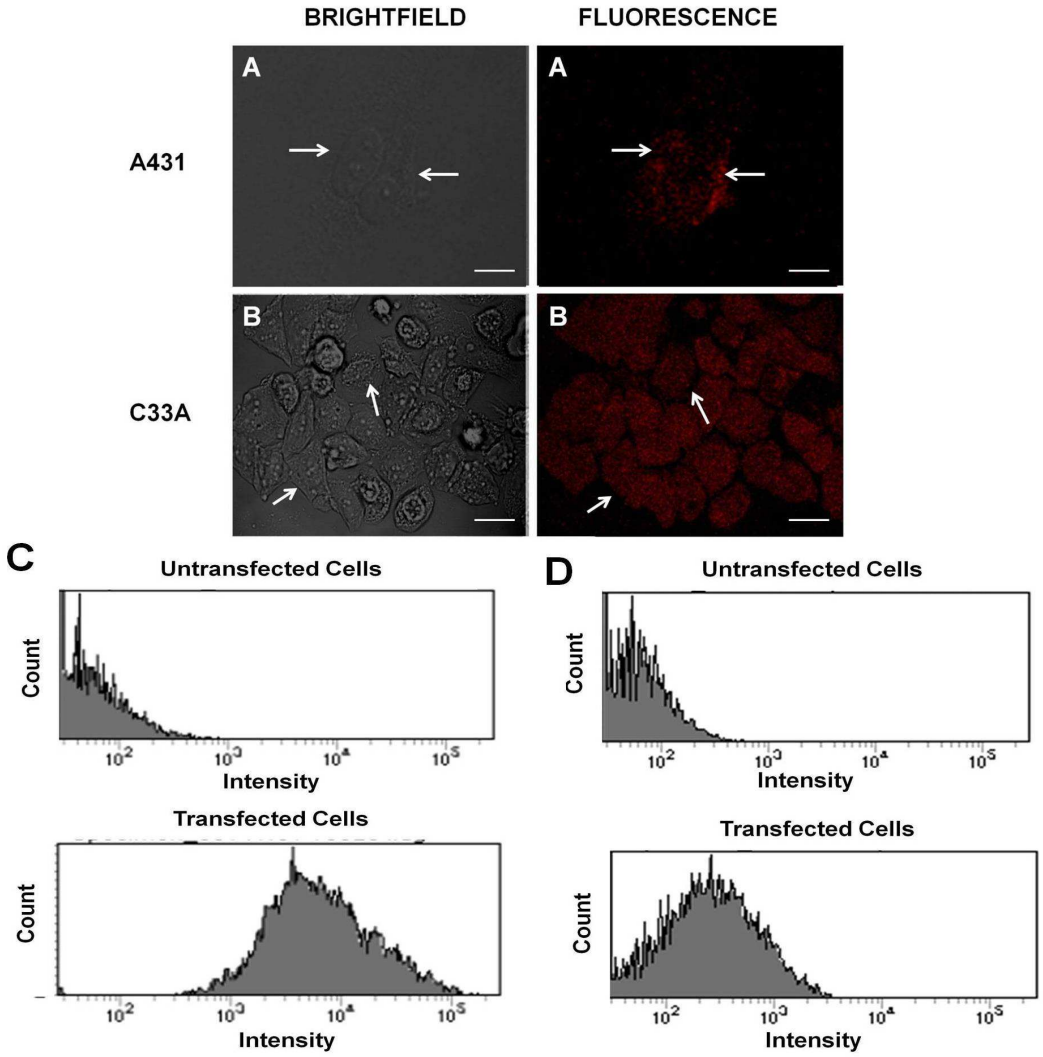

Figure 16. Representative bright field and fluorescence microscopy images depicting expression of MSCV-HPV16E5-FLAG plasmid in the following cell lines **(A)** A431 cells. **(B)** C33A cells. Flow cytometry mediated quantitative analysis of transfection efficiency and expression of MSCV-HPV16E5-FLAG plasmid in **(C)** untransfected and transfected A431 cells **(D**) untransfected and transfected C33A cells. Plasmid expression was assessed using a mouse anti-flag antibody and a rhodmine tagged goat-anti mouse secondary antibody. Size bar= 20 μm

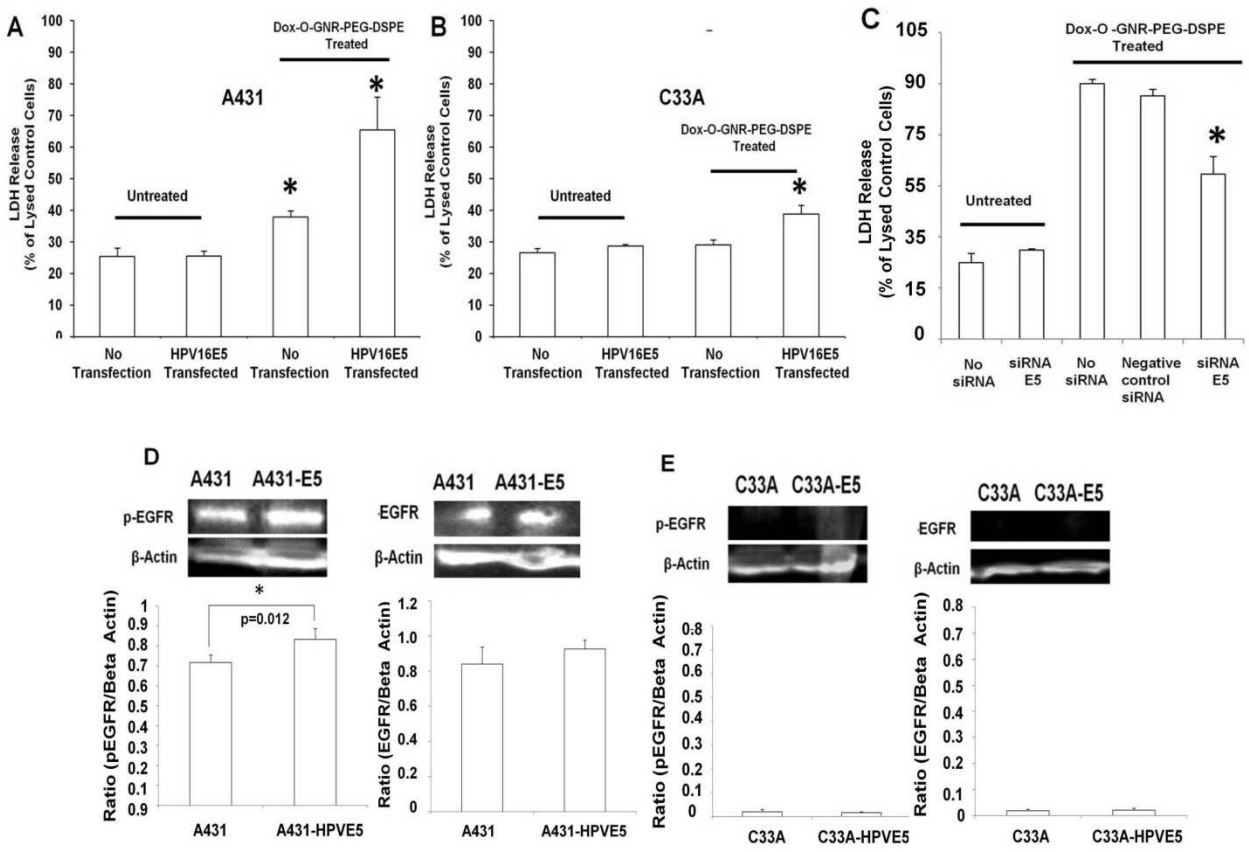

Figure 17. (A-D) LDH Release from Dox-loaded O-GNR-PEG-DSPE treated with the following in A431, C33A or HeLa cells: **(A)** A431 cells transfected with HPV16 E5. **(B)** C33A cells transfected with HPV16 E5. Untransfected and untreated cells were used as controls. Data are presented as mean +SD (n = 3 per group). * indicates significant increase ($p < 0.05$) in LDH release compared to untreated control cells. All data are normalized to LDH release from lysed control cells. **(C)** HeLa cells transfected with siRNA against HPV18 E5. For A, B and C, data are presented as mean +SD (n = 3 per group). * indicates significant decrease ($p < 0.05$) in LDH release compared to uninhibited cells treated with Dox-O-GNR-PEG-DSPE. All data are normalized to the LDH released from uninhibited Dox-O-GNR-PEG-DSPE treated cells. **(D)** Western blot and densitometric quantification of EGFR activation (phosphorylated EGFR) and

expression in A431 cells before and after transfection with the HPV 16 E5 expressing plasmid. **(E)** Western blot and densitometry quantification depicting EGFR activation (phosporylated EGFR) and expression in C33A cells before and after transfection with the HPV 16 E5 expressing plasmid after treatment with Dox-loaded O-GNR-PEG-DSPE.

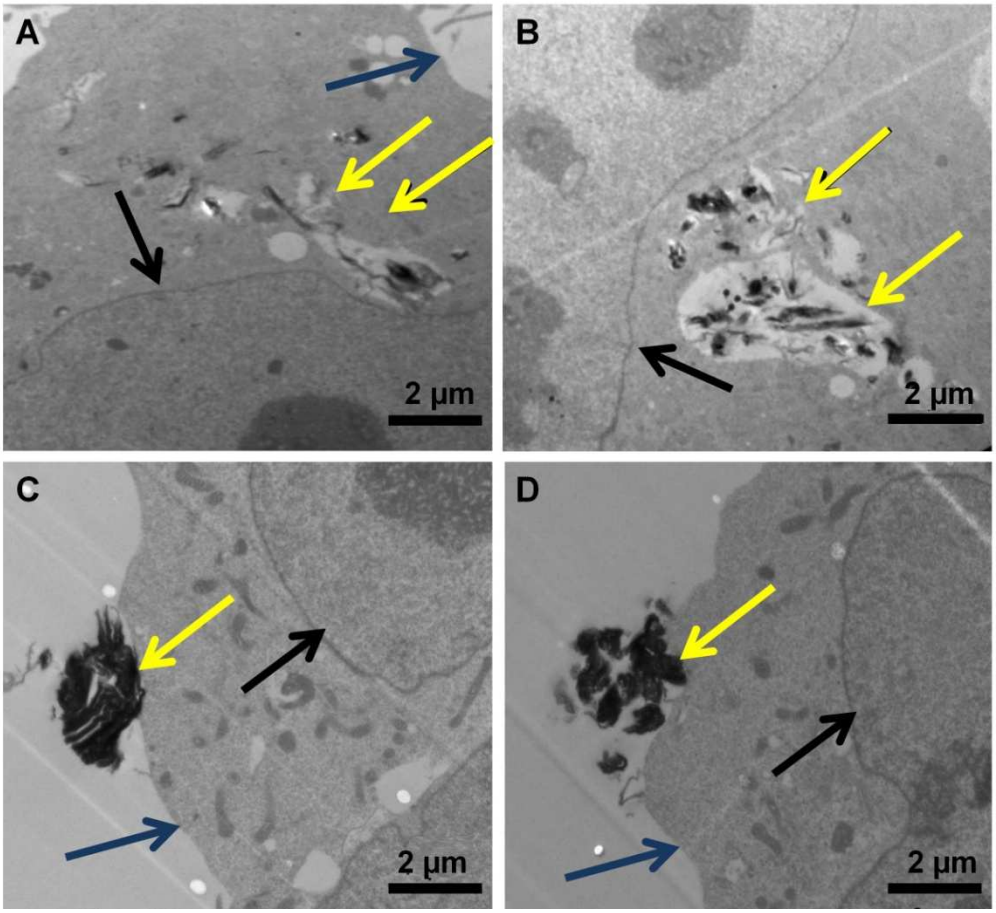

Figure 18. Representative high-resolution TEM images of A431 and C33A cells. All cells were treated with 40µg/ml O-GNR-PEG-DSPE for 30 minutes. **(A)** O-GNR-PEG-DSPE aggregate uptake into small vesicles of A431 cells (yellow arrows). **(B)** A431 cells transfected with MSCV- HPV16E5 plasmid show O-GNR-PEG-DSPEs in small and large vesicular structures (yellow arrows). **(C and D)** C33A cells and C33A cells transfected with MSCV HPV16E5 plasmid cells, respectively, do not show O-GNR-PEG-DSPE aggregate uptake; instead O-GNR-PEG-DSPEs remain on the surface of the cells. Black arrows point to the cell nucleus, and blue arrows to the cell membrane.12 cells per analyzed per type of cell line.

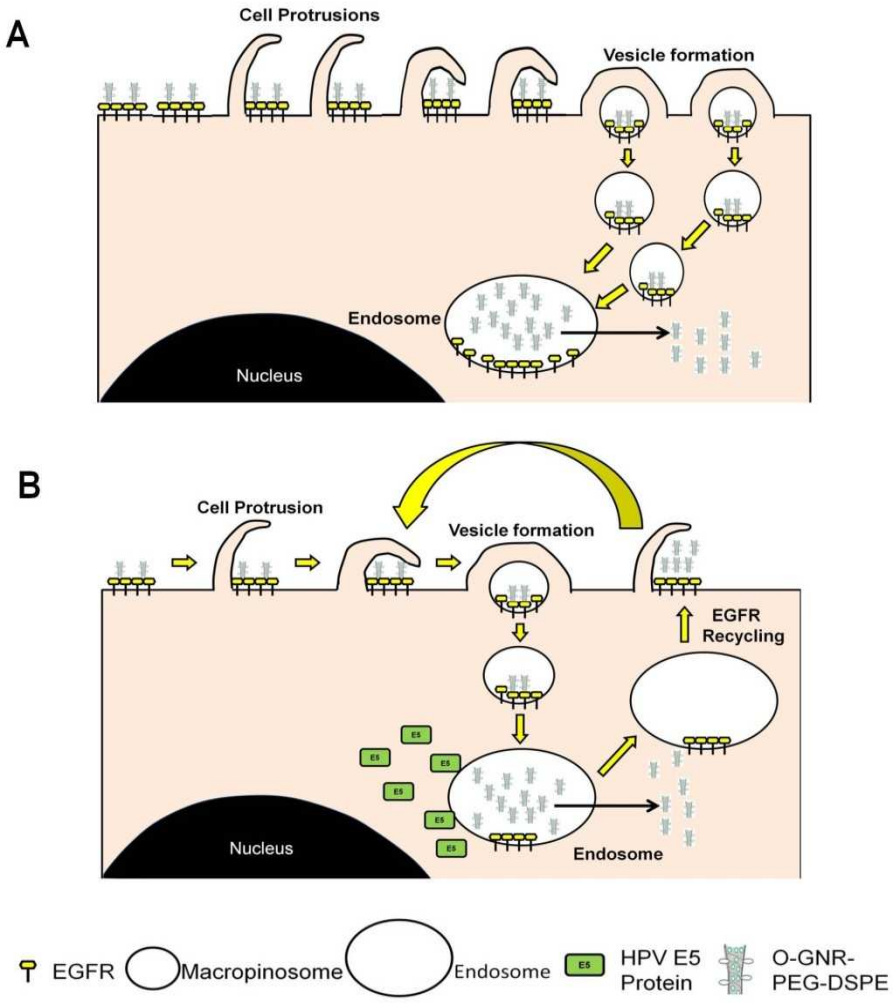

Figure 19. Schematic representation of mechanism of uptake postulated for O-GNR-PEG-DSPEs into **(A)** EGFR over expressing cells. O-GNR-PEG-DSPEs activate dense EGFR clusters at different locations on cell membrane surface. Simultaneous activation of these EGFRs results in a predominantly macropinocytotic response for uptake of O-GNR-PEG-DSPEs along with these receptors. **(B)** Cells with an integrated HPV genome. E5 prevents degradation of activated EGFR receptors, instead recycling them onto the cell surface; this results in a repeated uptake process without further EGFR activation and additional uptake of on nanoparticles on the cell surface or the surrounding regions.

Chapter 5

IN VIVO DRUG DELIVERY AND MECHANISM OF EGFR ACTIVATION

5.1 Introduction

Epidermal growth factor receptors (EGFR) play a very important role in initiation of intracellular signaling cascades that ultimately lead to increased metabolism, growth and cell division related effects(Yarden, 2001, Wells, 1999). Thus, to avoid aberrant growth and cell division, the body controls the number of EGFR activated at a particular time, and the time span of activation of each receptor. This is achieved through controlling the number of receptors that are expressed on the cell surface; use of ligands (EGF and related ligands) designed to specifically activate these receptors and initiation of degradation mechanisms for the activated receptors (Alwan et al., 2003, Yarden, 2001, Wells, 1999). However, mutations in the genes coding these receptors can lead to their over-expression on the cell surface, resulting in over-activation of signaling cascades (Barker II et al., 2001, Bhargava et al., 2005). Similarly, mutations in the receptors, especially in its tyrosine kinase domain and extracellular domain can lead to ligand free constitutive activation of the receptors(Nishikawa et al., 1994, Voldborg et al., 1997). This can lead to different kinds of cancers depending on the tissue type and the extent of up regulation. For example, over-expression or mutation of epidermal growth factor receptors in breast and lung tissue may lead to formation of breast carcinoma and non small cell lung carcinoma respectively(Nicholson et al., 2001, Dimri et al., 2007, Paez et al., 2004, Brabender et al., 2001, Mukohara et al., 2003). Similarly EGFR over-expression or mutation along with other factors in

glial cells can lead to formation of glioblastoma multiformae (Barker II et al., 2001, Ohgaki and Kleihues, 2007, Shinojima et al., 2003).

The existence of over-expression or mutation of EGF receptors in multiple forms of cancer has made it a very attractive target for anti cancer therapeutic measures. Antibodies have been designed to directly bind the ligand binding pocket of EGF receptors, thus competitively inhibiting ligand binding and receptor activation(Bonner et al., 2004, Cai et al., 2007). Tyrosine kinase inhibitors have also been designed to bind the tyrosine kinase domain and inhibit their activation in receptors containing its mutant constitutively active form (Paez et al., 2004, Maemondo et al., 2010). However, as mentioned in Chapter 1, mutations resulting in resistance have been found in to occur in cancers receiving these treatments (Gazdar, 2009, Sordella et al., 2004, Pao et al., 2005, Normanno, 2013, Bardelli and Jänne, 2012). This results in cancer cells becoming unresponsive to these treatments. Hence, chemotherapy, radiation therapy and surgery are the primary methods for treatment of EGFR related cancers.

A negative aspect of untargeted chemotherapy is their non-specific toxicity on normal non-cancerous tissue(Erban and Lau, 2006, Curigliano et al., 2012). Hence, as an alternative to the above mentioned treatments, and to utilize the EGF receptor over-expression in tumors, drug delivery agents functionalized with antibodies that bind to EGF receptors have also been created to achieve targeted chemotherapeutic drug delivery(Mamot et al., 2003, Mamot et al., 2006). However, since these agents also rely on receptor binding, resistance causing mutations in the extracellular ligand binding domain can potentially affect uptake of the agents into cancer cells. As such, for targeted therapy of EGFR over-expressing cancers, a chemotherapeutic drug delivery agent that can cause EGFR activation independent of receptor binding and get uptaken into the cells in the process will be the most efficient.

Activation of EGFR, which occurs through receptor clustering, is usually initiated through ligand binding(Wells, 1999). However, ligand independent activation of EGFR can take place through several other processes that can initiate clustering of EGFR. A study by Yu et al showed that in serum free media, association of EGFR with integrins could initiate EGFR clustering and activation(Yu et al., 2000). Takahashi et al showed a similar observation with extracellular matrix glycans and ErbB3 (a receptor belonging to EGFR family)(Takahashi et al., 2008). Oxidative stress has also been shown induce phosphorylation and activation of EGFR in multiple studies (Wang et al., 2000, Takeyama et al., 2000, Nishinaka and Yabe-Nishimura, 2001). Membrane depolarization has also can also be a cause for ligand free EGFR activation as shown in PC12 cells and cardiomyocytes(Ca influx dependent) (Zwick et al., 1997, Rosen and Greenberg, 1996) and vascular smooth muscle cells (Ca influx independent)(Norton et al., 2013).

In some recent studies it has been shown that nanoparticles can lead to the ligand free activation of EGF receptors. For example, in lung epithelial cells, Unfried *et al* showed that ultrasmall carbon nanoparticles can interact with EGFR and integrin directly to initiate growth related signaling cascades (Unfried et al., 2008, Rauch et al., 2013). In another study, Sydlik *et al* showed that both ultrafine carbon black and silica nanoparticles (both ~14 nm in size) initiated either pro-growth or pro-apoptosis pathways depending on the way they interacted with EGFR(Sydlik et al., 2006, Rauch et al., 2013). Another study showed that PM 2.5 particles could bind to the EGF receptors and initiate signaling leading to ERK mediated amphiregulin expression and initiation of an autocrine loop that sustains receptor signaling for a long time(Blanchet et al., 2004, Rauch et al., 2013). It was later indentified that this EGFR activation was initiated through ROS production in the cells on exposure to the particles(Blanchet et al., 2004, Rauch et al., 2013). Small negatively charged SPIONs have also been shown to activate

EGFR without ROS production probably through receptor cross-linking(Rauch et al., 2012, Rauch et al., 2013). Although these studies have shown that it is possible to activate EGFR receptors with nanoparticles no study has explored if the receptor activation by these particles can influence their mechanism of uptake and if that can be utilized to specifically deliver drugs to EGFR over-expressing cells.

In the last chapter I have shown that O-GNRs (prepared by oxidative unzipping of multi walled carbon nanotubes) functionalized with PEG-DSPE can activate EGFR and gets uptaken into cells over-expressing EGF receptors. This phenomenon can be utilized to specifically deliver chemotherapeutic drugs loaded onto O-GNR-PEG-DSPE to EGFR over-expressing cancer cells or HPV induced cancers that modulate EGFR recycling through the E5 protein. However, those studies were done on cells lines only and the effects observed needs to be validated in a setting that better mimics the tumor milieu. To this end, in this chapter, I report the results from drug delivery and uptake studies with O-GNR-PEG-DSPE in immune-compromised mice containing HeLa and MCF7 xenograft tumors. I also focus on finding a mechanism for EGFR activation by O-GNR-PEG-DSPE so that I can gather a better understanding of the drug delivery process and gauge the potential of the particles as a delivery agent that can overcome resistance.

5.2 Materials and Methods

5.2.1 Animal Care and Induction of xenograft tumors

All the experiments were performed according to the guidelines of Institutional Animal Care and Use Committee at Stony Brook University, NY. HeLa cells and MCF7 cells were plated at a density of $3x10^6$ cells in 10 cm plates and grown in Dulbecco's Modified Eagle Medium (DMEM) and Roswell Park Memorial Institute (RPMI) media respectively. The cells were grown to confluency after which the media was removed and replaced with fresh media. The

cells were allowed to grow for 6 hrs in fresh media after which they were trypsinized and resuspended in equal volumes of DPBS and Corning matrigel matrix to a concentration of 5 $x10^7$ cells/ml. Immunocompromised male mice were injected with 200 μl of each cell suspension on each flank and allowed to grow for 4 weeks.

5.2.2 Drug Loading onto Graphene Nanoribbons

The protocol used to load doxorubicin (Dox) onto O-GNR-PEG-DSPEs was the same as reported in Chapter 4. Briefly, 1 mg of Dox was mixed with 2 ml of 500μg/ml O-GNR-PEG-DSPE, bath sonicated for 30 minutes, and stirred for 48 hours. Post 48 hours of stirring, the mixture was centrifuged at 14000 rpm for 45 minutes and the supernatant containing unloaded Dox was separated from the pelleted O-GNR-PEG-DSPEs containing loaded Dox using a pipette. The amount of drug in the supernatant (i.e. drug not loaded) was calculated using the Dox absorbance spectra from the supernatant at 490 nm and the absorbance vs. Dox concentration standard curve shown in Chapter 4. The amount of drug loaded on O-GNR-PEG-DSPEs was calculated by subtracting the total drug in the supernatant from the starting amount of Dox (i.e., 1 mg). The drug-loaded O-GNR-PEG-DSPE was resuspended in PEG-DSPE at 500μg/ml (of O-GNR-PEG-DSPE) before being used as stock solutions for drug delivery and drug release experiments respectively.

5.2.3 Tumor Injection studies

Post 4 weeks of tumor growth the size of each tumor was measured using calipers and 50 μl of 500μg/ml drug loaded O-GNR-PEG-DSPE, 50 μl of PEG-DSPE, 50 μl of 500μg/ml O-GNR-PEG-DSPE and 50 μl of free Dox in PEG-DSPE were injected directly into 4 tumors each in the HeLa and MCF7 xenograft tumors (n=4). Tumor sizes were measured again 3 days after

injection of the particles using calipers. Tumor volume was calculated according to the formulae V=[W(2)x L]/2 where V is the volume of the tumor, W is the width and L is the length.

5.2.4 Histology

Tumors removed from mice were fixed for 24 hours by immersing into 4% paraformaldehyde Post fixation, the tumors were cut into 3 mm segments. All the tumors were dissected symmetrically for consistency. Tumor segments were then dehydrated using graded ethanol washes and then paraffin-embedded for further processing. 5 μm sections from each paraffin embedded tumor sample were cut using a microtome and stained with Hematoxylin and Eosin (H&E) for histological evaluation. Digital photo microscopy was performed using a bright field microscope at 400x and 100x magnification.

5.2.5 Drug delivery studies

Drug delivery in terms of cell death was conducted using a LDH release TOX-7 assay kit (Sigma-Aldrich, St Louis, MO) using a method discussed in the last chapter. Briefly, HeLa cells were plated, at a density of 10^4 cells per well, in 96 well cell culture plates, and allowed to grow for 24 hours. After 24 hours, the media was changed to either normal DMEM or DMEM without Ca^{2+} and the cells were treated with 1) different concentrations of Dox-loaded O-GNR-PEG-DSPE (10μg/ml, 25μg/ml 50μg/ml and 75μg/ml), for 24hours at 37 ^{o}C. 2) Dox loaded O-GNR-PEG-DSPE at 50μg/ml, O-GNR-PEG-DSPE at 50μg/ml, PEG-DSPE and Dox in PEG-DSPE (at the same concentration as loaded and double the concentration of loaded) 3) Dox loaded O-GNR-PEG-DSPE at 50μg/ml after pretreatment of HeLa cells with 65 nM, 130 nM and 200nM anti EGFR antibody specific to the ligand binding pocket of EGFR(Santa Cruz Biotechnology,Santa Cruz, CA). After 24 hours, media was collected from individual wells, and centrifuged at 1200 rpm for 5 minutes. 50 μl of the media supernatant was added to wells in a

fresh 96 well plate along with LDH assay reagent, and incubated for 45 minutes. Absorbance values were recorded at 490 nm. The positive control was prepared by adding 10 µl of lysis solution to control cells, 45 min before centrifugation. LDH secretion (% of positive control) was calculated using the formula $(OD_{test} - OD_{blank})/(OD_{positive} - OD_{blank})$, where OD_{test} is the optical density of control cells or cells exposed to O-GNR-PEG-DSPE, and $OD_{positive}$ is the optical density of the positive control cells, and OD_{blank} is the optical density of the wells without cells. Absorbance of culture media containing PEG-DSPE was used for baseline correction in all groups. LDH secretion (% of Dox-loaded O-GNR-PEG-DSPE treated cells) was calculated using the formula $(OD_{test} - OD_{blank})/(OD_{treatment} - OD_{blank})$, where OD_{test} is the optical density of the inhibited cells exposed to Dox-loaded O-GNR-PEG-DSPE, $OD_{treatment}$ is the optical density of the cells treated with only Dox-loaded O-GNR-PEG-DSPE, and OD_{blank} is the optical density of the wells without cells. Absorbance of culture media containing PEG-DSPE was used for baseline correction in all groups.

5.2.6 Confocal Microscopy

$7x\ 10^5$ cells were plated in glass bottom 35 mm plates and incubated for 24 hours. Post incubation, media was removed and replaced with fresh media and cells were further incubated for 24 hours. Following this,

1) Cells were treated with 130 nM anti EGFR antibody and then exposed to either 50µg/ml O-GNR-PEG-DSPE or EGF (10 nM)(Life Technologies, Carlsbad, CA) for 15 minutes. This step was followed by three washes with phosphate buffered saline and fixation for 30 minutes with 2.5% glutaraldehyde(Electron Microscopy Sciences, Hatfield,PA). Then, the fixed cells were treated with 0.5% Triton X-100, and washed 3 times with PBS; this was followed by incubation with anti-phospho EGFR antibody with attached Alexa fluor 488(Millipore, Billerica, MA).

2) Media was replaced with 200 µl of a 20µM working solution of 2', 7'-dichlorofluorescin diacetate (Sigma Aldrich, Grand Island, New York) in each well and incubated for 1 hour. Following this incubation, the solution was removed and the wells were washed thrice with DPBS. The cells were then treated with 10µg/ml, 25µg/ml, 50µg/ml and 75µg/ml O-GNR-PEG-DSPE for 15 minutes. The nanoparticles were then removed using 3 washes of DPBS and the cells were fixed with 2.5% glutaraldehyde before imaging.

3) Cells were treated with 10µg/ml, 25µg/ml, 50µg/ml and 75µg/ml O-GNR-PEG-DSPE followed by immediate addition of 50nM voltage sensitive dye $DiBAC_4(3)$ (Life Technologies, Carlsbad, CA) in KRH buffer for 15 minutes. This step was followed by removal of the nanoparticles and $DiBAC_4$ and three washes with phosphate buffered saline. The cells were then fixed for 30 minutes with 2.5% glutaraldehyde before imaging.

4) Cells were loaded with Fura 2-AM(Sigma Aldrich, Grand island, New York) by treating them with a 0.02 mM Fura 2-AM solution in DPBS for 60 minutes followed by its removal and three washes with DPBS. The cells were then treated with 50µg/ml and 100µg/ml O-GNR-PEG-DSPE for 15 minutes followed by their removal with multiple washes of DPBS. The cells were then fixed for 30 minutes with 2.5% glutaraldehyde before imaging.

Imaging was done using a Zeiss LSM 510 META NLO two photon laser microscope system. Quantification of fluorescence in confocal images was done using Image J with 15 cells per treatment group (n=15).

5.2.7 Oxidative stress

Oxidative stress in terms of ROS generation after 15 minutes incubation with O-GNR-PEG-DSPE was HeLa cells. Cells were plated at 5×10^4 cells per well in 96 well plates, and incubated

for 24 h. After 24 h, media was replaced with 200 µl of a 20µM working solution of 2', 7'-dichlorofluorescin diacetate (Sigma Aldrich, Grand Island, New York) in each well, and incubated for 1 h. This solution was replaced by 200 µl of DPBS (containing 10% FBS) followed by addition of 50 µl of different concentrations of O-GNR-PEG-DSPE to each well for final treatment concentrations of 10, 15, 25 and 50µg/ml. The O-GNR solutions were incubated for 15 minutes, and aspirated out. The wells were washed with DPBS, and 200 µl of DPBS (with 10% FBS) was added to each well. Fluorescence readings of the wells were recorded using a Cytofluor fluorescence multiwell plate reader (Series H4000 PerSeptive Biosystems, Framingham, MA) with excitation at 485 nm and emission at 530 nm. Untreated cells were used as a control.

5.2.8 Statistics

All data are presented as mean +standard deviation. Student's' test was used to analyze the differences among groups. All statistical analyses were performed using a 95% confidence interval ($p < 0.05$).

5.3 Results

5.3.1 Tumor Drug delivery

Efficiency of drug delivery by O-GNR-PEG-DSPE in xenograft tumors was evaluated by the change in tumor volume and morphological analysis of the tumors injected with the drug loaded nanoparticles. Efficient drug delivery to the tumor cells would decrease tumor volume because of cell death whereas low drug delivery will not be able to inhibit increase in tumor volume. HeLa cell tumors grew slower than the MCF7 tumors and on the day of injections the HeLa cell tumors had an average volume of 0.5±0.12 mm^3 whereas MCF7 tumors had a volume of 0.8±0.1mm^3. Figure 1 shows the change in volume of HeLa and MCF7 cell xenograft tumors in immune-

compromised mice injected directly injected with 50 µl of drug loaded O-GNR-PEG-DSPE and other controls (50 µl of O-GNR-PEG-DSPE, 50 µl of free Dox at the same concentration as loaded in PEG-DSPE, and 50 µl of PEG-DSPE). Figure 1A representing the data for HeLa cell xenografts shows that only the HeLa tumors injected with control showed significant increase in size over the next 3 days. Untreated HeLa cell tumors increased in volume by 38±13 mm^3. HeLa tumors treated with PEG-DSPE, O-GNR-PEG-DSPE showed an increase in tumor volume by 32±27 mm^3 and 34±31 mm^3 respectively. Free drug in PEG-DSPE showed an increase in tumor volume by 19±10 mm^3. In contrast to the control injected cells, the drug loaded O-GNR-PEG-DSPE showed a decrease in tumor volume by 31±10 mm^3. Figure 1B representing the data from MCF7 xenografts shows that all MCF xenograft tumors showed significant increase in size. . Untreated MCF7 cell tumors increased in volume by 61±31 mm^3. MCF7 tumors treated with PEG-DSPE, O-GNR-PEG-DSPE showed an increase in tumor volume by 52±41 mm^3 and 63±12 mm^3 respectively. Free drug in PEG-DSPE and drug loaded O-GNR-PEG-DSPE showed an increase in tumor volume by 45±29 mm^3 and 17±21 mm^3 respectively. Figure 2 shows bright field images of histological sections from the HeLa cell xenograft tumors stained with hematoxylin and eosin. Histology sections of the HeLa tumors showed that drug loaded O-GNR-PEG-DSPE treated HeLa tumors (Figure 2C-E, white arrows) showed higher number of necrotic cells compared other treatments (untreated cells showed as reference, other treatments showed similar number of necrotic cells as untreated cells)(Figure 2A-B, white arrows). Also, fibrosis was observed in the HeLa tumors treated with drug loaded O-GNR-PEG-DSPE (Figure 2E, yellow arrows). MCF7 tumors did not show any morphological change in the cells for all five treatment groups and hence are not shown.

5.3.2 Direct receptor binding

Treatment of cells with anti EGFR antibodies that block the ligand binding domain of the receptor followed by EGFR activation and drug delivery studies on the antibody treated cells was done to assess if O-GNR-PEG-DSPE acts an EGFR ligand and activates the receptor through the ligand binding domain. Figure 3 shows the results from two separate studies that evaluate the activation of EGFR and drug delivery efficiency in HeLa cells (pretreated with anti EGFR antibody) in response to O-GNR-PEG-DSPE and drug loaded O-GNR-PEG-DSPE treatment respectively. Figure 3 A-C represents fluorescence, bright field and merge images of HeLa cells treated with EGF after pre-treatment with anti-EGFR antibody (that blocks ligand binding domain of EGFR). The confocal images show almost no fluorescence indicating very little EGFR activation due to the EGFR blocking antibodies. Figure 3 D-F represents fluorescence, bright field and merge images of HeLa cells treated with O-GNR-PEG-DSPE after pre-treatment with anti-EGFR antibody (that blocks ligand binding domain of EGFR). The images show high fluorescence, especially in the areas where O-GNR-PEG-DSPE is being internalized into the cell (red arrows). Figure 3G represents the drug delivery efficiency of drug loaded O-GNR-PEG-DSPE on HeLa cells pretreated with increasing concentrations of anti-EGFR antibody (that blocks ligand binding domain of EGFR). Results show that LDH release in untreated HeLa cells was ~68% of lysed control cells. In comparison, LDH release in 65nM, 130 nM and 200 nM antibody treated cells was ~63%, ~64% and ~66% of lysed control cells respectively.

5.3.3 Drug delivery at different O-GNR-PEG-DSPE concentrations

Drug delivery efficiency of different O-GNR-PEG-DSPE concentrations in HeLa was calculated by cell death induced by drug loaded particles at different concentrations. Figure 4 shows the

drug delivery efficiency of different concentrations of O-GNR-PEG-DSPE evaluated by LDH release assay. Increasing LDH release implies increasing cell death due to higher drug delivery. Results show that LDH release was directly proportional to concentration of treatment. Treatment of the HeLa cells with 10μg/ml O-GNR-PEG-DSPE resulted in ~ 36% LDH release compared to lysed control cells. Similarly, treatment of the cells with 25μg/ml, 50μg/ml and 75μg/ml O-GNR-PEG-DSPE resulted in ~47%, ~65% and ~75% LDH Release compared to lysed control cells respectively.

5.3.4 Oxidative stress

Oxidative stress in terms of reactive oxygen species (ROS) production induced by different concentrations of O-GNR-PEG-DSPE was investigated using 2',7'–dichlorofluorescin diacetate (DCFDA)(Eruslanov and Kusmartsev, 2010). DCFDA can freely diffuse into cells and upon entry get deacetylated by cellular esterases to a non fluorescent compound. This non fluorescent compound can then react with ROS in the cell to produce highly fluorescent 2', 7'–dichlorofluorescin (DCF)(Eruslanov and Kusmartsev, 2010). Thus, higher amounts of ROS produced in the cell will produce increased fluorescence. Figure 5 shows the oxidative stress generated in terms of ROS production in HeLa cells treated with increasing concentrations of O-GNR-PEG-DSPE. Figure 5A-D are representative confocal images of HeLa cells treated with different nanoparticle concentrations and shows no change in fluorescence intensity due to ROS production. Figure 5E represents data obtained from multi well plate fluorescence assay using DCFDA for quantification of ROS in HeLa cells treated with O-GNR-PEG-DSPE concentrations. Results show that all tested concentrations produced ROS values above 150% of untreated cells. However, no statistical difference in ROS production was found in all the concentrations tested.

5.3.5 Membrane depolarization

The membrane depolarization of HeLa cells exposed to O-GNR-PEG-DSPE was investigated using the voltage sensitive dye $DiBAC_4$ (3). Entry of $DiBAC_4$ (3) into cells depends on the depolarization status of its membrane i.e increasing depolarization leads to increased uptake of the dye into the cells(Yamada et al., 2001). Once taken up into cells $DiBAC_4$ (3) can bind intracellular proteins or cell organelle membranes to exhibit fluorescence(Yamada et al., 2001). Thus, higher membrane depolarization would mean higher fluorescence in the cells. Figure 6 shows the representative images and fluorescence quantification of $DiBAC_4$ (3) in HeLa cells treated with different concentrations of O-GNR-PEG-DSPE. Figure 6A-E shows that increasing concentration of nanoparticle treatment produced increasing $DiBAC_4$ (3) fluorescence in HeLa cells. Figure 6F shows the fluorescence quantification of the images in Figure 6A-E. Quantification results also show a concentration of O-GNR-PEG-DSPE dependent increase in fluorescence intensity in the HeLa cells.

5.3.6 Membrane depolarization induced Ca^{2+} entry

The necessity of membrane depolarization induced Ca^{2+} entry for EGFR activation by O-GNR-PEG-DSPE was evaluated by treating the drug loaded O-GNR-PEG-DSPE to HeLa cells in normal and Ca^{2+} free media, and the change in intracellular Ca^{2+} on treating cells with different O-GNR-PEG-DSPE concentrations was evaluated using Fura 2-AM assay. Fura 2-AM is cell permeable dye that can enter cells and bind Ca^{2+} ions to form a complex with a distinct excitation and emission spectra very different from its unbound form(Roe et al., 1990). Thus in a cell pre-loaded with Fura-2AM increased Ca^{2+} concentration will result in increase in

fluorescence due greater Fura 2-AM –Ca^{2+} complex formation(Roe et al., 1990). Figure 7 shows the drug delivery efficiency of O-GNR-PEG-DSPE in HeLa cells grown in both normal media and Ca^{2+} free media. Figure 7A shows that HeLa cells grown in normal media produced ~ 100% more cell death compared to free drug at the same concentration as loaded (similar to what is reported in Chapter 4). Figure 7B shows that HeLa cells grown in Ca^{2+} free media produced ~36% more cell death compared to free drug at the same concentration as loaded onto the O-GNR-PEG-DSPE in these experiments.

Figure 8 shows the increase in intracellular Ca^{2+} ions in Fura 2-AM loaded HeLa cells treated with increasing concentrations of O-GNR-PEG-DSPE. Figure 8A-C shows the representative confocal images of the cells whereas Figure 8D shows the quantification of the fluorescence in these cells. Results show that fluorescence intensity in 50μg/ml and 100μg/ml O-GNR-PEG-DSPE treated cells were respectively ~5 times and ~8 times higher compared to untreated cells.

5.4 Discussion

The purpose of this study was two-fold. Firstly, I wanted to investigate if O-GNR-PEG-DSPE can activate EGFR receptors in an *in vivo* tumor environment and subsequently get internalized in EGFR over-expressing tumor cells to accomplish highly efficacious chemotherapeutic drug delivery. Secondly, I wanted to investigate the mechanism of EGFR activation by O-GNR-PEG-DSPE. A recent *in-vivo* study in mice exploring the tissue bio-distribution of O-GNR-PEG-DSPE reported that these particles were rapidly taken up and excreted from the liver and finally filtered to be excreted from the body through urine(Lu et al., 2014). The study concluded that O-GNR-PEG-DSPE is safe for *in-vivo* biomedical applications even at high concentrations (tested upto 200μg/ml)(Lu et al., 2014). Till date there is no reported *in vivo* study that has explored the efficiency of O-GNR-PEG-DSPE as a drug delivery agent.

For initial *in vivo* evaluation of drug delivery efficiency, xenograft tumors provide a suitable and highly researched model(Bae and Park, 2011). A decrease in tumor growth is a direct indication that the drug delivery system is highly efficacious(Bae and Park, 2011). In this study HeLa and MCF7 cells were chosen as the cell lines for inducing xenograft tumors as these cell lines had produced drastically opposite responses during the *in vitro* drug delivery studies. While HeLa cells treated with 50µg/ml drug loaded O-GNR-PEG-DSPE produced ~100% more cell death compared to free drug, MCF7 cells treated at the same concentration produced the same amount of cell death as free drug (discussed in Chapter 4). The probable reason for this was the activation of EGF receptors on HeLa cells by O-GNR-PEG-DSPE that leads to the uptake of these drug loaded particles. MCF7 cells, which have low EGFR expression, did not show the same response. For the *in vivo* study, the drug loaded O-GNR-PEG-DSPE along with its controls were injected into different tumors. Once present inside the tumor interstitium, uptake of the drug loaded particles into cells and resultant cell death depends on the efficiency of the cells in taking up these particles(Bryce et al., 2009). The HeLa xenograft tumors treated with drug loaded O-GNR-PEG-DSPE showed a significant decrease in tumor size, three days after the first injection (Figure 1A). This was probably because the HeLa cells in the tumor took up the drug loaded particles similar to *in vitro* studies. In contrast, MCF7 tumors treated with the drug loaded particles showed significant increase in size over the same period (Figure 1B). Histological evidence also suggested morphological changes in the HeLa cells indicating necrosis due to the drug treatment (Dox induces cell death through binding the genetic material and causing necrosis) (Figure 2). However, MCF7 cells showed no changes in cell morphology as they were not affected by the drug loaded particles (not shown). Normal tumor growth was observed in PEG-DSPE, free drug in PEG-DSPE and O-GNR-PEG-DSPE treated cells in

xenograft tumors of both cell lines (Figure 1). This suggests that they do not individually play a role in the toxicity observed in the HeLa cell xenografts treated with drug loaded O-GNR-PEG-DSPE. It is only when the drug loaded O-GNR-PEG-DSPEs are taken up in the cells that the toxicity is observed, reinforcing the observations from the *in vitro* study.

Similar to any other drug, it is essential to understand the underlying mechanism of EGFR activation by O-GNR-PEG-DSPE before it can be utilized for clinical applications in the future. Knowledge of the activation mechanism will not only help in assessing the pharmacodynamics of the drug delivery agent(Moreno et al., 2010) but also help in identifying other applications and potential toxicity of the agent(Kedmi et al., 2010, Deng et al., 2011). It may also help in modifying the structure of the particle in the future for more efficacious drug delivery. Epidermal growth factor receptors can get activated by several mechanisms including the normal ligand binding pathway and other pathways that induce receptor dimerization and clustering like oxidative stress and membrane depolarization(Schlessinger, 2002, Wells, 1999, Wang et al., 2000, Takeyama et al., 2000, Zwick et al., 1997). A recent study has also shown that magnetic nanoparticles targeted to EGFR using antibodies can induce clustering and activation of EGFR(Bharde et al., 2013). Epidermal growth factor receptors can be activated by eight different ligands which directly bind the extracellular domain of the receptor(Willmarth et al., 2009). It is possible that O-GNR-PEG-DSPE can act as a structural mimic of one of these ligands and activates these receptors by direct receptor binding. Blocking the ligand binding domain of EGF receptors with anti-EGFR antibodies could not decrease the drug delivery efficiency of the particles in HeLa cells suggesting that O-GNR-PEG-DSPE is not a ligand for the receptors (Figure 3G). This was further confirmed by presence of activated EGFR in confocal images of O-GNR-PEG-DSPE treated HeLa cells whose ligand binding domain was blocked by anti-EGFR

antibody (Figure 3D-F). Successful ligand blocking was confirmed in EGF treated blocked cells which showed no activation of EGFR (Figure 3 A-C).

Several studies have shown that oxidative stress can induce activation of EGFR. Khan *et al* showed that H_2O_2 induced oxidative stress can result in aberrant phosphorylation and activation of EGFR which prevents endocytosis and degradation of the receptors resulting in prolonged receptor signaling(Khan et al., 2006). Takeyama *et al* showed that exogenous H_2O_2 leads to EGFR activation mediated mucin synthesis in NCI-H292 cells(Takeyama et al., 2000). Peus *et al* showed that UV induced ROS generation leads to activation of EGFR signaling in keratinocytes (Peus et al., 1998). Wang *et al* showed that oxidative stress induces EGFR dependent Akt activation that improves cell survival in HeLa cells(Wang et al., 2000). Fischer *et al* provided a possible mechanism for oxidative stress mediated EGFR activation wherein oxidative stress was shown to cause ADAM protease activation leading to cleavage of pro-heparin binding EGF that leads to EGFR activation(Fischer et al., 2004). In several reports, graphene based nanostructures have been shown to cause oxidative stress in cell lines exposed to them(Chang et al., 2011). At high treatment concentrations, oxidative stress from graphene nanostructures leads to cyto-toxicity and geno-toxicity(Zhang et al., 2010, Akhavan et al., 2012). The geno-toxicity observed is often due to interruption of cell cycle related pathways(Akhavan et al., 2012). Since direct receptor interaction is not the mechanism of EGFR activation by O-GNR-PEG-DSPE, I investigated oxidative stress due to O-GNR-PEG-DSPE as a possible mechanism for EGFR activation. Chemotherapeutic drug delivery studies on HeLa cells at different treatment concentrations of Dox loaded O-GNR-PEG-DSPE showed a concentration dependent increase in cell death (Figure 4). Hence, if oxidative stress is responsible for the high uptake and drug delivery, oxidative stress generation should also be concentration dependent (i.e. higher

concentrations produce higher amounts of oxidative stress). Results showed that, although O-GNR-PEG-DSPE did induce oxidative stress, it was not concentration dependent. Increasing the treatment concentration from 10 to 50µg/ml did not lead to increased oxidative stress in HeLa cells (Figure 5E). This was further confirmed by confocal images of cells treated with different concentrations of O-GNR-PEG-DSPE (Figure 5A-D). This suggested that oxidative stress was not the mechanism of O-GNR-PEG-DSPE mediated EGFR activation. It should be mentioned here that previous studies reported in Chapter 2 evaluating oxidative stress generation in HeLa cells exposed to O-GNR-PEG-DSPE for 2 hours showed a concentration dependent increase in oxidative stress. However, we are only concerned with the 15 minute time point reported here as we had observed O-GNR-PEG-DSPE uptake into HeLa cells within 15 minutes of incubation.

Membrane depolarization has been linked to aberrant EGFR phosphorylation and activation in several studies(Zwick et al., 1997, Rosen and Greenberg, 1996). Membrane depolarization is defined as any change in the negative resting membrane potential because of the influx of positively charged ions. Zwick *et al,* Rosen *et al* and Bartel *et al* showed that membrane depolarization in PC12 cells can lead to further influx of Ca^{2+} ions that initiates downstream signaling cascades leading to phosphorylation of tyrosine kinase and activation of EGFR(Bartel et al., 1989, Zwick et al., 1997, Rosen and Greenberg, 1996). However, Norton *et al* showed that membrane depolarization in vascular smooth muscle cells under chronic hypoxia leads to EGFR activation independent of Ca^{2+} influx suggesting a different mechanism of EGFR activation from the previous three studies(Norton et al., 2013). Apart from EGFR tyrosine kinase, membrane depolarization has also been shown to induce phosphorylation of glycogen synthase kinase 3 β in neuroblastoma cells(Lee et al., 2005).

In several recent studies nanoparticles have been shown to induce cell membrane depolarization by interacting with the membrane and altering their resting membrane potential (Arvizo et al., 2010, Lin et al., 2008, Zhao et al., 2009). The extent of depolarization induced depends on the surface chemistry of the particle, especially on the type of material, its size and charge(Arvizo et al., 2010). Lin *et al* showed that 13nm Al_2O_3 particles showed more membrane depolarization than 30 nm Al_2O_3 particles in A549 cells(Lin et al., 2008). In comparison to both Al_2O_3 particles, similar CeO_2 particles caused less membrane depolarization(Lin et al., 2008). Gold nanoparticles have also been shown to induce membrane depolarization in CP70 and A2780 cell lines leading to Ca^{+2}entry into the cells(Arvizo et al., 2010). A recent study by Talukdar *et al* showed that O-GNR-PEG-DSPE contains large number of carboxyl and hydroxyl groups on its surface making the surface negatively charged. The negative charge on the surface was significantly higher than PEG-DSPE functionalized graphene nanoplatelets synthesized from graphite which did not show the same drug delivery response as O-GNR-PEG-DSPE(Talukdar et al., 2014). The negative charge of O-GNR-PEG-DSPE can potentially interact with the membrane of the cells making the resting membrane potential less negative (i.e. inducing membrane depolarization). Hence, I investigated the potential of O-GNR-PEG-DSPE in inducing membrane depolarization in HeLa cells.

Studies with the voltage sensitive dye $DiBAC_4$ showed that there was a concentration dependent increase in $DiBAC_4$ fluorescence indicating that treatment with increasing concentrations led to higher membrane depolarization and hence higher entry of the dye into the cells (Figure 6). Confocal images and their fluorescence intensity quantification showed higher fluorescence in 100µg/ml treated cells compared to lower concentrations (Figure 6). This suggested that

membrane depolarization was probably the mechanism by which O-GNR-PEG-DSPE could activate the EGFR receptors.

In both excitable and non-excitable cells, membrane depolarization results in entry of extracellular Ca^{+2} into the cells(Monteith et al., 2007, Chakrabarti and Chakrabarti, 2006). This Ca^{2+} entry can potentially lead to growth and proliferation promoting events like activation of EGFR signaling(Arvizo et al., 2010). Hence, I investigated if O-GNR-PEG-DSPE treatment induced EGFR activation and O-GNR-PEG-DSPE uptake was a direct consequence of membrane depolarization induced Ca^{2+} entry in to the cells. Drug delivery experiments in normal media (DMEM) containing Ca^{2+} showed ~100% more cell death in HeLa cells compared to free drug in O-GNR-PEG-DSPE as reported previously (Figure 7A). In contrast, repeating the same drug delivery experiment in cell media without Ca^{2+} resulted in a decrease of the drug delivery efficiency (i.e. cell death) to ~35% of free drug in PEG-DSPE (Figure 7B). This indicated that extracellular Ca^{2+} may be essential for the uptake of drug loaded O-GNR-PEG-DSPE through EGFR activation. This was further confirmed by Fura2-AM based analysis of Ca^{2+} entry into cells treated with different concentrations of O-GNR-PEG-DSPE. Confocal images of Fura 2-AM loaded HeLa cells showed concentration of O-GNR-PEG-DSPE treatment dependent increase in fluorescence (Figure 8A-C). In comparison to untreated cells, fluorescence quantification showed ~8 times increase in fluorescence intensity in cells treated with 100μg/ml O-GNR-PEG-DSPE (Figure 8D). This result suggests that O-GNR-PEG-DSPE treatment leads to Ca^{2+} entry from the extracellular space and this increased intracellular Ca^{2+} entry might be responsible for the EGFR activation observed on treatment with O-GNR-PEG-DSPE.

Activation of EGFR receptors by negatively charged magnetic particles has been reported before by *Rauch et al*. They found that these particles activated the receptors through a non oxidative

stress dependent pathway(Rauch et al., 2012). It is possible that these particles have a membrane depolarization dependent pathway for EGFR activation as in case of O-GNR-PEG-DSPE. However, further investigation will be necessary to understand how charge, shape and size of particles affect membrane depolarization by nanoparticles.

5.5 Conclusion

Results from this study suggest that the *in vitro* drug delivery efficiency of O-GNR-PEG-DSPE (evidenced by high cell death shown in Chapter 4) could be repeated in *in vivo* studies with HeLa xenograft tumors. This shows that highly efficacious and cell specific drug delivery through O-GNR-PEG-DSPE can be achieved even in the tumor microenvironment. This is critical for further clinical development of the particle as a drug delivery agent. Investigation of the mechanism through which O-GNR-PEG-DSPEs enter EGFR over-expressing cells indicates that these particles, probably because of their negative charge, can depolarize cell membranes. This membrane depolarization leads to entry of extracellular calcium into the cell and results in EGFR activation on the cell surface through activation of several signaling mechanisms. Activation of large number of EGFR on the cell surface leads to membrane protrusions that engulf the O-GNR-PEG-DSPE along with the activated EGFR receptors into the cells (Figure 9). This leads to the high drug delivery efficiency of O-GNR-PEG-DSPE in cells over-expressing EGFR. Moreover, the fact that O-GNR-PEG-DSPE can activate EGFR without direct ligand binding makes it an excellent choice for a drug delivery agent in EGFR over expressing tumors as mutations leading to resistance will not affect the uptake and drug delivery through these particles.

5.6 References

Akhavan, O., Ghaderi, E. & Akhavan, A. 2012. Size-dependent genotoxicity of graphene nanoplatelets in human stem cells. *Biomaterials,* 33**,** 8017-8025.

Alwan, H. A., Van Zoelen, E. J. & Van Leeuwen, J. E. 2003. Ligand-induced lysosomal epidermal growth factor receptor (EGFR) degradation is preceded by proteasome-dependent EGFR de-ubiquitination. *Journal of Biological Chemistry,* 278**,** 35781-35790.

Arvizo, R. R., Miranda, O. R., Thompson, M. A., Pabelick, C. M., Bhattacharya, R., Robertson, J. D., Rotello, V. M., Prakash, Y. & Mukherjee, P. 2010. Effect of nanoparticle surface charge at the plasma membrane and beyond. *Nano letters,* 10**,** 2543-2548.

Bae, Y. H. & Park, K. 2011. Targeted drug delivery to tumors: myths, reality and possibility. *Journal of Controlled Release,* 153**,** 198.

Bardelli, A. & Jänne, P. A. 2012. The road to resistance: EGFR mutation and cetuximab. *Nature medicine,* 18**,** 199.

Barker II, F. G., Simmons, M. L., Chang, S. M., Prados, M. D., Larson, D. A., Sneed, P. K., Wara, W. M., Berger, M. S., Chen, P. & Israel, M. A. 2001. EGFR overexpression and radiation response in glioblastoma multiforme. *International Journal of Radiation Oncology* Biology* Physics,* 51**,** 410-418.

Bartel, D. P., Sheng, M., Lau, L. F. & Greenberg, M. E. 1989. Growth factors and membrane depolarization activate distinct programs of early response gene expression: dissociation of fos and jun induction. *Genes & development,* 3**,** 304-313.

Bharde, A. A., Palankar, R., Fritsch, C., Klaver, A., Kanger, J. S., Jovin, T. M. & Arndt-Jovin, D. J. 2013. Magnetic Nanoparticles as Mediators of Ligand-Free Activation of EGFR Signaling. *PloS one,* 8**,** e68879.

Bhargava, R., Gerald, W. L., Li, A. R., Pan, Q., Lal, P., Ladanyi, M. & Chen, B. 2005. EGFR gene amplification in breast cancer: correlation with epidermal growth factor receptor mRNA and protein expression and HER-2 status and absence of EGFR-activating mutations. *Modern pathology,* 18**,** 1027-1033.

Blanchet, S., Ramgolam, K., Baulig, A., Marano, F. & Baeza-Squiban, A. 2004. Fine particulate matter induces amphiregulin secretion by bronchial epithelial cells. *American journal of respiratory cell and molecular biology,* 30**,** 421-427.

Bonner, J., Giralt, J., Harari, P., Cohen, R., Jones, C., Sur, R., Rabin, D., Azarnia, N., Needle, M. & Ang, K. 2004. Cetuximab prolongs survival in patients with locoregionally advanced squamous cell carcinoma of head and neck: a phase III study of high dose radiation therapy with or without cetuximab. *J Clin Oncol,* 22**,** 5507a.

Brabender, J., Danenberg, K. D., Metzger, R., Schneider, P. M., Park, J., Salonga, D., Hölscher, A. H. & Danenberg, P. V. 2001. Epidermal growth factor receptor and HER2-neu mRNA expression in non-small cell lung cancer is correlated with survival. *Clinical Cancer Research,* 7**,** 1850-1855.

Bryce, N. S., Zhang, J. Z., Whan, R. M., Yamamoto, N. & Hambley, T. W. 2009. Accumulation of an anthraquinone and its platinum complexes in cancer cell spheroids: the effect of charge on drug distribution in solid tumour models. *Chem. Commun.***,** 2673-2675.

Cai, W., CHen, K., He, L., Cao, Q., Koong, A. & Chen, X. 2007. Quantitative PET of EGFR expression in xenograft-bearing mice using 64Cu-labeled cetuximab, a chimeric anti-EGFR monoclonal antibody. *European journal of nuclear medicine and molecular imaging,* 34**,** 850-858.

Chakrabarti, R. & Chakrabarti, R. 2006. Calcium signaling in non-excitable cells: Ca2+ release and influx are independent events linked to two plasma membrane Ca2+ entry channels. *Journal of cellular biochemistry,* 99**,** 1503-1516.

Chang, Y., Yang, S.-T., Liu, J.-H., Dong, E., Wang, Y., Cao, A., Liu, Y. & Wang, H. 2011. In vitro toxicity evaluation of graphene oxide on A549 cells. *Toxicology letters,* 200**,** 201-210.

Curigliano, G., Cardinale, D., Suter, T., Plataniotis, G., De Azambuja, E., Sandri, M., Criscitiello, C., Goldhirsch, A., Cipolla, C. & Roila, F. 2012. Cardiovascular toxicity induced by chemotherapy, targeted agents and radiotherapy: ESMO Clinical Practice Guidelines. *Annals of Oncology,* 23**,** vii155-vii166.

Deng, Z. J., Liang, M., Monteiro, M., Toth, I. & Minchin, R. F. 2011. Nanoparticle-induced unfolding of fibrinogen promotes Mac-1 receptor activation and inflammation. *Nature nanotechnology,* 6**,** 39-44.

Dimri, M., Naramura, M., Duan, L., Chen, J., Ortega-Cava, C., Chen, G., Goswami, R., Fernandes, N., Gao, Q. & Dimri, G. P. 2007. Modeling breast cancer–associated c-Src and EGFR overexpression in human MECs: c-Src and EGFR cooperatively promote aberrant three-dimensional acinar structure and invasive behavior. *Cancer research,* 67**,** 4164-4172.

Erban, J. K. & Lau, J. 2006. On the toxicity of chemotherapy for breast cancer—the need for vigilance. *Journal of the National Cancer Institute,* 98**,** 1096-1097.

Eruslanov, E. & Kusmartsev, S. 2010. Identification of ROS using oxidized DCFDA and flow-cytometry. *Advanced Protocols in Oxidative Stress II.* Springer.

Fischer, O. M., Hart, S., Gschwind, A., Prenzel, N. & Ullrich, A. 2004. Oxidative and osmotic stress signaling in tumor cells is mediated by ADAM proteases and heparin-binding epidermal growth factor. *Molecular and cellular biology,* 24**,** 5172-5183.

Gazdar, A. 2009. Activating and resistance mutations of EGFR in non-small-cell lung cancer: role in clinical response to EGFR tyrosine kinase inhibitors. *Oncogene,* 28**,** S24.

Kedmi, R., Ben-Arie, N. & Peer, D. 2010. The systemic toxicity of positively charged lipid nanoparticles and the role of Toll-like receptor 4 in immune activation. *Biomaterials,* 31**,** 6867-6875.

Khan, E. M., Heidinger, J. M., Levy, M., Lisanti, M. P., Ravid, T. & Goldkorn, T. 2006. Epidermal growth factor receptor exposed to oxidative stress undergoes Src-and caveolin-1-dependent perinuclear trafficking. *Journal of Biological Chemistry,* 281**,** 14486-14493.

Lee, Y.-I., Seo, M., Kim, Y., Kim, S.-Y., Kang, U. G., Kim, Y.-S. & Juhnn, Y.-S. 2005. Membrane depolarization induces the undulating phosphorylation/dephosphorylation of glycogen synthase kinase 3β, and this dephosphorylation involves protein phosphatases 2A and 2B in SH-SY5Y human neuroblastoma cells. *Journal of Biological Chemistry,* 280**,** 22044-22052.

Lin, W., Stayton, I., Huang, Y.-W., Zhou, X.-D. & Ma, Y. 2008. Cytotoxicity and cell membrane depolarization induced by aluminum oxide nanoparticles in human lung epithelial cells A549. *Toxicological and Environmental Chemistry,* 90**,** 983-996.

Lu, Y.-J., Lin, C.-W., Yang, H.-W., Lin, K.-J., Wey, S.-P., Sun, C.-L., Wei, K.-C., Yen, T.-C., Lin, C.-I. & Ma, C.-C. M. 2014. Biodistribution of PEGylated graphene oxide nanoribbons and their application in cancer chemo-photothermal therapy. *Carbon,* 74**,** 83-95.

Maemondo, M., Inoue, A., Kobayashi, K., Sugawara, S., Oizumi, S., Isobe, H., Gemma, A., Harada, M., Yoshizawa, H. & Kinoshita, I. 2010. Gefitinib or chemotherapy for non–small-cell lung cancer with mutated EGFR. *New England Journal of Medicine,* 362**,** 2380-2388.

Mamot, C., Drummond, D. C., Greiser, U., Hong, K., Kirpotin, D. B., Marks, J. D. & Park, J. W. 2003. Epidermal growth factor receptor (EGFR)-targeted immunoliposomes mediate specific and efficient drug delivery to EGFR-and EGFRvIII-overexpressing tumor cells. *Cancer research,* 63**,** 3154-3161.

Mamot, C., Ritschard, R., Küng, W., Park, J. W., Herrmann, R. & Rochlitz, C. F. 2006. EGFR-targeted immunoliposomes derived from the monoclonal antibody EMD72000 mediate specific and efficient drug delivery to a variety of colorectal cancer cells. *Journal of drug targeting,* 14**,** 215-223.

Monteith, G. R., McAndrew, D., Faddy, H. M. & Roberts-Thomson, S. J. 2007. Calcium and cancer: targeting Ca2+ transport. *Nature Reviews Cancer,* 7**,** 519-530.

Moreno, D., Zalba, S., Navarro, I., Tros de Ilarduya, C. & Garrido, M. J. 2010. Pharmacodynamics of cisplatin-loaded PLGA nanoparticles administered to tumor-bearing mice. *European Journal of Pharmaceutics and Biopharmaceutics,* 74**,** 265-274.

Mukohara, T., Kudoh, S., Yamauchi, S., Kimura, T., Yoshimura, N., Kanazawa, H., Hirata, K., Wanibuchi, H., Fukushima, S. & Inoue, K. 2003. Expression of epidermal growth factor receptor (EGFR) and downstream-activated peptides in surgically excised non-small-cell lung cancer (NSCLC). *Lung Cancer,* 41**,** 123-130.

Nicholson, R., Gee, J. & Harper, M. 2001. EGFR and cancer prognosis. *European journal of cancer,* 37**,** 9-15.

Nishikawa, R., Ji, X.-D., Harmon, R. C., Lazar, C. S., Gill, G. N., Cavenee, W. K. & Huang, H. 1994. A mutant epidermal growth factor receptor common in human glioma confers enhanced tumorigenicity. *Proceedings of the National Academy of Sciences,* 91**,** 7727-7731.

Nishinaka, T. & Yabe-Nishimura, C. 2001. EGF receptor-ERK pathway is the major signaling pathway that mediates upregulation of aldose reductase expression under oxidative stress. *Free Radical Biology and Medicine,* 31**,** 205-216.

Normanno, N. 2013. The S492R EGFR ectodomain mutation is never detected in KRAS wild-type colorectal carcinoma before exposure to EGFR monoclonal antibodies. *Cancer biology & therapy,* 14**,** 1143-1146.

Norton, C. E., Broughton, B. R., Jernigan, N. L., Walker, B. R. & Resta, T. C. 2013. Enhanced depolarization-induced pulmonary vasoconstriction following chronic hypoxia requires EGFR-dependent activation of NAD (P) H oxidase 2. *Antioxidants & redox signaling,* 18**,** 1777-1788.

Ohgaki, H. & Kleihues, P. 2007. Genetic pathways to primary and secondary glioblastoma. *The American journal of pathology,* 170**,** 1445-1453.

Paez, J. G., Jänne, P. A., Lee, J. C., Tracy, S., Greulich, H., Gabriel, S., Herman, P., Kaye, F. J., Lindeman, N. & Boggon, T. J. 2004. EGFR mutations in lung cancer: correlation with clinical response to gefitinib therapy. *Science,* 304**,** 1497-1500.

Pao, W., Miller, V. A., Politi, K. A., Riely, G. J., Somwar, R., Zakowski, M. F., Kris, M. G. & Varmus, H. 2005. Acquired resistance of lung adenocarcinomas to gefitinib or erlotinib is associated with a second mutation in the EGFR kinase domain. *PLoS medicine,* 2**,** e73.

Peus, D., Vasa, R. A., Meves, A., Pott, M., Beyerle, A., Squillace, K. & Pittelkow, M. R. 1998. H2O2 is an important mediator of UVB-induced EGF-receptor phosphorylation in cultured keratinocytes. *Journal of Investigative Dermatology,* 110**,** 966-971.

Rauch, J., Kolch, W., Laurent, S. & Mahmoudi, M. 2013. Big signals from small particles: regulation of cell signaling pathways by nanoparticles. *Chemical reviews,* 113**,** 3391-3406.

Rauch, J., Kolch, W. & Mahmoudi, M. 2012. Cell type-specific activation of AKT and ERK signaling pathways by small negatively-charged magnetic nanoparticles. *Scientific reports,* 2.

Roe, M., Lemasters, J. & Herman, B. 1990. Assessment of Fura-2 for measurements of cytosolic free calcium. *Cell calcium,* 11**,** 63-73.

Rosen, L. B. & Greenberg, M. E. 1996. Stimulation of growth factor receptor signal transduction by activation of voltage-sensitive calcium channels. *Proceedings of the National Academy of Sciences,* 93**,** 1113-1118.

Schlessinger, J. 2002. Ligand-induced, receptor-mediated dimerization and activation of EGF receptor. *Cell,* 110**,** 669-672.

Shinojima, N., Tada, K., Shiraishi, S., Kamiryo, T., Kochi, M., Nakamura, H., Makino, K., Saya, H., Hirano, H. & Kuratsu, J.-I. 2003. Prognostic value of epidermal growth factor receptor in patients with glioblastoma multiforme. *Cancer research,* 63**,** 6962-6970.

Sordella, R., Bell, D. W., Haber, D. A. & Settleman, J. 2004. Gefitinib-sensitizing EGFR mutations in lung cancer activate anti-apoptotic pathways. *Science,* 305**,** 1163-1167.

Sydlik, U., Bierhals, K., Soufi, M., Abel, J., Schins, R. P. & Unfried, K. 2006. Ultrafine carbon particles induce apoptosis and proliferation in rat lung epithelial cells via specific signaling pathways both using EGF-R. *American Journal of Physiology-Lung Cellular and Molecular Physiology,* 291**,** L725-L733.

Takahashi, M., Yokoe, S., Asahi, M., Lee, S. H., Li, W., OSUMI, D., MIYOSHI, E. & TANIGUCHI, N. 2008. N-glycan of ErbB family plays a crucial role in dimer formation and tumor promotion. *Biochimica et Biophysica Acta (BBA)-General Subjects,* 1780**,** 520-524.

Takeyama, K., Dabbagh, K., Shim, J. J., Dao-Pick, T., Ueki, I. F. & Nadel, J. A. 2000. Oxidative stress causes mucin synthesis via transactivation of epidermal growth factor receptor: role of neutrophils. *The Journal of Immunology,* 164**,** 1546-1552.

Talukdar, Y., Rashkow, J. T., Lalwani, G., Kanakia, S. & Sitharaman, B. 2014. The effects of graphene nanostructures on mesenchymal stem cells. *Biomaterials,* 35**,** 4863-4877.

Unfried, K., Sydlik, U., Bierhals, K., Weissenberg, A. & Abel, J. 2008. Carbon nanoparticle-induced lung epithelial cell proliferation is mediated by receptor-dependent Akt activation. *American Journal of Physiology-Lung Cellular and Molecular Physiology,* 294**,** L358-L367.

Voldborg, B. R., Damstrup, L., Spang-Thomsen, M. & Poulsen, H. S. 1997. Epidermal growth factor receptor (EGFR) and EGFR mutations, function and possible role in clinical trials. *Annals of Oncology,* 8**,** 1197-1206.

Wang, X., McCullough, K. D., Franke, T. F. & Holbrook, N. J. 2000. Epidermal growth factor receptor-dependent Akt activation by oxidative stress enhances cell survival. *Journal of Biological Chemistry,* 275**,** 14624-14631.

Wells, A. 1999. EGF receptor. *The international journal of biochemistry & cell biology,* 31**,** 637-643.

Willmarth, N. E., Baillo, A., Dziubinski, M. L., Wilson, K., Riese II, D. J. & Ethier, S. P. 2009. Altered EGFR localization and degradation in human breast cancer cells with an amphiregulin/EGFR autocrine loop. *Cellular signalling,* 21**,** 212-219.

Yamada, A., Gaja, N., Ohya, S., Muraki, K., Narita, H., Ohwada, T. & Imaizumi, Y. 2001. Usefulness and limitation of DiBAC4 (3), a voltage-sensitive fluorescent dye, for the measurement of membrane potentials regulated by recombinant large conductance Ca2+-activated K+ channels in HEK293 cells. *The Japanese journal of pharmacology,* 86**,** 342-350.

Yarden, Y. 2001. The EGFR family and its ligands in human cancer: signalling mechanisms and therapeutic opportunities. *European journal of cancer,* 37**,** 3-8.

Yu, X., Miyamoto, S. & Mekada, E. 2000. Integrin alpha 2 beta 1-dependent EGF receptor activation at cell-cell contact sites. *Journal of Cell Science,* 113**,** 2139-2147.

Zhang, Y., Ali, S. F., Dervishi, E., Xu, Y., Li, Z., Casciano, D. & BIRIS, A. S. 2010. Cytotoxicity effects of graphene and single-wall carbon nanotubes in neural phaeochromocytoma-derived PC12 cells. *Acs Nano,* 4**,** 3181-3186.

Zhao, J., Xu, L., Zhang, T., Ren, G. & Yang, Z. 2009. Influences of nanoparticle zinc oxide on acutely isolated rat hippocampal CA3 pyramidal neurons. *Neurotoxicology,* 30**,** 220-230.

Zwick, E., Daub, H., Aoki, N., Yamaguchi-Aoki, Y., Tinhofer, I., Maly, K. & Ullrich, A. 1997. Critical role of calcium-dependent epidermal growth factor receptor transactivation in PC12 cell membrane depolarization and bradykinin signaling. *Journal of Biological Chemistry,* 272**,** 24767-24770.

5.6 Figures

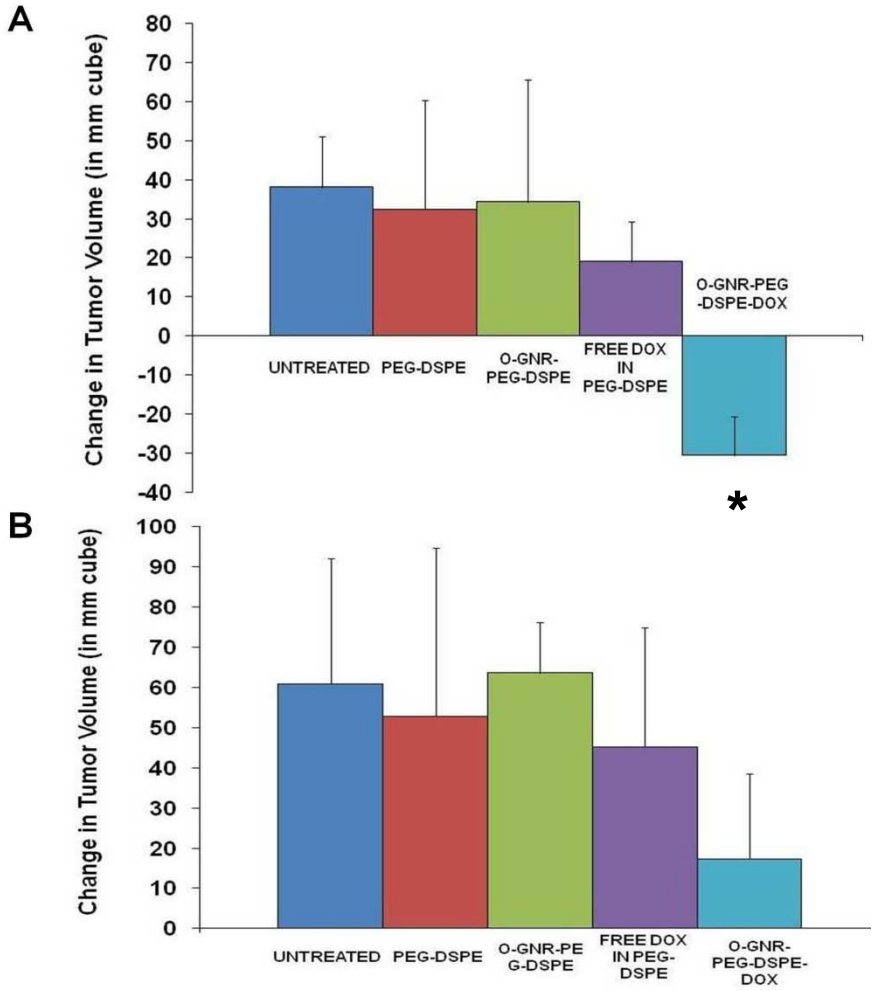

Figure 1 Change in volume of (A) HeLa xenograft tumors (B) MCF7 xenograft tumors injected with 50 μl each of Dox loaded O-GNR-PEG-DSPE, PEG-DSPE, O-GNR-PEG-DSPE and Free Dox in PEG-DSPE or left untreated. n=4. Data presented as mean+standard deviation. * = $p<0.05$ and represents a statistically significant difference from untreated cells.

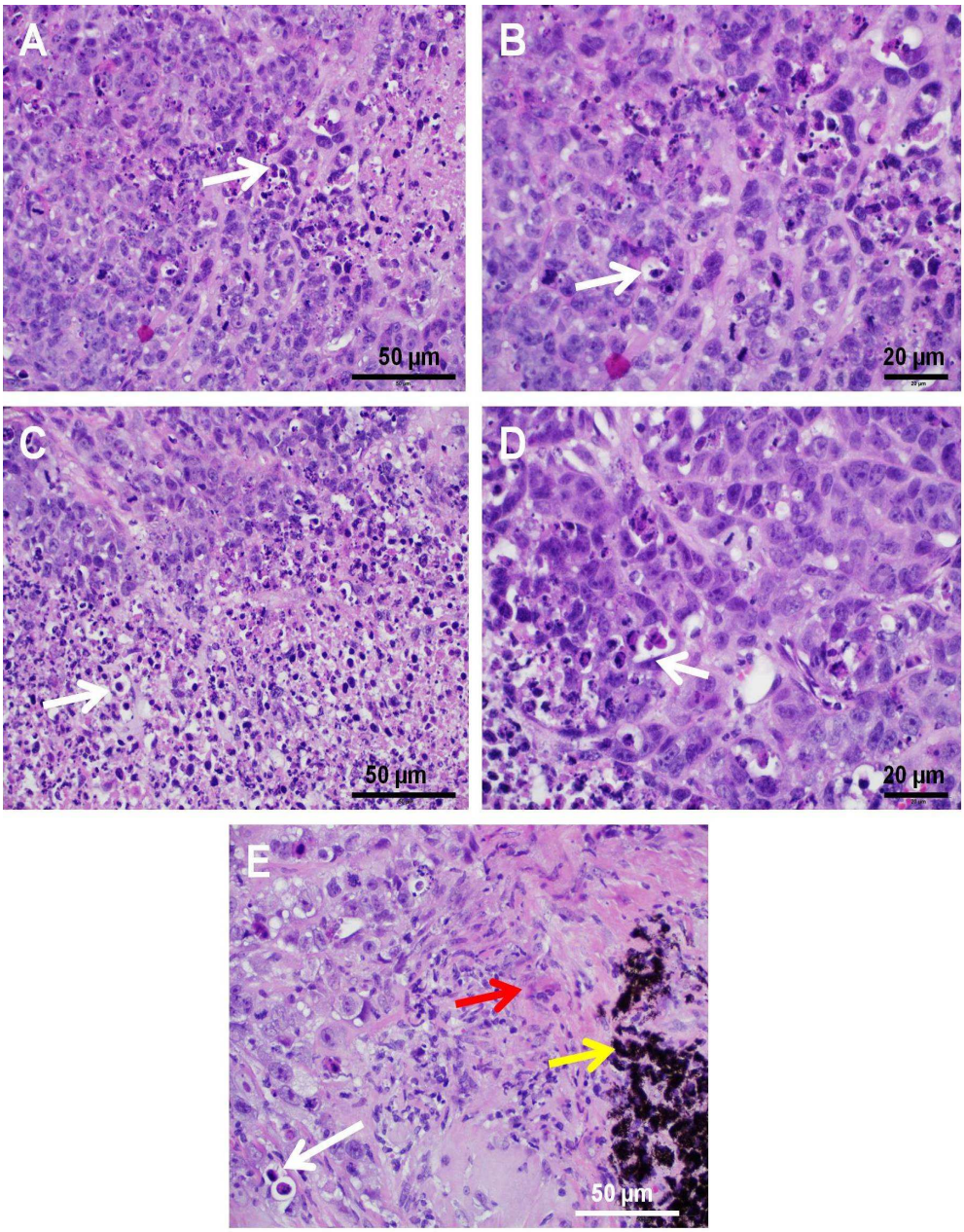

Figure 2 (A-E)Hematoxylin and Eosin stained histology sections of HeLa xenograft tumors (A-B) Untreated (C-E) injected with 50 µl of Dox loaded onto O-GNR-PEG-DSPE. White arrows indicate necrotic cells. Yellow arrows indicate O-GNR-PEG-DSPE and red arrows indicate fibrosis

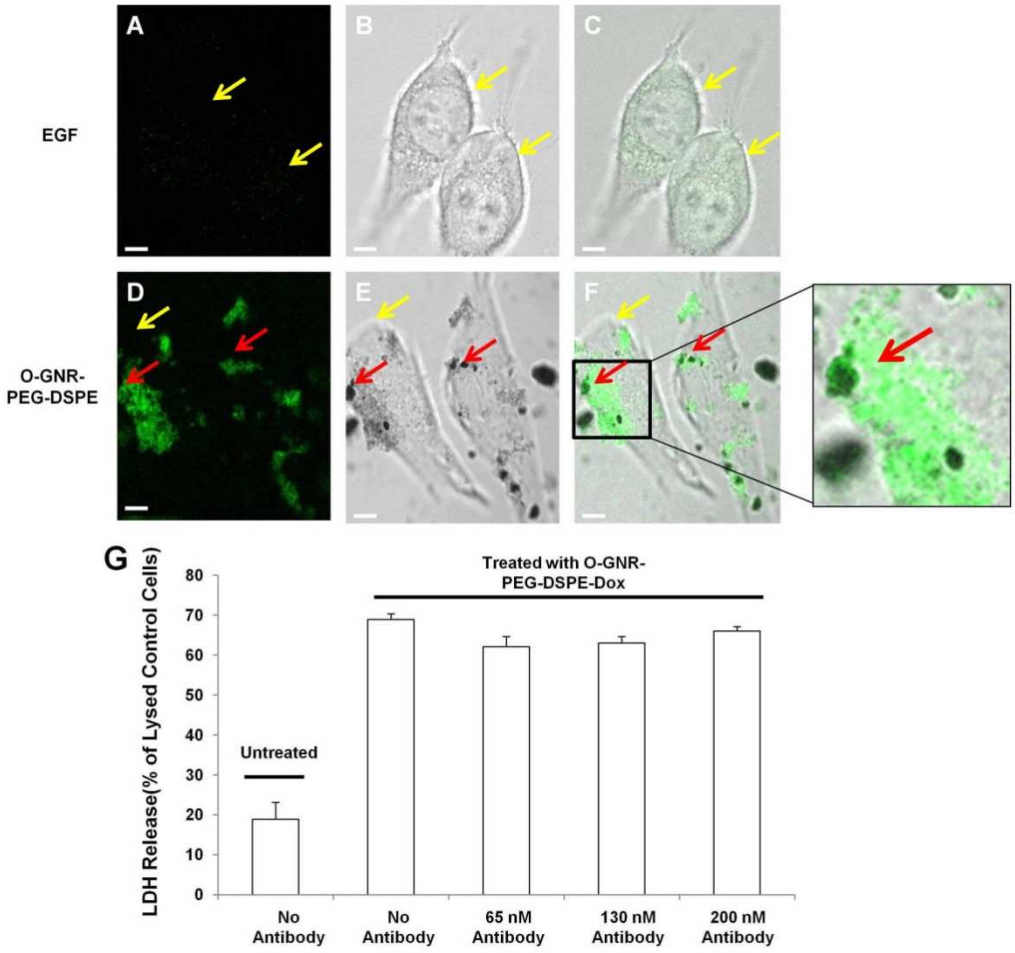

Figure 3. Representative fluorescence, bright field and merge images of HeLa cells treated with 130 nM anti-EGFR antibody and exposed to (A-C) EGF (D-F) O-GNR-PEG-DSPE. (G) Lactate dehydrogenase release after treatment of with doxorubin (Dox)-loaded O-GNR-PEG-DSPEs to untreated or anti-EGFR antibody treated HeLa cells. Red arrows indicate EGFR activation and yellow arrows indicate cells. N=4. Data presented as mean+standard deviation

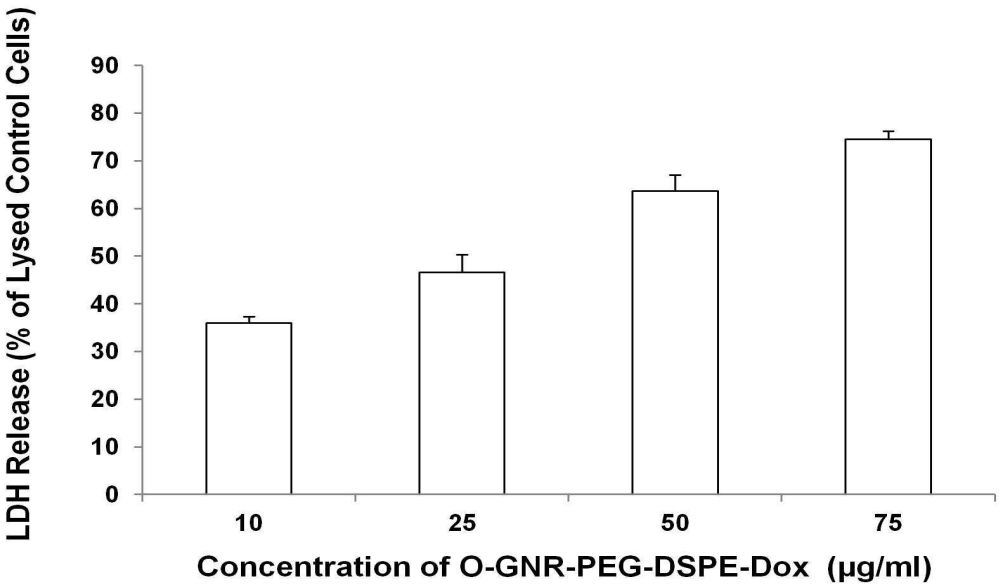

Figure 4 Lactate dehydrogenase release after treatment of HeLa cells with different concentrations of doxorubin-loaded O-GNR-PEG-DSPEs.N=4.Data presented as mean+standard deviation.

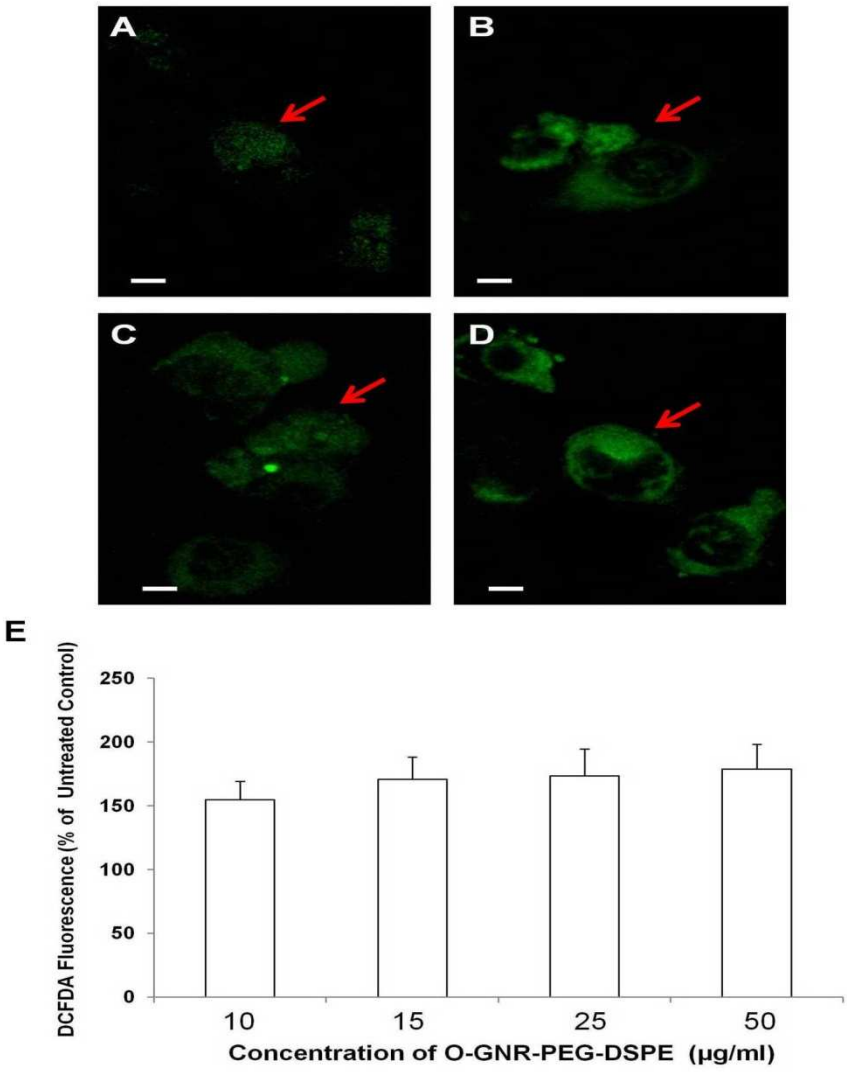

Figure 5 Representative DCFDA fluorescence images of HeLa cells treated with (A) 10µg/ml (B) 15µg/ml (C) 25µg/ml (D) 50µg/ml O-GNR-PEG-DSPE.Red arrows indicate individual cells (E) Multiwell plate based DCFDA fluorescence assay in HeLa cells exposed to 10-50µg/ml O-GNR-PEG-DSPE. N=4. Data presented as mean+standard deviation

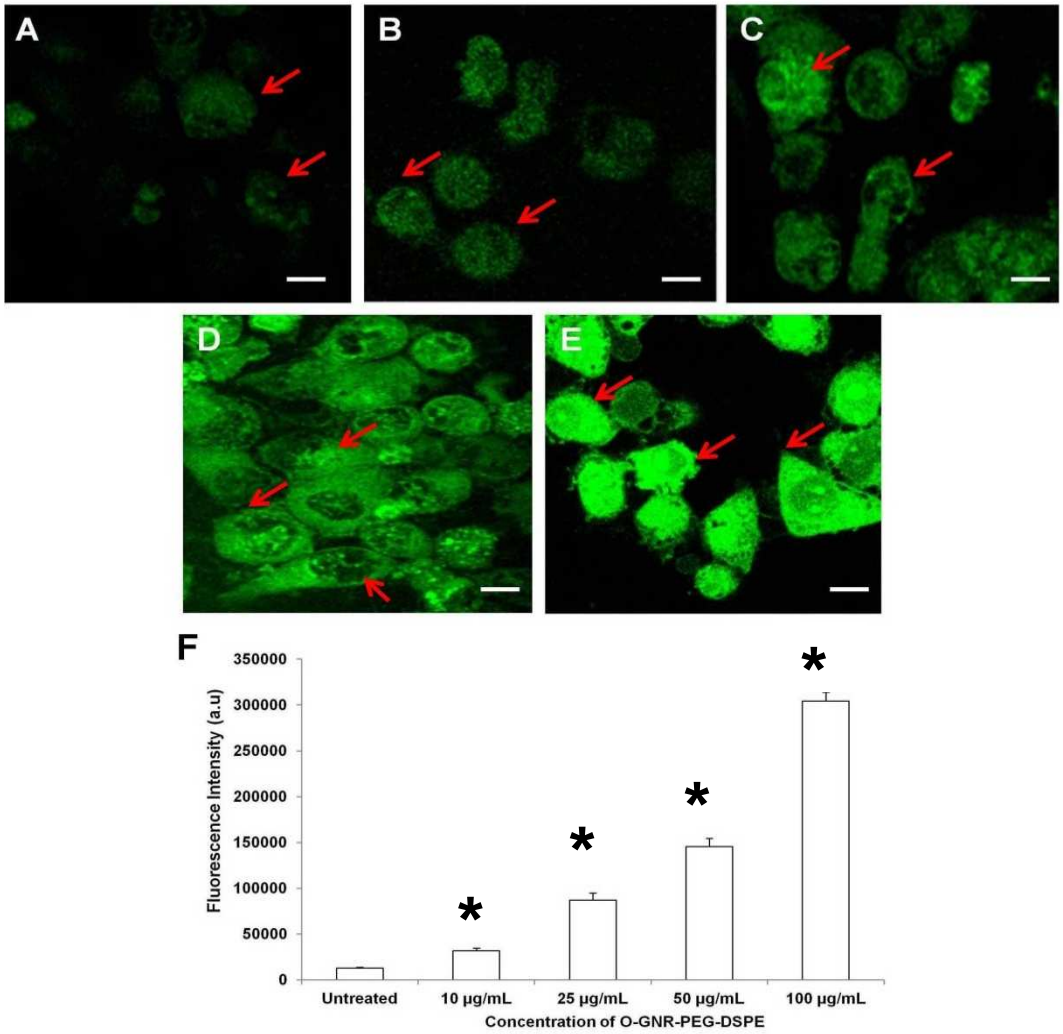

Figure 6 Representative $DiBAC_4(3)$ fluorescence images of HeLa cells treated with (A) 0µg/ml (B) 10µg/ml (C) 25µg/ml (D) 50µg/ml (E) 75µg/ml O-GNR-PEG-DSPE. Red arrows indicate individual cells (E) Quantification of fluorescence from representative images of each treatment group. 15 cells from each treatment group were analyzed for fluorescence quantification. Data presented as mean + standard deviation * indicates significant increase ($p < 0.05$) in fluorescence intensity compared to untreated cells.

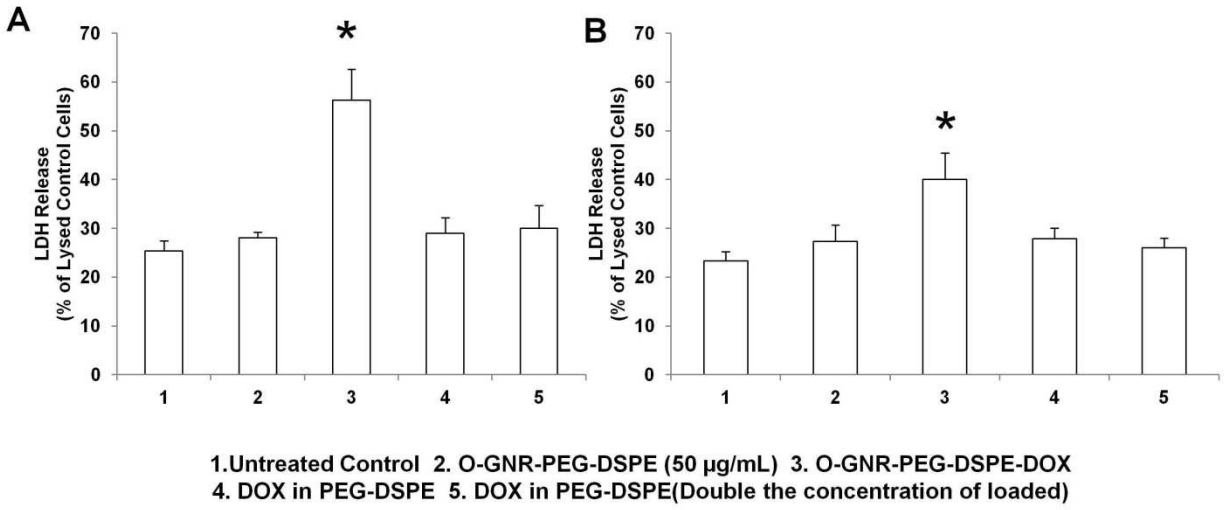

Figure 7 Lactic dehydrogenase (LDH) release after treatment with doxorubin (Dox)-loaded O-GNR-PEG-DSPEs in HeLa cells grown in (A) Normal DMEM (B) DMEM without Ca^{2+}. Untreated cells, cells treated with free Dox in PEG-DSPE, and lysed cells were additional controls. All data are normalized to LDH released from lysed control cells. Data are presented as mean +standard deviation (n = 6 per group). * indicates significant increase ($p < 0.05$) in LDH release compared to cells exposed to Dox in PEG-DSPE at the same concentration as loaded onto O-GNR-PEG-DSPEs. 1= Untreated Control 2= O-GNR-PEG-DSPE (50µg/ml) 3= O-GNR-PEG-DSPE-Dox 4= DOX in PEG-DSPE (Same concentration as loaded) 5= DOX in PEG-DSPE (Double concentration as loaded)

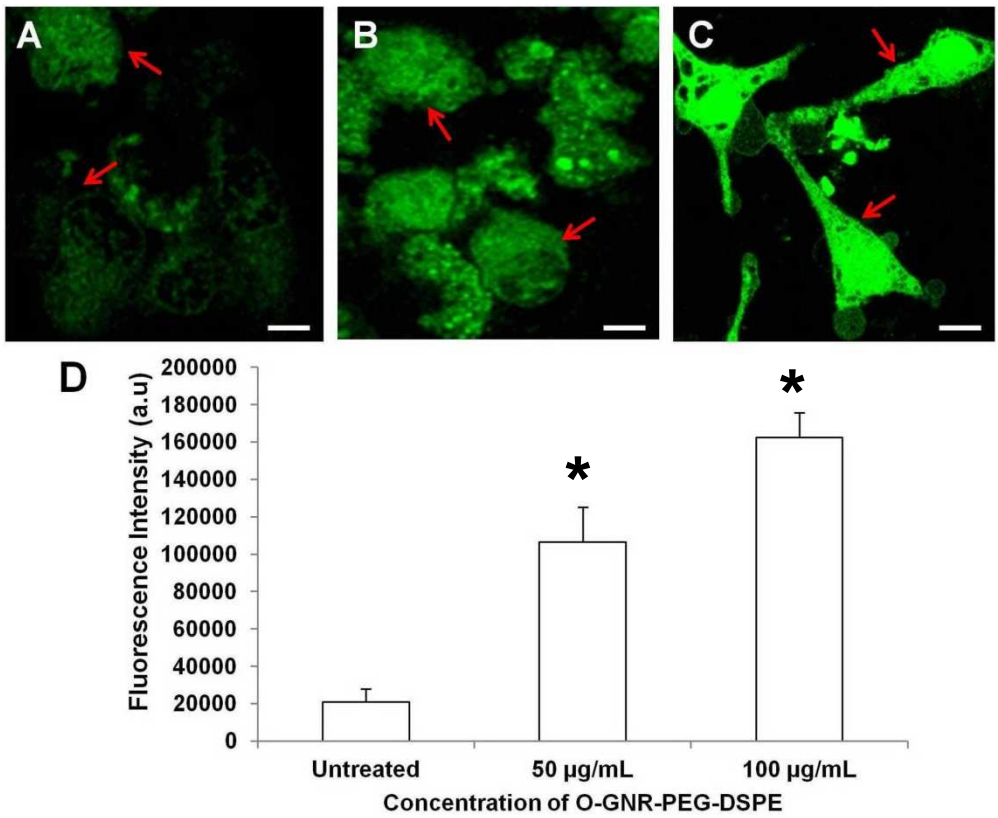

Figure 8 Representative Fura2-AM-Ca^{2+} fluorescence images of HeLa cells treated with (A) 0 µg/ml (B) 50µg/ml (C) 100µg/ml O-GNR-PEG-DSPE. Red arrows indicate individual cells (C) Quantification of fluorescence from representative images of each treatment group. 15 cells from each treatment group were analyzed for fluorescence quantification. Data presented as mean + standard deviation * indicates significant increase ($p < 0.05$) in fluorescence intensity compared to untreated cells.

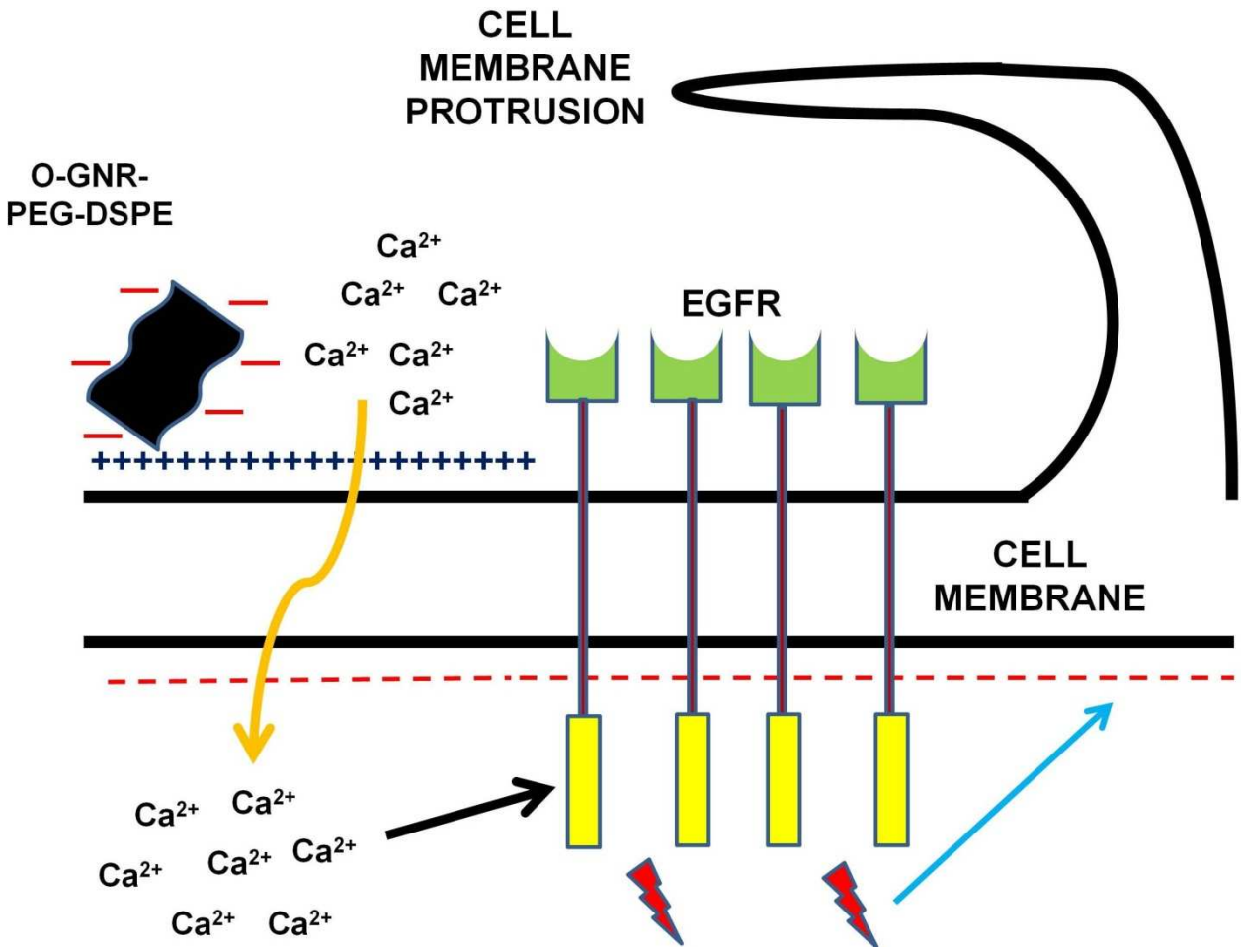

Figure 9 Schematic representation of probable mechanism of EGFR activation by O-GNR-PEG-DSPE

CONCLUSION AND FUTURE DIRECTIONS

This dissertation explores the suitability of graphene nanoribbons (O-GNR) for biomedical applications by finding its *in vitro* toxicity, hematological compatibility, and mechanism of uptake in different cell lines and blood. We also explore the potential of these particles as agents for cell specific drug delivery by utilizing their uptake mechanism.

O-GNRs were non-covalently coated with PEG-DSPE to increase their stability in water and decrease protein binding in both cell culture media and blood. O-GNR-PEG-DSPEs were significantly more soluble in water as well as saline compared to un-functionalized O-GNR's. Also, significant decrease in albumin binding was observed in the PEG-DSPE functionalized particles. However, even after PEG-DSPE functionalization, increasing concentration did result in increased protein binding albeit lesser than the unfunctionalized nanostructures. Toxicity screening performed using 5 assays tested (alamar blue, neutral red, trypan blue, LDH release, clonogenic assay and live cell assay) on four cell lines (HeLa, MCF7, SKBR3 and NIH3T3) indicated that O-GNR-PEG-DSPEs have a dose-dependent and time-dependent, and differential cytotoxic effects on the four cell lines .HeLa, exhibited greater toxicity compared to the other cell lines in all the 5 assays. TEM images of cell specimens showed higher uptake of the O-GNR-PEG-DSPE formulations into HeLa cells compared to other cells, which show very little or no uptake. The higher uptake could affect the cellular machinery of HeLa cells, and is probably the major reason for observed differences in cytotoxicity results between HeLa, and other cell lines. The results of this study suggested that O-GNRs synthesized from CNTs have a cell-specific cytotoxic effect and significantly different cytotoxicity profile compared to graphene nanoparticles prepared by the modified Hummer's method (graphene nanoparticles prepared by

oxidation of graphite, and its mechanical exfoliation) or its variations. Exposure of O-GNR-PEG-DSPE to red blood cells showed that nanoparticle-red blood cell interaction can result in structural changes to the red blood cells. These structural changes (probably caused due to interaction of the particles with cytoskeletal elements of the red blood cells) can potentially lead to formation of spherocyte like structures. However, this structural change in RBC's did not lead to hemolysis in red blood cells. Evaluation of the effects of O-GNR-PEG-DSPE on other aspects of the hematological system showed that exposure of these particles to whole blood did not lead to increase in histamine release or platelet activation. Also, no increase in complement activation was observed. Although, no change was observed in the levels of pro-inflammatory cytokine TNF-Alpha a small decrease (~5-10%) was observed in the levels of anti-inflammatory cytokine IL-10. Treatment of O-GNR-PEG-DSPE's to human umbilical vein endothelial cells showed that a decrease of ~15% cell viability at 100 µg/ml and ~40% at 600 µg/ml. Transmission electron microscopy analysis showed that the endothelial cells could take up large amounts of these particles in vesicular structures. Overall, both the *in vitro* and hematological toxicity suggested that concentrations ~50µg/mL are relatively non-toxic for biomedical applications. However, further steps should be taken to minimize RBC-nanoparticle interactions. Since toxicity analysis of HeLa cells had showed high uptake in these cells, further detailed analysis of uptake mechanism of O-GNR-PEG-DSPE in these cells indicated that on coming in contact with the particles, HeLa cells initiated membrane protrusions that engulfed O-GNR-PEG-DSPE aggregates into large vesicular macropinosome like structures. Use of inhibitors to assess uptake showed that nanoparticle uptake maybe a dynamin dependent macropinocytosis like process. Also, during the uptake process formation of circular dorsal ruffles were observed on staining the actin filaments. Previous studies have shown that dynamin dependent macropinocytosis like

uptake and dorsal ruffle formation during activation and uptake to epidermal growth factor receptors(Orth et al., 2006). Further analysis by confocal miscroscopy and western blots (using anti activated EGFR antibodies) showed that O-GNR-PEG-DSPEs activate epidermal growth factor receptors (EGFRs) and are taken up in significant amounts in cells with high EGFR expression. This phenomenon coupled to the fact that O-GNR-PEG-DSPE's can load high amounts of aromatic drugs through pi stacking interactions leads to differential and increased intracellular drug delivery efficacy in EGFR over-expressing cells. Results showed that, in cells with high EGFR expression or with integrated HPV genome [Cells with integrated human papilloma virus (HPV) genomes, which express EGFR (at normal or elevated levels), elicit enhanced O-GNR-PEG-DSPE uptake via the modulation of EFGR by the viral protein E5], the intracellular delivery of the drug Dox by O-GNR-PEG-DSPE increases its efficacy by 100% greater compared to drug alone. Even in cells with high EGFR expression, or with HPV genome, that express the multidrug resistant protein 1 (MDR1), the drug efficacies increase upto 75% compared to drug alone. Drug alone dispersed in PEG-DSPE at the same or twice the concentration loaded onto O-GNR-PEG-DSPEs did not show any statistically significant increase in its efficacy compared to untreated cells.

Further evaluation of the mechanism of EGFR activation due to O-GNR-PEG-DSPE treatment showed that EGFR activation does not occur due to direct receptor binding of the particle, although, treatment of increasing concentration of O-GNR-PEG-DSPE leads to increasing uptake and drug delivery. Also, O-GNR-PEG-DSPE did not show a concentration dependent increase in oxidative stress (which has been reported in some studies to cause ligand free activation of EGFR) indicating that it is not the cause for EGFR activation(Wang et al., 2000). Membrane depolarization has also been shown as a possible mechanism for ligand free

activation of EGFR. Treatment of increasing concentrations of O-GNR-PEG-DSPE showed increasing membrane depolarization (evaluated using a voltage sensitive dye in HeLa cells) indicating that membrane depolarization may be the cause for EGFR activation in O-GNR-PEG-DSPE treated cells(Zwick et al., 1997). A possible reason for this might be the negative zeta potential on O-GNR-PEG-DSPE due to the large number of hydroxyl and carboxyl groups on its surface that causes temporary depolarization of the cell membrane on coming in contact with it(Talukdar et al., 2014).

In vivo study in xenograft tumors of MCF7 and HeLa cells showed that Dox loaded O-GNR-PEG-DSPE could significantly retard tumor growth in HeLa xenograft tumors but not in MCF7 xenograft tumors establishing the cell specific uptake and drug delivery of O-GNR-PEG-DSPE. Free drug in PEG-DSPE, PEG-DSPE alone as well as O-GNR–PEG-DSPE did not retard tumor growth in either type of xenograft tumors.

This intriguing cell specific uptake of O-GNR-PEG-DSPEs together with its other attributes (i.e., high drug loading efficiencies, drug release at acidic pH, and other nanoparticle-related properties such as enhanced permeability-and-retention (EPR) effect(Haley and Frenkel, 2008)) suggest strong potential for the use of O-GNR-PEG-DSPE as a pharmaceutical delivery agent to treat pathologies that over-express EGFR or are mediated by HPV (Siddiqui et al., 2012). Such a delivery agent could mitigate the problem encountered with presently used agents such as drug resistance and toxicity to normal cells (Ogino et al., 2007, Lynch et al., 2007).

Confirmation of HPV infection is usually done through pap smear tests(Clarke and Anderson, 1979). However, pap smear tests can only confirm HPV infection at the later stages when there is histological evidence of the viral infection and visible changes in cell morphology(Clarke and

Anderson, 1979). Since O-GNR-PEG-DSPE particles show high uptake in HPV mediated tumors (due to the modulation of EGFR by the viral protein E5), O-GNR-PEG-DSPE (functionalized with a fluorescent or other tags that enhances contrast in imaging modalities) can be used for early detection of HPV infection (since E5 is expressed as soon as the viral genome starts proliferating). Thus there is potential to develop alternative to pap smear tests using these particles.

O-GNR-PEG-DSPE's consist of several sheets of graphene stacked together using weak interactions. The gaps between these sheets can be easily intercalated and coordinated with trace amounts of agents that can enhance contrast during imaging. Examples of such agents include Mn^{2+} for MRI and Iodine ions for enhancement of contrast in CT(Paratala et al., 2012, Lalwani et al., 2014). Moreover, graphene itself has NIR absorbing capabilities leading to contrast enhancement during photoacoustic imaging(Wang et al., 2013). This property of O-GNR-PEG-DSPE, along with its high drug loading and delivery capacity in EGFR over-expressing and HPV induced cancer cells, can be utilized for image guided therapy of cancer.

In recent years gene therapy has been explored by various research groups as a treatment option for cancer. Therapeutic gene delivery allows replacement of a mutated gene(Roth and Cristiano, 1997), production of therapeutic proteins (from delivered genes) inside target cells (Tremblay et al., 2012), delivery of inhibitory RNA for down-regulation of a mutated or over-expressed gene (Medarova et al., 2007, Liu et al., 2007, Chu et al., 2006) and in some cases for "suicide therapy" to guide the diseased cells towards apoptosis(Morgan, 2012). Due to the pi bonds present on O-GNR surface they can also be used to load genetic material onto on them. This is possible because purines and pyrimidines in DNA and RNA contain pi bonds which can be utilized to stack them on the O-GNR surface. Similar to drug delivery, the loaded genes on O-GNR can be

specifically delivered to EGFR over-expressing tumors or HPV induced tumors for efficient gene therapy. Hence the potential of O-GNR's as a gene delivery agent can also be explored in the near future.

In the future, further development of O-GNR-PEG-DSPE as a drug delivery agent would require more detailed toxicological analysis of these nanostructures in terms of detailed pharmacodynamics, pharmacokinetics and dose ranging of the drug loaded particles. A recent study has shown that O-GNR-PEG-DSPE, on intravenous injection, accumulates mostly in the liver(Lu et al., 2014). However, accumulation was also found to occur in other tissues like heart and kidney(Lu et al., 2014). The tissue specific effects of the nanoparticles that accumulate in different organs have to be completed in detail to ensure complete pharmacodynamic knowledge of the particles. Pharmacokinetics plays an important role in determining the potential toxicity or safe dosage of any drug delivery agent(Sheiner and Steimer, 2000). It also provides an idea about the primary mode of excretion or removal of the particles(Sheiner and Steimer, 2000). However, to get the complete idea about the metabolism, removal and maximum tolerated dose of O-GNR-PEG-DSPE, both pharmacodynamic and pharmacokinetic information will be needed(Sheiner and Steimer, 2000).

During intravenous injection of drug delivery agents, the vessel at the site of injection is subjected to several times higher concentration of the agent compared to the steady state blood concentration(Frame et al., 2014, Chowdhury et al., 2013). Hence, these vessels are prone to endothelial dysfunction if the concentration of the injected agent exceeds its maximum tolerated level(Frame et al., 2014, Chowdhury et al., 2013). Thus, a detailed analysis of endothelial effects due to injection of different concentrations of O-GNR-PEG-DSPE injection needs to be completed. This can be done by direct injection of various concentrations of O-GNR-PEG-DSPE

onto arterioles and measuring their vasodilatory and vasoconstrictory response over time in response acetylcholine, adenosine and phenylephrine as previously reported by Frame et al and Chowdhury et al(Chowdhury et al., 2013, Frame et al., 2014).

During flow of the O-GNR-PEG-DSPE through blood, the nanoparticles will also be subject to hemodynamic shear stress due to blood flow(Nollert et al., 1991). This shear stress may lead to disintegration of the particles resulting in unwanted toxicity. It has recently been shown that structural disintegration increases toxicity of O-GNR's. Hence, proper characterization and toxicity assessment of the disintegration products (if any) of O-GNR's formed due to shear stress in blood flow needs to be completed.

To be developed for clinical applications, more in depth physicochemical characterization is also needed for the drug loaded O-GNR-PEG-DSPEs. Intravenous injection of O-GNR-PEG-DSPEs would mean that they would flow along with blood into various blood vessels. Thus, it is very important to determine the value of the viscosity, osmolarity and patition coefficient of different concentrations of the nanoparticle. It is extremely difficult to inject solutions with higher viscosity than blood and if injected may cause various problems in renal output and perfusion.(Lancelot et al., 2002) Osmolarity of the O-GNR-PEG-DSPE solutions also affects vasodilation, vasoconstriction and release of vasopressin in the blood vessels(Vogler et al., 1995, Barrett and Carlisle, 1993). Hyper osmolar solutions usually produce more pain at injection site(Vogler et al., 1995). Partition coefficient is a measure of the hydrophobicity or hydrophilicity of the particles and determines biodistribution of the particles(Vogler et al., 1995, Caravan, 2009).

Future work to develop this nanoparticle as a drug delivery agent for EGFR over-expressing tumors would involve further *in vivo* drug delivery studies in orthotopic (EGFR over-expressing) tumor models of mice. Orthotopic tumors provide a more realistic model for tumor growth, and drug delivery studies in them would further prove the efficacy of this agent after intravenous injection(Burgos et al., 2003). Orthotopic tumor models to be utilized for this study should be tumors induced in breast tissue or lung tissue (which are the most common areas for cancers over-expessing EGFR)(de Palazzo et al., 1993, Miller et al., 1994). Orthotopic tumors for head and neck cancers have also been reported recently as mouse models for HPV mediated tumors(Masood et al., 2013). This orthotopic tumor model can be used for checking O-GNR-PEG-DSPE drug delivery efficacy in HPV mediated tumors.

The versatility of O-GNR-PEG-DSPE also needs to be established in terms of loading different chemotherapeutic drugs on its surface. Till now Dox (an anthracycline drug) and lucanthone (a thioxanthanone drug) has been loaded onto O-GNR-PEG-DSPE with high loading efficiency(Chowdhury et al., 2014). Depending on the drug being loaded, the loading protocol may need to be optimized to ensure maximum loading. Also, due to the varying number of pi bonds forming between O-GNR-PEG-DSPE and different aromatic drugs the drug release characteristics will also be different. Hence, it is necessary to characterize the drug release properties of each loaded drug to get an idea about release of the drugs in circulation after intravenous injection.

Although, membrane depolarization and Ca^{2+} entry is the probable mechanism for activation of EGFR, the events that lead to EGFR activation starting from the mechanism of Ca^{2+} entry needs to be further investigated. Similar to our findings it has been shown that in PC12 cells, that membrane depolarization induced calcium influx occurs through voltage gated channels (Zwick

et al., 1997). It remains to be seen if a similar mechanism occurs in other cells which shows high uptake of O-GNR-PEG-DSPE. However, HeLa cells do not contain voltage gated channels and some other mechanism may be at play for EGFR activation in terms of Ca^{2+} entry. Also, signaling events occurring downstream of Ca^{2+} entry that lead to the EGFR activation need to be better characterized.

In conclusion, it can be said that O-GNR-PEG-DSPE shows promise for a variety of applications in biomedicine including targeted drug and gene delivery to EGFR over-expressing and HPV mediated cancers as well as an agent for image guided therapy. They are multi-functional particles that can provide the solution to several unmet needs in the field of cancer drug delivery like low drug loading and tumor cell uptake. Although, I have provided an initial toxicological screening of these particles in this dissertation, further characterization of its possible toxic effects is still needed. If the maximum tolerated dose of these particles shows enough efficacy in both large and small animal models, this delivery agent has the potential to be a high impact discovery in the field of drug delivery.

References

Barrett, B. & Carlisle, E. 1993. Metaanalysis of the relative nephrotoxicity of high-and low-osmolality iodinated contrast media. *Radiology,* 188**,** 171-178.

Burgos, J., Rosol, M., Moats, R., Khankaldyyan, V., Kohn, D., Nelson Jr, M. & Laug, W. 2003. Time course of bioluminescent signal in orthotopic and heterotopic brain tumors in nude mice. *Biotechniques,* 34**,** 1184-1188.

Caravan, P. 2009. Protein-targeted gadolinium-based magnetic resonance imaging (MRI) contrast agents: design and mechanism of action. *Accounts of chemical research,* 42**,** 851-862.

Chowdhury, S. M., Kanakia, S., Toussaint, J. D., Frame, M. D., Dewar, A. M., Shroyer, K. R., Moore, W. & Sitharaman, B. 2013. In Vitro Hematological and In Vivo Vasoactivity Assessment of Dextran Functionalized Graphene. *Scientific reports,* 3.

Chowdhury, S. M., Surhland, C., Sanchez, Z., Chaudhary, P., Kumar, M. A. S., Lee, S., Peña, L. A., Waring, M., Sitharaman, B. & Naidu, M. 2014. Graphene Nanoribbons as a Drug Delivery Agent for Lucanthone Mediated Therapy of Glioblastoma Multiforme. *Nanomedicine: Nanotechnology, Biology and medicine.,* (Under review).

Chu, T. C., Twu, K. Y., Ellington, A. D. & Levy, M. 2006. Aptamer mediated siRNA delivery. *Nucleic acids research,* 34**,** e73-e73.

Clarke, E. A. & Anderson, T. 1979. Does screening by" Pap" smears help prevent cervical cancer?: a case-control study. *The Lancet,* 314**,** 1-4.

De Palazzo, I. E. G., Adams, G. P., Sundareshan, P., Wong, A. J., Testa, J. R., Bigner, D. D. & Weiner, L. M. 1993. Expression of mutated epidermal growth factor receptor by non-small cell lung carcinomas. *Cancer research,* 53**,** 3217-3220.

Frame, M. D., Dewar, A. M., Mullick ChowdhurY, S. & Sitharaman, B. 2014. Vasoactive effects of stable aqueous suspensions of single walled carbon nanotubes in hamsters and mice. *Nanotoxicology,* 8**,** 867-875.

Haley, B. & Frenkel, E. 2008. Nanoparticles for drug delivery in cancer treatment. *Urologic Oncology: Seminars and Original Investigations,* 26**,** 57-64.

Lalwani, G., Sundararaj, J. L., Schaefer, K., Button, T. & Sitharaman, B. 2014. Synthesis, characterization, in vitro phantom imaging, and cytotoxicity of a novel graphene-based multimodal magnetic resonance imaging-X-ray computed tomography contrast agent. *Journal of Materials Chemistry B,* 2**,** 3519-3530.

Lancelot, E., Idee, J.-M., Lacledere, C., Santus, R. & Corot, C. 2002. Effects of two dimeric iodinated contrast media on renal medullary blood perfusion and oxygenation in dogs. *Investigative radiology,* 37**,** 368-375.

Liu, Z., Winters, M., Holodniy, M. & Dai, H. 2007. siRNA Delivery into Human T Cells and Primary Cells with Carbon-Nanotube Transporters. *Angewandte Chemie International Edition,* 46**,** 2023-2027.

Lu, Y.-J., Lin, C.-W., Yang, H.-W., Lin, K.-J., Wey, S.-P., Sun, C.-L., Wei, K.-C., Yen, T.-C., Lin, C.-I. & Ma, C.-C. M. 2014. Biodistribution of PEGylated graphene oxide nanoribbons and their application in cancer chemo-photothermal therapy. *Carbon,* 74**,** 83-95.

Lynch, T. J., Kim, E. S., Eaby, B., Garey, J., West, D. P. & Lacouture, M. E. 2007. Epidermal growth factor receptor inhibitor–associated cutaneous toxicities: an evolving paradigm in clinical management. *The Oncologist,* 12**,** 610-621.

Masood, R., Hochstim, C., Cervenka, B., ZU, S., Baniwal, S., Patel, V., Kobielak, A. & Sinha, U. 2013. A novel orthotopic mouse model of head and neck cancer and lymph node metastasis. *Oncogenesis,* 2**,** e68.

Medarova, Z., Pham, W., Farrar, C., Petkova, V. & Moore, A. 2007. In vivo imaging of siRNA delivery and silencing in tumors. *Nature medicine,* 13**,** 372-377.

Miller, D. L., El-Ashry, D., Cheville, A. L., Liu, Y., McLeskey, S. W. & Kern, F. G. 1994. Emergence of MCF-7 cells overexpressing a transfected epidermal growth factor receptor (EGFR) under estrogen-depleted conditions: evidence for a role of EGFR in breast cancer growth and progression. *Cell growth & differentiation: the molecular biology journal of the American Association for Cancer Research,* 5**,** 1263-1274.

Morgan, R. A. 2012. Live and let die: a new suicide gene therapy moves to the clinic. *Molecular Therapy,* 20**,** 11.

Nollert, M., Diamond, S. & McIntire, L. 1991. Hydrodynamic shear stress and mass transport modulation of endothelial cell metabolism. *Biotechnology and bioengineering,* 38**,** 588-602.

Ogino, A., Kitao, H., Hirano, S., Uchida, A., Ishiai, M., Kozuki, T., Takigawa, N., Takata, M., Kiura, K. & Tanimoto, M. 2007. Emergence of epidermal growth factor receptor T790M mutation during chronic exposure to gefitinib in a non–small cell lung cancer cell line. *Cancer Research,* 67**,** 7807-7814.

Orth, J. D., Krueger, E. W., Weller, S. G. & McNiven, M. A. 2006. A novel endocytic mechanism of epidermal growth factor receptor sequestration and internalization. *Cancer research,* 66**,** 3603-3610.

Paratala, B. S., Jacobson, B. D., Kanakia, S., Francis, L. D. & Sitharaman, B. 2012. Physicochemical characterization, and relaxometry studies of micro-graphite oxide, graphene nanoplatelets, and nanoribbons. *PloS one,* 7**,** e38185.

Roth, J. A. & Cristiano, R. J. 1997. Gene therapy for cancer: what have we done and where are we going? *Journal of the National Cancer Institute,* 89**,** 21-39.

Sheiner, L. & Steimer, J.-L. 2000. Pharmacokinetic/pharmacodynamic modeling in drug development. *Annual review of pharmacology and toxicology,* 40**,** 67-95.

Siddiqui, S., Fang, M., Ni, B., Lu, D., Martin, B. & Maudsley, S. 2012. Central role of the EGF receptor in neurometabolic aging. *International Journal of Endocrinology,* 2012.

Talukdar, Y., Rashkow, J. T., Lalwani, G., Kanakia, S. & Sitharaman, B. 2014. The effects of graphene nanostructures on mesenchymal stem cells. *Biomaterials,* 35**,** 4863-4877.

Tremblay, J. P., Chapdelaine, P., Coulombe, Z. & Rousseau, J. 2012. Transcription activator-like effector proteins induce the expression of the frataxin gene. *Human gene therapy,* 23**,** 883-890.

Vogler, H., Platzek, J., Schuhmann-Giampieri, G., Frenzel, T., Weinmann, H.-J., Radüchel, B. & Press, W.-R. 1995. Pre-clinical evaluation of gadobutrol: a new, neutral, extracellular contrast agent for magnetic resonance imaging. *European journal of radiology,* 21**,** 1-10.

Wang, X., McCullough, K. D., Franke, T. F. & Holbrook, N. J. 2000. Epidermal growth factor receptor-dependent Akt activation by oxidative stress enhances cell survival. *Journal of Biological Chemistry,* 275**,** 14624-14631.

Wang, Y.-W., Fu, Y.-Y., Peng, Q., Guo, S.-S., Liu, G., Li, J., Yang, H.-H. & Chen, G.-N. 2013. Dye-enhanced graphene oxide for photothermal therapy and photoacoustic imaging. *Journal of Materials Chemistry B,* 1**,** 5762-5767.

Zwick, E., Daub, H., Aoki, N., Yamaguchi-Aoki, Y., Tinhofer, I., Maly, K. & Ullrich, A. 1997. Critical role of calcium-dependent epidermal growth factor receptor transactivation in PC12 cell membrane depolarization and bradykinin signaling. *Journal of Biological Chemistry*, 272**,** 24767-24770.